Beyond Jack-Ups

A Moonshot for Future Offshore Wind Turbine Installation Vessels for an Uncertain Market

MSc. Thesis

J.J. de Ridder

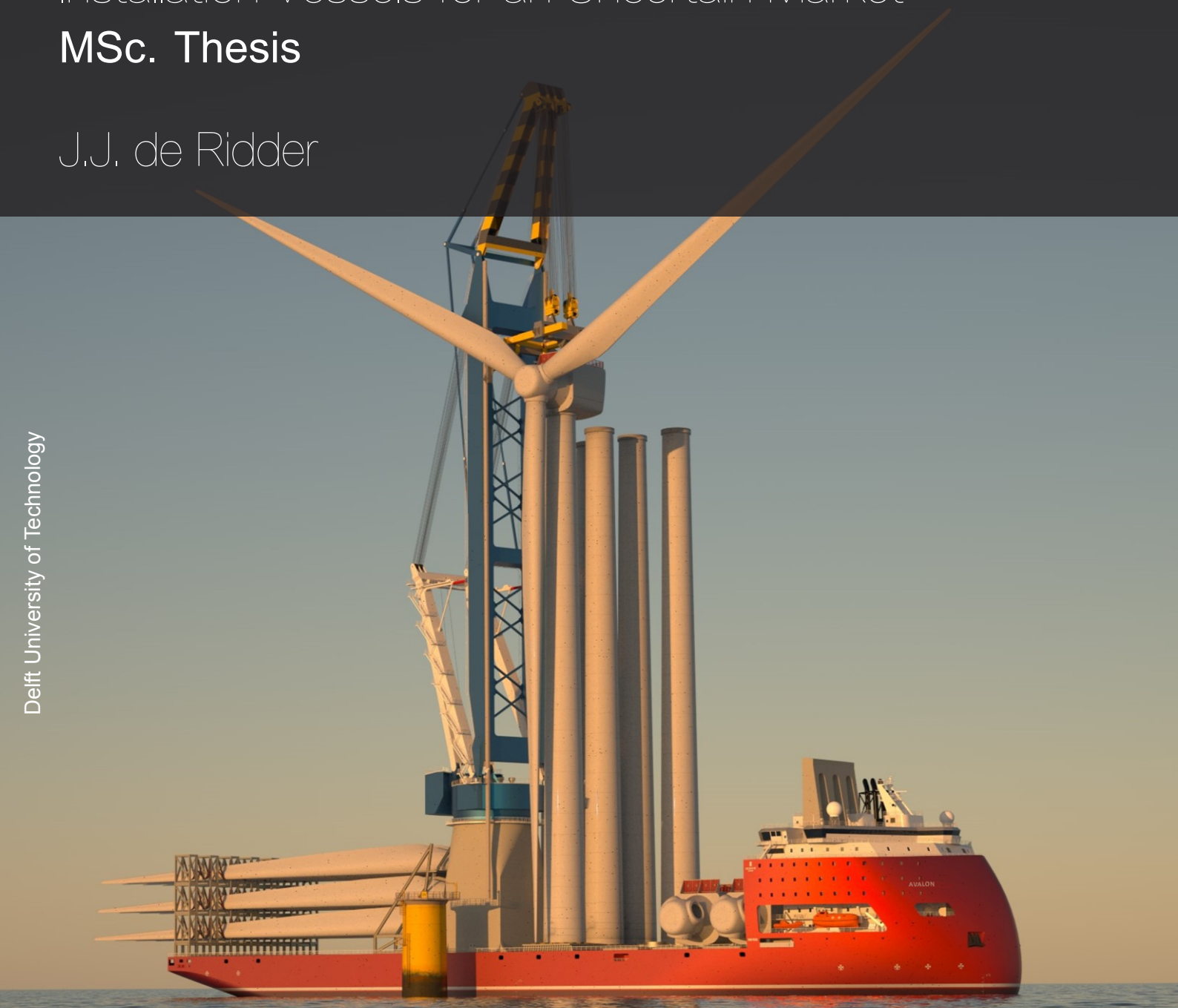

Delft University of Technology

TUDelft

ULSTEIN®

Beyond Jack-Ups

A Moonshot for Future Offshore Wind Turbine Installation Vessels for an Uncertain Market

MSc. Thesis

by

J.J. (Jesse) de Ridder

to obtain the degree of Master of Science in Marine Technology
at the Delft University of Technology,
to be defended publicly on November 8, 2023 at 14:00

Report number: **MT.23/24.004.M**
Student number: 4478851
Project duration: February 13, 2023 - November 8, 2023
Department: Maritime and Transport Technology

Supervisors: Dr. A. A. Kana, TU Delft
Ir. J. D. Stroo, Ulstein Design & Solutions B.V.

Thesis committee: Dr. A. A. Kana, TU Delft - Chair
Dr. H. C. Seyffert, TU Delft
Dr. Ir. M. B. Zaayer, TU Delft
Ir. J. D. Stroo, Ulstein Design & Solutions B.V.

An electronic version of this thesis is available at `http://repository.tudelft.nl/`

Cover image: Artist impression of *Moonshot*

TU Delft ULSTEIN®

Preface

This report marks the end of my journey as a student, and what a ride it has been. It all began with four years in Rotterdam. I then felt it was not enough, so I continued the journey in Delft, starting in 2021 with a bridging program for the Master in Marine Technology. And now, here we are.

Interestingly, this is not my first time graduating at *Ulstein Design & Solutions B.V.* (*UDSBV*); we already go way back. In 2020, I wrote my bachelor thesis at the company. After that, I stayed with them, while during my pre-master and Master, working part-time as a Naval Architect alongside my studies. I am incredibly grateful for the opportunities they provided me to develop on a professional level, besides developing academically. Initially, I had the plan to find a graduation research at another company, but *UDSBV* proposed the *Moonshot* project to me, I knew this would be the perfect topic for me. A big thank you to *UDSBV* for trusting me with the development of *Moonshot*.

This topic really appealed to me because it aligns perfectly with my passion: ship design. It was a fascinating and at the same time challenging subject. Through the process, I learned a lot about the offshore wind industry and how to design innovative solutions, while also designing for an uncertain market. This research also helped me improve my coding skills. It was great to use *Blended Design* in my research and to further develop it. Funnily enough, *Blended Design* was created by Jesper, who also graduated at *UDSBV* in 2020, during the same period I was there for my graduation.

I am very proud of my final work, but I could not have done it alone. Therefore, I would really like to thank Austin Kana for his guidance during these nine months. The progress meetings and regular feedback on my research were incredibly valuable. I had a great time with all my colleagues at *UDSBV* for which I would like to thank them. Ko, I would like to sincerely thank you for you daily supervision, support, and insights; this really took my research to a higher level.

Additionally, I would like to thank my family and friends for their unconditional support and the relaxation they provided. Last but certainly not least, I want to express my gratitude to my girlfriend, Avalon, who is my rock for over a decade now.

I hope you enjoy reading this thesis.

J.J. de Ridder
Delft, October 2023

Abstract

The offshore wind market is rapidly growing, resulting in increasing wind turbine sizes, increasing distances to port, and a shift to deeper waters. A literature study in this thesis shows that existing wind turbine installation vessels, vessels under construction, and future concepts will not be able to install next-generation turbines or that they would have installation bottlenecks, making them cost-inefficient. This goes against the goal of decreasing the Levelized Cost of Energy (LCOE) of wind energy, to ensure that offshore wind stays competitive with other energy sources, enabling the energy transition. There is thus a gap between future demand of offshore wind installation vessels and current and near-term solutions. The research proposes a new floating monohull vessel concept, called *Moonshot*, to fill this gap. *Moonshot* will thus be different than traditional jack-up or semi-submersible installation vessel options.

In this research, various design strategies were analyzed. Based on the findings, a design strategy is developed to design and analyze *Moonshot*. A combination of *Ulstein Design and Solution B.V.*'s *Controlled Innovation* process and *Blended Design* were used and extended to develop this new concept. First, the important functions and design aspects of the design were established using *Controlled Innovation*. *Blended Design* was then used to create a design space of the design configurations and to explore multiple market scenarios to establish optimal ship parameters for further development. As part of the research, the existing design process and model were modularized and new features were developed to suit wind turbines, assess seakeeping behavior, and explore the design space of the future wind turbine installation vessel.

The results of this research aim to elucidate optimal design parameters across certain market scenarios. Results show how optimizing the design for financial performance, seakeeping behavior, or a combination of the two, influences the optimal design point. With the optimal design ranges, the initial design parameters for the next stage in the design of *Moonshot* are established. Finally, *Blended Design* is used to benchmark *Moonshot* against existing wind turbine installation solutions to assess its performance. A version of *Moonshot* is developed as a direct competitor for the largest jack-up design available, the *NG-20000X*. Benchmarking with the jack-up, an SSCV, and *Huisman*'s *WIV* concept showed that *Moonshot* would be a more efficient solution, capable of installing a larger number of turbines per year at a considerably lower cost per megawatt compared to other solutions.

In summary, this research concludes *Moonshot* as an innovative concept to address the evolving challenges of offshore wind turbine installation. By combining innovative design strategies, extensive assessment, and optimization, *Moonshot* emerges as a promising contender in the quest for effective and cost-efficient installation solutions for offshore wind.

Contents

Preface ii

Abstract iv

Nomenclature ix

List of Figures xiv

List of Tables xviii

1 Introduction 2
- 1.1 Background information . . . 2
  - 1.1.1 Offshore wind energy is rapidly growing . . . 2
  - 1.1.2 Installation of offshore wind farms . . . 6
  - 1.1.3 Moonshot . . . 12
  - 1.1.4 Company introduction . . . 12
- 1.2 Problem statement . . . 12
- 1.3 Research objective . . . 12
- 1.4 Relevant research and literature . . . 13
- 1.5 Research questions . . . 13
- 1.6 Scope . . . 14
- 1.7 Scientific and societal relevance . . . 14
- 1.8 Content description . . . 14

2 State-of-art in ship design 16
- 2.1 About innovation . . . 16
- 2.2 Design strategies . . . 17
  - 2.2.1 Evaluating strategies . . . 17
- 2.3 Design strategies by Ulstein . . . 18
  - 2.3.1 Controlled Innovation . . . 18
  - 2.3.2 Blended Design . . . 20
  - 2.3.3 Evaluating UDSBV design strategies . . . 24
- 2.4 Chapter conclusion . . . 25

3 Developing Moonshot 26
- 3.1 The design process . . . 26
- 3.2 High-level objective, Functions, and Design aspects . . . 27
- 3.3 Design aspects evaluation . . . 29
- 3.4 Development packages . . . 31
  - 3.4.1 Development package 1 - Lifting equipment . . . 31
  - 3.4.2 Development package 2 - Size, mass, and CoG of components . . . 34
  - 3.4.3 Development package 3 - Deck layout . . . 39
- 3.5 Chapter conclusion . . . 47

4 Blended Design for Moonshot **48**
4.1 Solution approach . . . 48
4.2 Method for seakeeping analysis . . . 50
4.2.1 Definition of motions . . . 51
4.2.2 Response Amplitude Operators . . . 51
4.2.3 Local RAOs . . . 58
4.2.4 Acceleration RAO . . . 59
4.2.5 Wave scatter diagram . . . 59
4.2.6 Wave spectra . . . 61
4.2.7 Motion response spectra . . . 63
4.2.8 Response maxima . . . 63
4.2.9 Validation of the seakeeping analysis module (SAM) . . . 65
4.3 Wind turbine mission module . . . 67
4.3.1 Crane capacity constraint . . . 68
4.3.2 Deck area constraint . . . 68
4.3.3 Deadweight constraint . . . 69
4.3.4 Stability constraints . . . 69
4.4 Chapter conclusion . . . 70

5 Evaluating the performance of Moonshot **72**
5.1 Results and findings . . . 72
5.2 Financial performance . . . 73
5.2.1 Market scenarios . . . 73
5.2.2 Financial performance in different market scenarios . . . 75
5.2.3 Influence of distance to port . . . 77
5.2.4 Splitting the turbine towers . . . 79
5.3 Seakeeping performance . . . 81
5.3.1 Local displacements while weathervaning . . . 81
5.3.2 Local accelerations while weathervaning . . . 84
5.4 Seakeeping performance meets financial performance . . . 85
5.5 Optimal design ranges for Moonshot . . . 87
5.6 Chapter conclusion . . . 88

6 Benchmarking the design **90**
6.1 Strategy for benchmarking . . . 90
6.2 Optimal financial performance . . . 91
6.3 Optimal seakeeping performance . . . 92
6.4 Optimal design parameters for the 20 MW *Moonshot* . . . 93
6.5 Comparing *Moonshot* with other solutions . . . 93
6.6 Visualization of *Moonshot* . . . 96
6.7 Chapter conclusion . . . 96

7 Conclusion **98**

8 Discussion **102**

References **104**

A Offshore wind **118**
A.1 Wind energy . . . 118
A.2 Offshore wind farms . . . 119
A.2.1 Electrical energy generation . . . 119

A.2.2 Electrical energy transportation . . . 120
A.3 Life cycle . . . 121
A.4 Economics of offshore wind farms . . . 122
A.4.1 Levelized cost of energy . . . 122
A.4.2 Decreasing the LCOE . . . 123

B Wind turbine installation solutions 126
B.1 Existing solutions . . . 126
B.1.1 Jack-up vessels . . . 126
B.1.2 Floating vessels . . . 128
B.2 Gap between offshore wind market and current installation fleet . . . 131
B.2.1 Ordering new vessels . . . 132
B.2.2 Upgrading existing vessels . . . 133
B.2.3 Designing new concepts . . . 134

C Design strategies 138
C.1 Point-based design . . . 138
C.2 Set-based design . . . 139
C.3 Systems engineering . . . 140
C.4 Systems-based design . . . 141
C.5 Optimization-based design . . . 142

D Offshore wind turbines 144

E Alternative non-feasible deck layouts 146

F Validation of CFEs and SAM 150

G Validation of WTG module 151

H Wind turbine installation cycles 152

I Estimation of installation contract rates 153

J RAO calculation with simplified formulas for Froude-Krylov force 154

K Additional results 160
K.1 Significant wave height limit of 1.5m . . . 160
K.2 Significant wave height limit of 3.5m . . . 162

L Small analysis on environmental performance 164

M Artist impressions of Moonshot 168

Nomenclature

Abbreviations

Abbreviation	Definition
APS	Announced Pledges Scenario
BEM	Boundary Element Method
CAPEX	Capital Expenditure
CDF	Cumulative distribution function
CFE	Closed-form expression
CI	Controlled Innovation
CO_2	Carbon dioxide
CoG	Center of Gravity
CTV	Crew Transfer Vessel
DNV	Det Norske Veritas
DWT	Deadweight
DP	Dynamic Positioning
EEXI	Energy Efficiency eXisting ships Index
EPCI	Engineering, Procurement, Construction and Installation
FIV	Foundation Installation Vessel
GHG	Greenhouse Gases
GW	Gigawatt
HAWT	Horizontal-axis Wind Turbine
HAS	Hydrodynamic analysis software
HTV	Heavy Transport Vessel
IEA	International Energy Agency
JONSWAP	Joint North Sea Wave Project
LCOE	Levelized cost of energy
LSW	Lightship weight
MDO	Marine Diesel Oil
MPE	Most Probable Extreme
MPM	Most Probable Maximum
MW	Megawatt
NM	Nautical Miles
NWEA	The Netherlands Wind Energy Association
OPEX	Operational Expenditure
OWF	Offshore Wind Farm
O&M	Operations and Maintenance
PDF	Probability density function
POB	People on board
PS	Port side
PWT	Parallelogram Wind Turbine
RAO	Response Amplitude Operators
RNA	Rotor Nacelle Assembly

Abbreviation	Definition
ROI	Return on Investment
SAM	Seakeeping analysis module of *Blended Design*
SB	Starboard
SOV	Service Operation Vessels
SSCV	Semi-submersible Crane Vessels
SWATH	Small Waterplane Area Twin Hull
T&I	Transportation and Installation
UDSBV	Ulstein Design & Solutions B.V.
US	United States
VOYEX	Voyage Expenses
WIV	Windfarm Installation Vessel by *Huisman*
WTG	Wind Turbine Generator
WTIV	Wind Turbine Installation Vessel
WTS	Wind Turbine Shuttle by *Huisman*

Symbols

Symbol	Definition	Unit
a	Acceleration	[m/s²]
a_i	Coefficients estimated on actual data	[-]
b_i	Coefficients estimated on actual data	[-]
A_{wl}	Waterplane area	[m²]
A_γ	Normalizing factor	[-]
B_0	Breadth	[m]
B_0	Ship breadth for RAO calculation	[m]
B_{blade}	Blade breadth	[m]
$B_{nacelle}$	Nacelle breadth	[m]
C_{ii}	Restoring spring term	[N/m or Nm]
C_b	Block coefficient	[-]
C_{wp}	Waterplane coefficient	[-]
C_m	Midship coefficient	[-]
DWT	Deadweight	[t]
D_{hub}	Hub diameter	[m]
D_{rotor}	Rotor diameter	[m]
D_t	Decommissioning cost in year t	[EUR]
D_{tower}	Tower base diameter	[m]
E_t	Energy generation in year t	[MWh]
$F_{ex,i}$	Wave excitation force or moment	[N or Nm]
$F_{d,i}$	Diffraction force or moment	[N or Nm]
$F_{w,i}$	Undisturbed wave/Froude-Krylov force or moment	[N or Nm]
f_{H_s}	Cumulative probability function	[-]
F_t	Fuel expenditure in year t	[EUR]
$f_{T_z\|H_s}$	Joint probability distribution	[-]
g	Gravitational constant (=9.81)	[m/s^2]
$\overline{GM_L}$	Longitudinal metacentric height	[m]
$\overline{GM_T}$	Transverse metacentric height	[m]
H_{hub}	Hub height	[t]
$H_{nacelle}$	Nacelle height	[m]
H_s	Significant wave height	[m]
I_t	Investment expenditure in year t	[EUR]
k	Effective wave number	[1/m]
$\overline{KG}$	Distance from keel to center of gravity	[m]
$\overline{KM}$	Distance from keel to metacenter	[m]
L	Length	[m]
L_{blade}	Blade length	[m]
L_{deck}	Deck length	[m]
L_{hub}	Hub length	[m]
$L_{nacelle}$	Nacelle length	[m]
L_{tower}	Tower length	[m]
LCF	Longitudinal center of floatation	[m]
LCG	Longitudinal center of gravity	[m]
LSW	Lightship weight	[t]
M_{blade}	Blade mass	[t]

Symbol	Definition	Unit
M_{hub}	Mass of hub	[t]
$M_{nacelle}$	Nacelle mass	[t]
M_t	O&M expenditure in year t	[EUR]
M_{tower}	Tower mass	[t]
m_{WTG}	Total mass of turbine	[t]
N	Number of zero-up-crossing wave period	[-]
N	Number of turbines	[-]
n	Lifetime of structure	[-]
n	Number of zero-up-crossing wave periods	[-]
N_A	Number of turbines according to deck area	[-]
N_{CC}	Number of turbines according to crane capacity	[-]
N_{DWT}	Number of turbines according to deadweight	[-]
$N_{tot,lift}$	Number of turbines according to lifting stability	[-]
$N_{tot,tr}$	Number of turbines according to transit stability	[-]
P	Available power in wind	[W]
P_{rated}	Rated power of turbine	[MW]
r	Discount rate	[-]
S_J	JONSWAP wave spectrum	[m^2s]
S_{PM}	Pierson-Moskowitz wave spectrum	[m^2s]
S_{ζ_i}	Motion response spectrum	[m^2s or rad^2s]
S_ζ	Wave spectrum	[m^2s]
$t_{'name'}$	Duration of 'name'	[h]
T	Time period	[s]
T	Draft	[m]
T_n	Natural period	[s]
$T_{n,roll}$	Natural roll period	[s]
T_p	Peak period	[s]
T_z	Zero-up-crossing wave period	[s]
U_w	Wind speed	[m/s]
V_s	Sailing speed	[kn or m/s]
VCG	Vertical center of gravity	[m]
x_p	Longitudinal local motion in point P	[m]
y_p	Transverse local motion in point P	[m]
z_p	Vertical local motion in point P	[m]
α	Risk factor	[-]
α_{Hs}	Scale parameter in Weibull distribution	[-]
β	Wave heading angle	[rad]
β_{Hs}	Shape parameter in Weibull distribution	[-]
γ	Peak enhancement factor	[-]
γ_{Hs}	Location parameter in Weibull distribution	[-]
δ	Shape parameter in Weibull distribution	[-]
ϵ	Phase angles	[rad]
ϵ	Spectral width parameter	[-]
ζ_a	Wave elevation amplitude	[m]
ζ_{a_i}	Motion amplitude	[m or rad]
λ	Wavelength	[m]
μ	Function of significant wave height	[-]

Symbol	Definition	Unit
ρ	Density of water	[kg/m^3]
ρ_a	Density of air	[kg/m^3]
σ	Function of significant wave height	[-]
σ	Spectral width parameter	[-]
σ	Standard deviation of spectrum	[m or rad]
ω	Wave frequency	[rad/s]
ω_e	Encounter frequency	[rad/s]
ω_p	Angular spectral peak frequency	[rad/s]
∇	Hull volume	[m^3]

List of Figures

1.1 Global evolution of wind turbine capacity, based on author's analysis of *4C Offshore* data (February 24, 2023). . . . 3
1.2 Offshore wind turbine size comparison, from [15]. . . . 4
1.3 Global average distance to shore by year, from [21]. . . . 5
1.4 Marshalling ports in the logistic process, from [22]. . . . 5
1.5 Global evolution of water depth, based on author's analysis of *4C Offshore* data (February 24, 2023). . . . 6
1.6 General overview of the ships involved in the installation of an OWF with monopile foundations. . . . 7
1.7 Overview of common methods for offshore wind turbine installation, based on [28], [29], [30]. . . . 7
1.8 Visualization of the RNA installation method, from [37]. . . . 9
1.9 The structure of this research. . . . 15

2.1 Classification of innovation, from [57]. . . . 16
2.2 Venn diagram showing the position of *UDSBV* design strategies. . . . 18
2.3 Model of cohesion in a system-of-systems, from [52]. . . . 19
2.4 Design strategy, based on the interaction between system and ship design, from [52]. . . . 19
2.5 *UDSBV*'s *Controlled Innovation* Process. . . . 20
2.6 Schematic of *Blended Design* method and its place in the design process, from [49]. . . . 21
2.7 Forecast of market trend using extrapolation from data scatter, from [49]. . . . 22
2.8 Visualization of transforming forecasting trend lines into probability functions, from 2020 [49]. . . . 22
2.9 Visualisation of the coupling between market and ship model, from [62]. . . . 23
2.10 ROI results of three different future market projections, from [49]. . . . 24

3.1 Schematic of the design strategy for this research. . . . 26
3.2 Overview of the defined high-level objective, functions, and design aspects for the design of *Moonshot*. . . . 27
3.3 Visualization of the identified lifting mechanisms: Free-hanging lift (left) and guided lift (right). . . . 32
3.4 Artist impressions of mast crane (left) and tub mounted crane (right), from *Huisman*. . . . 32
3.5 An impression of the *Zephyr* crane concept, received from *Huisman*. . . . 34
3.6 Example scaling laws for (a) rated power and (b) blade mass. . . . 37
3.7 Scaling laws for nacelle mass 38
3.8 Visualization of assumed CoG locations. . . . 39
3.9 Picture of the blade rack on *Aeolus, from [79]*. . . . 40
3.10 Deck layout 1 showing the positioning of components, crane, assembly location, and installation position. . . . 42

3.11 Deck layout 2 showing the positioning of components, crane, assembly location, and installation position. . . . 43
3.12 Deck layout 3A showing the positioning of components, crane, assembly location, and installation position. . . . 44
3.13 Deck layout 3B showing the positioning of components, crane, assembly location, and installation position. . . . 45
3.14 Visualization of weathervaning. . . . 46

4.1 Integration of functions for *Moonshot* in *Blended Design*. . . . 48
4.2 The proposed approach for determining seakeeping behavior with *Blended Design*. . . . 50
4.3 Definition of ship motions in six degrees of freedom, from [84]. . . . 51
4.4 Comparison of different seakeeping analysis methods on accuracy and calculation time. . . . 52
4.5 Simplified ship model used in roll motion analysis, from [88]. . . . 53
4.6 Heave, roll, and pitch RAOs of HX104 as function of wave frequency for different headings. . . . 55
4.7 Schematic of the location of point P for local motions. . . . 59
4.8 Nautical zones for estimation of the wave distribution parameters, from [82]. . . . 60
4.9 Wave scatter diagram calculated for zone 11. . . . 61
4.10 From wave signal to wave spectrum, from [93]. . . . 62
4.11 Rayleigh PDF and CDF (ϵ=0) of responses for m_0=8.02$\cdot 10^{-4}$. . . . 64
4.12 Rayleigh PDF and CDF ($\epsilon = 0$) for $m_0 = 8.02 \cdot 10^{-4}$ and n=2,207 waves (T_p =5.5s). 65
4.13 Wave headings in an omnidirectional environment. . . . 66
4.14 Wave headings in a weathervaning environment with +- 30 degrees offset. . . . 66
4.15 Division of deck area. . . . 68

5.1 Visual guide on how to interpret the result plots. . . . 73
5.2 Visualization of the unbound market. . . . 74
5.3 Visualization of the 16 MW bound market. . . . 74
5.4 Visualization of the 22 MW and 1,000 feet bound market. . . . 74
5.5 Visualization of the results for the four market scenarios. . . . 75
5.6 Multivariate visualization of the results for a 1,000ft bound market. . . . 76
5.7 Parallel coordinates plot of the financial performance in a 1,000ft bound market. 77
5.8 Visualization of the results of a 1,000ft bound market with three distances to port. 78
5.9 Distribution of limiting factors for feasible ship configurations. . . . 79
5.10 Distribution of limiting factors for feasible ship configurations, grouped per turbine size. . . . 79
5.11 Distribution of limiting factors for feasible ship configurations with towers carried in two parts. . . . 80
5.12 Distribution of limiting factors for feasible ship configurations with towers carried in two parts, grouped per turbine size. . . . 80
5.13 Visualization of limiting factors and number of turbines for the two tower strategies. 80
5.14 Visualization of the results for two different tower transportation strategies in a 1,000ft bound market. The distance to port is 140 NM. . . . 81
5.15 Visualization of the MPE displacements during weathervaning. . . . 82
5.16 Visualization of the MPE displacements during weathervaning. . . . 83
5.17 Parallel coordinates plot of motion performance. . . . 84
5.18 Visualization of the MPE acceleration vector results. . . . 85

5.19 Visualization of the financial results with motion performance penalty in a 1,000ft bound market with an operational H_s limit of 2.5 meters. 86
5.20 Parallel coordinates plot of the financial performance at a motion compensation cost of €10,000/(t·m). 87

6.1 Render of an *NG-20000X* jack-up, currently under construction for *Havfram*. From [104]. 90
6.2 Visualization of the financial performance results for the 20 MW *Moonshot*. . . 91
6.3 Visualization of the seakeeping performance results for the 20 MW *Moonshot* with fixed displacement. 93
6.4 Artist impression of the 20 MW *Moonshot* 96

A.1 Global electricity generation by source, from [107]. 118
A.2 Anatomy of an offshore wind turbine, from [3]. 120
A.3 Schematic of typical offshore wind farm, showing the energy transportation to shore, from [6]. 121
A.4 Life cycle of an offshore wind farm, adapted from [6] and [28]. 121
A.5 *IEA* 2020 LCOE comparison by technology (left) and median LCOE comparison by region for different technologies (right), adapted from [8]. 123
A.6 Capital cost breakdown for bottom-fixed (left) and floating (right) offshore wind farms, from [10]. 124

B.1 Timeline showing the T&I process for a jack-up vessel. The timeline is not to scale. 127
B.2 Main crane capacity and maximum speed of jack-up fleet, own analysis of *4C Offshore* fleet data. 127
B.3 Visualization of relevant findings of the current jack-up fleet, own analysis of *4C Offshore* fleet data. 128
B.4 *Saipem 7000* [44] (left) and *Thialf* [132] (right) installing wind turbines. 129
B.5 Timeline showing the T&I process for an SSCV. The timeline is not to scale. . . 129
B.6 Sheerleg crane *Rambiz* lifting a 5 MW turbine, from [134]. 130
B.7 Timeline showing the T&I process for a sheerleg. The timeline is not to scale. . 130
B.8 *Aegir* installing a wind turbine, from [138]. 130
B.9 Timelines showing the T&I process for *Aegir* (top) and a floating monohull using installation method 2 (bottom). The timelines are not to scale. 131
B.10 Scatter plot displaying the lifting height of jack-up vessels and the required lifting height for various wind turbine sizes, own analysis of *4C Offshore* fleet data. . 132
B.11 Selection of new concepts, showing *Windlifter* (top left) [156], *WTS* (middle) [157], *WIV* (top right) [158], *PWT* (bottom left) [48] and *Feederdock* (bottom right) [159]. 134
B.12 Visualization of the assembly process with the assembly tower, snapshots from [163]. 135

C.1 Traditional design spiral from 1959, from [168]. 138
C.2 Relationship between freedom, knowledge, and uncertainty in design during design process, from [170]. 138
C.3 Set-based design approach, from [172]. 139
C.4 Systems Engineering life cycle model, from [175]. 140
C.5 Concept development phases of system life cycle, from [175]. 140
C.6 The system-based design process, from [179]. 141

J.1 Froude-Krylov forces for all six degrees of freedom of HX104 as function of wave frequency for different wave heading angles. 155
J.2 RAOs for all motions, excluding roll, of HX104 as function of wave frequency for different headings. 158

K.1 Visualization of the MPE displacements while weathervaning with a maximum H_s of 1.5 meters. 160
K.2 Visualization of the financial results while weathervaning with a maximum H_s requirement of 1.5 meters. 161
K.3 Visualization of the MPE displacements while weathervaning with a maximum H_s of 3.5 meters. 162
K.4 Visualization of the financial results while weathervaning with a maximum H_s requirement of 3.5 meters. 162

L.1 Visualization of the environmental performance results for the 20 MW *Moonshot* with a fixed displacement. 165
L.2 Visualization of the environmental performance results for sailing speed. 166

List of Tables

1.1 Size and mass comparison of 10, 15, and 20 MW wind turbines. 4
1.2 Overview of the considered vessels and concepts. 11
1.3 Overview of relevant research and literature. 13

2.1 Evaluation of the main design strategies. 17
2.2 Evaluation of *UDSBV* design strategies. 25

3.1 Evaluation of the design aspects. 30
3.2 Assessment of the different lift mechanisms. 33
3.3 Spearman's rank correlation coefficients for all turbine data. 36
3.4 Spearman's rank correlation coefficients for direct and semi-direct driven turbines 36
3.5 Scaling laws for each parameter based on a heuristic engineering approach and best power fit, based on the database with 23 offshore wind turbine models. 37
3.6 Overview of assumed CoG locations. 39
3.7 Evaluation of deck layout 1. 42
3.8 Evaluation of deck layout 2. 43
3.9 Evaluation of deck layout 3A. 44
3.10 Evaluation of deck layout 3B. 45
3.11 Results of motion analysis for all deck layouts. 46
3.12 Evaluation of all deck layouts. 47

4.1 Comparison of the areas under RAO curves for results from HAS and CFEs. . 56
4.2 Comparison of the standard deviation (σ) of the response spectra at $T_p = 7s$, calculated using the RAOs from HAS and CFEs. 57
4.3 Validation of weathervaning MPE motion-induced displacements from the sea-keeping analysis module (SAM) with hydrodynamic analysis software (HAS). . 66
4.4 Validation of omnidirectional MPE motion-induced displacements from the sea-keeping analysis module (SAM) with hydrodynamic analysis software (HAS). . 67

5.1 Input for *Blended Design* to create the design space. 72
5.2 Summary of optimal design ranges for *Moonshot*. 87

6.1 Input for *Blended Design* to create the design space for benchmarking. 91
6.2 Summary of optimal design ranges for the 20 MW *Moonshot*. 93
6.3 Comparison of different installation solutions to benchmark *Moonshot*. 95

D.1 Offshore wind turbine database 145

(This page intentionally left blank)

1 Introduction

In this chapter, relevant background information and the problem statement will be presented, along with the objective and main research question and sub-questions. Additionally, a review of available literature and relevant research on the problem solution will be conducted. The research scope and relevance of the study will be established. Finally, the structure of the report and a description of the content will be given.

1.1. Background information

The following sections provide background information for this research. The background information is a product of literature and market research. More information regarding offshore wind and installation vessels can be found in Appendix A and B.

1.1.1. Offshore wind energy is rapidly growing

Today's society faces growing concerns over climate change, which is primarily caused by the release of greenhouse gases (GHG) and other hazardous emissions. These gases trap heat and warm the planet, leading to rising temperatures, changing weather patterns, and a range of other impacts, including sea level rise, and damage to ecosystems. A large part of global emissions comes from generating electricity and heat by burning fossil fuels [1]. In order to mitigate, or at least reduce the impacts of climate change, it is essential to reduce our reliance on fossil fuels and transition to cleaner, renewable energy sources. One of those sources is wind [2].

The kinetic energy from the wind can be captured and converted into usable electrical energy by wind turbines, typically horizontal-axis wind turbines (HAWTs) [3]. The offshore environmental offers favorable wind conditions because there are no psychical obstructions to block the wind flow, and wind conditions are more consistent than on land. Moreover, offshore wind turbines can be built much larger than onshore wind turbines, resulting in higher power outputs [4]. Offshore wind energy is harvested by means of offshore wind farms (OWFs), which are made up of dozens or even hundreds of turbines [5]. An OWF can be defined as a power plant that contains all the required facilities to capture the kinetic energy from wind, transform it to electric energy, and supply it to the main electricity network on the mainland [6].

An important metric in the energy generation space is the Levelized cost of energy (LCOE). The LCOE is a measure of the average net present cost of energy generation over its assumed lifetime, allowing for the comparison of different power-generating technologies with unequal

life span, risk, return, and capacity [7]. To make offshore wind a competitively priced renewable energy source in comparison to other sources, there is a strong focus on reducing the LCOE [8]. One way to lower the LCOE is to reduce investment expenditures. Cost reduction can be achieved through economies of scale, which often leads to the design and construction of larger turbines [9]. A portion of investment expenditures is also related to the assembly and installation of the wind turbines at sea [10].

The offshore wind energy industry rapidly growing. The global offshore wind market has experienced significant growth in recent years, with total installed capacity increasing from zero in the 1990s to over 40 gigawatts (GW) in 2020. This growth is expected to continue towards 630 GW in 2050 [11]. Due to the improvements in offshore wind energy, growing demand, and the aim to reduce the LCOE, the landscape of the offshore wind market is also evolving. An analysis of *4C Offshore Wind Farm Database* has been performed, revealing three trends: (1) increasing capacity of wind turbines, (2) increasing distances from shore to OWFs, and (3) increasing water depths at OWF locations [12].

Increasing size of wind turbines

Figure 1.1 presents the global evolution of offshore wind turbine capacity from 1990 to 2040. The data, from the *Offshore Wind Farm Database* from *4C Offshore* (February 24, 2023), reveals a clear trend of increasing wind turbine capacity over the years, driven by technological improvements and the aim to reduce the LCOE. In 2010, the weighted average size was only 3.6 MW. However, in 2020, this had already increased to 6.0 MW. Projections suggest that the average turbine capacity will increase to 10.8 MW in 2050, and over 15 MW in 2030. Concepts for OWFs with turbine capacities of more than 20 MW have already been established [13]. It should be noted that a large portion of the displayed data beyond 2030 consists of concepts for OWFs. At this moment, the largest available offshore wind turbine is the *Vestas* V236-15.0MW with a power rating of 15 MW [14]. However, it is uncertain what the exact (technological) boundary for future wind turbines would be [13].

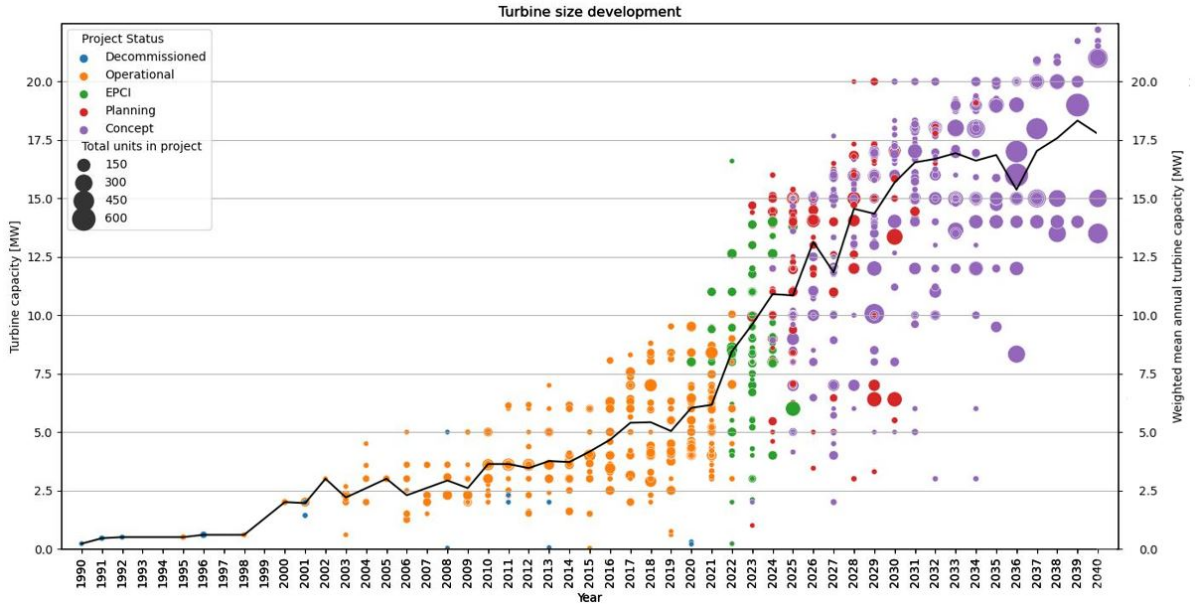

Figure 1.1: Global evolution of wind turbine capacity, based on author's analysis of *4C Offshore* data (February 24, 2023).

As turbines grow in capacity, their physical size also increases. This is displayed in Figure

1.2. The increase in size and mass of the wind turbine and its components poses new challenges in terms of installation. To install the future wind turbines, vessels with greater lifting capacity, higher lifting heights, and increased carrying capacity are needed.

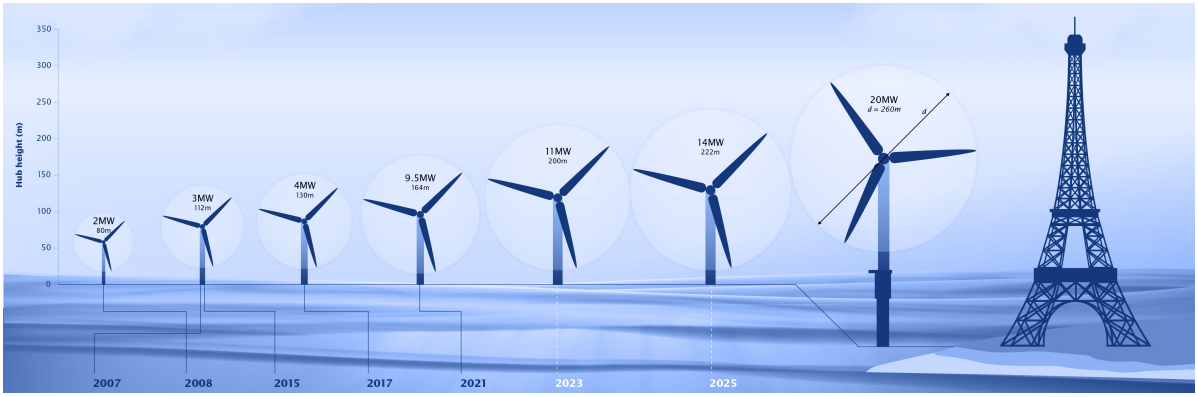

Figure 1.2: Offshore wind turbine size comparison, from [15].

Table 1.1 shows a comparison of component sizes and mass for wind turbines of different capacities.

Table 1.1: Size and mass comparison of 10, 15, and 20 MW wind turbines.

Parameter		DTU 10-MW	IEA Wind 15-MW	20 MW concept
Capacity	[MW]	10	15	20
Rotor diameter	[m]	178.3	240	276
Hub height	[m]	119	150	160.2
Blade mass	[t]	41	65	77.7
Nacelle mass	[t]	446	631	945
Rotor nacelle assembly	[t]	675	1,017	1,431
Tower mass	[t]	987	860/1,528*	2,070
Tower base diameter	[m]	8	10	12
Reference		[16], [17]	[16]	[18]

*1,528t is the result of linear interpolation 10 and 20 MW.

Increasing distance from shore

Along with the trend of larger turbines, another significant development is the increasing distance between OWFs and the nearest marshalling port [19]. This shift is driven by the limited availability of near-shore locations. Especially in the North Sea near-coast locations are getting scarce [20]. Also, farther from the shore, the wind speeds are higher and thus more favorable, making these locations more attractive [6]. Figure 1.3 shows the global average distance from OWFs to shore by year. From 2011 to 2023, the average distance from OWF to shore is more than doubled. What also stands out, is that the extremities have become much higher. In Europe and the United states, there is a trend to build OWFs in far-offshore locations. Until 2030, the trend of moving towards the far-offshore will be offset by the development of near-shore projects in Japan, Taiwan, and Vietnam [21].

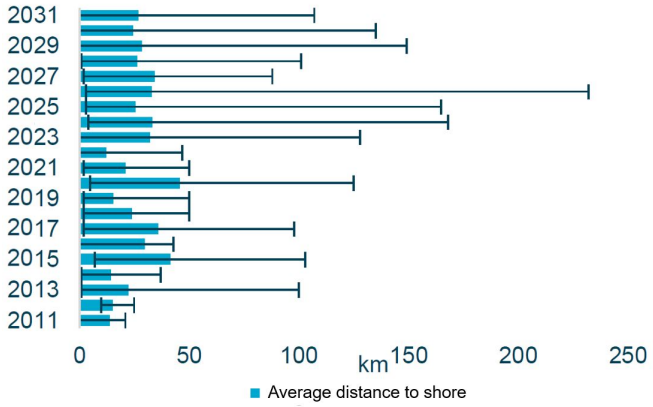

Figure 1.3: Global average distance to shore by year, from [21].

Generally speaking, the far-offshore environment is harsher. This has to be taken into account during installation. Wind turbine installation vessels (WTIVs) must be capable of withstanding such conditions. This all imposes challenges during the design and operation of such a vessel.

When developing an OWF, it is important to consider not only the distance from shore but also the distance from marshalling port to the OWF location. Offshore wind projects involve large-scale components, such as foundations and turbine parts. These are normally transported from manufacturing facilities to an intermediate facility. The intermediate facilities are called marshalling, or staging ports, and serve as locations where the components are brought together, stored, and prepared for transportation to the OWF [22]. Figure 1.4 provides a schematic representation of this logistic process. Preferably, marshalling ports are located near the OWF site, are very large, and have unlimited air draft. However, the number of marshalling ports is limited, especially in the US [23]. Consequently, the actual distance from the marshalling port to the OWF site can be much larger than the distance from shore to the farm. Unfortunately, there is no information available on the evolution of distance from marshalling ports to OWFs.

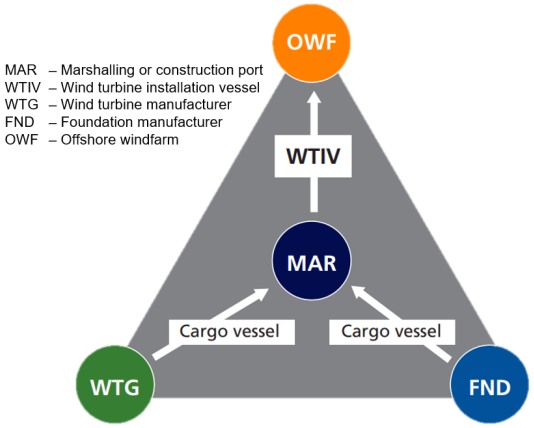

Figure 1.4: Marshalling ports in the logistic process, from [22].

With OWFs being constructed farther from the shore, wind turbine installation vessels must sail greater distances to the construction sites, increasing the sailing time. Consequently, it can be beneficial to have a vessel with larger cargo capacity or use a feeder system [24]. The latter has advantages and disadvantages, which will be discussed later in this report.

Increasing water depths

Due to the trend of building OWFs farther from shore, water depths at OWF locations also tend to increase. Typically, the farther from shore, the deeper the waters [9]. Figure 1.5 provides the evolution of water depth over the years. Before 2010, the average water depth at OWF locations was not more than 20 meters. Nowadays, the average water depth is increased to almost 40 meters. This number is expected to increase in the future. Additionally, there is even a concept for an offshore wind project in 2032 with a water depth as deep as 1,000 meters. For projects in the far-future, the exact water depths are yet unknown, making it challenging to determine the weighted average water depth of projects beyond 2035.

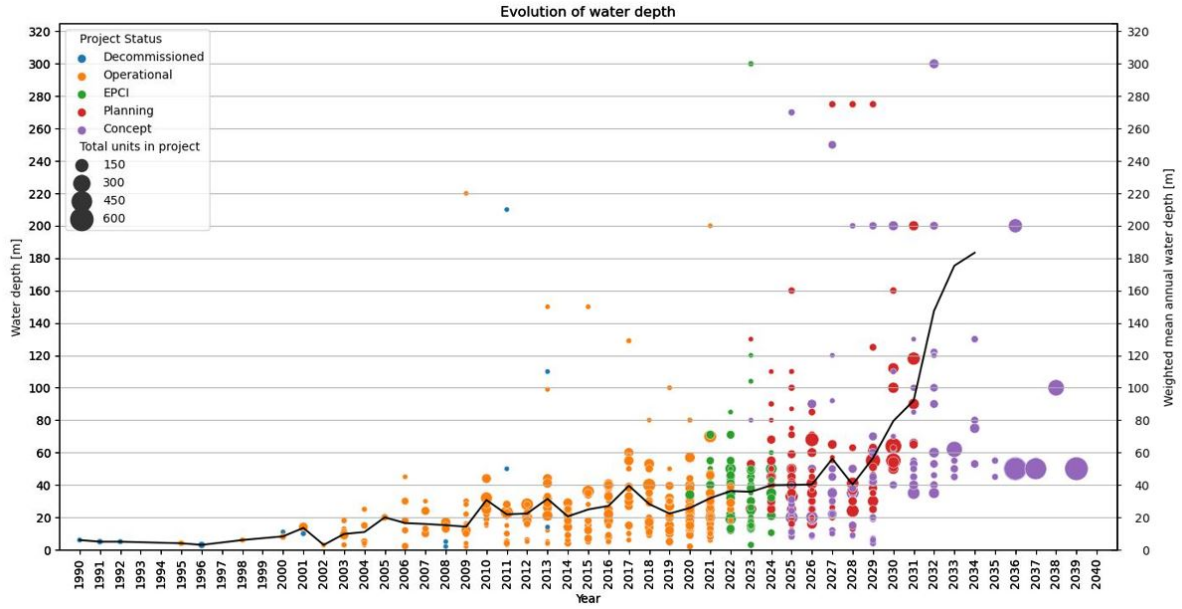

Figure 1.5: Global evolution of water depth, based on author's analysis of *4C Offshore* data (February 24, 2023). (Not showing 1000m and 700m (2032), 723m (2033), 750m (2034) and 600m (2035)).

Larger water depths do not necessarily impact the design of wind turbines. The increased water depths primarily impact the choice of foundation type for the wind turbines and the wind turbine installation vessels. For water depths exceeding 60 meters, the use of floating foundations becomes technologically and economically more attractive [6]. In the context of this research, which will focus on the installation of wind turbines, the specific foundation type may not be the primary concern. However, water depths do have an impact on the selection and design of the vessels used for the installation of the offshore wind turbines

1.1.2. Installation of offshore wind farms

The construction of an OWF consists of various stages, including foundation installation, wind turbine installation, cable-laying, subsea rock installation for scour protection, and substation installation [25]. A visualization of the ships involved in the construction process of an OWF with monopile foundations is displayed in Figure 1.6.

Figure 1.6: General overview of the ships involved in the installation of an OWF with monopile foundations.

Nowadays, wind turbine and foundation transportation and installation (T&I) is typically carried out by the same vessels. However, due to the increasing weight and size of foundations, which are growing faster than turbines, foundation installation work is shifting towards purpose-built foundation installation vessels (FIVs) [26]. As a result, wind turbine installation is expected to be handled in the future by dedicated WTIVs, which would have different design requirements than FIVs. This research concentrates on the process of wind turbine installation, so all other elements of OWF installation will not be taken into account. The offshore wind turbine installation cycle typically consists of loading at a marshalling port, transportation to the offshore construction site, turbine installation, and returning to the marshalling port to repeat the cycle [27], [24]. Below, different strategies for wind turbine installation and transportation will be discussed.

Wind turbine installation methods

Regarding offshore wind turbine installation with vessels, seven methods have been identified. Figure 1.7 provides an overview of the different installation methods. The methods differ in terms of the number of onshore preassembled components and, consequently, the number of required offshore lifts.

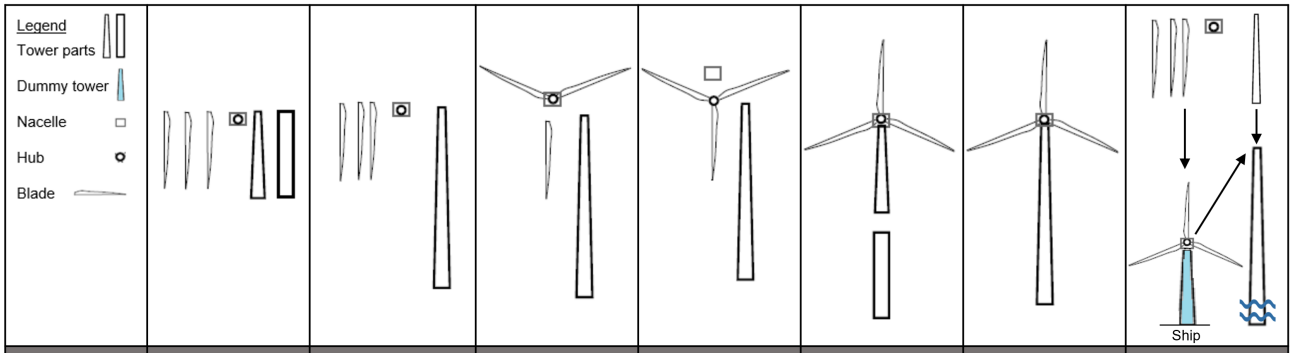

Method	1	2	3	4	5	6	7
Name	Single-blade	Single-blade with preassembled tower	Bunny ears	Star assembly	Fully preassembled with split tower	Fully preassembled	RNA method
Number of offshore lifts	6	5	3 or 4	3 or 4	2	1	**6**
Of which overboard	6	5	3 or 4	3 or 4	2	1	**2**

Figure 1.7: Overview of common methods for offshore wind turbine installation, based on [28], [29], [30].

1. **Single-blade** - This method involves no preassembly of components, and all components are assembled offshore. The tower pieces are installed first. Then, the nacelle

with hub is lifted onto the tower, followed by installation of each blade. This methods requires six lifts. Since the blades are lifted one by one, the lifts are more susceptible to delays due to high winds. Because the components are not preassembled, they can be transported more easily [31]. For example, the blades can be stacked in a rack, enabling the transportation of more turbine components on the same deck area and reducing the number of round-trips. However, there are some disadvantages to this method, such as potentally long installation times and a higher likelihood of difficulties or vulnerabilities when aligning components due to the higher number of lifts [32];

2. **Single-blade with preassembled tower** - This method is similar to the first method but with the tower preassembled onshore. This reduces the number of lifts to five. Most OWFs are installed using this method [25];
3. **Bunny ears** - In this method, two of the three blades are pre-fitted on the hub and nacelle onshore. The third blade will be added offshore. The tower can consist of two pieces or may be preassembled onshore. Therefore, the number of offshore lifts is either three or four. This approach is efficient in terms of offshore lifting but inefficient in terms of deck space usage [33]. This is because the bunny ear assemblies cannot be stacked and have an awkward shape because of the V-shape of the blades;
4. **Star assembly** - In the star assembly method, the hub and three blades are assembled onshore. This assembly is lifted onto an installation vessel together with the nacelle and either the full tower or two tower parts. At the offshore location, the turbine is then installed in three or four lifts, depending on the tower. A drawback of this method is the size of the rotor assembly, which is substantial, especially for future turbines. It takes up a lot of deck space on the vessel [25]. To address this, it is possible to stack multiple rotors, which requires a special structure on the deck for load handling and to prevent damage to the rotors. This has been done, for instance, in *Iberdrola's Wikinger* OWF in 2017. In this project, three rotor assemblies were stacked on the WTIV. However, it should be noted that the capacity of this turbines was 5 MW. The current and future turbines are much bigger and subsequently the rotor is heavier and the diameter larger [34];
5. **Fully preassembled with split tower** - In this method, the rotor nacelle assembly (RNA) is preassembled onshore and placed on top of one of the two tower pieces [29]. At sea, the lower tower piece is lifted onto the foundation, and the upper tower with RNA is lifted on top of it. In this way only two offshore overboard lifts are needed. In comparison to fully preassembled, the lower lifting capacities and heights are sufficient for this method;
6. **Fully preassembled** - The entire wind turbine is assembled onshore and lifted onto the installation vessel. At the wind farm location, the turbine is lifted onto the foundation. This method requires a vessel with high lift capacity and substantial lifting height [31]. An advantage of this method is that only one overboard lift is needed and that there is no difficulty in handling and assembling rotor components. However, vulnerability of the rotor to damage during installation is a drawback of this method [32]. In addition, this method results in heavier and more complex transport, subject to more restrictive weather limitations [35]. Especially for next-generation turbines, that would be very tall, this would be a challenge;
7. **RNA method** - The RNA method is a relatively new installation method, which was developed in a joint cooperation of *Heerema Marine Contractors*, *MHI Vestas*, and *Parkwind*. This method does not involve onshore preassembly. The wind turbine parts are transported separately. However, the number of offshore overboard lifts is only two, but the number of offshore overboard lifts is only two, due to the so-called dummy tower on the vessel's deck. This dummy tower serves as a safe platform for assembling the nacelle

and blades on board of the vessel. The installation process is as following: The turbine tower is lifted onto the foundation, while simultaneously, with another crane, the nacelle is lifted onto the dummy tower, and the blades are attached one by one. Once the RNA is assembled on the dummy tower, the entire RNA is lifted as one piece onto the already installed turbine tower. As a result, the number of offshore overboard lifts is only two [30]. The installation process is visualized in Figure 1.8. The onboard preassembly process ensures a safe and reliable installation environment, while the reduced number of overboard lifts lowers the risk of damage to the structure [36]. Furthermore, this method offers the advantages of method 1 or 2 because the wind turbines are transported separately, allowing for a more efficient use of deck space. This method is especially suited for floating installation due to the reduced number of overboard lifts. As of now, the method has only been used on the semi-submersible crane vessel *Thialf*.

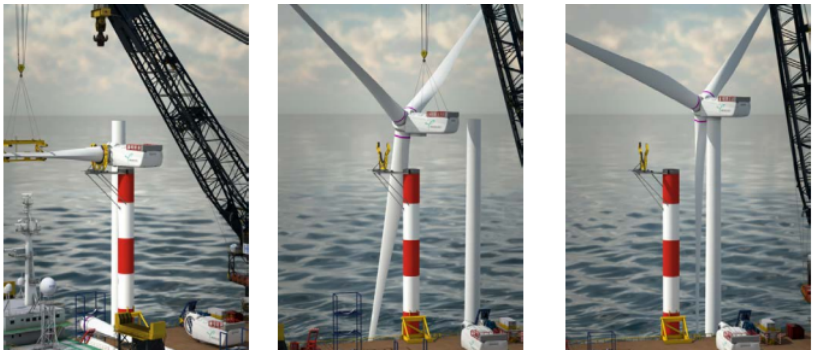

Figure 1.8: Visualization of the RNA installation method, from [37].

The choice of installation method and the level of preassembly significantly affects the number of offshore (overboard) lifts. Given the risks and susceptibility to delays or damage due to environmental conditions during offshore lifts, the preference is to minimize offshore assembly [31]. Moreover, from a cost perspective, it is beneficial to reduce the number of lifts offshore. For instance, if construction costs $1 onshore, it is $2 in port, and increases to $10 offshore [38]. The preferred method also depends on the location of the OWF. example, the second method (single-bade lift with preassembled tower) is more suitable for far-offshore wind farm sites due to its more efficient use of deck space. The chosen installation method determines the maximum lifted weight, which, in turn, dictates the minimum crane capacity requirement for a vessel [31]. Also, the available deck space determines the maximum number of turbines that can fit on a vessel. The required space depends on the chosen method [24]. Since the chosen method has a significant impact on the vessel requirements, it is very important to consider this aspect at an early design stage.

Wind turbine transportation

Besides the installation of wind turbines, the other important phase in the construction of an OWF is the transportation of components. Two possibilities for transportation of wind turbine components are identified:

1. **All-in-one or shuttling** - The first transportation strategy is the all-in-one strategy, also sometimes referred to as shuttling. This involves the installation vessel both transporting and installing the turbine components. The vessel loads at the marshalling port and sails to the installation site. There, the turbines are assembled and installed by the same vessel. When empty, the vessel returns to the marshalling port, and the cycle repeats [24];
2. **Feeder system** - The second strategy is the feeder system. In this approach, the WTIV remains at the installation site and is supplied with components by other, so-called,

feeder vessels or barges. These feeders shuttle between port and construction site to be loaded and unloaded. The installation vessel stays at location and installs the turbines using the provided components. This strategy improves productivity of the installation vessel, as it does not have to travel to port. However, lifting components from another vessel at sea, which is subject to wave-induced motions, can be very risky [24]. Additionally, nacelles are susceptible to damaging the mechanical and electrical components due to acceleration [39]. Due to the increased size of turbine components and the fragility, wind turbine components are currently not lifted from a moving vessel at sea. [24]. As a result, current feeders for wind turbine components are, therefore, more likely to be self-elevating vessels or barges [40]. Using such vessels would help mitigating motions and reducing the risks associated with offshore transfers. However, these vessels would be dependent on soil conditions, jacking time, and have a limited working depth due to the length of the legs. Instead of self-elevating feeders, active motion compensation platforms could be used to reduce the motion of the components and enhance the lifting process from a floating feeder vessel or barge [41].

The decision of whether to use a feeder system or adopt an all-in-one strategy depends on several factors, including transit speed, costs of the installation vessel, available deck space and capacity, the distance to marshalling port, and the size of the turbine components [31]. As a result, the chosen installation method plays an important role in deciding which transportation strategy is most suitable.

Wind turbine installation vessels

Currently, mostly jack-up vessels are used for wind turbine T&I [25]. These vessels can elevate themselves above the sea surface, using their legs, providing a stable base for lifting operations. This eliminates the impact of vessel and crane motions caused by waves and surges, making them suitable for offshore wind turbine installation [42], [40]. An analysis into the main particulars of different generations of jack-up vessels within the existing wind turbine T&I fleet was conducted using the *4C Offshore Wind vessel database* (as of March 10, 2023). The analysis, along with additional information can be found in Appendix B. The analysis revealed that the current fleet will not be able to lift the next-generation turbines, mainly due to their lifting height. Moreover, the length of the legs of these vessels dictate the maximum working depth [40], which becomes a limiting factor with the increasing water depths. In addition, because of their interaction with the seabed, jack-ups are dependent on soil conditions. Before deploying such as vessel, a survey of the seabed is therefore required. This must be done by dedicated survey vessels. Consequently, installation of wind turbines by jack-up vessels requires a complete support fleet [43], and these vessels cannot be deployed at all locations. Additionally, lowering and raising the legs takes up a considerable amount of time [33], especially considering the fact that this must be done at every turbine location and in port. All of the above makes jack-up vessels very inefficient and sometimes unsuitable for offshore wind turbine installation.

Alternatively, floating solutions, such as semi-submersible crane vessels (SSCVs), are sometimes used for wind turbine installation. However, a major drawback of these vessels is that their day rates are very high [28] and their capabilities exceed what is needed for offshore wind turbine installation [31], making them cost-inefficient. In addition, these vessels require a feeder system, despite having substantial deck space. The transit draft of SSCVs ranges from 10 to 12 meters, while their maximum draft during lifting operations is between 25 to 32 meters [44], [45]. The water depth at marshalling ports is typically not larger than 9 to 13 meters [23]. As a result, SSCVs are not able to enter the marshalling ports to load turbine components, requiring a feeder system with all risks associated. Alternatively, other vessel

types are sometimes used, such as sheerlegs and once a monohull crane vessel. These were found to all be cost-inefficient or unsuitable for the installation of next-generation turbines. All information on existing wind turbine installation vessel solutions can be found in Appendix B.

A noticeable gap can be identified between the existing wind turbine installation fleet and the evolving market needs. Various ways to bridge this gap have been investigated, including: (1) ordering new vessels, (2) upgrading existing vessels, and (3) developing new concepts. These pathways were all explored and are described in Appendix B. Vessels currently on order or being built were found to be just larger jack-up vessels. While the first two pathways may enable the installation of larger turbines, they do not address the installation bottlenecks associated with jacking systems. Research into a number of concepts for future wind turbine installation has shown a shift towards floating installation solutions that rely on fully preassembled installation methods. While these methods reduce the number of offshore overboard lifts, there are stability and seakeeping risks when transporting fully preassembled turbines [32], [35]. Other innovative concepts were found to still have installation bottlenecks, such as jacking or the need for a feeder system. Additionally, most of the concepts involve complex hull types, such as semi-submersibles, catamarans, or SWATHS, which are expensive to build, leading eventually to higher day rates [46]. Additionally, operational costs are generally higher for these hull types [47], which may not contribute to decreasing the LCOE. Table 1.2 presents an overview of all investigated vessels and concepts, summarizing the findings from Appendix B.

Table 1.2: Overview of the considered vessels and concepts.

	Name	Vessel type	Transit speed	Installation method		Day rate	H_s limit	Lifting height$^+$	Lifting capacity	Installation bottleneck	Note
	[-]	[-]	[kn]	Number	Name	[-]	[m]	[m]	[t]	[-]	[-]
Existing	1st generation 2nd generation 3rd generation 4th generation	Jack-up	0 - 8 0 - 12 0 - 13 12	1, 2, 3, 4	Single-blade, Bunny ears or Star Assembly	High	1.5 - 2.0#	up to 110 70 - 125 95 - 159 158 - 170	up to 800 800 - 1,000 1,200 - 1,600 2,000 - 3,200	Jacking time	
		SSCV	10	6 or 7	Fully preassembled or RNA	Very high	3.0*	up to 165^o	up to 2x 10,000	Feeder system	
		Sheerleg	5*	6	Fully preassembled	Low	0.75	?	300-10,000	Low workability	
	Aegir	Monohull	15	6	Fully preassembled	Medium	2.0*	96	5,000	-	
Ordered	Boreas	Jack-up	12	1 or 2	Single-blade	High	1.5 - 2.0#	?	3,200	Jacking time	Max. 20 MW
	Seaway Ventus	Jack-up	10	1 or 2	Single-blade	High	1.5 - 2.0#	156 - 116.5	1,600 - 2,500	Jacking time	
	Siren	Jack-up	10	1 or 2	Single-blade	High	2.0	?	2,600	Jacking time	
	X-class	Jack-up	10*	1 or 2	Single-blade	High	1.5 - 2.0#	200+	2,600	Jacking time	
	F-class	Jack-up	10*	1 or 2	Single-blade	High	1.5 - 2.0#	200+	2,600+	Jacking time	
Upgrades	Aeolus	Jack-up	11	1 or 2	Single-blade	High	1.5 - 2.0#	?	1600	Jacking time	Max. 12-15 MW
	Sea Installer	Jack-up	12	1 or 2	Single-blade	High	2	?	1600	Jacking time	
	Wind Osprey	Jack-up	13	1 or 2	Single-blade	High	2.5	160	1600	Jacking time	Max. 14 MW
	Wind Orca	Jack-up	13	1 or 2	Single-blade	High	2.5	160	1600	Jacking time	Max. 14 MW
Concepts	Windlifter	Monohull	12+*	6	Fully preassembled	Medium	2.0 - 2.5	NA	NA	-	
	WTS Huisman	SWATH	14	6	Fully preassembled	Low	3.5	?	2x 2,000	-	Max. 12 MW
	WIV Huisman	Semi-submersible	12	-	Assembly tower	High	3.5	?	3,000	Feeder system	Max. 20 MW
	PWT	Monohull	14	6	Fully preassembled	Medium	?	NA	2x 5,000	-	
	Feederdock	U-shaped jack-up	12*	1 or 2	Single-blade	High	1.5 - 2.0#	?	3,000	Feeder system and jacking time	Max. 25 MW

* Estimated values, # Based on [40], $^+$ Measured from main deck, ^{o} Measured from sea level, NA Not Applicable

Based on the market and concept analysis, it is concluded that there is a need for a new cost-effective and efficient solution. The research suggests that the new vessel should meet he following requirements:

- Relatively high transit speed of at least 12 knots;
- Competitive day rate, lower than jack-up vessels or SSCVs;
- Higher installation efficiency than jack-up vessels, SSCVs, or other concepts;
- Good workability, capable of operating in significant wave heights of at least 2.0 meters;
- Capability to transport and install next-generation wind turbines;
- Has no installation bottlenecks, such as jacking systems, and the ability to enter ports and load, mitigating the need for a feeder system (at least in non-US waters).

1.1.3. Moonshot

Based on the findings from the literature study, this research proposes a new floating monohull vessel concept, named *Moonshot*, to address the gap between (future) market demand and current and near-term solutions. Monohulls generally have a large open deck area and are therefore capable of carrying a lot of cargo. Also, day rates are generally lower than for the other types of mentioned WTIVs [28]. In addition, this type of vessel would be capable of higher transit speeds than, for example, jack-ups and SSCVs [46], which is beneficial when travelling large distances between port and the OWF site. Above all, this vessel type would not have any of the mentioned installation bottlenecks. However, a floating monohull would be more susceptible to motions because of waves during the installation of the turbines, which is important to consider when designing the vessel. Besides fully preassembled floating installation of turbines with a monohull, no other floating monohull solutions can be found in literature.

1.1.4. Company introduction

The research on *Moonshot* will be carried out in collaboration with *Ulstein Design & Solutions B.V. (UDSBV)*. *UDSBV* develops innovative ships for the offshore renewable market and offshore oil and gas industry. The company is located in Rotterdam, The Netherlands, and specializes in the design of complex offshore vessels. These vessels are, amongst others, turbine installation vessels, heavy lift crane vessels, rock installation vessels, cable installation vessels, pipelay, drillships and other construction (support) vessels.

1.2. Problem statement

As a result of the booming offshore wind industry and the resulting advancements and evolution, the current WTIVs will no longer be adequate. Currently, wind turbine installation is mostly done by jack-ups, which are limited by their legs, because of maximum operational water depths and soil dependency. Also, raising and lowering the legs at every wind turbine location takes a considerable amount of time, which slows down the installation process. In order to increase the competitiveness of offshore wind energy compared to other electricity sources, reducing the LCOE is crucial. A cost-effective, efficient, and future-proof solution is required to achieve this objective. *UDSBV* believes that a floating monohull could be that solution. This project has been named *Moonshot*. The mission of this research is therefore to develop *Moonshot* into a viable concept, suitable for installing next-generation offshore wind turbines, and ready for the unpredictable and uncertain nature of the offshore wind market.

1.3. Research objective

The objective of this thesis is to explore the feasibility of a floating monohull vessel (*Moonshot*) for installation of offshore wind turbines and develop it in a viable concept for future offshore wind markets. Due to the uncertain nature of the offshore wind market, it is important to elucidate optimal design parameters for *Moonshot*, based on its financial performance in the market. Because the proposed hull type would be susceptible to wave-induced motions, the vessel should also be optimized for seakeeping performance. The aim during the graduation process is to answer the following main research question:

“What should optimal design parameters be for the innovative Moonshot concept, a floating monohull vessel for offshore wind turbine installation, taking into account financial and seakeeping performance, while considering the uncertainties and evolving requirements of the offshore wind market?”

1.4. Relevant research and literature

The table below provides an overview of relevant research that has already been conducted on the topic, including research goals, usefulness, and limitations. Additionally, relevant literature for this project has been included in the table.

Table 1.3: Overview of relevant research and literature.

Author(s)	Title	Goal	Usefulness	Limitations
G. Hoogendoorn, 2020 [48]	Design in principle for flexible fully assembled wind turbine installation	Investigation into promising installation solutions for large next-generation turbines.	Investigation of multiple options and installation from monohull.	Focus mainly on operational efficiency and installation of only fully preassembled wind turbines. No seakeeping analysis and technical feasibility is questionable.
J.J. Zwaginga, 2020 [49]	Exploring market uncertainty in early ship design	Explore effect of design parameters on vessel performance in uncertain market.	Uncertainty modelling offshore wind market and lifetime financial performance assessment.	Limited to foundation installation market and vessels. Only looks at financial performance.
C. van Lynden, 2021 [50]	Offshore Wind Installation Vessels	Generating insight about the driving factors behind design of future installation vessels.	Insight in driving factors and Epoch-era analysis for uncertain future.	Not about designing future wind turbine installation vessel specifically.
R. Krishnakanth, 2014 [51]	Concept design of an installation vessel to install fully preassembled next-generation offshore wind energy turbines	Design new wind turbine installation solution.	The report covers the whole design process.	No monohull-type solution. Very basic design method used (design spiral). Only designed for market at that time, so for significantly smaller turbines.
T.M. van Bruinessen, 2016 [52]	Towards controlled innovation of complex projects. A social-technological approach to describing ship design	Create insight in design process and develop new method for innovative ship design.	Insight in design process for innovative and complex ships.	Not about optimization or designing for uncertain markets.
S. Ove Erikstad and B. Lagemann, 2022 [53]	Design Methodology State-of-the-Art Report	Generate insight in various design strategies.	Comprehensive overview of state-of-the-art design strategies and recent developments in ship design practice.	Hard to not get lost in all the described design method options.
Z. Jiang, 2021 [28]	Installation of offshore wind turbines: A technical review	Generate (technical) insight in offshore wind.	Very useful to get understanding about installation of offshore wind turbines and important aspects.	Only gives overview of most important aspects and summarizes other literature. Detailed information is missing.
Edited by: C. Ng and L. Ran, 2016	Offshore Wind Farms: Technologies, Design and Operation	Covers all relevant aspects in the development of an offshore wind farm.	Very useful for detailed information about everything related to offshore wind energy.	Not about the design of installation vessels.

1.5. Research questions

To reach the objective and answer the main research question, the following sub-questions have been established:

1. *What are state-of-the-art ship design strategies and how can they cope with innovation and the uncertainty of the offshore wind market and requirements for future offshore wind installation vessels?*
2. *How can the Moonshot idea for turbine installation from a floating monohull be developed into a viable ship concept using UDSBV's Controlled Innovation process?*

3. *What modifications to Blended Design are needed to properly explore the design space for Moonshot and evaluate financial and seakeeping performance?*
4. *How would the main particulars of the Moonshot design influence its financial and seakeeping performance in various future offshore wind market scenarios?*
5. *How does the performance of the proposed Moonshot concept design compare to other vessels for future offshore wind turbine installation?*

1.6. Scope

This research is limited in scope as follows:

- This research focuses exclusively on the **installation of offshore wind turbines**. As a result, installation of foundations, which is expected to be done in the future by other ship types [26], will not be considered;
- As the philosophy behind *Moonshot* is to install wind turbines from a **floating monohull**, the final proposed solution must also be of this type;
- The term wind turbine in this research specifically refers to **horizontal axis wind turbines (HAWTs)**, disregarding other types of wind turbine designs currently under exploration or development;
- While environmental performance nowadays is an important consideration in ship design, this research does **not** assess **alternative fuels** or the **environmental performance** of *Moonshot* to limit the workload.

1.7. Scientific and societal relevance

This research is unique as it focuses on wind turbine installation using a floating monohull. The topic of this thesis has received limited attention in existing literature and prior research. Table 1.3 shows that G. Hoogendoorn, 2020 [48] looked into turbine installation with a floating monohull, but his research was focused on the installation of fully preassembled wind turbines. This research, on the other hand, will not be restricted to fully preassembled wind turbine installation. By exploring an innovative installation method and vessel designs, and optimizing for performance, this study aims to develop a future-proof and more cost-efficient design over the vessel's lifespan, compared to traditional WTIVs. Additionally, this research will perform an extensive exploration of the design space, considering both financial and seakeeping performance, which is something that has not been done in previous studies. The findings from this study could serve as a foundation for further development in this field or, at least, offer valuable insights into the challenges associated with constructing wind farms of the future using an innovative and optimized vessel.

In additional to the scientific relevance, this research also holds societal relevance. The research is driven by the transition towards renewable energy sources. The development of a new, more cost-efficient concept for offshore wind turbine installation plays an important role in reducing the LCOE and ensuring the ability to install the next-generation turbines. This, in turn, will make offshore wind energy more appealing and competitive, accelerating the transition towards sustainable energy sources. Ultimately, this research has the potential to benefit both current and future generations.

1.8. Content description

The sub-questions can generally be categorized into three categories, as shown in Figure 1.9. Each sub-question will be addressed in separate chapters, providing a structured approach to answering the main research question and fulfilling the research objective.

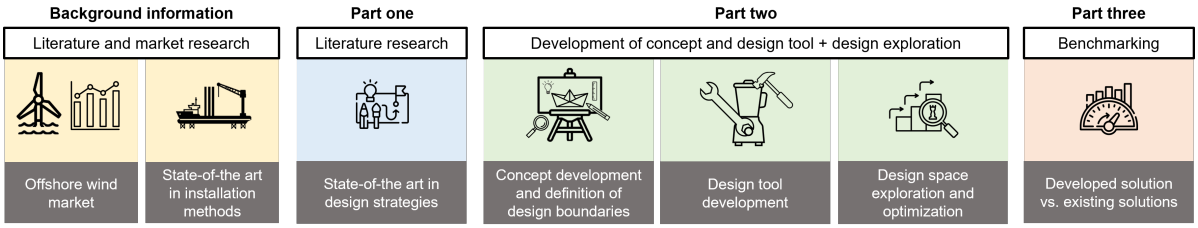

Figure 1.9: The structure of this research.

Chapter 2 covers various design strategies for ship design, discussing the main state-of-the-art design strategies and their principle, benefits, and drawbacks. Various design strategies will be evaluated on the requirements for the purpose of designing *Moonshot*.

In Chapter 3, the *Moonshot* concept will be developed. *UDSBV*'s *Controlled Innovation* process will be employed to determine the value drivers and design aspects. The design aspects will then be evaluated to determine what areas of the design would require the most attention. Some of them will be investigated in so-called development packages and others will later be covered with *Blended Design*.

Chapter 4 introduces the modifications made to the existing *Blended Design* model to properly explore the design space of *Moonshot*. Also, the underlying theory behind the approach will be discussed.

Chapter 5 will explore the design space of *Moonshot* to elucidate optimal design parameters and investigate how ship particulars would influence the financial and seakeeping performance in different scenarios, using *Blended Design*. Eventually, optimal design ranges for the different scenarios are established, providing a basis for further development of *Moonshot*.

Chapter 6 examines the performance of *Moonshot* in comparison with other wind turbine installation solutions. *Blended Design* will be used once again to create a version of *Moonshot* to directly compete with the largest available jack-up design. The resulting *Moonshot* configuration will then be compared to various wind turbine installation vessel solution to determine if the proposed concept is superior to other alternatives.

This thesis is concluded by stating the answers to the sub-questions and main research question. Finally, recommendations for further research will be given.

2

State-of-art in ship design

Before starting the development of *Moonshot*, it is important to establish the appropriate design strategy. As previously noted, the offshore wind market is highly unpredictable, making it challenging to design the ideal WTIV for the evolving market needs. In Appendix B clear examples of this unpredictability are provided where existing jack-ups have been retrofitted to install larger turbines. For instance, jack-ups like *Aeolus* and *Wind Osprey* have undergone two upgrades within their relatively short lifetimes to keep up with growing turbines. This situation can be described as underdesign, where vessels no longer can perform what they were originally designed for, or even becoming obsolete. Conversely, overdesigning is also a potential risk. Overdesigned vessels would have capabilities that surpass the market demand, rendering them expensive and not competitive [54], [55]. The question is how to design a ship that hits the sweet spot, enabling it to operate effectively in the unpredictable and evolving market. This chapter aims to create an understanding of various state-of-the-art ship design strategies and their respective benefits and drawbacks. The ultimate objective is to identify the strategy most suitable for the specific requirements of designing *Moonshot*. By the end of this chapter, the following sub-question is answered: *"What are state-of-the-art ship design strategies and how can they cope with innovation and the uncertainty of the offshore wind market and requirements for future offshore wind installation vessels?"*.

2.1. About innovation

Innovation can be described as: *"An iterative process initiated by the perception of a new market and/or new service opportunity for a technology-based invention which leads to development, production, and marketing tasks striving for the commercial success of the invention."* [56]. When discussing innovation, it is important to consider that there are different levels of innovation. A classification of innovation is depicted in Figure 2.1.

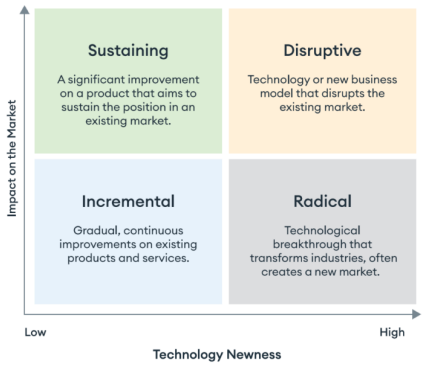

Figure 2.1: Classification of innovation, from [57].

Minor innovations are often described as incremental or sustaining, while major innovations are expressed as radical and disruptive [56]. Incremental innovation is the most common type of innovation in ship design, where the developed vessel is a derivative of a previously designed vessel [58]. On the other hand, major innovative designs, like radical or disruptive ones, often start with a clean sheet of paper. Typically, in such projects, the project duration is lengthy, and there is a high number of iterations [58]. The level of innovation significantly impacts the development of a ship design [52]. Major innovation requires different design strategies than, for example, incremental innovation. Given that *Moonshot* falls into the higher end of the innovation spectrum, it is important to select the right design strategy for the development of the concept.

2.2. Design strategies

A strategy is a high-level plan for achieving an overall goal. In the context of ship design methodology, it can be translated as the organization of the design process, starting from initial capture of client needs and expectations until a final design solution is reached. This section will discuss state-of-the-art design strategies for ships. It is important to note that it is not possible to discuss all available ship design strategies within this thesis. Therefore, focus will be on only the main design strategies as described by Erikstad et al. (2022) [53] and Van Bruinessen et al. (2013) [58]. These strategies are considered fundamental in ship design and other methods. The five strategies are extensively discussed in Appendix C. For additional information on other strategies and derivatives of the discussed methods, refer to the papers by Andrews et al. (2015) [59], Andrews et al. (2018) [60] and Erikstad et al. (2022) [53].

2.2.1. Evaluating strategies

Table 2.1 shows the considered design strategies and evaluates them on applicability on different points that are deemed important for the design development of the future WTIV *Moonshot*.

Table 2.1: Evaluation of the main design strategies.

	Point-based	Set-based	Systems Engineering	System-based	Optimization -based
Applicable in ship design					
Enables innovative solutions					
Global optimization with parametric (ship) model					
Flexibility with changing requirements or market uncertainty					

Green indicates that the requirement is met. Yellow indicates that meeting the requirement is questionable or requires more effort. Red means the requirement is not met.

As indicated, all methods, except for optimization-based design, are applicable in ship design. As described, the typical ship design problem is too complex for a mathematical optimization model. However, there have been some efforts in multi-objective ship design optimization. Therefore, this method is colored in yellow for both its applicability in ship design and optimization with a parametric (ship) model. Regarding the enablement of innovative solutions, almost all discussed strategies are not suitable. For example, point-based design only allows for incremental innovation, but not for major innovations. As demonstrated by Van Bruinessen, Systems engineering is also not applicable for major innovations due to the independent design of different decomposition levels within the system in Systems Engineering. Only set-based design is superior when it comes to innovation. Concerning optimization with

a parametric (ship) model, we observe that point-based design is not suitable for this purpose because of the iterative nature. For the other strategies, except optimization-based, it could be possible. When considering the flexibility to handle market uncertainty and changing requirements, both point-based and optimization-based strategies are not suitable. This is because one must restart the design the design process, when requirements change. For the other strategies, it is applicable to a certain extent.

In conclusion, the discussed strategies show limitation on aspect that are deemed important for the development of the *Moonshot* concept. Especially, when it comes to (major) innovation, none of the strategies are really applicable and fulfills the intended objective.

2.3. Design strategies by Ulstein

In addition to the discussed fundamental state-of-the-art design strategies, two other design strategies can be identified. These strategies are developed and used by *UDSBV* and are referred as *Controlled Innovation* (CI) and *Blended design*. The strategies are in fact amalgamations of the general design methods, combining their strengths. The relationship is illustrated in the Venn diagram in Figure 2.2. The Venn diagram depicts the position of the two *UDSBV* design strategies within the main design strategies, highlighting the areas of overlaps.

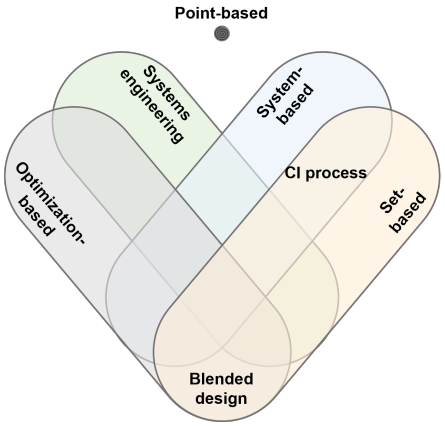

Figure 2.2: Venn diagram showing the position of *UDSBV* design strategies.

The two design strategies by *UDSBV* will be discussed in detail in the following subsections.

2.3.1. Controlled Innovation

As we have seen, the general design strategies often leave limited room for highly innovative solutions. When designing such an innovative solution as *Moonshot*, the *UDSBV Controlled Innovation* process appears to be a more suitable approach. The method was initiated and developed by T. M. van Bruinessen as part of his PhD dissertation in 2016 [52]. The starting point of the dissertation was to explore, identify, and evaluate how innovative, large, and complex vessels are designed in practice. An analysis of the current state-of-the-art in ship design showed that most design methods do not describe the full scope of creative activities. Instead, they often only concentrate on specific parts of the ship design process. The author found that creative ship design, system-based design, and requirement elucidation explore a broader scope of the design process. These approaches enable the full creative design of the ship, in the case of requirement elucidation, both the requirements and the ship design.

A critical aspect in innovative ship design is a concept known as co-evolution. Co-evolution

shifts the focus away from a single-level decomposition, being either the business case, ship design, system design, or component design, and instead emphasizes on developing multiple levels of decomposition in parallel. Co-evolution between solutions on different levels of decomposition enables creative solutions to evolve and influence each other. To enhance the development of co-evolving innovative solutions, a design process should focus on multiple levels of decomposition; allow for weak system boundaries and take into account technical dimensions of the interaction. Figure 2.3 illustrates the cohesion of a system-of-systems and is based on the individual system description, using the form, characteristics, performance, and functions, which is the same on each level of decomposition.

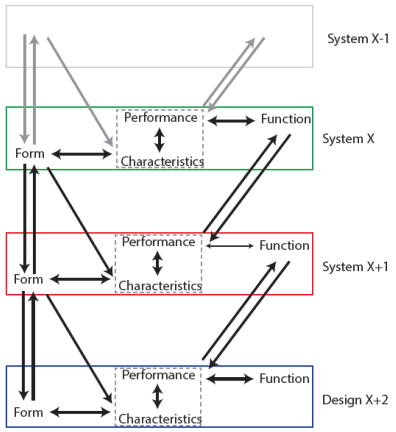

Figure 2.3: Model of cohesion in a system-of-systems, from [52].

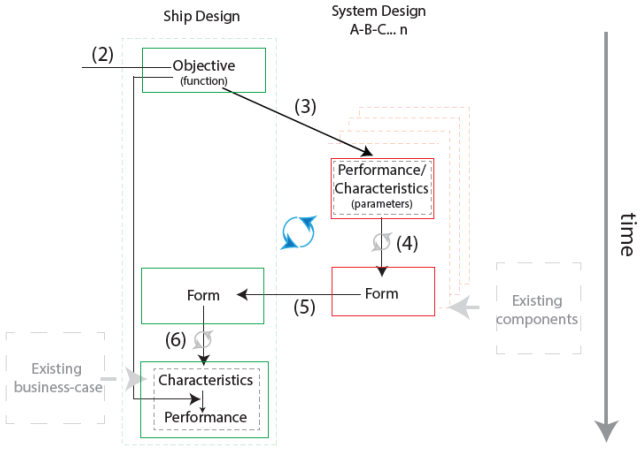

Figure 2.4: Design strategy, based on the interaction between system and ship design, from [52].

The model of cohesion then served as a basis for development of the design strategy (Figure 2.4). The developed strategy starts with a required ship functionality, which is further elaborated into various sets of system performance parameters. These parameters subsequently lead to the development of individual system. Later in the process, these individual system developments are integrated into the overall ship design (form) and undergo evaluation.

T. M. van Bruinessen's [52] method eventually evolved into the *Controlled Innovation* process. Ships design is a complex network of disciplines. When applying systems-thinking, a ship can be decomposed into systems and components that are often interconnected with other systems. As a result of the decomposition, co-evolution between ship design and system design exists. The *Controlled Innovation* process ensures focus on the right performance parameters, systems, or components to identify risks in the design. Eventually, it aims that these aspects are independently reviewed and developed. A practical way to apply this in the ship design process is to use a five-step approach. Figure 2.5 shows the approach of the *Controlled Innovation* process. Each of the five steps will be explained in detail below.

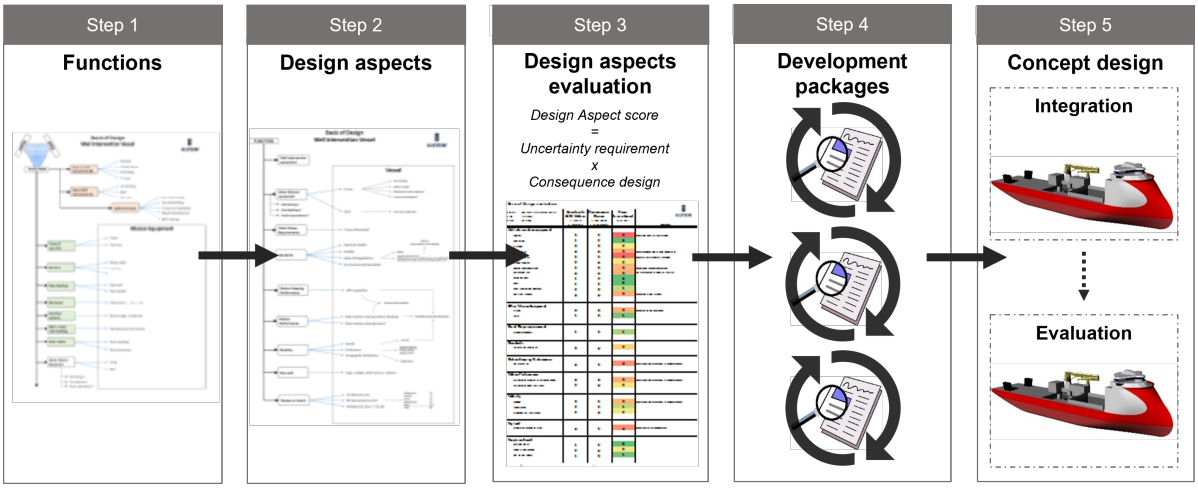

Figure 2.5: *UDSBV*'s *Controlled Innovation* Process.

1. **Functions** - First, the high-level objectives of the vessel are defined. These include, for instance, a specific function the ship has to fulfill, maximum requirements for CAPEX, or OPEX. Following this, more detailed functions are determined, covering mission equipment, payload, accommodation, mobility, performances etc.;
2. **Design aspects** - After defining the functions, the underlying design aspects are determined. For instance, an underlying design aspect of mission equipment could be lifting capacity;
3. **Design aspects evaluation** - All identified design aspects then undergo evaluation. In this evaluation, the uncertainty associated with the requirement of the design aspect is multiplied by the expected impact the design aspect would have on the ship design. Here, uncertainty relates to the likelihood a requirement will change and whether sufficient knowledge is available on the design aspect. Essentially, the evaluation is a risk analysis of the design aspects;
4. **Development packages** - Design aspects with high scores indicate a need for extra attention. Based on that, development packages are formulated. Development packages are small studies focusing on specific design aspects. Their purpose is to support the functions and are well-suited for development of new solutions. Given the limited context often available, these development packages involve conceptual and creative elements, ultimately generating new knowledge on the design aspect;
5. **Concept design** - Once all development packages are completed, and the design aspects are satisfied, the knowledge generated from these packages, together with existing knowledge, is integrated into a concept design. The integration aims to fulfill the set functions for the ship. Following the integration, the concept is evaluated and optimized in alignment with the high-level objective.

Concluding, *UDSBV*'s *Controlled Innovation* process is an elegant strategy to evaluate functions and design aspects in the ship design process. The application of development packages for high-risk design aspects allows for knowledge generation and often results in new solutions and an improved design. Therefore, this method proves to be very useful when innovating in the realm of ship design.

2.3.2. Blended Design

Another strategy that is commonly used at *UDSBV* is *Blended Design*. It is debatable whether *Blended Design* should be considered a design method or more of a tool. Some view *Blended*

design as a life cycle assessment design method that connects to financial performance indicators, while others see it as a tool for generating and assessing thousands of configurations. What we do know is that we are always designing for the future but that the future is inherently uncertain. The previously discussed design strategies have in common that they are not particularly well-suited for designing in markets characterized by uncertainty and evolving requirements. Therefore, *UDSBV* came up with *Blended design*. This has been developed by J.J. Zwaginga for *Ulstein* in 2020 as part of his graduation project [49]. The so-called *Blended Design* tool is developed explicitly to account for market uncertainty within the design process, explore the design space, and elucidate optimal design parameters in the early-stage of design.

Blended Design is capable of generating a large number of unique ship configurations and calculating their financial performance over their lifetimes. It does so by generating tens of thousands of design variations of a parent design, each with varying particulars, such as dimensions, speed, and crane capacity. Subsequently, lifetime costs (OPEX, VOYEX, and CAPEX) and financial indicators like return on investment (ROI) are calculated for each configuration within a simulated market environment. It can do so for different market scenarios, which are modelled with uncertainty modelling. The model was originally intended to design and evaluate the economic performance of foundation installation vessels (FIVs) for the offshore wind industry. In 2022, V.P.M. Peeten [61] extended the original model to assess environmental performance of Heavy Transport Vessels (HTVs). A schematic of the *Blended Design* method, as developed by J.J. Zwaginga [49] is shown in Figure 2.6.

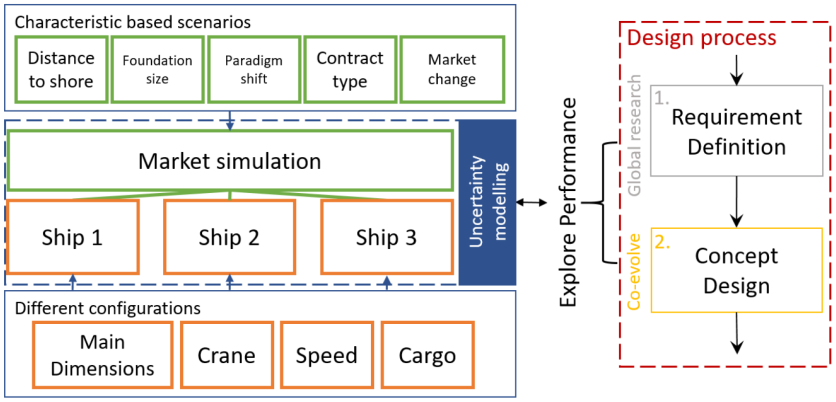

Figure 2.6: Schematic of *Blended Design* method and its place in the design process, from [49].

As shown in the schematic above, the tool consists of three main modules. These will be discussed in the following parts together with the output and the limitations of the model.

Market model

The first module of *Blended Design* is the market model, which simulates the development of the offshore wind market. The model uses market data from the *4C Offshore* wind farm database. It first extrapolates a trend line from the available data, but it also allows designers to adjust and shift the trend line. Designers can choose to examine a broader market with smaller size foundations or a narrower market with larger foundation sizes. This is visualized in Figure 2.7.

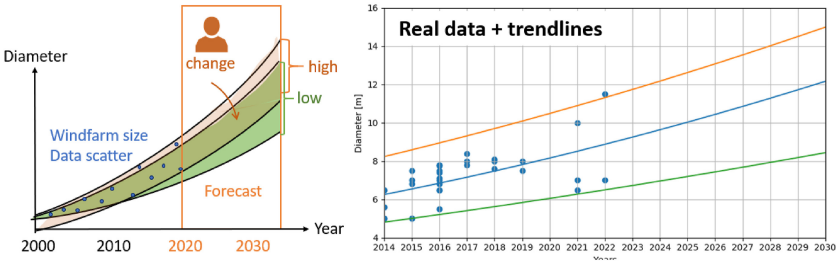

Figure 2.7: Forecast of market trend using extrapolation from data scatter, from [49].

For each time step in the market, lower and upper bounds are determined to account for outliers and represent market uncertainty. These bounds create a range in which contracts might occur each year. To simulate the market, the market prediction with its boundaries is used to generate probability density functions for each year, which is depicted in Figure 2.8. The probability density functions determine the probability of a certain foundation size occurring in a certain year. The output of the market model is the expected growth of the market itself, the corresponding physical growth of the monopiles and jackets, and a matrix with probabilities for each foundation size per year.

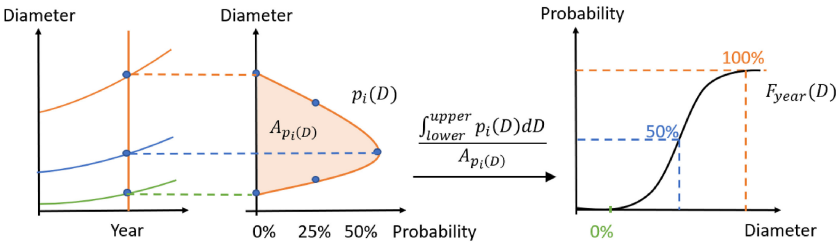

Figure 2.8: Visualization of transforming forecasting trend lines into probability functions, from 2020 [49].

At this moment, the market model is focused on monopile foundations and its mass and dimensions. The original market model has been later extended with a database on alternative fuels by V.P.M. Peeten [61], enabling projections on future alternative fuel prices based on historical and current fuel price data.

Ship model

The second module, the ship model, aims to generate a wide range of design configurations and evaluate their capabilities and performance. The model uses a parent *UDSBV* vessel design and scales the main particulars, including length, breadth, depth, speed, and crane capacity. The inputs for the ship model are ranges with step sizes for each design parameter.

The ship model is divided into multiple parts, each of which is executed for every design configuration. The process consists of scaling of the parent design. Thereafter, calculations are performed to determine resistance, power, and propulsion characteristics. Subsequently, the model estimates the weight of the configuration and the available deadweight for cargo. For each configuration, a stability curve is generated. This depicts the stability and the maximum allowable vertical center of gravity for cargo. Simple scalar checks are incorporated to check the feasibility of all configurations and to eliminate infeasible ones. In 2022, an additional part was integrated, allowing for alternative fuel selection.

Uncertainty model

The third and final model of *Blended Design* is the uncertainty model, which connects the market model to the ship model. The uncertainty model calculates the performance of every

configuration within the market context. It uses the probability matrix from the market model, which provides information about the likelihood of various monopile sizes occurring in a year. An example of this is shown in Figure 2.9. For instance, about 85 percent of the contracts in 2030 will result in three monopiles of a certain size on deck, which decreases to only 40 percent in 2040. For each monopile size, the model calculates the maximum capacity of each configuration and the yearly amount of piles that can be transported. Eventually, the cost, revenue, and profit of a configuration for a range of monopiles sizes is calculated.

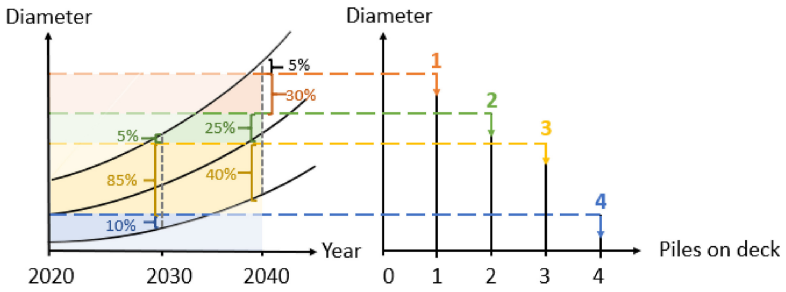

Figure 2.9: Visualisation of the coupling between market and ship model, from [62].

To quantify the performance of a vessel throughout its operational lifetime, the expected value is used as a measure of merit. This value uses the probability of profit and calculates the mean profit of an investment. Eventually, a decision can be made by doing this for multiple investments. The expected value is calculated using a discounted Markov Chain with rewards with a finite horizon. It calculates performance values based on each cut-off diameter or the number of piles on deck and considers the probability of occurrence. Ultimately, the ROI is used to evaluate performance.

In 2022, the model was extended with modules determining equivalent CO_2 emissions. This impacts the Energy Efficiency eXisting ship Index (EEXI), which is a measure of environmental performance of the configurations. Also, alternative fuels were taken into account, affecting the design and cargo capacity of the configurations. This also has an effect on the financial performance of the configuration, but increases the environmental performance. As a result, penalties in the form of carbon tax were introduced as an incentive for low- or zero-emission fuels.

Output of blended design

The output of *Blended Design* is the financial performance of all design configurations in various market scenarios. With the market model, it is possible to generate different market scenarios, and analyze bound markets and non-bound markets. The output of *Blended Design* consists of plots with on the horizontal axis a design parameter and on the vertical axis a performance indicator. An example is shown in Figure 2.10. This example shows that for a non-bound market it is more optimal to have more length but the overall ROI will be lower than for a bound market. *Blended Design* is also capable of investigating the impact of other scenarios, such as increasing distance to shore, difference between contract types or a paradigm shift towards monopiles without transition piece. This shows the strength and versatility of the *Blended Design* strategy.

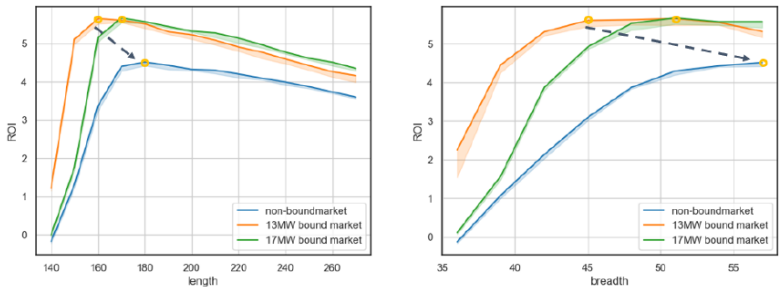

Figure 2.10: ROI results of three different future market projections, from [49].

Limitations of Blended Design

Although *Blended Design* proves to be very powerful and flexible for early-stage ship design, it has some limitations. The first limitation has already been pointed-out in the thesis by J.J. Zwaginga [49] and relates to workability assessment. Workability refers to the percentage of time a vessel can successfully execute a certain operation, taking into account weather conditions such as waves, wind, and currents. As stated by J.J. Zwaginga [49], workability is not implemented into the *Blended Design* tool. During the early-design stages, determining seakeeping and workability is complex since the hull geometry is not yet defined. Even in later design phases, quantifying workability is challenging due to assumptions and time-consuming simulations. In the original model, seakeeping behavior is not assessed and workability is a fixed number for every design configuration. However, research has shown that various installation solutions and hull types (Table 1.2 in Chapter 1) can significantly affect workability. For example, floating monohulls are particularly susceptible to wave-induced motions. When installing wind turbines, motion amplitudes must be low enough to prevent impact and damage to the turbine or foundation. Literature research also showed that accelerations in the nacelle must be limited. Due to the philosophy behind *Moonshot* to use a floating monohull during installation, seakeeping behavior and workability are considered critical in this research. Therefore, it is essential to include a seakeeping analysis and determine workability percentages during the early design phases when applying the Blended Design method for Moonshot design. In this way, *Blended Design* could reward and highlight design configurations that can operate under harsher conditions.

The second limitation arises from the fact that *Blended Design* has been developed for a specific part of the offshore wind market. The first version was developed for FIVs, focusing on monopile transport and installation. Later, HTVs were included, these vessels transport monopiles and transition pieces. Consequently, every part of *Blended Design* is currently focused on monopiles and not on wind turbines. Therefore, modifications to *Blended Design* are needed for designing *Moonshot*. These will mostly impact the ship model and the uncertainty model, since the way of fitting the components on deck will also be different.

2.3.3. Evaluating UDSBV design strategies

Table 2.2 evaluates the two UDSBV design strategies on the same aspects as the general design strategies were evaluated on earlier in Section 2.2.1, and are deemed important for the design of the future WTIV *Moonshot*.

Table 2.2: Evaluation of *UDSBV* design strategies.

	Point-based	Set-based	Systems Engineering	System-based	Optimization -based	Controlled Innovation	Blended Design
Applicable in ship design							
Enables innovative solutions							
Global optimization with parametric (ship) model							
Flexibility with changing requirements or market uncertainty							

Green indicates that the requirement is met. Yellow indicates that meeting the requirement is questionable or requires more effort. Red means the requirement is not met.

The *Controlled Innovation* process shows to be a great approach when it comes to developing innovative ship designs. On the other hand, *Blended Design* is a very versatile approach to evaluate the performance of a wide range of different configurations. If it is not exactly clear what the requirements are and what to design for, this method is an elegant way to explore the design space and to give insight in how changes in the design influence the performance. Eventually, optimum design points for different market scenarios can be established in early-design. However, *Blended Design* needs some constraints for the configurations and therefore relies on a reference design. For example, the tool requires information on what locations are reserved for mission equipment and what deck space is available for cargo. As a result, it is not a great design strategy for innovation.

When combining the two design strategies into one design strategy, all four points are satisfied. First, *Controlled Innovation* could be used to develop a ship concept and to determine what parts of the design need attention and require extra knowledge. This can then be used as constraint in *Blended Design* to evaluate the performance and determine optimum design ranges. This will result in the basis for further development of *Moonshot*, the next-generation WTIV. Therefore, the preferred strategy for the development of *Moonshot* would be a combination of the *Controlled Innovation* process and *Blended Design*.

2.4. Chapter conclusion

This chapter discussed state-of-the-art ship design strategies. A lot of different strategies are available and described in literature. The main strategies, that are the foundation of many other strategies, have been discussed in this chapter. The main strategies are: point-based design, set-based design and Systems Engineering, system-based and optimization-based design. The approach and goal of each strategy has been reviewed, along with their respective advantages and disadvantages. The five strategies were evaluated on aspects that are important for the development of *Moonshot*. These consider innovation, optimization with a parametric model, and flexibility in dealing with changing requirements or market uncertainty. No design strategy was found to be particularly suitable for the development of *Moonshot*. In response to this, two strategies by *UDSBV* have been introduced and explained in detail. These methods are: *Controlled Innovation* and *Blended Design*. An evaluation of the capabilities of these strategies was also conducted. Analysis showed that combining the two strategies, results in a robust strategy, perfectly applicable for the development of *Moonshot*. The main characteristic of the *Controlled Innovation* process is that it enables the design of major innovations, while *Blended Design*'s strength is that it can account for uncertain markets and evaluate the performance of a wide range of design variations. However, *Blended Design* requires modifications to tailor it to the specific needs of *Moonshot*.

3

Developing Moonshot

The goal of this chapter is to develop *Moonshot* and explore ways to make the idea work. To accomplish this, the *Controlled Innovation* process will be used. The following sub-question will be answered in this chapter: *"How can the Moonshot idea for turbine installation from a floating monohull be developed into a viable ship concept using UDSBV's Controlled Innovation process?"*.

3.1. The design process

As determined earlier, the combination of the *Controlled Innovation* and *Blended Design* is deemed to be the most effective strategy for this project. Figure 3.1 provides a schematic representation of the design process adopted for this research.

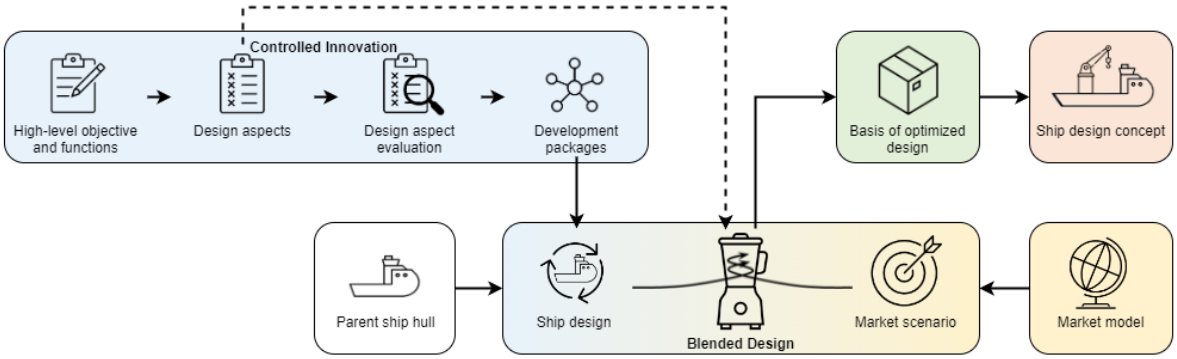

Figure 3.1: Schematic of the design strategy for this research.

Controlled Innovation is used to determine the functions of *Moonshot*, as well as to establish the underlying design aspects. These design aspects are then evaluated to pinpoint those that require additional focus or extra knowledge. It is then important to differentiate between the design aspects that should be addressed in the development packages of the *Controlled Innovation* process and those that can be handled through *Blended Design*. The results obtained from the development packages will eventually serve as input and boundaries for the *Blended Design* model. This chapter and the subsequent sections will focus on the *Controlled Innovation* part. The next chapters will delve into *Blended Design* and assess the performance of *Moonshot*.

3.2. High-level objective, Functions, and Design aspects

The first step in the design process involves defining the high-level objective of the design. The high-level objective corresponds to the primary goal or purpose for which the vessel is being designed. This could, for instance, be for certain functions, minimizing CAPEX or OPEX. In this case, there are no strict CAPEX or OPEX requirements but the design should aim to be competitive in the offshore wind market and be efficient. Hence, the high-level objective of *Moonshot* is more inclined towards the function of the ship design. Subsequently, the targeted high-level objective of the design is further subdivided into functions, which are then broken down into design aspects. Figure 3.2 provides an overview of the high-level objective, functions, and design aspects of *Moonshot*. These elements are based on the findings from the literature and market research, together with input from *UDSBV* Naval Architects. More details regarding the functions and design aspects will be provided below the figure.

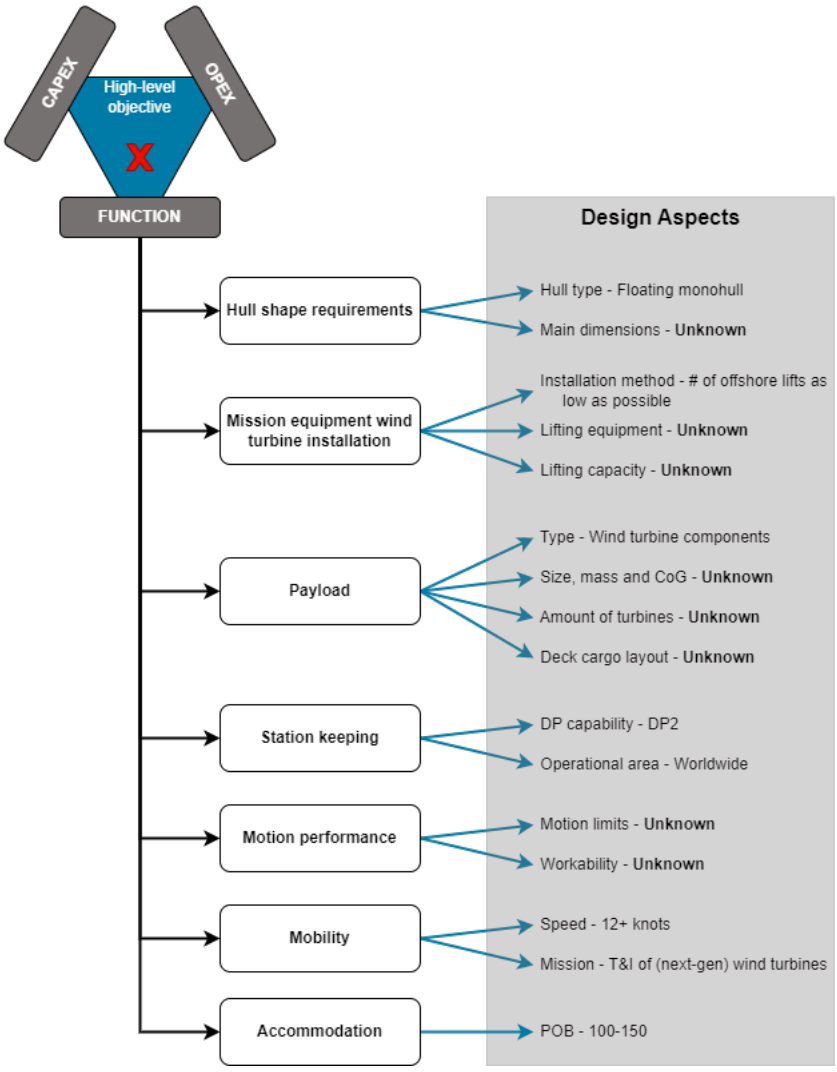

Figure 3.2: Overview of the defined high-level objective, functions, and design aspects for the design of *Moonshot*.

- **Hull shape requirements** - The first function of the design pertains to the hull shape. The following two design aspects are associated with this function:
  - *Hull type*: The requirement for the hull type of *Moonshot* is evident, as it must be a floating monohull;

  - *Main dimensions*: The main dimensions are closely related to the mass, size, number of turbines that must be transported and installed, and both financial and seakeeping performance. Therefore, the requirements for this design aspect are not yet known.

- **Mission equipment wind turbine installation** - One of the most important functions of the WTIV design is the mission equipment for wind turbine installation. The following design aspects are related to this function:
  - *Installation method*: The literature review on installation methods for turbines showed that it is preferable to minimize the number of offshore overboard lifts while ensuring efficient use of deck space capacity by transporting the turbine components separately. There are ways to achieve this, such as the RNA method or the proposed method of *Huisman*'s *WIV* concept (Section B.2.3 in Appendix B) with its assembly tower. *Moonshot* aims to employ a similar installation method;
  - *Lifting equipment*: At this moment, the appropriate type of lifting equipment for *Moonshot* is unknown. However, it is important for the design to have an understanding of the required lifting equipment, such as the working principle, mass, physical dimensions, and footprint. This will influence the ship design, performance, and the deck cargo layout;
  - *Lifting capacity*: The lifting capacity will determine the maximum size of turbine components that can be lifted. The lifting capacity affects the overall performance in the market. The best lifting capacity for *Moonshot* is not yet known.

- **Payload** - Payload is one of the most important functions of *Moonshot* because it represents the part through which the vessel would generate income. Four design aspects related to this function have been identified:
  - *Cargo type*: As *Moonshot* is a WTIV, the cargo type will obviously be wind turbine components;
  - *Size, mass, and center of gravity (CoG)*: This design aspect directly influences the cargo capacity and performance of the vessel. The size, mass, and CoG also affect the required main dimensions and the required lifting capacity of the design, among other factors. At this stage, the size, mass, and CoG of next-generation turbine components remain uncertain due to the evolving offshore wind market;
  - *Amount of turbines*: The amount of turbine components that can be transported depends on the size, mass, and CoG of the total payload of the design. Specific requirements for this are also not known at this stage;
  - *Deck cargo layout*: The other design aspects do not determine the placement of all turbine components on board of the vessel. This depends on the mission equipment, layout of the ship design, and other factors. Therefore, there are many possible deck layouts. The best deck cargo layout for *Moonshot* is unknown at this moment.

- **Station keeping** - This function encompasses two design aspects:
  - *DP capability*: DP capability refers to the station keeping capabilities and redundancy. As *Moonshot* is intended for floating wind turbine installation, a DP system is essential. There are different DP classes, with DP1 representing the lowest level of capability and DP3 the highest. The higher the DP class, the more demanding the operational requirements and the greater the vessel's capability to maintain its position accurately and safely, even when systems fail. The choice of DP class is often influenced by client preferences. The market research in the existing and future

fleet in Appendix B shows that the majority of WTIVs has DP2 capability. Hence, it is assumed for now that DP2 capability would be sufficient for *Moonshot*;
  - *Operational area*: The vessel should be capable of operating globally.

- **Motion performance** - The motion performance function can be divided into two design aspects:
  - *Motion limits*: The operational limits define the acceptable range of motion or acceleration in which the vessel can operate without compromising safety or risking damage to the turbine, foundation, or vessel. The limits dictate in what sea states operations can be continued and when these should be terminated, with the vessel waiting for better weather conditions. The operational limits during installation are currently not readily available;
  - *Workability*: Eventually, the seakeeping behavior in combination with the operational limits will result in a workability percentage. The seakeeping behavior and this percentage are highly dependent on the geometry of the hull, operational limits, as well as the distribution of sea states in a specific offshore environment.

- **Mobility** - The mobility function encompasses everything that is related to the ship's mission. The following important design aspects were identified:
  - *Sailing speed*: The main advantage of a monohull vessel is the capability of higher speeds [46]. Based on analysis of other vessels, the requirement for sailing speed was set to a minimum of 12 knots (Section 1.1.2). However, it is not yet known what the exact speed of the design should be, as it relates to the main dimensions, propulsion systems, and performance in the market;
  - *Mission*: *Moonshot*'s mission is to transport and install next-generation wind turbines without the need for a feeder system.

- **Accommodation** - People on board (POB) is the most important design aspect related to the function accommodation. The POB is the number of marine crew, special personnel for operations, services, maintenance, and other stakeholders. The required POB is influenced by the number of shifts per day, which typically depends on the preferences of the ship operator. POB provides insight into the size of accommodation required for the ship design, impacting the ship mass and superstructure footprint. Analysis of the existing fleet of WTIVs (Appendix B) indicates that POB typically ranges from 100 to 150.

At this stage of the design process, some design aspects still have unknown requirements. In the upcoming section, all design aspects will be evaluated to identify which ones need significant attention and require knowledge generation.

3.3. Design aspects evaluation

In the design aspect evaluation, all design aspects are ranked. The first step involves assessing the level of uncertainty for each requirement of a design aspect. Thereafter, the expected impact of an aspect on the ship design is determined. The two scores are then multiplied to generate a score between 1 and 5. Design aspects with higher scores indicate greater risks to the ship design, typically due to uncertainty and substantial impact. To decrease these risks, it is crucial to reduce uncertainty of the high-scoring design aspects and generate more knowledge to establish requirements with more certainty. Following *Controlled Innovation*, these high-risk design aspects are covered in detail in development packages. However, not all aspects will be covered in development packages, as some are more suitable to be addressed through *Blended Design*. Table 3.1 shows the evaluation of design aspects, also indicating

whether the path of development packages or *Blended Design* is proposed for high-scoring design aspects.

Table 3.1: Evaluation of the design aspects.

	Uncertainty 1 = certain 5 = uncertain	Consequence Design 1 = low impact 5 = high impact	Score Design Aspect U x C x 0.2	Assigned solution
Hull shape requirements				
Hull type	1	5	1.0	
Main dimensions	5	5	5.0	Blended design
Mission equipment wind turbine installation				
Installation method	2	5	2.0	
Lifting equipment	5	5	5.0	**Development package**
Lifting capacity	5	5	5.0	Blended design
Payload				
Type	1	4	0.8	
Size, mass and CoG of components	5	4	4.0	**Development package** and Blended design
Amount of turbines	5	5	5.0	Blended design
Deck cargo layout	4	4	3.2	**Development package**
Station keeping				
DP capability	2	4	1.6	
Operational area	1	3	0.6	
Motion performance				
Motion limits	5	3	3.0	
Workability	5	5	5.0	Blended design
Mobility				
Speed	4	5	4.0	Blended design
Mission	1	5	1.0	
Accommodation				
People on board	3	3	1.8	

While the hull type design aspect has a significant impact on the ship's overall design, the requirement for it to be a floating monohull is highly certain. Consequently, the design aspect of hull type is very low. On the other hand, main dimensions have also a great impact in determining the ship's capabilities, like deck area, resistance, stability, and other factors. However, as the requirements for this design aspect are unknown, the uncertainty of the requirements is very high. Hence, this design aspect receives a maximum design aspect score, indicating high risk. Main dimensions should, therefore, receive great attention during this research. As explained, *Blended Design* can provide valuable insights into how ship parameters, like main dimensions, affect performance in an uncertain market, making it the preferred solution for reducing this uncertainty.

Lifting equipment and lifting capacity are other high-scoring design aspects. At this moment, it is very unclear what type of lifting equipment should be used for offshore wind turbine installation in alignment with the chosen method. Therefore, this design aspect requires an development package to determine the appropriate equipment for the desired installation method. The lifting capacity depends on a lot of other parameters, such as the size of turbines in the market and main dimensions, and will influence the ship design's performance directly. Consequently, *Blended Design* seems to be the perfect solution for defining the right lifting capacity requirements

Another function with multiple high-scoring design aspects, thus risks involved, is payload. The size, mass, and CoG of the turbine components are very uncertain, as it is not known what kind of wind turbines will be transported and installed by *Moonshot*, due to the unpredictable and evolving offshore wind market. The turbine component properties are closely related to the ship capabilities and performance of the ship design. Therefore, *Blended Design* appears to be the preferred solution for determining the properties of next-generation turbines. How-

ever, since only data about existing wind turbines is available and the size of future turbines is uncertain, this design aspect will also require a development package. This package aims to establish relationships between turbine parameters, identify trends, and enable extrapolation for next-generation turbine components. The requirement for the number of turbines carried per round-trip is also uncertain and can have a substantial impact on the ship design, making it another aspect to investigate with *Blended Design*. The optimal deck layout for *Moonshot* will also be explored in a development package.

Workability is also a risky design aspect. Workability is highly-dependent on the seakeeping behavior of a ship and thus related to the hull dimensions and loading conditions. Since the main dimensions and design aspects related to payload are uncertain, the seakeeping behavior and workability are also uncertain. This design aspect would be suitable to be covered by *Blended Design*. However, the existing *Blending Design* tool does not include a workability or motion assessment, so the existing tool needs to be upgraded.

Regarding mobility, the mission requirement is highly certain, while the speed requirements are less certain. Since *Moonshot* will transport and install the wind turbines, the speed is very important. Too slow will increase the cycle times and make the design less cost-efficient, while too high speed will result in bigger and more expensive propulsion equipment. *Blended Design* is able to create various vessel configuration with varying vessel speeds, so the assigned solution to find the requirements for the vessel speed design aspect will be *Blended Design*.

All other design aspects with lower scores are important to the overall function of the ship design. However, the risks associated with their requirements is much lower due to lower uncertainty or impact on the design. As a result, they do not need additional knowledge generation or a strong focus in this research.

3.4. Development packages

Following the evaluation of design aspects, there are three design aspects that require extra attention in the form of a development package. These will be discussed in the following subsections.

3.4.1. Development package 1 - Lifting equipment

It is essential for the lifting solution to align with the preferred installation method. The preferred method is similar to the RNA method (Figure 1.7), emphasizing on as low as possible offshore overboard lifts while the components are transported individually. When it comes to the design and development of the lifting equipment for *Moonshot*, it is important to rely on existing technologies and the expertise of equipment specialists. While it may be tempting to explore innovative ideas for lifting equipment, it is crucial to consider practicality and feasibility, as ship owners are often hesitant to invest in costly experimental solutions. In this development package, requirements for the lifting equipment will be set-up and various solutions for lifting equipment will be explored and evaluated.

Vertical lift options

The goal of the lifting equipment is straightforward: to vertically move the turbine components during assembly and subsequently lift the assembled turbine onto the foundation. Two types of vertical lifting mechanisms can be identified when examining the existing turbine installation vessels and future concepts: free-hanging lifts and guided lifts. The principles of these mechanisms are visualized in Figure 3.3.

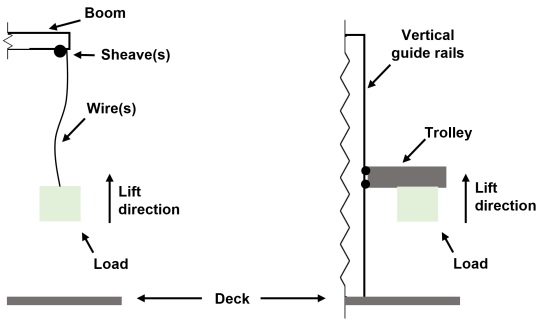

Figure 3.3: Visualization of the identified lifting mechanisms: Free-hanging lift (left) and guided lift (right).

1. **Free-hanging lift** - In a free-hanging vertical lift, the load is suspended and lifted vertically without constraints or a guiding system. This principle is used in conventional cranes. Examples of conventional offshore heavy-lift cranes include mast cranes and tub mounted cranes. These are depicted in Figure 3.4. These cranes often have a high lifting capacity of thousands of tonnes and have a high lifting height. Tub mounted cranes generally have a larger lifting capacity, but a larger footprint because the overturning moment of the crane is transferred by a large slew bearing [63].

Figure 3.4: Artist impressions of mast crane (left) and tub mounted crane (right), from *Huisman*.

2. **Guided lift** - The guided lifting mechanism involves a lifting system where the load is constrained and guided during the lifting process to ensure controlled movement without swinging loads. The mechanism is often seen on land-based pile drivers used for civil construction, in the form of a *vertical travel lead* system. An example of an offshore lifting solution with this mechanism would be the assembly tower from *Huisman*'s *WIV* concept, as discussed in Section B.2.3 in Appendix B. This tower uses vertical guide rails to guide and constrain the turbine components during vertical lifting. A drawback of the guided lift mechanism is its ability to only lift vertically, whereas a free-hanging lifting solution usually also allows for horizontal load movement by luffing the crane boom.

Both free-hanging and guided lifting mechanisms could benefit from 3D motion compensation technology to mitigate the effects of ship and crane motions due to external forces, such as waves. For example, *Huisman* designed a 3D Motion compensated crane for a company called *OWL* in 2020 [64]. The crane looks like a tub mounted crane, but has a special jib, which is able to compensate for the motions of the vessel and crane boom. The assembly tower of the *WIV* concept also employs 3D motion compensation. The tower has multiple motion compensated grippers holding the wind turbine and compensating for the vessel motions. Incorporating 3D motion compensation is worth considering for enhancing the workability of *Moonshot*.

Criteria for lifting equipment
The following criteria have been formulated for the lifting equipment, based on consultations with *UDSBV* naval architects and findings from the literature research.

- **Sufficient lifting capacity** - It is crucial that the lifting equipment of *Moonshot* has sufficient lifting capacity for installation of current and next-generation wind turbines. Given the uncertainty surrounding the exact lifting capacity required for future wind turbines, it is essential that the lifting equipment is at least scalable. This means that it should be capable of having larger capacities than the current standard;
- **Prevention of swinging loads** - Another criterion for the lifting equipment is the prevention of swinging loads. As discussed in Chapter 1, the lifting of wind turbine components, particularly blades, can be hazardous and vulnerable to delay or damage caused by wind conditions. When combined with the motion of the vessel due to waves, it is important to mitigate the swinging of crane loads to ensure a safe and efficient installation environment;
- **Stored position during sailing** - The preferred lifting solution should enable a secure storage position during sailing. It is undesirable for the equipment to remain fixed and protrude several hundreds of meters above the vessel while sailing. Therefore, the lifting equipment should be designed in a way that allows it to be safely stored to a lower position during transport, ensuring a lower profile, lower center of gravity, and reducing potential hazards;
- **Flexible** - *UDSBV* always strives to design a ship that is not a “one-trick pony”. This means that the concept should be able to perform other tasks in the offshore wind industry or even other industries, rather than being limited to wind turbine installation alone. This inherent flexibility of the vessel enhances its value and usefulness. Consequently, the lifting equipment should also be flexible, allowing for the executing of diverse heavy-lift operations;
- **Acceptable** - The last criterion is that the lifting equipment should be acceptable. The lifting solution should not be overly complex to understand or too advanced. The lifting solution should fulfill the requirements for the goal of floating installation of wind turbines, while also meeting the expectations from the industry. An guiding example of this is the MAYA principle, which stands for Most Advanced, Yet Acceptable. This principle refers to finding the optimal balance between pushing the boundaries of innovation and technology while ensuring that the solution remains acceptable and practical for its intended purpose [65].

Table 3.2 provides an evaluation of the two lifting mechanisms based on the set criteria. A column has been added for a hybrid solution that combines elements from both mechanisms.

Table 3.2: Assessment of the different lift mechanisms.

	Free-hanging lift	Guided lift	Hybrid solution
Sufficient lifting capacity			
Prevention of swinging loads			
Stored position during transport			
Flexible			
Acceptable			

Green indicates a positive score. Yellow indicates that it is questionable.
Red indicates a negative score

A free-hanging lift solution scores very positive, but would not be able to prevent swinging loads. Although 3D motion compensation could be considered, it is assumed that it may not fully eliminate blade swinging caused by wind. On the other hand, guided lifting equipment is considered to be not as flexible as a free-hanging lift solution, lacking the ability to move objects horizontally. Also, it is questionable if a guided lift solution would be able to be stored during transport, as the assembly tower is not capable of that. It is also expected that the assembly tower may be too advanced and considered too experimental for the market to be accepted. However, a guided lift solution would be very suitable for preventing swinging loads. As a result, it would be very beneficial to combine the strengths of the two mechanisms into a hybrid solution.

An example of such as hybrid solution is the *Zephyr* crane concept, developed by *Huisman*. An impression of this crane concept is given in Figure 3.5. It functions as both a conventional offshore crane for heavy-lifting and as a guided lifting system. This crane achieves its guided lifting capability by positioning the boom vertically and employing a trolley that moves along rails along the boom structure. The trolley serves as the lifting mechanism during guided lifting operations. With this system, the *Zephyr* crane concept combines the flexibility of a conventional offshore crane with the ability to perform guided lifts. Such an equipment solution or comparable solution would be highly suitable for *Moonshot*.

Figure 3.5: An impression of the *Zephyr* crane concept, received from *Huisman*.
The left render shows the free-hanging mode, while the right shows the guided lift mode.

3.4.2. Development package 2 - Size, mass, and CoG of components

This design aspect heavily relies on the size of the wind turbine being transported and installed. However, due to the unpredictable and uncertain nature of the offshore wind market, it is currently unknown what capacity *Moonshot* will be designed for. Therefore, one would expect that this design aspect should solely be addressed by *Blended Design*. This is only partially true because there is no knowledge about the properties of the components too. The development of size and mass properties for larger turbines remains unknown. Hence, an analysis needs to be conducted.

Size and mass of components

Information about the properties of next-generation offshore wind turbines is not available, resulting in uncertainty regarding the size and mass of turbine components. To estimate the

properties of future wind turbine components, the relationship between different parameters of existing wind turbine parts will be examined. By extrapolating these relationships, the properties of future wind turbines and their components can be estimated. unfortunately, detailed information about existing offshore wind turbines is limited and often not publicly available. To address this, a database has been created based on information from various public sources. This database, which is included in Appendix D, contains data on 16 commercially available wind turbines. Also, 7 generic reference offshore wind turbine models provided by research institutions were included.

Thirteen different parameters from the database were subjected to statistical analysis for correlation. Spearman's rank correlation has been used for this purpose. Spearman's rank correlation is a widely used statistical measures for assessing the relationship between multiple variables. It is used to evaluate the monotonic relationship between variables. In a monotonic relationship the variables tend to change in the same relative direction but not at a constant rate [66]. In a Spearman's rank correlation procedure, values of the variables are ranked and correlation is calculated based on the ranks, rather than the values of the variables. The main advantage of Spearman's rank correlation over other correlation measures is that it is more robust and less affected by outliers [67]. In the case of ties, where two or more variables have the same value, tied observations receive the same average rank [67]. Equation 3.1 demonstrates the Spearman's rank correlation formula [68].

$$\rho = \frac{\frac{1}{n}\sum_{i=1}^{n}\left(\left(R(x_i) - \overline{R(x)}\right)\cdot\left(R(y_i) - \overline{R(y)}\right)\right)}{\sqrt{\left[\frac{1}{n}\sum_{i=1}^{n}\left(R(x_i) - \overline{R(x)}\right)^2\right]\cdot\left[\left(R(y_i) - \overline{R(y)}\right)^2\right]}} \tag{3.1}$$

where:

ρ = Spearman's correlation coefficient
n = Number of observations
$R(x_i)$ = Rank of x variable for i^{th} observation
$R(y_i)$ = Rank of y variable for i^{th} observation
$\overline{R(x)}$ = Mean rank of x variable
$\overline{R(y)}$ = Mean rank of y variable

The correlation coefficients were calculated for each variable of the wind turbine components. The results are presented in Table 3.3. Definitions and units of the used symbols are shown in the Symbols list at the beginning of this thesis. Variable sets with a correlation coefficient denoted by '-' indicate that there are insufficient values available for conducting a valid correlation test. Nacelle and hub length are treated as a single variable because in a lot of instances in the wind turbine database, the hub length is included in the nacelle length.

Table 3.3: Spearman's rank correlation coefficients for all turbine data.

	P_{rated}	D_{rotor}	L_{blade}	M_{blade}	$L_{nacelle}$ + L_{hub}	$B_{nacelle}$	$H_{nacelle}$	$M_{nacelle}$	M_{hub}	L_{tower}	D_{tower}	M_{tower}	H_{hub}
P_{rated}	1	0.92	0.92	0.87	0.81	0.86	0.30	0.95	0.32	0.89	0.93	0.89	0.91
D_{rotor}		1	1.00	0.82	0.52	0.60	0.60	0.91	0.30	0.88	0.93	0.88	0.83
L_{blade}			1	0.71	0.52	0.60	0.60	0.87	0.02	0.88	0.89	0.88	0.79
M_{blade}				1	0.33	0.60	0.60	0.88	0.38	0.68	0.98	0.88	0.80
$L_{nacelle}$ + L_{hub}					1	0.86	-0.04	0.72	-	-	-	-	0.22
$B_{nacelle}$						1	0.19	0.86	-	-	-	-	0.90
$H_{nacelle}$							1	0.45	-	-	-	-	0.38
$M_{nacelle}$								1	0.24	0.76	0.96	0.88	0.78
M_{hub}									1	0.38	0.66	0.40	0.46
L_{tower}										1	0.59	0.96	0.77
D_{tower}											1	0.79	0.92
M_{tower}												1	0.93
H_{hub}													1

Based on the analysis of turbine variables, it can be concluded that there is correlation among most parameters of offshore wind turbines. However, correlation between nacelle size and other turbine properties is not very high. Also, hub mass is not strongly correlated with other variables. The correlations above are based on the entire database, containing all turbine drive types. An additional correlation analysis was conducted solely on direct and semi-direct drive turbines, resulting in the correlation coefficients in Table 3.4.

Table 3.4: Spearman's rank correlation coefficients for direct and semi-direct driven turbines

	P_{rated}	D_{rotor}	L_{blade}	M_{blade}	$L_{nacelle}$ + L_{hub}	$B_{nacelle}$	$H_{nacelle}$	$M_{nacelle}$	M_{hub}	L_{tower}	D_{tower}	M_{tower}	H_{hub}
P_{rated}	1	0.89	0.89	0.82	1.00	0.70	0.21	0.98	-0.25	0.80	0.63	0.50	0.88
D_{rotor}		1	1.00	0.78	0.74	0.53	0.54	0.91	-0.31	0.80	0.63	0.50	0.88
L_{blade}			1	0.78	0.74	0.53	0.54	0.91	-0.31	0.80	0.63	0.50	0.88
M_{blade}				1	0.32	0.53	0.54	0.87	-0.11	-0.50	0.95	0.50	0.91
$L_{nacelle}$ + L_{hub}					1	0.70	0.21	0.94	-	-	-	-	-
$B_{nacelle}$						1	0.05	0.76	-	-	-	-	-
$H_{nacelle}$							1	0.48	-	-	-	-	-
$M_{nacelle}$								1	-0.26	0.00	0.83	0.50	0.91
M_{hub}									1	0.00	0.50	-0.50	0.00
L_{tower}										1	-0.87	1.00	0.50
D_{tower}											1	0.00	0.63
M_{tower}												1	0.65
H_{hub}													1

As shown in the table, correlation between the nacelle mass and other variables is higher, as is the correlation of the nacelle length, including hub length, with other variables. However, it is important to consider that the data set is relatively small, and further research would be needed to determine whether the found correlations are representative.

Overall, it is confirmed that there is (some) correlation between different variables of offshore wind turbines, it is important to establish the exact relationship between the turbine properties. The design of a wind turbine directly depends on the rated power, which, in turn, is linked to a function of the squared rotor diameter, as indicated in the equation on page 120. To understand how other mass and size properties scale with increased turbine size, scaling laws have been established primarily using the independent variable rotor diameter (D_{rotor} or D). Two approaches, described in [69], have been employed:

1. **Heuristic engineering fit** with $y = cx^d + f$, where x is the independent variable and the exponent d is constant and based on expected geometric upscaling from physical laws or literature. Coefficients c and f are unknown and f is non-zero for linear scaling;

2. **Best power fit** with $y = ax^b$, where coefficients a and b are unknown.

The unknown coefficients have been determined by fitting curves through the data points. The coefficient of determination (R^2) indicates how well the curves fit the data. Table 3.5 shows the derived scaling laws. Figure 3.6 displays two examples of these fits. The validity of the obtained fits has been verified by a wind turbine manufacturer, who confirmed that the fits align with their expectations for next-generation turbines.

Table 3.5: Scaling laws for each parameter based on a heuristic engineering approach and best power fit, based on the database with 23 offshore wind turbine models.

Parameter	Heuristic engineering fit	R²	Best power fit	R²
P_{rated}	-	-	-	-
D_{rotor}	$5.98 \times 10^{1} \cdot P_{rated}^{0.5}$	0.913	$6.02 \times 10^{1} \cdot P_{rated}^{0.497}$	0.913
L_{blade}	$4.86 \times 10^{-1} \cdot D^{1} + 0.113$	1.000	$4.89 \times 10^{-1} \cdot D^{0.999}$	1.000
M_{blade}	$1.16 \times 10^{-3} \cdot D^{2}$	0.903	$5.58 \times 10^{-3} \cdot D^{1.707}$	0.929
$L_{nacelle} + L_{hub}$*	$8.23 \times 10^{-2} \cdot D^{1} + 2.112$	0.819	$1.66 \times 10^{-1} \cdot D^{0.890}$	0.815
$B_{nacelle}$*	$7.03 \times 10^{-2} \cdot D^{1} - 4.433$	0.834	$1.47 \times 10^{-3} \cdot D^{1.658}$	0.882
$H_{nacelle}$	$6.13 \times 10^{-2} \cdot D^{1} - 2.136$	0.719	$1.98 \times 10^{-2} \cdot D^{1.175}$	0.703
$M_{nacelle}$	$1.20 \times 10^{-2} \cdot D^{2}$	0.866	$1.59 \times 10^{-2} \cdot D^{1.947}$	0.867
M_{hub}	$2.76 \times 10^{-3} \cdot D^{2}$	0.584	$1.08 \times 10^{-3} \cdot D^{2.174}$	0.588
L_{tower}	$3.80 \times 10^{-1} \cdot D^{1} + 39.328$	0.730	$4.27 \times 10^{0} \cdot D^{0.622}$	0.735
D_{tower}	$3.89 \times 10^{-2} \cdot D^{1} + 0.766$	0.888	$6.38 \times 10^{-2} \cdot D^{0.924}$	0.885
M_{tower}	$3.07 \times 10^{-2} \cdot D^{2}$	0.624	$5.89 \times 10^{-2} \cdot D^{1.880}$	0.626
H_{hub}	$4.68 \times 10^{-1} \cdot D^{1} + 32.540$	0.822	$2.56 \times 10^{0} \cdot D^{0.737}$	0.822

* Only the direct and semi-direct drive turbines were used for this parameter. The complete database, with all drive types, produced fits with an R^2 below 0.02, which is too low.

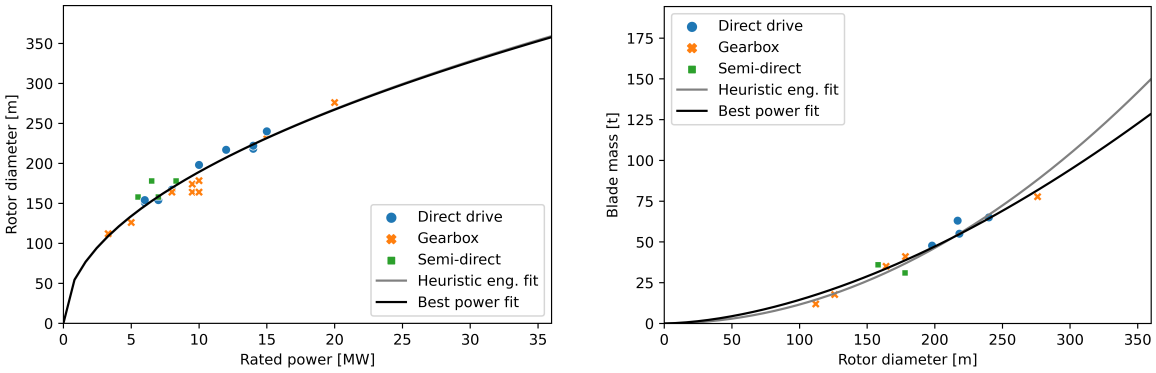

Figure 3.6: Example scaling laws for (a) rated power and (b) blade mass.

The following subsections provide a detailed description of the identified trends in the components, along with the reasoning behind the coefficients.

Rotor and blades

The available power in wind and the rated power of a wind turbine depend on various factors, including wind speed, rotor diameter, and efficiency. Theoretically, the rated power exhibits a quadratic relationship with rotor diameter, as depicted in Equation A.2.1. As a result, the rotor diameter has a square root dependency to the rated power. Hence, $P^{0.5}$ is used in the heuristic engineering fit. However, for the best power fit, the scaling exponent is slightly lower than the theoretical value (0.497). This difference could be attributed to factors associated

with the effects of aerodynamic, elastic, inertial, or gravitational forces [70].

Following normal scaling laws, the blade length must scale linearly with the rotor diameter. This is also confirmed. According to normal scaling laws, the mass of turbine blades should increase with the cube of the length. However, due to improved aerodynamic performance, the use of more advanced materials, and improved manufacturing, the mass of turbines blades has historically only increased to a power between 2 to 2.5 [71], [72]. For larger turbines, the blade mass scales with an even lower exponent. This is demonstrated in Table 3.5, aligning with findings presented in [69].

Nacelle

The mass of the nacelle primarily depends on the mass of its components, which typically includes the nacelle structure, drive train, generator, brake, controller, yaw system, and electronics [73]. Among these components, the drive train and generator contribute the most to the nacelle's mass. The choice of drive train, whether with a gearbox or direct-drive, significantly influences the mass of the nacelle. Gearbox are used between the rotor and the generator to increase the rotational speed, allowing for the use of high-speed, low-torque generators. These generators are relatively small, lightweight, and inexpensive. This technology originates from land-based wind turbines [74]. However, gearboxes can be susceptible to reliability issues, which is disadvantageous for offshore wind farms due to the limited accessibility and higher maintenance costs. As a result, direct-drive configurations have been introduced. However, direct-drive systems tend be larger and heavier due to the size and mass of the generator required for low-speed, high-torque power generation [75]. These generators are generally also more expensive [69]. Analysis of the database showed that larger and most recent turbines mostly have direct-drives. This is also visible in Figure 3.7. The nacelle mass follows roughly quadratic scaling. The exponent for the best power fit is lower, having a value of 1.947. This is in accordance with the scaling exponent reported by [69].

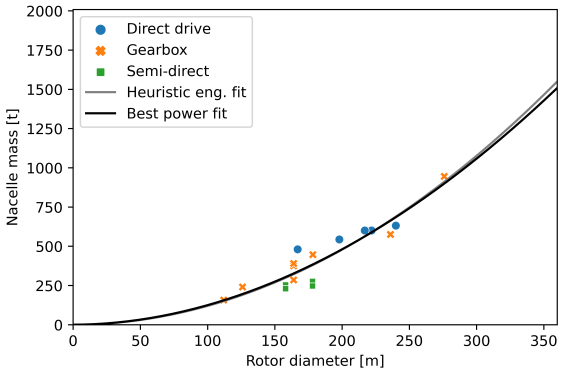

Figure 3.7: Scaling laws for nacelle mass

The dimensions of the nacelle are influenced by the components housed inside it. Although no specific scaling laws regarding nacelle dimensions are found in literature. The best power fits provide the closest fit to the data points, exhibiting acceptable coefficients of determination for the length, breadth, and height of the nacelle.

Tower

Information about tower properties is limited due to their strong dependency on the installation site and the used type of foundation [69]. Additionally, towers should be designed in such a way that the natural frequency does not coincide with the blade passing or rotational frequency of the turbine. Initially, linear scaling laws were expected for linear tower dimensions, including

length, base diameter, and hub height, with the rotor diameter, following conventional scaling laws. However, fitting of the data points, especially from the generic reference turbines, revealed that the exponent for the best power fit is lower than 1 for the tower length and base diameter. The base diameter often follows a stepwise regime [17], rounded to whole meters rather than decimal values. This could be a contributing factor to the less accurate fit.

The heuristic engineering and best power fits can be used to estimate the properties of larger, next-generation wind turbines. These estimates can then be incorporated in the uncertainty model of *Blended Design*, which aims to account for market uncertainties and include the component properties in the forecasting.

Center of gravity of components

The CoG of the individual components is important to determine the CoG of the total deck cargo, for among others, ship stability. Information on the CoG of offshore wind turbine components is not publicly available. Therefore, geometry-based assumptions will be made. A wind turbine tower is typically tapered with a decreasing diameter along the the height of the tower. At the bottom and top of a turbine tower the wall thicknesses are largest, due to the loads at the bottom and yaw system at the top. In between, the wall thickness typically decreases over the height [17], [76]. Consequently, the CoG is expected to be below half the height of the tower. For the generic 12 MW turbine in [17], the CoG was calculated to be at around 41 percent of the tower height. This percentage will be adopted for this research. CoGs of the hub and nacelle are assumed to be at the center of the components. Wind turbine blades are complex three dimensional geometries. The CoG of turbine blades is typically located between the 25 and 35 percent chord line [77]. In this research, the value of 35 percent of the blade length has been chosen to adopt for the location of CoG. Figure 3.8 and Table 3.6 present an overview of the assumed CoG locations for this research.

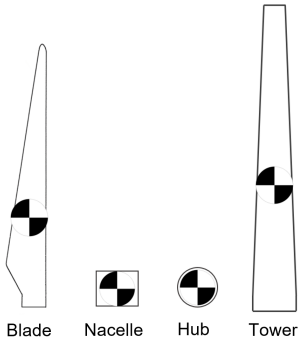

Figure 3.8: Visualization of assumed CoG locations.

Component	CoG location	Reference
Tower	41% of tower height	From tower base
Nacelle	Center	-
Hub	Center	-
Blade	35% of blade length	From blade root

Table 3.6: Overview of assumed CoG locations.

3.4.3. Development package 3 - Deck layout

The deck layout is a combination of the location of the crane, positioning of the components, and the preferred installation location, either at the stern or side. The deck layout plays an important role in the design of *Moonshot* and is important to consider for logistics, stability, and motion behavior. By choosing the best deck layout, wind turbine installation can be enhanced, improving installation efficiency and safety. There are many options, but it is important to start by exploring different solutions of transporting the components and how they are normally transported on a ship.

Handling of tower
The tower of an offshore wind turbine is typically transported vertically [22], [78] for several reasons. Since the towers are tapered, they are normally manufactured in sections that are stacked on top of each other. Constructing a tapered structure horizontally could be challenging. Also, it would be inefficient if the constructed tower had to be laid flat again to be transported horizontally by the WTIV, to be upended again at the offshore installation site. It is also questionable whether the long and slender turbine towers would be strong enough to be upended, and not bend, deform, or even break during the procedure. Ideally, the entire tower is transported as a single piece, but if it is too heavy or tall, it may need to be divided into multiple sections for transportation [22].

Handling of nacelle and hub
The nacelle is a heavy component but has a relatively compact size and shape. Typically, the hub and nacelle are transported as a single component. During transportation, the nacelle is bolted onto a dedicated transport frame made from steel beams. This deck may be welded to the deck of the WTIV [22], [39]. It is important to note that nacelles are never stacked on top of each other.

Handling of blades
Turbine blades are commonly stored in blade racks, which are used to support the blades in a horizontal position during transportation. The blade racks allow for stacking of the blades and can be oriented either in a transverse or longitudinal direction. On jack-up vessels, transverse placement is often preferred. This is illustrated in Figure 3.9

Figure 3.9: Picture of the blade rack on *Aeolus, from [79]*.

Jack-up vessels are generally wider than conventional monohull vessels. Given the significant increase in the size of future wind turbine blades compared to the current ones, transverse storage would result in a very large protrusion over the sides of the vessel. This poses risks such as potential collisions. Hence, it is assumed that transverse storage of the blades may not be feasible on *Moonshot*.

Wind turbine blades are lifted using specialized lifting tools or yokes. Typically, the contact points are located around the center of gravity of the blade to ensure an evenly distributed load and balanced lift. The lifting tools are often controlled remotely, allowing to control the lift without the need for manual sling-handling or working on heights [22], [80]. There are various types of lifting tools available, and ongoing developments aim to improve them.

Layouts
Many options exist with regard to crane positioning and component placement on the deck of the ship design. Therefore, a small study will be conducted to determine the best deck layout for *Moonshot*. This study will involve creating and evaluating multiple layouts. The

components of 15 MW turbine and a typical *UDSBV* design will be used. The evaluation will be based on several key points, including:

- Port logistic and transit
  - Loading
  - Transit
- Offshore operations
  - Tower lifting
  - Nacelle lifting
  - Blade lifting
  - Assembly lifting
- Capacity
  - Number of turbines
  - Efficient deck space use
- Motions
  - Assembly location
  - Installation location

The logistics and operations points address the efficiency of the lifts and the challenges related to lifting the components in the different deck layouts. Furthermore, capacity is about the number of 15 MW turbines that could be transported and how efficient the deck space is used. Additionally, the motion behavior of the turbine in both the assembly location and installation position of the different layouts will be assessed. The optimal deck layout for *Moonshot* will be determined by assessing the evaluation scores of each layout on these key points. The following assumptions will be taken into account when developing the deck layouts:

- Nacelles can be moved horizontally across the deck using a skidding system;
- Towers cannot be moved across the deck and must, therefore, be within reach of the crane during offshore operations. The maximum lifting radius for a tower lift is assumed to be 50 meters;
- To minimize the risk of losing control of the blades due to the wind, it is preferable to install the blades in the same orientation as they are located on deck and lifted. The airfoil shape of the blades makes them susceptible to wind, and turning the blades during installation increases the chances of encountering the unfavorable wind angles, increasing the risk of losing control;
- The complete wind turbine assembly, with its large size and three delicate blades extending outward, should be lifted with caution and minimal rotation.

The following section will cover the developed deck layouts, meeting the set assumptions and demonstrating the greatest potential to become the optimal deck layout for *Moonshot*. In the process of creating these layouts, 18 potential deck layout were drawn. These were developed and evaluated in collaboration with naval architects and a product manager from *UDSBV*. The other, non-feasible deck layouts, accompanied by commentary, are displayed in Appendix E.

Layout 1 - Crane at the side

The first deck layout is shown in Figure 3.10. In this layout, the wind turbine is assembled on and installed over the side of the vessel. The crane is located slightly inward of the side of the vessel to make sure the crane does not obstruct the blades when assembly. Otherwise, the assembly area should be located more outward of the vessel. The blade only has to be translated towards the assembly location. The installation direction of the blades is also indicated in the figure. After the first blade is installed, the hub is rotated 120 degrees to facilitate the installation of the second blade, which is common practice. After the first set of blades is installed, the consecutive blades require bigger rotation from the crane and the blades. To mitigate this, it would be beneficial to consider a solution for relocating the blades to the first stack location by, for example, using a smaller deck crane. The blades are positioned

aft of the crane, extending over the stern. Deck space and the ship length are in this way efficiently used. Table 3.7 presents the scores of deck layout 1 scores on the established key points.

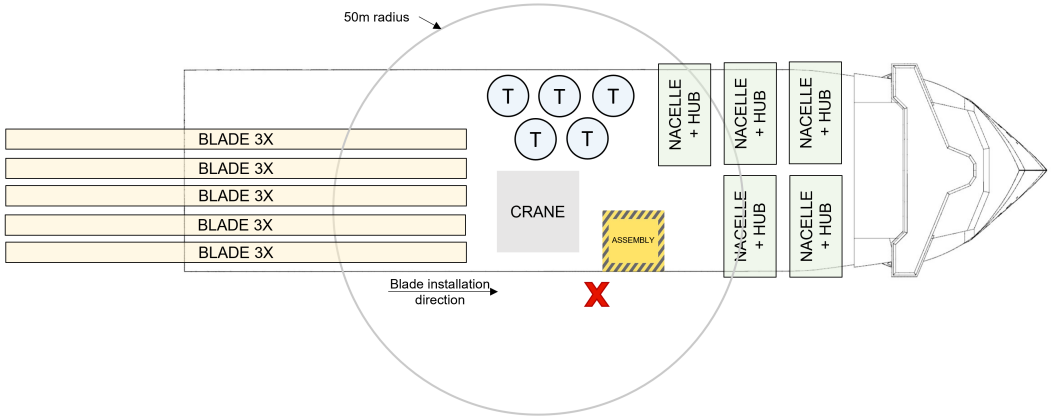

Figure 3.10: Deck layout 1 showing the positioning of components, crane, assembly location, and installation position.

Table 3.7: Evaluation of deck layout 1.

Key point	Explanation	Score
Port logistics and transit		
Loading	No challenges	✓
Transit	When crane is in storage position, it is likely that boom protrudes over the bow, potentially obstructing the vision from bridge. Challenging to fit boomrest.	✓
Offshore operations		
Tower lifting	All towers in 50m range. Crane slewing 90 degrees.	✓
Nacelle lifting	Skidding required. Crane slewing <90 degrees.	✓
Blade lifting	Only translation of blades needed, no rotation. Additional equipment for restacking blades or special blade lifting tool required.	✓
Assembly lifting	-	✓
Capacity		
Number of turbines	Components for 5 turbines.	✓
Efficient deck space use	PS aft unused but could potentially be used for lifting tools.	✓

Layout 2 - Crane at stern

The second deck layout is shown in Figure 3.11. In this layout, the crane and assembly location are located at the stern, and installation is performed over the stern of the vessel. The blades are positioned between the accommodation area and the crane. The blades are positioned in such a way that they do not have to be rotated during installation. However, a drawback of this layout is that a large part of the lifting range of the crane is outside the vessel. Consequently, the deck area that is within the lifting range is limited, limiting the cargo that can be transported and lifted. Table 3.8 presents the scores of deck layout 2 scores on the established key points.

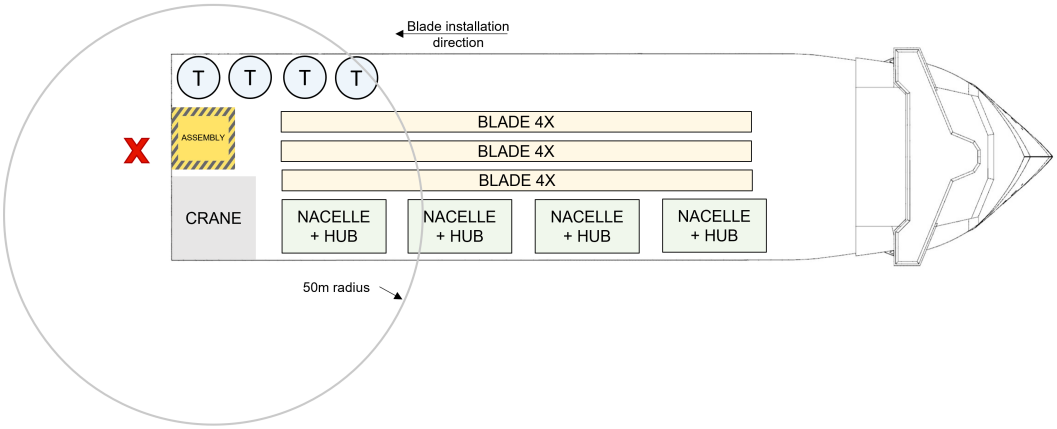

Figure 3.11: Deck layout 2 showing the positioning of components, crane, assembly location, and installation position.

Table 3.8: Evaluation of deck layout 2.

Key point	Explanation	Score
Port logistics and transit		
Loading	No challenges	✓
Transit	No challenges	✓
Offshore operations		
Tower lifting	All towers in 50m range. Crane slewing <90 degrees.	✓
Nacelle lifting	Skidding required. Crane slewing ≈90 degrees.	✓
Blade lifting	Only translation of blades needed, no rotation.	✓
Assembly lifting	Risk of collision with 2nd tower.	✓
Capacity		
Number of turbines	Components for 4 turbines.	✓
Efficient deck space use	Deck behind accommodation and at PS unused.	✓

Layout 3 - U-stern

Layout 3 features a U-stern recess in the aft of the vessel. The patent pending U-Stern has recently been developed by *UDSBV* for monopile installation. For monopile installation, the U-stern enables longitudinal pile upending in the ship centerline. While the U-Stern offers advantages for monopile installation, such as perfect weathervaning with stern operation, improved control by pile upending, and a sheltered installation position, not all of the benefits apply to wind turbine installation due to the difference in procedures and challenges involved. The primary expected benefit of a U-Stern for wind turbine installation could be improved motion behavior, as the assembly and installation locations are more towards the center of the vessel. The U-Stern, as shown in the deck layouts, is a conceptual representation to demonstrate the idea. The exact dimensions have not been determined yet. Two deck layouts with a U-Stern have been created.

Layout 3A

The first layout with a U-Stern is depicted in Figure 3.12. A drawback of this layout is that the ship length limits the turbine size that could be transported due to the tight fit between assembly location and accommodation of the blades. To accommodate longer blades, the vessel length would increase proportionally with the blade length. Another issue is that positioning of the towers near the near the installation position of the wind turbine, poses a significant collision risk during installation. Given the large size of the complete assembly, with the blades

extending outward, there is a high potential for collision between the assembly and the towers. Therefore, it is advisable that the area surrounding the installation site remains clear of towers to minimize the risk. Table 3.9 presents the scores of deck layout 3A on the established key points.

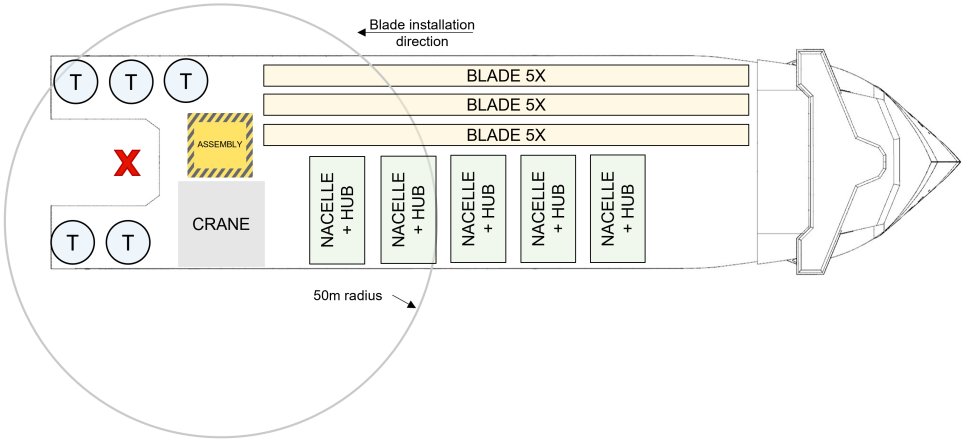

Figure 3.12: Deck layout 3A showing the positioning of components, crane, assembly location, and installation position.

Table 3.9: Evaluation of deck layout 3A.

Key point	Explanation	Score
Port logistics and transit		
Loading	No challenges	✓
Transit	No challenges	✓
Offshore operations		
Tower lifting	All towers in 50m range. Crane slewing <90 degrees	✓
Nacelle lifting	Skidding required. Crane slewing ≈90 degrees.	✓
Blade lifting	Only translation of blades needed, no rotation.	✓
Assembly lifting	Towers around installation position. Risk of collision.	✗
Capacity		
Number of turbines	Components for 5 turbines.	✓
Efficient deck space use	Deck area efficiently used.	✓

Layout 3B

Based on the insights gained from layout 3A, a fourth layout has been made, without towers around the installation location. In this new layout, the towers have been repositioned to the SB side of the vessel and the nacelles have been rotated and placed between the blade racks and the towers. To accommodate this, the blade racks extend over the side of the vessel. Layout 3B is displayed in Figure 3.13. A drawback of this layout is that allows for the transport of only four 15 MW turbines. Additionally, the towers must be slewed within the space between crane and blades, as it can be assumed that lifting the towers over the blade racks would not be feasible. Table 3.10 presents the scores of deck layout 3B scores on the key points.

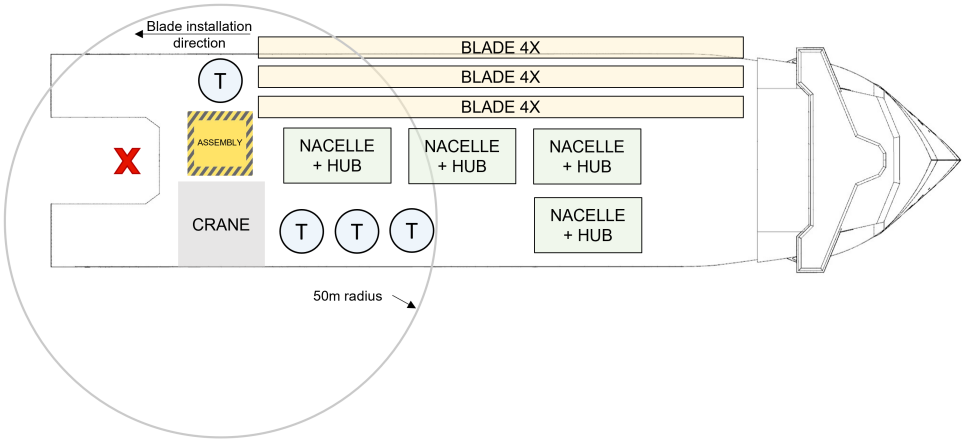

Figure 3.13: Deck layout 3B showing the positioning of components, crane, assembly location, and installation position.

Table 3.10: Evaluation of deck layout 3B.

Key point	Explanation	Score
Port logistics and transit		
Loading	No challenges	✓
Transit	Blades extending over the side. Not deemed to be much of an issue	✓
Offshore operations		
Tower lifting	All towers in 50m range.	✓
Nacelle lifting	Skidding and crane slewing <90 degrees. Nacelles must be rotated 90 degrees.	✓
Blade lifting	Only translation of blades needed, no rotation.	✓
Assembly lifting	-	✓
Capacity		
Number of turbines	Components for 4 turbines.	✓
Efficient deck space use	Large unused deck area.	✓

Motion analysis of all deck layouts

A motion analysis of all deck layouts was conducted under two loading conditions: a fully-loaded condition and a condition where the last turbine is lifted. These loading conditions primarily differed in terms of displacement, draft, and metacentric height. The analysis was performed using hydrodynamic analysis software from the *SESAM* software package, developed by classification society DNV [81]. The used modules from the package included *GeniE* for creating a numerical panel model of the hull and *HydroD* for modelling the environment and hydrodynamic analysis in the frequency domain, employing *WADAM* as a solver.

The calculations were done for a significant wave height of 2.5 meters with wave peak periods (T_p) in accordance with DNVGL-RP-C205 *Recommended practice for environmental conditions and environmental loads* [82]. Ten different T_p values were included, ranging from 4.1s ($2.6\sqrt{H_s}$) to 7.9s ($5.0\sqrt{H_s}$), with increments of 0.4s. The wave spectrum used was the Joint North Sea Wave Project (JONSWAP) spectrum with a peak enhancement factor (γ) of 3.3. The JONSWAP spectrum is commonly used for describing ocean waves statistically and is based on measurements of wave data from the North Sea.

To assess the seakeeping behavior for the different deck layouts, the most probable maximum (MPM) local motion-induced displacements were calculated at the hub height for both the assembly and installation locations. The MPM value represents the maximum value of

a variable with the highest probability of occurring over a specified time period. In this case, the MPM displacements were determined for a three-hour period, which is commonly used in the offshore industry as it is normally the average duration of a sea state. Therefore this time period allows for a good representation of the motions during a typical sea state.

It is assumed that the vessel is allowed to weathervane with a maximum heading offset of 30 degrees on either side during offshore operations, as shown in Figure 3.14. Weathervaning refers to aligning the bow of the vessel with the incoming environment; waves, current, and wind. This reduces vessel motions and the power required for station keeping.

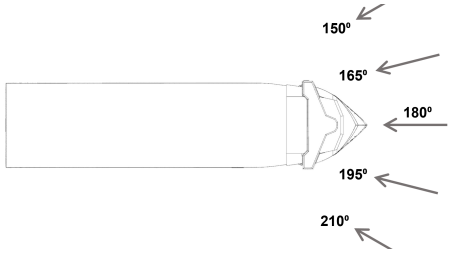

Figure 3.14: Visualization of weathervaning.

Table 3.11 displays the results of the seakeeping analysis for the different deck layouts, showing MPM displacements in the hub at both the assembly and installation locations for the two loading conditions. Layout 3A and 3B have identical assembly and installation locations, resulting in similar motion behavior. Therefore, the motion behavior of these two layouts can be considered to be comparable. It is important to note that the focus of the motion analysis focuses is on the variations between the different layouts, rather than the absolute results.

Table 3.11: Results of motion analysis for all deck layouts. The table shows MPM motion displacements.

		Fully-loaded			Lifting last turbine			
	Position	Long. Motion [m]	Trans. Motion [m]	Vertical Motion [m]	Long. Motion [m]	Trans. Motion [m]	Vertical Motion [m]	Score
Layout 1	Assembly	1.60	0.26	0.57	1.73	0.45	0.60	✓
	Installation	1.68	0.26	0.58	1.80	0.45	0.61	
Layout 2	Assembly	1.54	0.47	0.93	1.68	0.62	1.04	✗
	Installation	1.54	0.59	1.19	1.68	0.71	1.33	
Layout 3	Assembly	1.54	0.32	0.62	1.68	0.51	0.68	✓
	Installation	1.54	0.43	0.83	1.68	0.59	0.93	

Deck layout 2 demonstrates the worst seakeeping behavior. The benefit of using a U-Stern over stern installation is clearly visible when comparing layout 3 to deck layout 2. Deck layouts 1 and 3 show comparable motion behavior, with deck layout 3 performing slightly better in the longitudinal direction. Deck layout 1 demonstrates better results in both transverse and vertical direction, particularly at the installation position.

Evaluation of all deck layouts

Table 3.12 summarizes the scores of all deck layout scores based on the key points. The scores are rated on a scale from 1 to 5, with weights assigned to the key points to reflect their relative importance. For instance, blade and assembly lifting are deemed more critical compared to tower and nacelle lifting.

Table 3.12: Evaluation of all deck layouts.

		Layout			
Key point	Weight	1	2	3A	3B
Port logistics and transit					
Loading	3	5	5	5	5
Transit	3	4	5	5	5
Offshore operations					
Tower lifting	4	4	5	5	5
Nacelle lifting	4	5	4	4	4
Blade lifting	5	4	5	5	5
Assembly lifting	5	5	4	2	5
Capacity					
Number of turbines	4	5	4	5	4
Efficient deck space use	3	4	3	5	3
Motions					
Assembly location	4	5	2	4	4
Installation location	4	5	2	4	4
Total weighted score		180	152	168	165

After evaluating all four deck layouts, it is concluded that layout 1, installation over the side, would be the most favorable deck layout for *Moonshot*. This layout will be further used throughout this research.

3.5. Chapter conclusion

This chapter introduced the design process for the development of *Moonshot*. The approach combines *Controlled Innovation* and *Blended Design*. Initially, it was unclear which parts of the design process would be best suited for *Controlled Innovation* and where *Blended Design* should be used. To address this, *Controlled Innovation* was employed to establish the high-level objective and functions of the design. Subsequently, the underlying design aspects associated with the functions were identified. Following a systematic approach, the design aspects have been evaluated on uncertainty of their requirements and the consequence on the design. In this way, high-risk design aspects, requiring extra focus or knowledge generation, were identified. Eventually, a differentiation between those design aspects has been made whether they could be covered in development packages, which are part of the *Controlled Innovation* process, or that a design aspect could be covered in *Blended Design*. Three designs aspects that needed knowledge generation within development packages were identified, including the lifting equipment, turbine component properties, and optimal deck layout. Requirements of other high-risk design aspects were found to be best addressed with *Blended Design*.

The three development packages were also covered in this chapter. The conclusion of the development package about lifting equipment was that a combination of a free-hanging and guided lift solution, such as *Huisman*'s *Zephyr* crane concept, would be the preferred solution for *Moonshot*. In the second development package, correlations between size and mass properties of wind turbine components were investigated with data on wind turbine models and literature. Correlations between most of the parameters were found. Based on the data points, fitting curves were established. These curves can later be used for extrapolation to estimate the size and mass properties of next-generation wind turbine components. Also, CoG locations of wind turbine components were identified. The third development package explored various deck layouts. Following an extensive analysis of different options on various criteria, the research concluded that the most favorable deck layout would have the lifting equipment and assembly location on the side of the vessel, with installation of the turbine over the side. The results from the development packages will be used in the subsequent stages of this research and integrated in *Blended Design*.

4

Blended Design for Moonshot

As previously discussed, *Blended Design* will be employed to explore the design space of *Moonshot* and to obtain optimal ship parameters, based on financial and seakeeping performance. As discussed, the existing model is not ready to use for *Moonshot* yet. The existing model was created for vessels with different cargo. Also, the needs of the *Moonshot* design will be different and other performances have to be investigated. The objective of this chapter is therefore to formulate an answer to the sub-question: *"What modifications to Blended Design are needed to properly explore the design space for Moonshot and evaluate financial and seakeeping performance?"*.

4.1. Solution approach

To prepare *Blended Design* for *Moonshot*, existing assumptions and functions required to be updated or changed. Furthermore, new functionalities are added. Figure 4.1 shows the new *Blended Design* model as used for the assessment of *Moonshot*. The figure also shows the connection between different functions of the entire model.

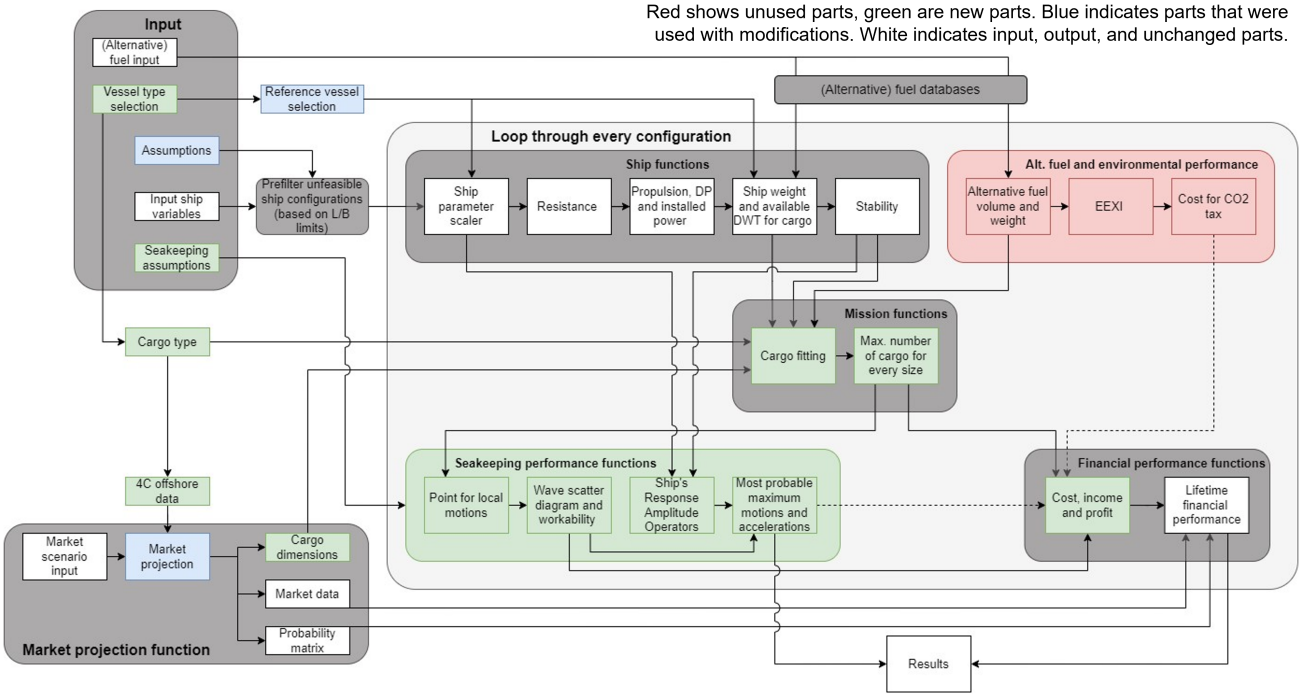

Figure 4.1: Integration of functions for *Moonshot* in *Blended Design*.

For this research, the environmental performance of *Moonshot* will not be taken into consideration. As a result, alternative fuel and environmental performance functions of *Blended Design* will be switched off. In the following part, the new and modified parts of the model will be discussed.

- **Vessel and cargo type selection** - To facilitate the implementation of *Moonshot* in *Blended Design*, the existing code has been modularized to allow the analysis of different vessels and cargo types. The modularization allows the user to specify what type of vessel and cargo to analyze. The model then selects the relevant functions and input. This adaption also provides future benefits to *UDSBV*, as it eases the ability to seamlessly integrate other vessel and cargo types.
- **Seakeeping performance and assumptions** - Since the seakeeping performance is a whole new functionality of *Blended design*, a separate section will be dedicated for the adopted method for evaluating seakeeping performance evaluation, along with the underlying assumptions. This can be found in Section 4.2.
- **Market projection functions** - First of all, the market database had been updated with the most recent *4C Offshore* OWF data from February 24, 2023. The existing code determined the development of monopile diameters over the years for the market projections. A new function has been added that filters the turbine capacity from the market data and establishes the evolution of turbine capacity over the years. Also, the relations from Section 3.4.2 have been integrated in the market projection. In this way, the model calculates the dimensions and mass of components for each turbine size that could occur in a market scenario. These properties are ultimately used in the mission functions of *Blended Design*.
- **Mission functions** - The mission functions calculate the cargo capacity of a given ship configuration for all possible cargo sizes within a certain market scenario. The process of calculating the maximum number of wind turbine components differs significantly from assessing monopiles. Because of this, a new mission module for wind turbines is created. This new module is explained in Section 4.3.
- **Assumptions and reference vessel** - When using *Blended Design*, the user has the flexibility to decide which fuel types are used in the analysis. As the current research excludes environmental performance, no alternative fuels will be taken into account. Hence it is assumed that the vessel will operate on marine diesel oil (MDO).

  Furthermore, the user can specify the number of operational days per year. It is assumed that the vessel will be available for projects 300 days annually. The remaining 65 days are allocated for repairs, maintenance, and relocation of the vessel.

  In addition, in the existing model the user can specify the workability as input. In the new model, this number will be calculated based on a selected wave scatter diagram and the desired maximum significant wave height, which is a new input parameter. The determination of workability using the wave scatter diagram and the input will be explained in Section 4.2.

  The most recent version of the HX118 design will be used as reference vessel, serving as a basis for determining ship coefficients for scaling when creating different ship configurations.
- **Cost, income, and profit** - To calculate the harbour and installation times, number of trips per year, and the number of installed turbines per year , wind turbine installation cycle times have been established. A detailed breakdown of the envisioned operational cycle for *Moonshot* is provided in Appendix H.

In *Blended Design*, vessels can either be rewarded via charter contracts (fixed income per day) or by installation contracts (income per MW installed). For the purpose of this project, assuming a fixed day rate would be unfair. This is because smaller vessels would then have the same income as larger vessels in a market, even though smaller vessels might not be able to transport and install larger wind turbines. This would nullify the competitive position of larger installation vessels. Therefore, a more reasonable approach is to compensate vessels based on the quantity and size of turbines they install. Under installation contracts, all vessels will receive rewards for each MW installed.

Information about installation contracts or rates per MW installed for WTIVs is not publicly available. Therefore, this rate has been estimated with information on charter rates, particulars of purpose-built jack-up vessels, and their estimated cycle times. This estimation is explained in Appendix I. The calculated reward is approximately **45,000 €/MW**. it is important to note that this reward is only an approximation to measure the relative merit between the different ship configurations in *Blended Design*. This method was chosen to make sure that the number is based on realistic numbers and falls within the right order of magnitude. The approximated rate was validated with [83], which states that the costs for turbine installation are typically around 50,000 £/MW (corresponding to 58,500 €/MW at an exchange rate of 1.17 £/€).

4.2. Method for seakeeping analysis

Currently, *Blended Design* lacks the capability to determine and assess seakeeping behavior. Environmental factors contributing to operational disturbances, and consequently ship motions, include wind, waves, current, and tides [82]. To evaluate seakeeping behavior, the analysis will only focus on first-order wind-generated waves. Originally, the intention was to include a workability assessment in *Blended Design*. However, the main challenge with this approach is to find the operational motion limits for the installation process. Given that the installation method and lifting equipment of *Moonshot* will be different from existing vessels, the the operational limits for this design would be unknown. For example, *Moonshot* aims to perform blade installation with a controlled lift to mitigate swinging or movement during mating with the hub. Additionally, motion compensation may be employed during the installation of the complete assembly onto the foundation. Without operational limits, a comprehensive workability assessment of each of the design configurations in the design space cannot be conducted. Therefore, an alternative approach has been proposed. Figure 4.2 illustrates the proposed approach for determining seakeeping behavior with *Blended Design*.

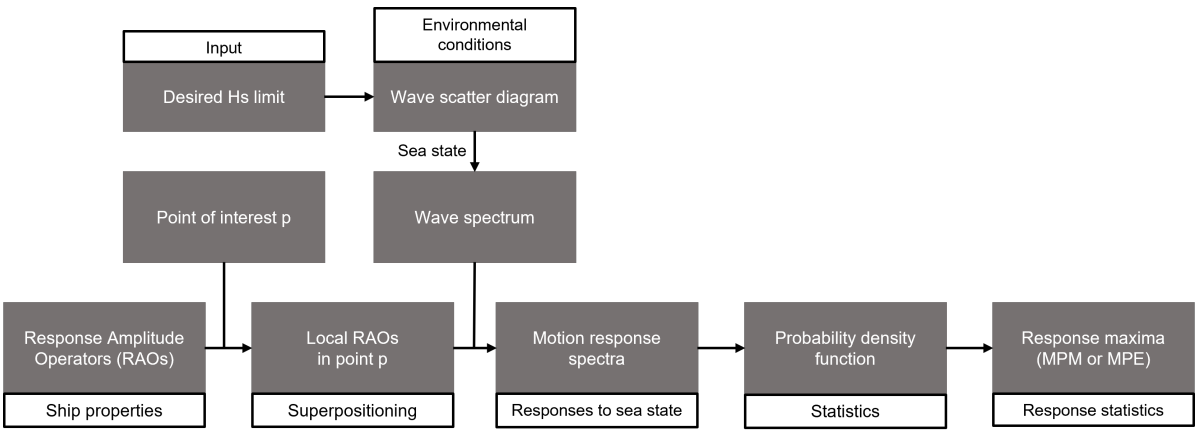

Figure 4.2: The proposed approach for determining seakeeping behavior with *Blended Design*.

The output of this approach aims to provide data on the response maxima for the most-occurring sea state within the operational range of a vessel configuration. Users would be able to specify the operational range by setting a desired significant wave height (H_s) limit, such as 2.5 meters, according to the set requirements from Section 1.1.2. The upcoming sections will provide details on the procedure and underlying assumptions. Furthermore, the challenge of obtaining the RAOs for every ship configuration will be addressed.

4.2.1. Definition of motions

The six ship motions and the axis convention are defined as shown in Figure 4.3.

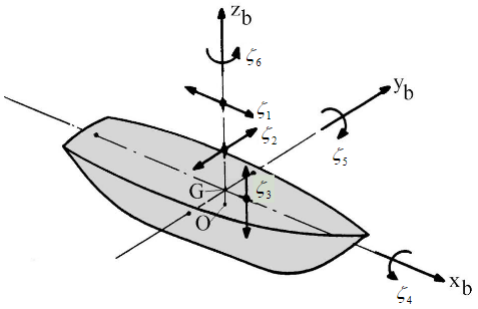

Figure 4.3: Definition of ship motions in six degrees of freedom, from [84].

- Three translations of the ship's CoG in the direction of the x-, y- and z-axes:
  - Surge (ζ_1) in the longitudinal x-direction, with positive values towards the bow;
  - Sway (ζ_2) in the lateral y-direction, with positive values to port side;
  - Heave (ζ_3) in the vertical z-direction, with positive values upwards.
- Three rotations about the axes:
  - Roll (ζ_4) around the x-axis, with positive values representing right-turning motion;
  - Pitch (ζ_5) around the y-axis, with positive values representing right-turning motion;
  - Yaw (ζ_6) around the z-axis, with positive values representing right-turning motion.

Environmental directions, such as waves, are measured counterclockwise starting with 0 degrees at the stern (following sea) and 180 degrees at the bow (head sea). It is important to also note that motions will be treated as linear in this analysis. This allows for the use of transfer functions and superposition to obtain the motion response in irregular waves.

4.2.2. Response Amplitude Operators

Response Amplitude Operators (RAOs) are frequency-dependent transfer functions that describe the relation between incoming regular waves and the linear response of a vessel in a specific motion direction. This relationship is represented by Equation 4.1.

$$RAO_i(\omega) = \frac{\zeta_{a_i}(\omega)}{\zeta_a(\omega)} \tag{4.1}$$

where ω is the angular wave frequency, ζ_{a_i} the motion amplitude, and ζ_a the wave elevation amplitude. The RAO is influenced by the characteristics and shape of a floating body. Typically, the RAO consists of the terms depicted in Equation 4.2.

$$RAO_i(\omega) = \frac{|F_{ex,i}|}{\sqrt{\left[c_i - (m_i + a_i)\omega^2\right]^2 + \left[b_i\omega\right]^2}} \tag{4.2}$$

in which the wave excitation force $F_{ex,i} = F_{w,i} + F_{d,i}$, is the combination of the undisturbed wave (Froude-krylov) force or moment and the diffraction force or moment. a, b, and c are the

added mass, damping, and restoring spring terms.

Various methods are available for calculating the RAOs and evaluating motion behavior. The most-used methods include strip theory and 3D boundary element methods (BEM). Strip theory can be further subdivided into 2D and 2.5D strip theory. In 2D strip theory, a ship's hull is divided into a finite number of transverse 2D sections its length. The shape of each slice closely relates to the corresponding hull segment. The 3D potential problems are then approximated by 2D problems in the transverse planes. This method yields reliable results for the ship motions for conventional hull shapes with a relatively low calculation time. 2D strip theory is particularly suited for low ship speeds, head waves, and at high wave frequencies. [85]. 2.5D strip theory is an enhancement of 2D strip theory, improving accuracy of the results in general and for higher ship speeds [86]. 3D BEM includes more advanced methods, such as Wave Green's Function or Rankine Source [86], and involves discretizing the hull and free surface into a mesh of panels. The 3D potential flow problems are solved by satisfying boundary conditions of the body and free surface. 3D BEMs are capable of solving more complex hull shapes and provide more accurate results than strip theory methods. However, these methods are more computationally intensive [85], [87].

All of these methods have in common that they require the hull-form geometry to calculate the RAOs. However, this specific information is unavailable during the early-design stage and, as a result, is not included in *Blended Design*. Moreover, these methods could result in very long calculation times when calculating seakeeping behavior for numerous ship configurations. Consequently, the described methods will not be applicable. Instead, a simpler method which only depends on ship parameters is needed. Two papers that describe methods fulfilling this requirement were identified. One of these papers presents closed-form expressions (CFEs) to estimate the RAOs, while the other uses simple formulas to estimate the Froude-Krylov forces and moments, which are substantial components of the RAOs. In both methods, the coupling effects between different motions, such as roll-pitch, surge-heave etc., are not considered. In general, often a trade-off exists between simplicity and accuracy of calculation methods. Figure 4.4 illustrates this relationship.

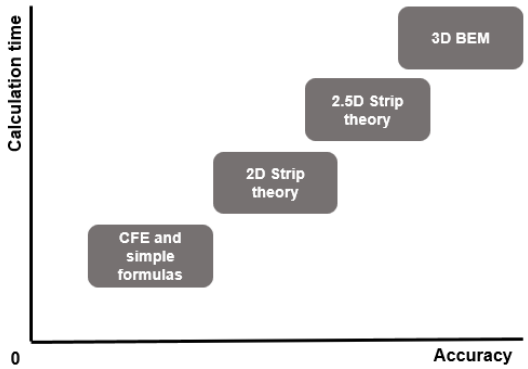

Figure 4.4: Comparison of different seakeeping analysis methods on accuracy and calculation time.

Closed-form expressions by Jensen

The paper by Jensen et al. [88] introduces a semi-analytical approach for estimating the RAOs for **heave**, **pitch**, and **roll** wave-induced motions of monohull vessels. The estimation method relies on closed-form expressions (CFEs).

The RAOs for heave and pitch motions are derived analytically by assuming the vessel to be a homogeneously loaded box and applying linear strip theory. The method also assumes

a constant sectional added mass equal to the displaced water. The equations of motions in regular waves with unit wave amplitude are then expressed as follows:

$$2\frac{kT}{\omega^2}\ddot{\zeta_3} + \frac{A^2}{kB_0C_b\alpha^3\omega}\dot{\zeta_3} + \zeta_3 = F_3\cos(\omega_e t) \tag{4.3}$$

$$2\frac{kT}{\omega^2}\ddot{\zeta_5} + \frac{A^2}{kB_0C_b\alpha^3\omega}\dot{\zeta_5} + \zeta_5 = F_5\sin(\omega_e t) \tag{4.4}$$

where ζ_3 and ζ_5 are the heave and pitch motion. The time derivative is denoted with a dot. ω and ω_e are respectively the wave frequency and encounter frequency. $k = \omega^2/g$ is the wave number. A represents the wave sectional hydrodynamic damping, which is approximated by a dimensionless ratio between the incoming and diffracted wave amplitudes. α represents the Doppler shift, which would be 1 for zero-speed. To account for the actual ship-shape of a vessel, instead of a box-shaped vessel, the maximum beam on the waterline of the vessel B_0 is multiplied by the block coefficient C_b.

$$RAO_3 = \frac{|F_3|}{\sqrt{(1-2kT\alpha^2)^2 + \left(\frac{A^2}{kB_0C_b\alpha^2}\right)^2}} \tag{4.5}$$

$$RAO_5 = \frac{|F_5|}{\sqrt{(1-2kT\alpha^2)^2 + \left(\frac{A^2}{kB_0C_b\alpha^2}\right)^2}} \tag{4.6}$$

The CFEs for determining the RAOs for heave and pitch motion (Equation 4.5 and 4.6) require input parameters such as: length (L), breadth (B_0), draft (T), block coefficient (C_b), waterplane coefficient (C_{wp}), forward speed (V_s), transverse metacentric height ($\overline{GM_t}$), and wave heading angle (β). These inputs are either already input values of the existing *Blended Design* or could be calculated by it. All RAOs will be calculated during the wind turbine installation process. This implies that the vessel is performing DP operations and is stationary. Therefore, forward speed will be zero, which implies that the encounter frequency (ω_e) is equal to the wave frequency (ω).

To calculate the RAO for roll motion, a more complex model is used compared to heave and pitch. The ship is simplified to two prismatic breams with a draft T, but different breadths B_0 and B_1. The ratio between the two breadths is such that the waterplane coefficient C_{wp} of the actual hull matches that of the simplified model. An additional parameter δ, representing a fraction of the length L, must be specified. δ cannot be greater than C_{wp}. The simplified model to estimate the roll RAO is shown in Figure 4.5.

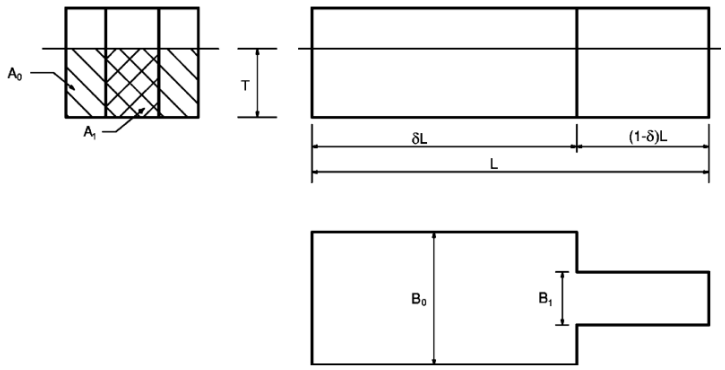

Figure 4.5: Simplified ship model used in roll motion analysis, from [88].

The equation of motion for roll in regular waves with unit wave amplitude, as established by Jensen et al., is formulated as:

$$\left[\frac{T_{n,roll}}{2\pi}\right]^2 c_{44}\ddot{\zeta_4} + b_{44}\dot{\zeta_4} + c_{44}\zeta_4 = F_4 \tag{4.7}$$

where $T_{n,roll}$ is the natural roll period. The solution to the equation of motion gives the RAO for roll. This is shown in Equation 4.8.

$$RAO_4 = \frac{|F_4|}{\sqrt{\left[-\omega_e(T_{roll}/2\pi)^2 + 1\right]^2 c_{44}^2 + \omega_e^2 b_{44}^2}} \tag{4.8}$$

To determine the RAO for the roll motion, additional input parameters are needed. These parameters are: roll natural period ($T_{n,roll}$) and delta (δ). The influence of the value for δ on the resulting RAO was found to be not significant. Therefore, for this project, the value will be set at 0.95% of C_{wp}.

Determine natural roll period

The natural roll period an essential parameter for determination of the roll RAO but is not known and cannot be directly calculated by *Blended Design*. To address this and calculate it for every configuration in *Blended Design*, a simple and fast estimation method for the natural roll period is needed. Various empirical methods exist to estimate a ship's natural roll period. However, these were found to not be a good fit for *UDSBV*'s offshore vessels. As a result, the following formula was adopted to determine the roll natural period, denoted as $T_{n,roll}$.

$$T_{n,roll} = 2\pi\sqrt{\frac{I_{xx} + a_{44}}{\rho g \nabla \overline{GM_t}}} \tag{4.9}$$

where I_{xx} is the moment inertia around x-axis and a_{44} the roll added mass. As the hull shapes of the different configurations in *Blended Design* are unknown, it is not possible to calculate a_{44} exactly. It would also be too time-consuming. Therefore, the relation between the added mass and main dimensions of 25 *UDSBV* designs has been investigated. Eventually, a trend line was established with draft as the independent variable. The moment of inertia around the x-axis can be calculated with the formula below. According to [89], the radius of gyration can be estimated using the empirical ratio of k_{xx} and B. It was determined that the most suitable fit *UDSBV* designs would be 0.4. This conclusion was validated using 25 different loading conditions of *UDSBV* designs.

$$I_{xx} = k_{xx}^2 \cdot \Delta \tag{4.10}$$
$$0.35 < k_{xx}/B < 0.45$$

where k_{xx} is the radius of gyration around the x-axis, Δ the ship's displacement, and B the breadth of the ship.

Limitations

The closed-form expressions have some accuracy limitations. The limitations, as identified by the author of the paper, are as follows:

- Heave response is too small for wavelengths larger than the ship length ($\lambda/L > 1$);
- Pitch response is too large where wave length is around the same as the ship length ($\lambda/L = 1$) for Froude numbers larger than 0.2;
- Roll motion is too large around the resonance frequency;
- Only valid for deep water.

Validation

Jensen et al. describe a validation process for the CFEs in their paper. They conducted a comparison of the results obtained for various ship using model tests and strip theory. Their conclusion was that the established CFEs provided reasonably accurate estimates for the three RAOs. In this research, the results from the CFEs are also validated for a *UDSBV* design. The three RAOs were computed for an HX104 design with the following main particulars: L = 185.0 m, B_0 = 36 m, T = 7 m, C_b = 0.777, $\overline{GM_t}$ = 5m, V_s = 0 m/s. Below, the obtained results are validated with the actual RAOs as calculated with hydrodynamic analysis software (HAS).

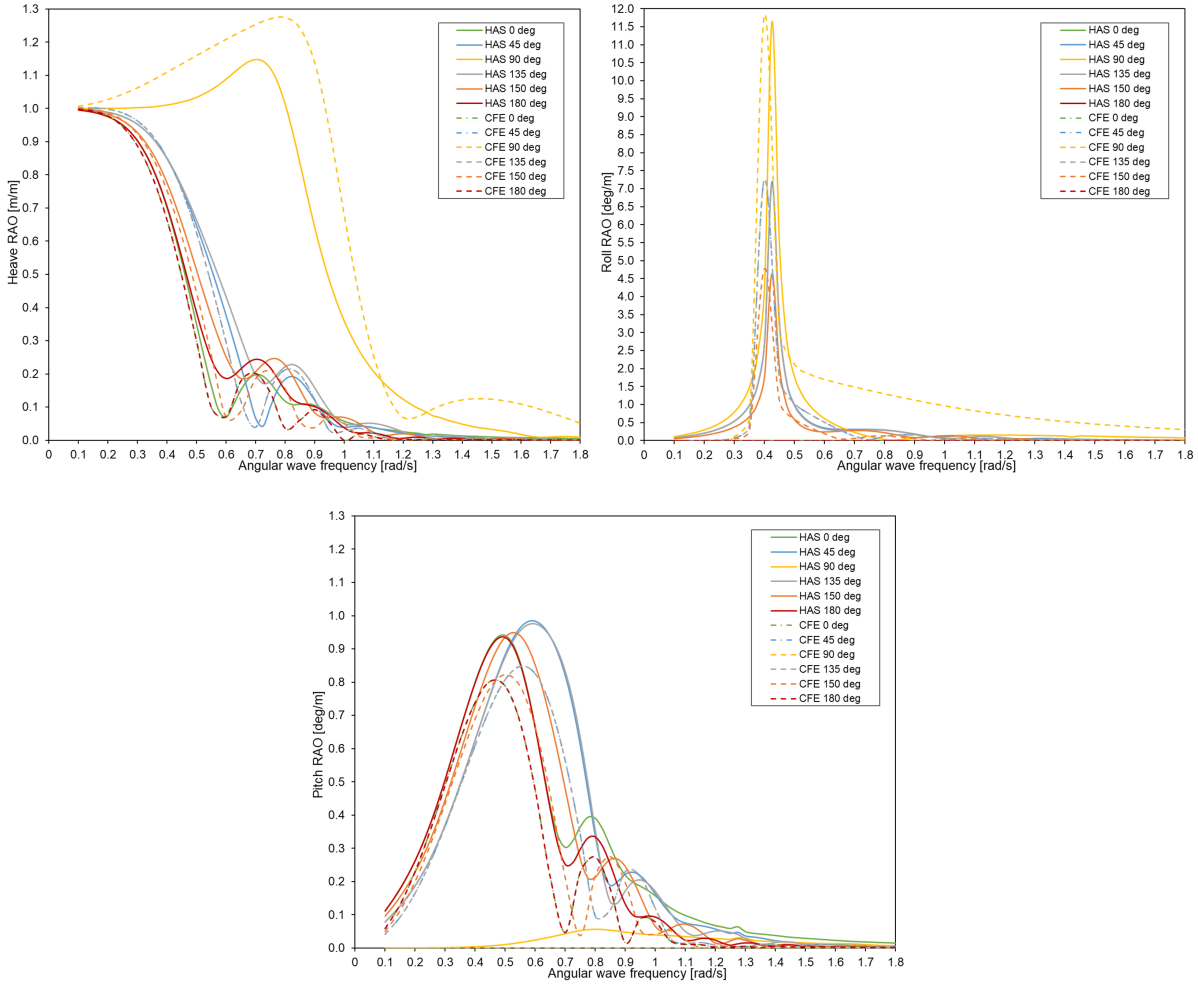

Figure 4.6: Heave, roll, and pitch RAOs of HX104 as function of wave frequency for different headings. Continuous lines represent calculated results from CFE by Jensen et al. Dashed lines are results from *HydroD* hydrodynamic analysis software.

The plots reveal that the RAOs for the three motions, as calculated using the CFEs, do not exactly match the outcomes obtained from hydrodynamic analysis software (HAS). Nonetheless, upon visual inspection, they appear to be remarkably similar. The trajectory of the RAOs calculated with the CFEs aligns with the behavior of the RAOs from HAS. The amplitudes of the motion RAOs appear to be around the same angular wave frequency, and the order of magnitude of the RAOs falls within the same range. What stands out is that the method is not very accurate for beam seas (wave heading angles of 90 or 270 degrees). The RAO for pitch motion is underestimated due to neglecting coupling effects. For shorter waves the RAO for roll motion is too high.

In addition to visually comparing the resulting RAOS from the two methods, the results were also validated through other means. The first one involved comparing the areas under the different RAO curves. The area under an RAO curve is associated with the amount of transferred energy. These areas were calculated for both methods and compared for all different wave headings. The results are presented in Table 4.1.

Table 4.1: Comparison of the areas under RAO curves for results from HAS and CFEs.

			Wave heading angle										
	Method		**0°**	**15°**	**30°**	**45°**	**60°**	**90°**	**120°**	**135°**	**150°**	**165°**	**180°**
Heave	HAS	[s^{-1}]	0.41	0.42	0.44	0.48	0.57	0.93	0.61	0.51	0.46	0.43	0.42
	CFE	[s^{-1}]	0.38	0.39	0.41	0.47	0.57	1.13	0.57	0.47	0.41	0.39	0.38
	Error		**-9%**	**-8%**	**-5%**	**-3%**	**1%**	**21%**	**-6%**	**-8%**	**-10%**	**-11%**	**-11%**
Roll	HAS	[deg/ms]	0.00	0.24	0.49	0.72	0.93	1.11	0.90	0.70	0.48	0.24	0.00
	CFE	[deg/ms]	0.00	0.19	0.41	0.66	0.97	2.04	0.97	0.66	0.41	0.19	0.00
	Error		**0%**	**-21%**	**-16%**	**-9%**	**4%**	**84%**	**8%**	**-5%**	**-14%**	**-20%**	**0%**
Pitch	HAS	[deg/ms]	0.47	0.47	0.47	0.49	0.51	0.04	0.52	0.48	0.44	0.42	0.41
	CFE	[deg/ms]	0.33	0.33	0.35	0.39	0.45	0.00	0.45	0.39	0.35	0.33	0.33
	Error		**-30%**	**-29%**	**-25%**	**-20%**	**-12%**	**-100%**	**-13%**	**-19%**	**-20%**	**-20%**	**-21%**

The table shows the areas under each of the various RAO curves for different wave headings.

As displayed, the CFEs tend to underestimate the area under the RAO curves in comparison to the RAOs obtained from HAS. This implies that there is a difference in the total transferred energy across the entire range angular wave frequencies. The disparities between the two methods are most pronounced in beam seas. Therefore, the simplified method does not yield reliable results in that case.

Another way to validate the RAOs from CFEs is to compare the standard deviation (σ) of the resulting response spectra. This is because the distribution of the area under the RAO curves is also important to take into account. Therefore, the differences in transferred energy do not provide the complete picture. To incorporate the distribution into the validation, response spectra were calculated for all RAOs in a specific sea state. Details on calculating the wave and response spectrum can be found in later sections.

For the validation, a JONSWAP wave spectrum with $\gamma = 3.3$ and a significant wave height H_s of 2.5 meters was used. Wave spectra were computed for wave peak periods T_p of 4, 7, and 12 seconds, enabling an investigation of differences in the response standard deviations at various wave frequencies. The response spectra for the different motions and wave headings were then calculated, and the standard deviations of those spectra were determined. Standard deviation is the square root of the variance or area under the spectrum. Table 4.2 presents the Standard deviations of the calculated response spectra for different wave headings and motions. Only the results for a wave peak period of 7 seconds are displayed here. The results for other T_p values can be found in Appendix F.

Table 4.2: Comparison of the standard deviation (σ) of the response spectra at $T_p = 7s$, calculated using the RAOs from HAS and CFEs.

		Wave heading angle										
	Method	**0°**	**15°**	**30°**	**45°**	**60°**	**90°**	**120°**	**135°**	**150°**	**165°**	**180°**
Heave	HAS [m]	$5.8{\cdot}10^{-2}$	$5.7{\cdot}10^{-2}$	$5.9{\cdot}10^{-2}$	$6.8{\cdot}10^{-2}$	$8.0{\cdot}10^{-2}$	$3.9{\cdot}10^{-1}$	$1.1{\cdot}10^{-1}$	$8.8{\cdot}10^{-2}$	$7.3{\cdot}10^{-2}$	$6.5{\cdot}10^{-2}$	$6.3{\cdot}10^{-2}$
	CFE [m]	$4.2{\cdot}10^{-2}$	$4.4{\cdot}10^{-2}$	$4.9{\cdot}10^{-2}$	$7.2{\cdot}10^{-2}$	$8.4{\cdot}10^{-2}$	$5.7{\cdot}10^{-1}$	$8.4{\cdot}10^{-2}$	$7.2{\cdot}10^{-2}$	$4.9{\cdot}10^{-2}$	$4.4{\cdot}10^{-2}$	$4.2{\cdot}10^{-2}$
	Error	**-26%**	**-23%**	**-16%**	**7%**	**5%**	**46%**	**-21%**	**-18%**	**-32%**	**-32%**	**-32%**
Roll	HAS [deg]	0.0	$7.7{\cdot}10^{-4}$	$1.4{\cdot}10^{-3}$	$2.0{\cdot}10^{-3}$	$2.4{\cdot}10^{-3}$	$1.3{\cdot}10^{-3}$	$2.0{\cdot}10^{-3}$	$2.0{\cdot}10^{-3}$	$1.5{\cdot}10^{-3}$	$8.5{\cdot}10^{-4}$	0.0
	CFE [deg]	0.0	$3.2{\cdot}10^{-4}$	$7.2{\cdot}10^{-4}$	$1.2{\cdot}10^{-3}$	$2.0{\cdot}10^{-3}$	$1.1{\cdot}10^{-2}$	$2.0{\cdot}10^{-3}$	$1.2{\cdot}10^{-3}$	$7.2{\cdot}10^{-4}$	$3.2{\cdot}10^{-4}$	0.0
	Error	**0%**	**-59%**	**-49%**	**-38%**	**-17%**	**735%**	**-1%**	**-36%**	**-51%**	**-62%**	**0%**
Pitch	HAS [deg]	$2.5{\cdot}10^{-3}$	$2.5{\cdot}10^{-3}$	$2.6{\cdot}10^{-3}$	$3.0{\cdot}10^{-3}$	$5.0{\cdot}10^{-3}$	$4.7{\cdot}10^{-4}$	$5.1{\cdot}10^{-3}$	$2.9{\cdot}10^{-3}$	$2.3{\cdot}10^{-3}$	$2.0{\cdot}10^{-3}$	$1.9{\cdot}10^{-3}$
	CFE [deg]	$1.3{\cdot}10^{-3}$	$1.4{\cdot}10^{-3}$	$1.8{\cdot}10^{-3}$	$2.1{\cdot}10^{-3}$	$4.2{\cdot}10^{-3}$	0.0	$4.2{\cdot}10^{-3}$	$2.1{\cdot}10^{-3}$	$1.8{\cdot}10^{-3}$	$1.4{\cdot}10^{-3}$	$1.3{\cdot}10^{-3}$
	Error	**-46%**	**-42%**	**-32%**	**-29%**	**-15%**	**-100%**	**-17%**	**-27%**	**-22%**	**-28%**	**-30%**

The results indicate that the standard deviations and variances of the response spectra are also underestimated when using RAOs calculated with CFEs. The error is most pronounced for roll and pitch motion, with the standard deviation of the response spectra being more than 50 percent too low in this case. In beam seas, the error is particularly high for roll motion. When comparing the standard deviations of the response spectra for different T_p values, it can be observed that the error in the standard deviations decreases as wave periods increase, or wave frequencies decrease.

The validation demonstrates that a visual comparison of the RAOs alone does not provide a complete assessment of the accuracy of the method proposed by Jensen et al. Nevertheless, despite the observed differences in total transferred energy and the standard deviation of the response spectra, the method does provide results that are in the correct order of magnitude. Also, it is important to keep in mind the primary purpose of the method for determining the RAOs, which is to assess seakeeping behavior within *Blended Design* and predict the relative merits of various ship configurations. In this context, the method appears to be applicable. However, absolute results obtained from this method should be interpreted with caution.

Simplified formulas for Froude-Krylov force

The aforementioned method is only capable of calculating RAOs for three of the six degrees of freedom. Unfortunately, no comparable methods to the method by Jensen et al. were found in literature to estimate the surge, sway, and yaw RAOs. The only alternative approach is described in a paper by Matsui et al. (2021) [90]. This paper proposes simple formulas to determine the linear Froude-Krylov forces for the six degrees of freedom. A detailed explanation on the method, application, and a validation can be found in Appendix J. Visual validation of the estimated Froude-Krylov forces showed that they resemble the Froude-Krylov forces computed by HAS to a certain extend. However, other terms such as the diffraction force, added mass, hydrodynamic damping, and spring are also required to calculate the RAOs. The paper only focused on determination of the forces, so the other terms needed to be calculated using other methods. Unfortunately, no other alternative methods for estimating the diffraction forces were found. RAOs without the diffraction component were compared to RAOs from HAS, and it was observed that the results could not be used. This is also discussed in Appendix J. Ultimately, the decision was made to omit the remaining three RAOs from the seakeeping assessment module. The influence of excluding them is expected to be relatively small, as the RAO values from HAS for surge, sway, and yaw motions were found to be almost zero for higher wave frequencies. These wave frequencies were found to be the most common waves, according to wave scatter diagrams. This is also discussed in the Appendix.

4.2.3. Local RAOs

The RAOs are calculated in the CoG of the vessel. When linearizing for small motions, the independent RAOs can be translated to local motions in a point P through superpositioning. This is shown in Equation 4.11.

$$\begin{aligned} x_p(t) &= \zeta_1(t) - y_{bp}\zeta_6(t) + z_{bp}\zeta_5(t) \\ y_p(t) &= \zeta_2(t) + x_{bp}\zeta_6(t) - z_{bp}\zeta_4(t) \\ z_p(t) &= \zeta_3(t) - x_{bp}\zeta_5(t) + y_{bp}\zeta_4(t) \end{aligned} \tag{4.11}$$

where x_p, y_p, and z_p are the local motions in the x-, y-, and z-direction in point P. The coordinates of point P with respect to the original of the coordinate system are denoted with x_{bp}, y_{bp}, and z_{bp}. ζ_i represents the six ship motions. The terms that will not be used because of the omission of three of the six RAOs are marked with gray.

The phase angles $\epsilon_{\zeta_i,\zeta}$ of the RAOs are not known. Therefore, it is assumed that the phases of all motions are such that the maximum motions occur simultaneously. The resulting RAO in each of the three directions is then the sum of the associated RAOs in combination with the coordinates of point P with respect to the origin of the coordinate system, which is located at the the CoG of the ship. This approach is chosen as it yields the most conservative results. This leads to the following formulas to determine the local RAOs in point P for the three directions of motion.

$$\frac{x_{pa}}{\zeta_a}(\omega) = \left|\frac{\zeta_{1a}}{\zeta_a}(\omega)\right| + \left|y_{bp}\frac{\zeta_{6a}}{\zeta_a}(\omega)\right| + \left|z_{bp}\frac{\zeta_{5a}}{\zeta_a}(\omega)\right| \tag{4.12}$$

$$\frac{y_{pa}}{\zeta_a}(\omega) = \left|\frac{\zeta_{2a}}{\zeta_a}(\omega)\right| + \left|x_{bp}\frac{\zeta_{6a}}{\zeta_a}(\omega)\right| + \left|z_{bp}\frac{\zeta_{4a}}{\zeta_a}(\omega)\right| \tag{4.13}$$

$$\frac{z_{pa}}{\zeta_a}(\omega) = \left|\frac{\zeta_{3a}}{\zeta_a}(\omega)\right| + \left|x_{bp}\frac{\zeta_{5a}}{\zeta_a}(\omega)\right| + \left|y_{bp}\frac{\zeta_{4a}}{\zeta_a}(\omega)\right| \tag{4.14}$$

where $\frac{x_{pa}}{\zeta_a}$, $\frac{y_{pa}}{\zeta_a}$, and $\frac{z_{pa}}{\zeta_a}$ are the local motion RAOs in point P. $\frac{\zeta_{i,a}}{\zeta_a}$ represents the 6 ship RAOs.

For this project, point P will be located at the installation position at the hub height of the largest turbine that occurs in a market and a ship configuration is capable to install during its lifetime. The location of point P is illustrated in Figure 4.7.

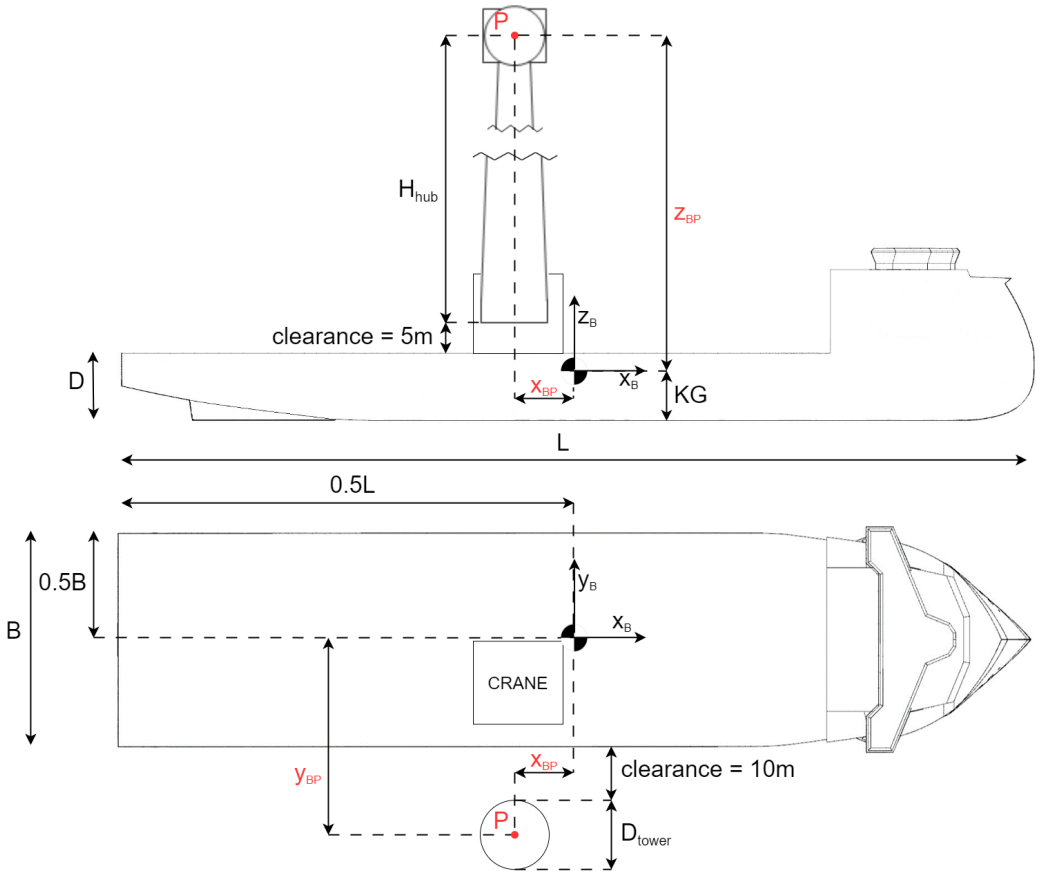

Figure 4.7: Schematic of the location of point P for local motions.

4.2.4. Acceleration RAO

Both displacements and accelerations are crucial in the seakeeping behavior of a vessel. The calculated RAOs represent displacement RAOs. However, it would also be valuable to investigate the acceleration behavior of the different ship configurations.

The accelerations in point P across the three directions can be found by taking the second time derivative of the displacement RAOs. An example for the vertical acceleration RAO in point P is shown in Equation 4.15.

$$\frac{\ddot{z_{pa}}}{\zeta_a}(\omega) = -\omega^2 \frac{z_{pa}}{\zeta_a} \cos(\omega t + \epsilon_{\zeta_{zp},\zeta}) = \omega^2 \frac{z_{pa}}{\zeta_a} \cos(\omega t + \epsilon_{\zeta_{zp},\zeta} + \pi) \tag{4.15}$$

where $\frac{\ddot{z_{pa}}}{\zeta_a}$ is the vertical acceleration RAO in point P. $\frac{z_{pa}}{\zeta_a}$ denotes the vertical displacement RAO in point P. The angle between vertical acceleration and wave elevation is represented by $\epsilon_{\zeta_{zp},\zeta}$. As the phase angles of the RAOs are not known and neglected, the phase angle of the acceleration $\epsilon_{\zeta_{zp},\zeta}$ will also be omitted. The acceleration RAOs can thus easily be calculated with Equation 4.16.

$$R\ddot{A}O = \omega^2 RAO \tag{4.16}$$

4.2.5. Wave scatter diagram

A wave scatter diagram presents the joint probability of significant wave height and wave zero-up-crossing period. First of all, the significant wave height is modeled by a 3-parameter Weibull probability density function. The formula to calculate this probability function f_{H_s} is shown in Equation 4.17.

$$f_{H_s}(H_s) = \frac{\beta_{Hs}}{\alpha_{Hs}} \left(\frac{H_s - \gamma_{Hs}}{\alpha_{Hs}} \right)^{\beta_{Hs}-1} exp\left\{ -\left(\frac{H_s - \gamma_{Hs}}{\alpha_{Hs}} \right)^{\beta_{Hs}} \right\} \tag{4.17}$$

where H_s is the significant wave height. β_{Hs}, α_{Hs}, and γ_{Hs} represent the shape, scale, and location parameters of the Weibull distribution. The zero-up-crossing wave period conditional on H_s can then be represented by the log-normal distribution. The join probability distribution $f_{T_z|H_s}$ is calculated in Equation 4.18.

$$f_{T_z|H_s}(T_z|H_s) = \frac{1}{\sigma T_z \sqrt{2\pi}} exp\left\{ -\frac{(\ln T_z - \mu)^2}{2\sigma^2} \right\} \tag{4.18}$$

where T_z is the zero-up-crossing wave period. μ and σ are dimensionless functions of the significant wave height: $\mu = E[\ln T_z] = a_0 + a_1 H_s^{a_2}$ and $\sigma = std[\ln T_z] = b_0 + b_1^{b_2 H_s}$. The values of parameters α_{Hs}, β_{Hs}, γ_{Hs}, and coefficients a_i and b_i have been derived using measurements and depend on the location for which a wave scatter diagram is desired. The division of nautical zones, for which the wave distribution parameters are available, is shown in Figure 4.8.

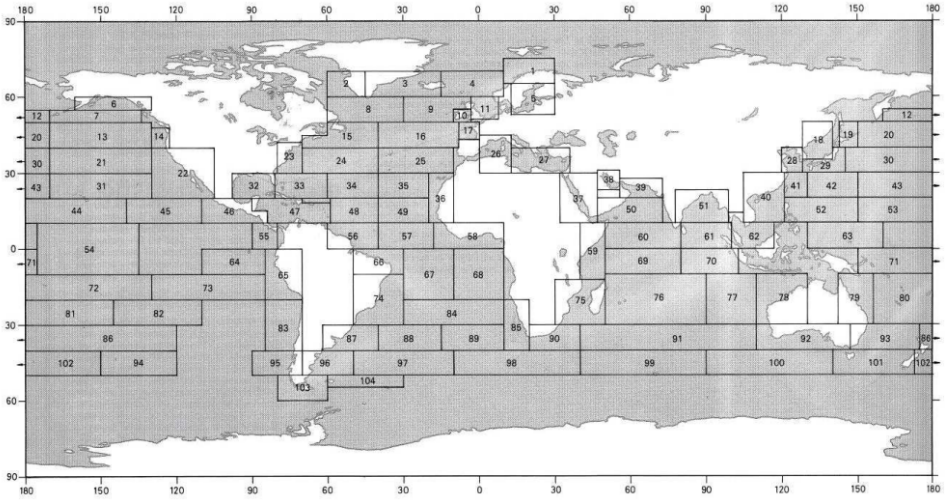

Figure 4.8: Nautical zones for estimation of the wave distribution parameters, from [82].

An example of a wave scatter diagram is shown in Figure 4.9. This wave scatter diagram represents zone 11, which is located in the North Sea. A wave scatter diagram displays the probability of occurrence of a certain sea state, which is a combination of H_s and T_z. In this wave scatter diagram, the sea state with highest probability of occurrence has a significant wave height of less than 1 meter with a zero-up-crossing period of 4 to 5 seconds. Empty cells in the data indicate that the probability of occurrence is approaching zero, which means that the corresponding sea state is highly unlikely to happen at that location.

Percent occurrence	Tz [s] 0.5	1.5	2.5	3.5	4.5	5.5	6.5	7.5	8.5	9.5	10.5	11.5	12.5	13.5	14.5	15.5	Sum
0.5			0.467%	8.780%	14.052%	7.111%	1.972%	0.392%	0.064%	0.010%	0.001%						**32.85%**
1.5			0.009%	1.083%	6.704%	9.701%	6.324%	2.576%	0.786%	0.200%	0.045%	0.010%	0.002%				**27.44%**
2.5				0.133%	1.868%	5.036%	5.401%	3.321%	1.436%	0.493%	0.145%	0.039%	0.010%	0.002%	0.001%		**17.89%**
3.5				0.017%	0.447%	1.954%	3.071%	2.580%	1.449%	0.623%	0.223%	0.070%	0.020%	0.006%	0.001%		10.46%
4.5				0.002%	0.098%	0.650%	1.413%	1.544%	1.078%	0.557%	0.234%	0.085%	0.028%	0.008%	0.002%	0.001%	5.70%
5.5					0.020%	0.195%	0.567%	0.782%	0.662%	0.402%	0.194%	0.079%	0.029%	0.010%	0.003%	0.001%	2.94%
6.5					0.004%	0.054%	0.206%	0.352%	0.355%	0.250%	0.136%	0.062%	0.025%	0.009%	0.003%	0.001%	1.46%
7.5					0.001%	0.014%	0.069%	0.144%	0.172%	0.138%	0.085%	0.042%	0.018%	0.007%	0.003%	0.001%	0.69%
8.5						0.003%	0.022%	0.055%	0.076%	0.070%	0.048%	0.026%	0.012%	0.005%	0.002%	0.001%	0.32%
9.5						0.001%	0.006%	0.019%	0.032%	0.033%	0.025%	0.015%	0.008%	0.003%	0.001%		0.14%
10.5							0.002%	0.007%	0.012%	0.014%	0.012%	0.008%	0.004%	0.002%	0.001%		0.06%
11.5								0.002%	0.005%	0.006%	0.006%	0.004%	0.002%	0.001%	0.001%		0.03%
12.5								0.001%	0.002%	0.002%	0.002%	0.002%	0.001%	0.001%			0.01%
13.5									0.001%	0.001%	0.001%	0.001%	0.001%				0.00%
14.5																	0.00%
15.5																	0.00%
Sum	0.00%	0.00%	0.48%	10.02%	23.19%	24.72%	19.05%	11.77%	6.13%	2.80%	1.16%	0.44%	0.16%	0.05%	0.02%	0.00%	**100%**

Hs [m]

Figure 4.9: Wave scatter diagram calculated for zone 11.
The red-outlined cell shows the sea state of interest for this zone.

By changing the parameters, it is possible to generate wave scatter diagrams for other zones and calculate the most probable sea state. For this research zone 11 will be used.

When designing a vessel, it is common practice to aim for a certain workability or to set the limits up to which it can operate. For *Moonshot*, one of the requirements is that it should be able to operate up to a minimum of 2.0 meters H_s, and preferably higher sea states. This is stated in Section 1.1.2 and based on market research. In the wave scatter diagram, sea states with H_s up to 2.5 meters are highlighted by a black outline. The sum of these occurrences would correspond to a workability of more than 75 percent, which is acceptable. Of the sea states with an H_s of 2.5 meters, a T_z of 6.5 seconds is most-occurring. For this research, this sea state (outlined in red) will be the sea state of interest, assuming that the other sea states with H_s up to 2.5 meters would result in less severe motions.

4.2.6. Wave spectra

An ocean wave cannot be described as a regular sinusoidal wave, but is rather irregular. Hence, it only makes sense to study the characteristics of such a wave in the frequency domain. To analyze ocean waves, a time trace containing many waves is needed. An assumption in the analysis is that the sea can be described as a stationary random process, which means that the signal would repeat itself after each interval. In practice, this time period ranges from 0.5 to about 10 hours. This is called the short-term description of the sea [91]. Linear theory allows the sea surface to be described as a linear superposition of several regular sinusoidal waves. This can be used to decompose the irregular signal and obtain statistical estimations. The wave elevation can then be written as the sum of a number of n wave components, as shown below.

$$\zeta(t) = \sum_{n=1}^{N} \zeta_{an} \cos(\omega_n t + \epsilon_n) \tag{4.19}$$

ζ_{an}, ω_n, and η_n are respectively the wave amplitude, angular wave frequency and random phase angle of a wave component n. In the linear approximation of ocean waves, the instantaneous (at one random moment in time) wave elevation is supposed to be Gaussian distributed with zero mean [92]. The wave amplitudes of the components ζ_{an} can be obtained by Fourier analysis of the wave signal. But, for each shift in time a new series of ζ_{an} will be found. However, a continuous function for the mean square value of ζ_{an} can be found, under the condition that there are no prevailing frequencies in the signal $\zeta(t)$ [93]. This eventually leads to the fact that ζ_{an} can be expressed by a wave spectrum $S(\omega)$, which is defined as:

$$\frac{1}{2}\zeta_{an}^2 = S_\zeta(\omega_n)d\omega \tag{4.20}$$

The variance σ_ζ^2 of the Gaussian distribution equals the area under the wave spectrum, as shown below.

$$\sigma_\zeta^2 = \int_0^\infty S_\zeta d\omega \tag{4.21}$$

The visual representation of the procedure above and the relationship between time domain of the wave signal and the frequency domain representation by a wave spectrum is shown in Figure 4.10

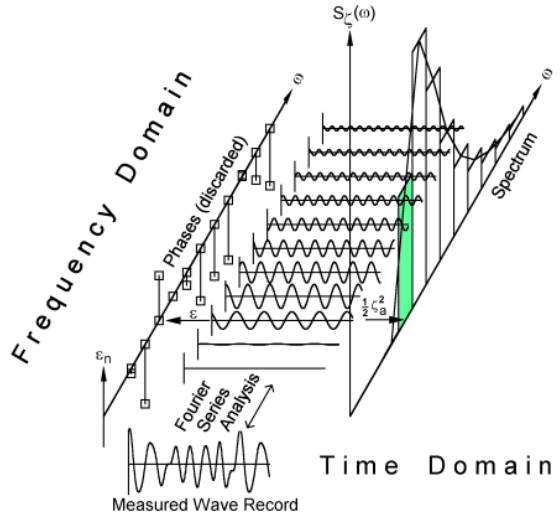

Figure 4.10: From wave signal to wave spectrum, from [93].

Thus, a wave spectrum is a mathematical representation of the distribution of wave spectral density across different wave frequencies. There are various empirical wave spectrum formulations that were derived from wave measurements. One of the most-used wave spectra is the Pierson-Moskowitz spectrum, which was developed in 1964 [94]. This formulation was later extended to the Modified two-parameter Pierson-Moskowitz spectrum, which was accepted in 1969 as the standard for seakeeping calculations [93]. This wave spectrum is particularly suitable for open seas. It assumes a deep sea and a fully developed sea state. Fully developed means that a constant wind has blown for a long time over a long fetch of the sea so that a steady-state and equilibrium with the wind is reached [95]. The mathematical description of the modified two-parameter Pierson-Moskowitz wave spectrum S_{PM} is shown in Equation 4.22.

$$S_{PM}(\omega) = \frac{5}{16} \cdot H_s^2 \omega_p^4 \cdot \omega^{-5} exp\left(-\frac{5}{4}\left[\frac{\omega}{\omega_p}\right]^{-4}\right) \tag{4.22}$$

where ω_p is the angular spectral peak frequency, which is calculated with the peak wave period T_p ($\omega_p = 2\pi/T_p$).

In reality, sea states are rarely fully developed due to non-linear wave-wave interactions [96]. To address this, the JONSWAP spectrum was developed with wave measurements from the North Sea. The JONSWAP spectrum represents a developing wind-generated sea state for a fetch-limited situation [93]. The wave spectrum S_J is defined in Equation 4.23. The JONSWAP spectrum is expressed as the modified Pierson-Moskowitz spectrum multiplied by the dimensionless peak enhancement factor γ. A typical γ value for the North sea is 3.3 [82].

For a fully developed sea state $\gamma = 1$ and the JONSWAP spectrum reduces to the modified Pierson-Moskowitz spectrum.

$$S_J(\omega) = A_\gamma S_{PM}(\omega)\gamma^{exp\left(-0.5\left[\frac{\omega-\omega_p}{\sigma\omega_p}\right]^2\right)} \tag{4.23}$$

where γ is the dimensionless peak enhancement factor. A_γ is a normalizing factor, which is calculated as $1-0.287\ln(\gamma)$. The spectral width parameter σ is calculated as $\sigma = \sigma_a$ for $\omega \leq \omega_p$ and $\sigma = \sigma_b$ for $\omega > \omega_p$.

Average values for the JONSWAP spectrum are σ_a=0.07 and σ_b=0.09 [82]. As noticed form the equations, the wave spectra are calculated for the wave peak period T_p, instead of T_z as is the case for the wave scatter diagram. The zero-up-crossing wave period T_z is related to T_p by the following relations, for $1 \leq \gamma < 7$.

$$\frac{T_z}{T_p} = 0.6673 + 0.05037\gamma - 0.006230\gamma^2 + 0.0003341\gamma^3 \tag{4.24}$$

So for example, when $\gamma = 3.3$ the peak period is $Tp = 1.2859 \cdot T_z$. In this study, the JONSWAP spectrum is used to be able to determine the wave spectrum for every combination of H_s and T_z from the wave scatter diagram. The primary focus is to identify the wave spectrum corresponding to the H_s and T_z combination that has the highest probability of occurrence in the specific nautic zone of interest.

4.2.7. Motion response spectra

A motion response spectrum describes the response to waves of a floating body at different wave frequencies. We know that a wave spectrum S_ζ can be defined as:

$$S_\zeta(\omega)d\omega = \frac{1}{2}\zeta_a^2(\omega) \tag{4.25}$$

where ω is the angular wave frequency and ζ_a the wave elevation amplitude. With this knowledge, the spectrum of the response in different motion directions can be derived. The steps are shown in Equation 4.26. Eventually, the response spectrum of a motion can be found by using the RAO of that motion and the wave spectrum, as expressed in Equation 4.27.

$$\begin{aligned} S_{\zeta_i}(\omega)d\omega &= \frac{1}{2}\zeta_{a_i}^2(\omega) \\ &= \left|\frac{\zeta_{a_i}(\omega)}{\zeta_a(\omega)}\right|^2 \cdot \frac{1}{2}\zeta_a^2(\omega) \\ &= \left|\frac{\zeta_{a_i}(\omega)}{\zeta_a(\omega)}\right|^2 \cdot S_\zeta(\omega)d\omega \end{aligned} \tag{4.26}$$

$$S_{\zeta_i}(\omega) = |RAO_i(\omega)|^2 \cdot S_\zeta(\omega) \tag{4.27}$$

where S_{ζ_i} is the motion response spectrum, ζ_{a_i} the motion amplitude, and S_ζ the wave spectrum. The response spectrum displays the response for every value of angular wave frequency. With the motion response spectra it is possible to determine response maxima in every motion direction.

4.2.8. Response maxima

To assess the seakeeping characteristics of the ship configurations, it is important to predict the highest response value within an irregular sea state within a certain time period. This can

be done with probability distributions. The first step in determining the relationship between the response spectra and statistics can be found by calculating the spectral moments. The n^{th} order spectral moment is computed using the formula:

$$m_n = \int_0^\infty \omega^n \cdot S(\omega) d\omega \tag{4.28}$$

The square root of the zeroth order spectral moment provides the standard deviation σ_S of the spectrum ($\sigma_S = \sqrt{m_0}$). A good approximation for the distribution of the response maxima can be obtained using a Rice distribution function. The probability distribution depends on the standard deviation of the spectrum and spectral width parameter. When the spectral width parameter $\epsilon = 0$, the Rice distribution reduces to the Rayleigh distribution. The spectral width parameter ϵ, which depends on m_n, the n^{th} order spectral moment, can be obtained by means of Equation 4.29.

$$\epsilon = \left[1 - \frac{m_2^2}{m_0 m_4}\right]^{\frac{1}{2}} \tag{4.29}$$

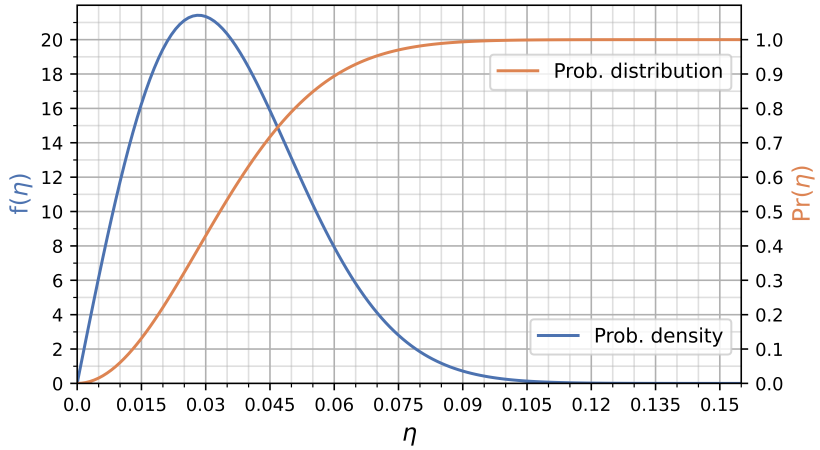

Figure 4.11: Rayleigh PDF and CDF (ϵ=0) of responses for m_0=8.02·10^{-4}.

Figure 4.11 illustrates a Rayleigh probability density function (PDF) and cumulative distribution function (CDF), representing the occurrence and probability of responses during one cycle of an irregular wave. Typically, the most probable largest values are calculated for a number of observations n within a time interval T. For spectral width parameter values where $\epsilon \leq 0.9$, the most probable largest value in n observations of a random process, as given in [97], is calculated with Equation 4.30.

$$\eta_n = \sigma_S \left[2 \ln\left(\frac{2\sqrt{1-\epsilon^2}}{1+\sqrt{1+\epsilon^2}} \cdot \frac{n}{\alpha}\right)\right]^{1/2} \tag{4.30}$$

where η_n is the most probable largest value of a random process. This depends on the standard deviation of the spectrum σ_S and number of zero-up-crossing wave periods n, which is calculated as $n = T/T_z$. Time interval T is 3 hours for the offshore industry as it is normally the average duration of a sea state. T_z is the zero-up-crossing wave period.

The most probable largest response of a random process also depends on a risk factor α. This variable is the probability that an extreme value will exceed η_n. For example, with $\alpha = 1$, the most probable maximum (MPM) value is calculated. This is the most-likely maximum response that will occur within the specified time interval T. The MPM response value typically has a 63 percent probability of being exceeded [98]. On the other hand, with $\alpha = 0.01$, the

exceedance probability is only 1 percent. This value is commonly referred to as the most probable extreme (MPE). A PDF and CDF for n response observations is depicted in the figure below. Additionally, the MPM and MPE values with an α of respectively 1.0 and 0.01 are displayed.

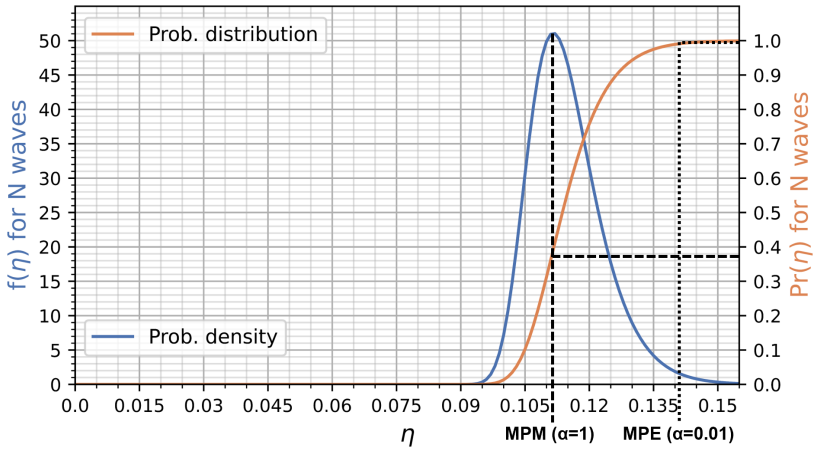

Figure 4.12: Rayleigh PDF and CDF ($\epsilon = 0$) for $m_0 = 8.02 \cdot 10^{-4}$ and n=2,207 waves (T_p =5.5s).

The choice of the α value depends on the acceptable risks and the designer's decision. When looking at the MPM and MPE responses of the CDF above, it stands out that the difference between the two values is relatively low, respectively 0.114 and 0.142 meters. This depends on the steepness of the CFD and is thus directly related to the properties of the response spectrum. It should be noted that the response spectrum will be different for every wave heading, ship motion direction, and sea state. Therefore, the MPM and MPE values of other cases might be further apart. Therefore, when interpreting results, it is important to keep in mind that the results are based on statistics and larger responses could potentially occur. When assessing workability, for example, MPM responses are acceptable and preferred.

For this research, however, the decision was made to calculate the MPE ($\alpha = 0.01$) responses, representing a more conservative approach. In addition, given that the seakeeping behavior is evaluated during offshore operations, where it is crucial to maintain low risks, it would be more appropriate to use the MPE response values rather than the MPM values.

The calculation of response values is executed for every wave heading. Ultimately, the MPE response across the three directions (x,y,z) for all wave headings are determined. With these results, the worst MPE responses across the longitudinal, transverse, and vertical direction can be determined for every ship configuration.

4.2.9. Validation of the seakeeping analysis module (SAM)

As briefly introduced in Section 3.4.3, a ship can be allowed to weathervane during offshore operations. Weathervaning involves aligning the bow of a vessel with the incoming environment. This improves seakeeping and reduces the power required for station keeping. When a vessel is not allowed to weathervane, its heading remains fixed, while the environment can be omnidirectional. The difference between the two scenarios is visualized in the following figures.

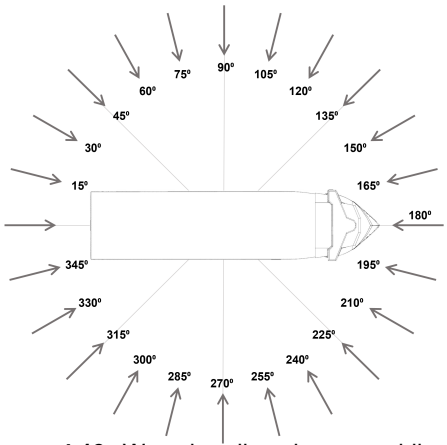

Figure 4.13: Wave headings in an omnidirectional environment.

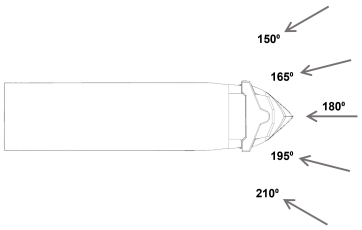

Figure 4.14: Wave headings in a weathervaning environment with +- 30 degrees offset.

The new seakeeping module in *Blended Design* allows for the designer to specify the wave headings for which seakeeping performance needs to be evaluated. It can also specify whether it wants to calculate MPM or MPE responses. Since a WTIV could install a wind turbine from every heading onto the foundation, this type of vessel should be allowed to weathervane. Therefore, weathervaning is deemed to be the most realistic operational scenario during wind turbine installation. However, both scenarios, weathervaning and omnidirectional are validated to check if the new seakeeping analysis module (SAM) would be applicable for both cases.

To validate the outcomes of the seakeeping module, the worst motion responses were calculated for the same HX118 design under the same conditions as the hydrodynamic analysis performed in Section 3.4.3. This enables a direction comparison between the obtained worst responses from the simple seakeeping analysis module (SAM) and HAS. Comparisons were done for three different T_p values and for two different loading conditions. Both MPM and MPE motion-induced displacements were calculated to also check whether Equation 4.30 is correctly implemented.

Weathervaning

Table 4.3 shows the comparison of obtained worst MPE results for $T_p = 6.2s$ from both SAM and HAS under a weathervaning assumption. The other comparisons of weathervaning MPM and MPE values and other T_p values are to be found in Appendix F.

Table 4.3: Validation of weathervaning MPE motion-induced displacements from the seakeeping analysis module (SAM) with hydrodynamic analysis software (HAS).

		Most probable extreme					
		Fully-loaded			Lifting last turbine		
Position	Method	Long. disp. [m]	Trans. disp. [m]	Vert. disp. [m]	Long. disp. [m]	Trans. disp. [m]	Vert. disp. [m]
Assembly location	HAS	0.77	0.15	0.26	0.94	0.25	0.32
	SAM	0.74	0.22	0.21	0.74	0.27	0.21
	Error	**-4%**	**44%**	**-21%**	**-21%**	**10%**	**-33%**
Installation location	HAS	0.84	0.15	0.27	1.01	0.25	0.32
	SAM	0.74	0.22	0.23	0.74	0.27	0.25
	Error	**-11%**	**44%**	**-14%**	**-26%**	**10%**	**-24%**

The table shows local MPE motion-induced displacements in a sea state with $H_s = 2.5$ and $T_p = 6.2s$.

The validation results demonstrate that the outcomes of the two methods are comparable

and within the same order of magnitude. Differences in the outcomes of the two methods can be observed. When comparing the results for the different T_p values shows that the error in the responses from SAM is highest for lower wave periods. When comparing the MPM and MPE displacements, the error percentage is the same, indicating that Equation 4.30 is correctly implemented. For the purpose of this research, the performance of the calculations from SAM are considered acceptable. Primarily because the results will be used to evaluate the relative differences among all ship configurations.

Omnidirectional

In addition to weathervaning, a comparison has been conducted on the results in an omnidirectional environment. The results are presented in Table 4.4. Further comparisons of the response maxima in an omnidirectional environment can be found in Appendix F.

Table 4.4: Validation of omnidirectional MPE motion-induced displacements from the seakeeping analysis module (SAM) with hydrodynamic analysis software (HAS).

		Most probable extreme					
		Fully-loaded			Lifting last turbine		
Position	Method	Long. disp. [m]	Trans. disp. [m]	Vert. disp. [m]	Long. disp. [m]	Trans. disp. [m]	Vert. disp. [m]
Assembly location	HAS	1.02	0.23	0.39	1.26	0.41	0.48
	SAM	2.09	4.00	1.69	4.46	5.03	3.03
	Error	**104%**	**1668%**	**329%**	**255%**	**1114%**	**534%**
Installation location	HAS	1.13	0.23	0.42	1.35	0.41	0.48
	SAM	2.09	4.00	2.21	4.46	5.03	3.73
	Error	**85%**	**1668%**	**432%**	**230%**	**1114%**	**671%**

The table shows local MPE motion-induced displacements in a omnidirectional sea state with $H_s = 2.5$ and $T_p = 6.2s$.

The table above reveals that SAM would highly overestimate the responses when all wave headings are taken into account. This also aligns with the earlier validation of the RAOs and response spectra, which showed significant errors in beam seas. The table above confirms that SAM is unsuitable for use in an omnidirectional environment because the results are notably inaccurate, while the results under the weathervaning assumption were at least within the correct order of magnitude.

4.3. Wind turbine mission module

The new wind turbine mission module connects the wind turbine market with the ship configurations. The objective of this module is to determine the feasible number of turbines that can be transported and installed by each ship configuration. Given the diversity of turbine sizes in the market, this calculation is performed for every turbine size. The number of turbines is dependent on multiple constraints. In the case of wind turbine installation, five different constraint were identified. The number of turbines is calculated for each of the constraints. Ultimately, for every turbine size, the module identifies the limiting factor that yields the smallest number of turbines of the five constraints, as shown in equation 4.31. This number is eventually the maximum number of turbines a configuration transport and install. The limiting constraint is also recorded in the results of *Blended Design*. This gives the designer an overview of the dominant limiting factor for this type of cargo and an understanding of what limits the number of turbines for different ship configurations or turbine sizes.

$$N = \min\{N_{CC}, N_A, N_{DWT}, N_{tot,tr}, N_{tot,lift}\} \tag{4.31}$$

In the following sections, each of the limiting factors and the corresponding calculation method will be explained.

4.3.1. Crane capacity constraint

The crane capacity constraint is a very significant constraint. It dictates whether the installation of wind turbines of a particular size is feasible or not. If a ship's crane capacity exceeds the mass of an assembled turbine, it essentially opens up the possibility for an unlimited number of turbines to be installed. In reality this that it automatically will be constraint by other limiting factors.

$$N_{CC} = \begin{cases} \infty & \text{if } m_{WTG} < crane\ capacity \\ 0 & \text{else} \end{cases} \tag{4.32}$$

4.3.2. Deck area constraint

The second constraint is the available deck area. Under this constraint, the number of turbine components that fit on the deck for all turbine sizes that might occur in the market are calculated. This limiting factor is based on the available deck space and the area occupied by the turbine components. For the analysis, the deck area is divided into two parts. This is illustrated in the figure below. It is assumed that the green area will be reserved for towers and nacelles. The yellow area, behind the crane, is exclusively designated for blade storage.

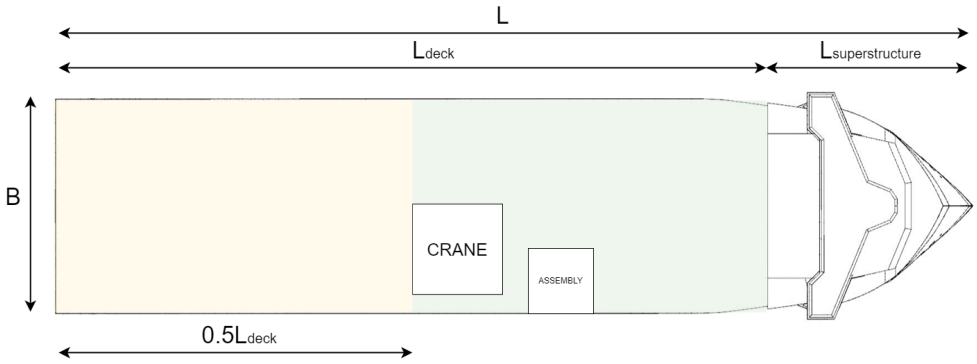

Figure 4.15: Division of deck area.

Certain areas of a ship cannot be occupied by turbine components. These areas are indicated in the figure with white. The first area is the superstructure. The second one is the are occupied by the crane pedestal. Not much is known yet about the lifting equipment. Therefore, the crane pedestal is assumed to be the same for all crane capacities, which is 20 by 20 meters. The third location is the assembly area, where the turbines will be assembled before installation onto the foundation. This area is assumed to be 15 by 15 meters, as the tower diameter is expected to always be less than this.

For the required area of all components for different turbine sizes, the relations from Section 3.4.2 are used. Additionally, to account for seafastening and to ensure sufficient spacing between the components, a margin of 1 meter around the nacelle is assumed. For the towers, a square of the tower diameter with an offset of 1 meter on each side is used as footprint. The blades are assumed to be stacked per three in blade racks. To determine the width of the blade racks, footprint relations adopted from [99], were divided by the respective blade lengths. Also, a margin of 1 meter on both side of the blades was added.

The algorithm within the model calculates the maximum number of towers and nacelles that can be accommodated within the green deck area, which is forward of the aft of the crane. In addition, a margin of 90 percent has been taken into account. The number of turbines, with the margin included, was found to better match drawn deck layouts.

$$N_{A,1} = 0.9 \cdot A_{deck,green} / \left[(L_{nacelle} + 2) \cdot (B_{nacelle} + 2) + (D_{tower} + 2)^2 \right] \tag{4.33}$$

Once the number of towers and nacelles that fit within the green are is calculated, the model knows how many blade stacks are required. The algorithm then checks if the width of all blade stacks does not exceed the breadth of the vessel. If the width exceeds the limit, the maximum number of turbines becomes equal to the number of blade stacks that can be fitted side-by-side within the ship's breadth.

$$N_{A,2} = \begin{cases} B/(B_{blade} + 2) & \text{if } N_{A,1} \cdot (B_{blade} + 2) > B \\ N_{A,1} & \text{else} \end{cases} \tag{4.34}$$

In this research, it is assumed that the blades can extend beyond the aft of the vessel. The estimated length that should fit on the length of the yellow part of the deck is set at 60 percent of the total blade length. A check is performed to verify if this requirement is satisfied. The blades are assumed to not be placed directly against the crane, so a margin of 5 meters is taken into account. If the length constraint is violated, the algorithm automatically sets the number of turbines to zero.

$$N_A = \begin{cases} N_{A,2} & \text{if } 0.5 L_{deck} - 5 \geq 0.6 L_{blade} \\ 0 & \text{else} \end{cases} \tag{4.35}$$

4.3.3. Deadweight constraint

The third limiting factor is associated with the deadweight available for cargo. The algorithm calculates the maximum number of turbines that can be accommodated within the vessel's deadweight. This calculation assumes that there is no ballast water present. The total mass of a single turbine is defined as follows:

$$m_{WTG} = m_{tower} + m_{nacelle} + m_{hub} + 3 \cdot m_{blade} \tag{4.36}$$

Additionally, an allowance of 10 percent is assumed for seafastening mass. The maximum number of turbines is then calculated by dividing the deadweight available for cargo by the turbine mass including the allowance. This calculation is performed for every turbine size that might occur within the market. The resulting numbers of turbines are rounded down to the nearest whole number.

$$N_{DWT} = DWT / (1.1 \cdot m_{WTG}) \tag{4.37}$$

Blended Design calculates two values for the deadweight. One for a transit condition and one for a lifting condition. In the lifting condition, the draft is assumed to increase due to the addition of water ballast to compensate for the increase in CoG due to crane operations. As a result of the increase in draft, the available deadweight would consequently be higher in the lifting condition. Thus, the relevant limiting factor is determined by the deadweight in transit condition. Therefore, only the maximum number of turbines for this condition is calculated.

4.3.4. Stability constraints

The fourth and fifth constraint are related to the stability of the ship configurations. The first limiting factor is the transit stability and the second lifting stability. *Blended Design* has already a stability function, which is extensively covered in [49]. This function calculates the distance from keel to metacenter ($\overline{KM}$) and is able to calculate the metacentric height ($\overline{GM_t}$) for each ship configuration. Based on this it calculates the maximum allowable $\overline{KG}$ value. It does this

both for transit and lifting conditions.

The algorithm for the stability limiting factors calculates the vertical center of gravity (VCG) for an increasing number of wind turbines of every size in the market simulation. It then checks if the VCG of the turbines is still below the allowable $\overline{KG}$. If not, the vessel will be unstable and not be able to carry that number of wind turbines. The algorithm eventually finds the maximum number of wind turbines for which the $\overline{KG}$ value is still positive.

For both conditions, the vessel is assumed to use water ballast. The difference between the mass of the turbines and the deadweight of a configuration is filled with ballast water, so that the vessel would reach the targeted draft. The VCG of the water ballast is a fixed ratio of the depth. Therefore, the VCG of the water ballast increases with the depth of a ship configuration.

$$m_{bal} = DWT - N_{WTG} \cdot m_{WTG} \tag{4.38}$$

The VCG of the individual components corresponds with the findings in section 3.4.2. To determine the resulting VCG of these components, when they are in storage position on deck during transit, the following equation is used.

$$VCG_{comp} = D + \frac{3m_{blade} \cdot 0.5 \cdot 3h_{blade} + m_{tower} \cdot VCG_{tower} + (m_{nacelle} + m_{hub}) \cdot VCG_{nacelle}}{m_{turbine}} \tag{4.39}$$

Transit
The VCG of the deck cargo in transit condition is calculated with the following equation.

$$VCG_{tr} = \frac{VCG_{LSW} \cdot LSW + N_{tot,tr} \cdot VCG_{comp} \cdot m_{WTG} + VCG_{bal} \cdot D \cdot m_{bal,tr}}{\Delta_{tr}} \tag{4.40}$$

Lifting
The VCG of the deck cargo in lifting condition is calculated with the following equation.

$$VCG_{lift} = \frac{VCG_{LSW} \cdot LSW + (N_{tot,lift} - 1) \cdot VCG_{comp} \cdot m_{WTG} + VCG_{bal} \cdot D \cdot m_{bal,lift} + z_{load} * m_{WTG}}{\Delta_{lift}} \tag{4.41}$$

The equation closely resembles the one for transit condition. The only difference is that one of the turbines is being lifted, instead of only individual components on deck. The point of lift, where the mass of turbine assembly applies, is located 20 meters above the hub height. This is assumed to allow for the use of lifting tools etc. The used hub height is of the largest turbine size a ship configuration can possibly carry in its lifetime.

The output of the created wind turbine mission module has been validated using an *UDSBV* design. The validation is presented in Appendix G.

4.4. Chapter conclusion

This chapter discussed what modifications to the existing *Blended Design* were required. *Blended Design* will be used to explore the design space of *Moonshot* and to asses the performance of ship configurations within the design space. Firstly, the existing model lacks the ability to assess seakeeping behavior. Secondly, the model is unsuitable for wind turbine installation vessels. As a result, several modifications were made to the model to address these limitations. All changes to the existing model and revised assumptions have been discussed, such

as the addition of a wind turbine deck cargo module.

The most substantial addition was the seakeeping analysis module (SAM). An approach for determining the response maxima for a set operational limit has been devised. The approach involved calculating the RAOs in six degrees of freedom for all ship configurations in the design space. Various methods were explored, such as the semi-analytical method proposed by Jensen et al. [88] for calculation of the heave, roll, and pitch RAOs. The resulting RAOs from this method were validated with RAOs from hydrodynamic analysis software. Various ways to validate the results were used, such as a visual comparison, comparison of the areas under the RAO curves, and the standard deviation of the response spectrum for different wave heading angles and three different wave periods. The validation showed that the method by Jensen et al. produces results in the correct order of magnitude and could be applicable to predict the relative merits of ship configurations within the design space. In addition, an attempt was made to calculate the RAOs for the remaining degrees of freedom, drawing upon a method by Matsui et al. [90]. Unfortunately, this method did not yield satisfactory results. Therefore, it was decided to only incorporate the three RAOs from the method by Jensen et al. in the module.

The output from SAM was further validated by comparing the results with those obtained from hydrodynamic software. Local response maxima for different wave periods in both omnidirectional and weathervaning conditions were calculated. The validation demonstrated that SAM provided accurate results for weathervaning conditions but was not suitable for use in an omnidirectional wave environment.

5

Evaluating the performance of Moonshot

In previous chapters, a solution for wind turbine installation using a floating monohull vessel has been developed. Modifications to the existing *Blended Design* model have been made to explore the design space of *Moonshot*. This chapter focuses on using the new model and evaluating the performance of *Moonshot* in future offshore wind markets and investigating how the ship parameters affect performance indicators. These will include financial and seakeeping performance. By analyzing these factors, the optimal design configurations for Moonshot can be determined. By the end of this chapter, the following sub-question is answered: *"How would the main particulars of the Moonshot design influence its financial and seakeeping performance in various future offshore wind market scenarios?"*

5.1. Results and findings

In this section, the results and findings will be presented. Firstly, the financial performance will be evaluated. Secondly, the seakeeping performance will be evaluated. The following input is used to study the performance and determine optimal design ranges for *Moonshot*. As shown in Table 5.1, the block coefficient is fixed for all configurations. This is to limit the amount of configurations and subsequently calculation time. Analysis of existing heavy-lift vessel designs by *UDSBV* showed that the block coefficient is generally around 0.77. This value was therefore adopted as input. In total, the created design space consisted of 158,340 unique ship configurations. Only 38,219 ship configurations were found to be feasible, according to the feasibility criteria of *Blended Design*. These criteria were discussed in the thesis by J.J. Zwaginga [49]. In total, seven runs were done to cover all scenarios. The total calculation time was about 13 hours with one computer.

Table 5.1: Input for *Blended Design* to create the design space.

Particular		Start	End	Step size	#
Length	[m]	140.0	280.0	5.0	29
Breadth	[m]	36.0	72.0	3.0	13
Depth	[m]	10.0	19.0	1.0	10
Sailing speed	[kn]	10.0	15.0	1.0	6
Crane capacity	[t]	1,000	7,000	1,000	7
Block coefficient	[-]	0.77	-	-	1

The results are depicted in graphs that show the performance of all the configurations for a specific ship parameter. The Pareto front of the best-performing configurations is displayed with a line. This is shown in the left graph in Figure 5.1. Instead of representing individual configurations with separate points, the data is visualized as a shaded region below the Pareto

front. To enhance readability of the plots, the shading is omitted in most of the plots in this report. As shown in the example on the right in Figure 5.1, the ship parameter value with the highest performance is indicated with a marker. Additionally, a bold line indicates the range of ship parameter values that perform within 2.5 percent of the best-performing value. The percentage is user-defined and can easily be changed.

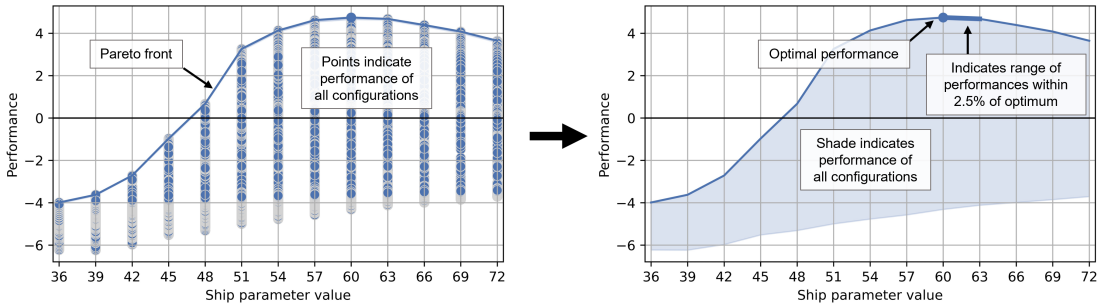

Figure 5.1: Visual guide on how to interpret the result plots.

5.2. Financial performance

Firstly, the influence of ship parameters on the financial performance will be investigated. Various scenarios will be included in the analysis, and optimal design configurations will be determined. The financial performance will be measured in return on investment (ROI), which is the ratio between the net profit over the lifetime and the investment costs.

5.2.1. Market scenarios

To start the research into the optimal design configuration for *Moonshot*, four different market scenarios have been analyzed. The first market scenario assumes unlimited growth of wind turbine capacity. The corresponding market projection is depicted in Figure 5.2. The market projection has been established by analysis of recent *4C Offshore* data (February 24, 2023). The data points within the figure correspond to various wind turbine projects with a bottom-fixed foundation. The size of each dot indicates the number of turbines in a project. Based on the data points, calculations were performed to derive the weighted mean, upper, and lower values, for every year. Subsequently, lines were fitted through these values, representing the weighted mean, upper, and lower boundaries. With extrapolation of these lines, a projection for the future trends in the market was made. The weighted mean and boundaries are eventually used for uncertainty modelling, as explained by J.J. Zwaginga [49].

Furthermore, a second scenario was established. This scenario assumes that the mean turbine capacity will not grow beyond the maximum turbine capacity of all offshore wind projects currently in operation, planned or within the Procurement, Construction, and Installation (EPCI) phase. Following this assumption, the market would be bound to a mean capacity of 16 MW. The market scenarios are displayed in Figure 5.3. The upper boundary extends over 16 MW to account for uncertainties in the wind turbine properties, such as mass and size of components.

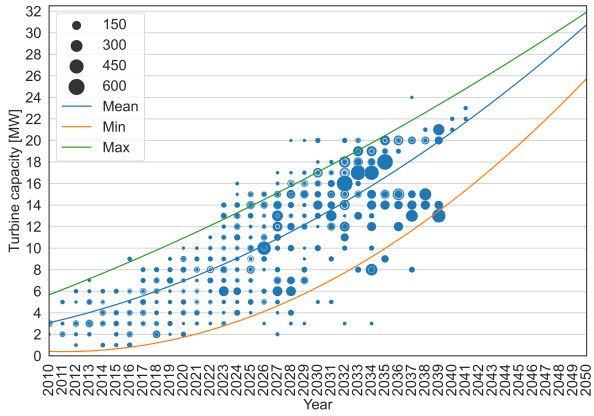

Figure 5.2: Visualization of the unbound market.

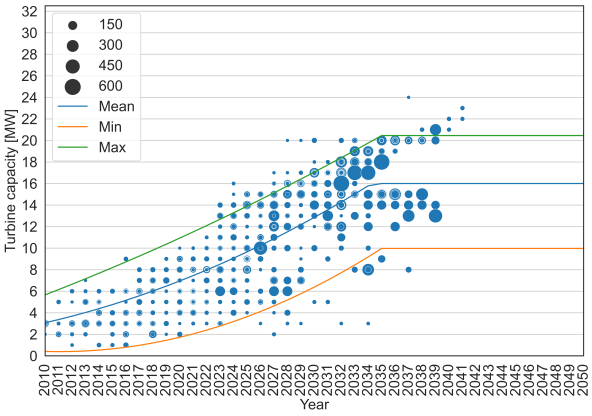

Figure 5.3: Visualization of the 16 MW bound market.

In the third scenario, growth of turbines is restricted to a tip height of 1,000 feet. Recently, there have been discussions about limiting the height of wind turbines to stabilize the rapid development of offshore wind turbines and to introduce more standardization in the industry. This will increase the stability in the offshore wind sector and make it more appealing for investments, ultimately accelerating the energy transition [100]. The Netherlands Wind Energy Association (NWEA) has proposed a tip height limit of 1,000 feet, which is approximately 305 meters. When considering a clearance of 25 meters between the water surface and the lowest blade tip, the maximum allowable rotor diameter would be 280 meters [101]. Based on the established relations in Section 3.4.2, this rotor diameter would correspond to a turbine with a rated power of around 22 MW.

The proposal applies to the Dutch offshore wind industry, but the expectation is that the European Union will support the initiative. Hence, this scenario is realistic market scenario for investigation in this research. Once the weighted mean capacity of the market reaches 22 MW, further growth is restricted. This is also depicted in Figure 5.4. The upper boundary in the context of a 1,000 feet bound market extends beyond 22MW to account for uncertainties in the mass of the turbine components.

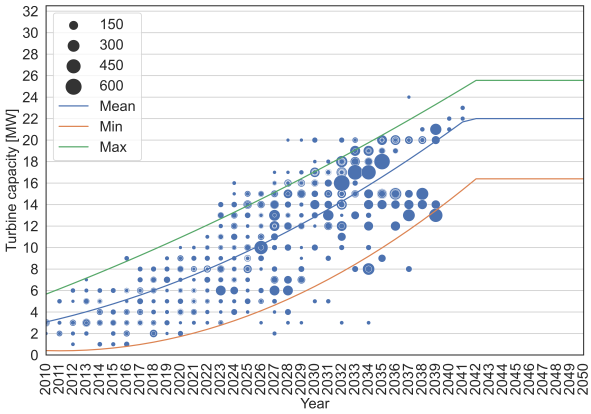

Figure 5.4: Visualization of the 22 MW and 1,000 feet bound market.

Additionally, a fourth market scenario will be explored, which involves a 22 MW capacity bound scenario. The market projection resembles that of the 1,000 ft bound market illustrated in Figure 5.4. The key difference lies in the fact that in this market scenario, the upper boundary takes into consideration not only the uncertainty of the mass of wind turbine components but also the uncertainty in size of these components. This 22 MW scenario is included to demon-

strate the impact of the differences between the upper boundary assumptions of a 1,000 ft bound market and a scenario where both size and mass are uncertain.

For the analysis in *Blended Design*, markets of 25 years starting from 2025 will be assumed. A 25-year duration aligns with the typical lifetime of a ship.

5.2.2. Financial performance in different market scenarios

This section investigates the financial performance of all ship configuration in the four different market scenarios. The results of *Blended Design* are shown in the figures below.

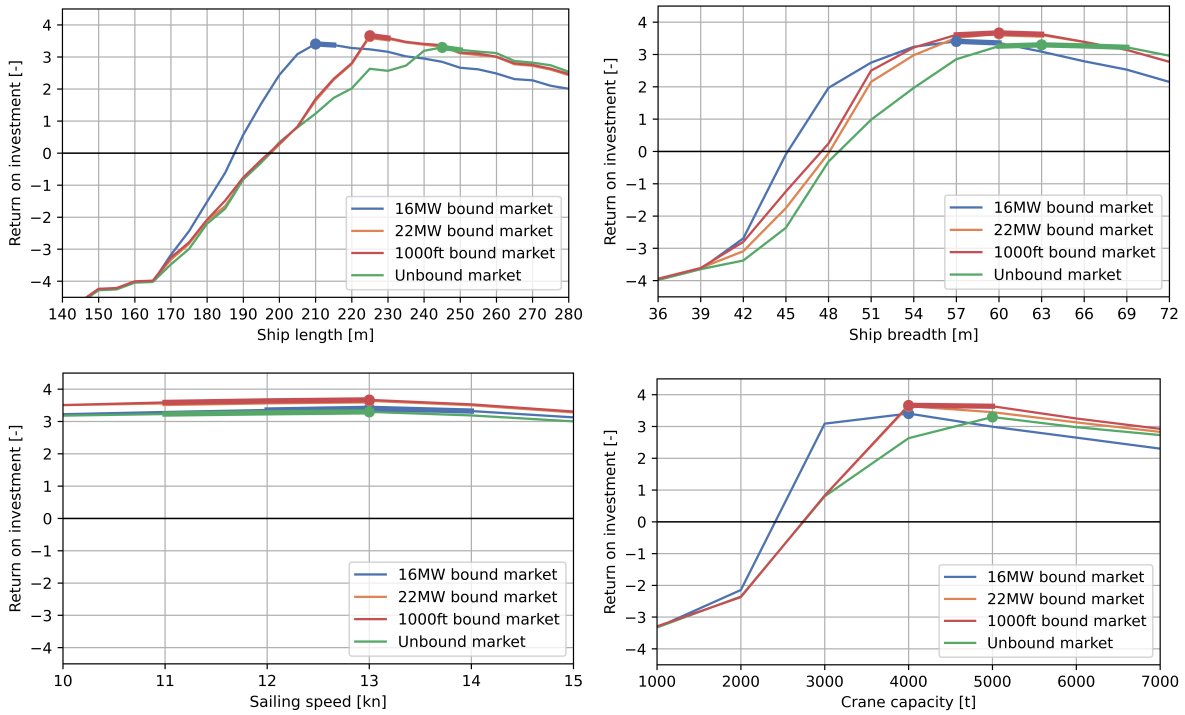

Figure 5.5: Visualization of the results for the four market scenarios.

The results indicate that the short vessels yield a negative ROI across all market scenarios. In the 16 MW bounded market, smaller vessels start generating a positive return sooner compared to the other market scenarios. What stands out, is that the configurations perform best in 1,000 ft and 22 MW markets. In terms of ship length, the lines of the 1,000 ft and 22 MW bound market are very close to each other.

In terms of optimal ship dimensions, the results reveal that the optimal ship length and breadth are the same for the 1,000 ft and 22 MW bound market. The optimal ship length increases for markets with larger turbines, which can be attributed to the fact that the longer blades of large turbines can only be transported by vessels that have sufficient deck length. When looking at breadth, the optimal breadth also increases for growing markets and the optimal ranges widen. This probably has to do with lifting stability. A larger ship breadth results in greater lifting stability, enabling larger ships to install the larger turbines in the market. Smaller vessels do not have the ability to install these turbines. Larger vessels, capable of installing them receive a more substantial reward compared to the smaller configurations, which are limited to smaller turbines, that that yield less reward. The results for ship depth are not displayed, as it showed comparable behavior. The optimal ship depth ranges from 14.0 meters to 15.0 meters in a 16 MW bound market, whereas in an unbound market, the optimum ranges

from 16.0 to 17.0 meters. The lines for sailing speed for the various market scenarios are very close to each other and are relatively flat, indicating that sailing speed does not impact the ROI significantly. Therefore, the optimal speed range is quite wide, from 11 to 13 knots, for most market scenarios. In a market with smaller turbines, the optimum ranges from 12 to 14 knots. The optimal crane capacity is 4,000 tonnes for the turbine-capacity bound markets. In the unbound market, a crane capacity of 5,000 tonnes is required to lift the larger turbines. In a 1,000 ft bound market, a 4,000 or 5,000 tonnes crane results in roughly the same ROI, which is interesting because this range is not visible for a 22 MW bound market. This can probably be attributed to the uncertainty in the mass of turbine components in a 1,000 ft market.

The results from *Blended Design* also enable exploration of the relationship between multiple ship parameters. Crane capacity dictates what turbine sizes can be installed, making it a critical parameter for WTIVs. Therefore, multivariate visualizations were made to display how different crane capacities perform in relation to other ship parameters. For the remainder of this research, the 1,000 ft bound market scenario will be used because as it represents a highly realistic future scenario.

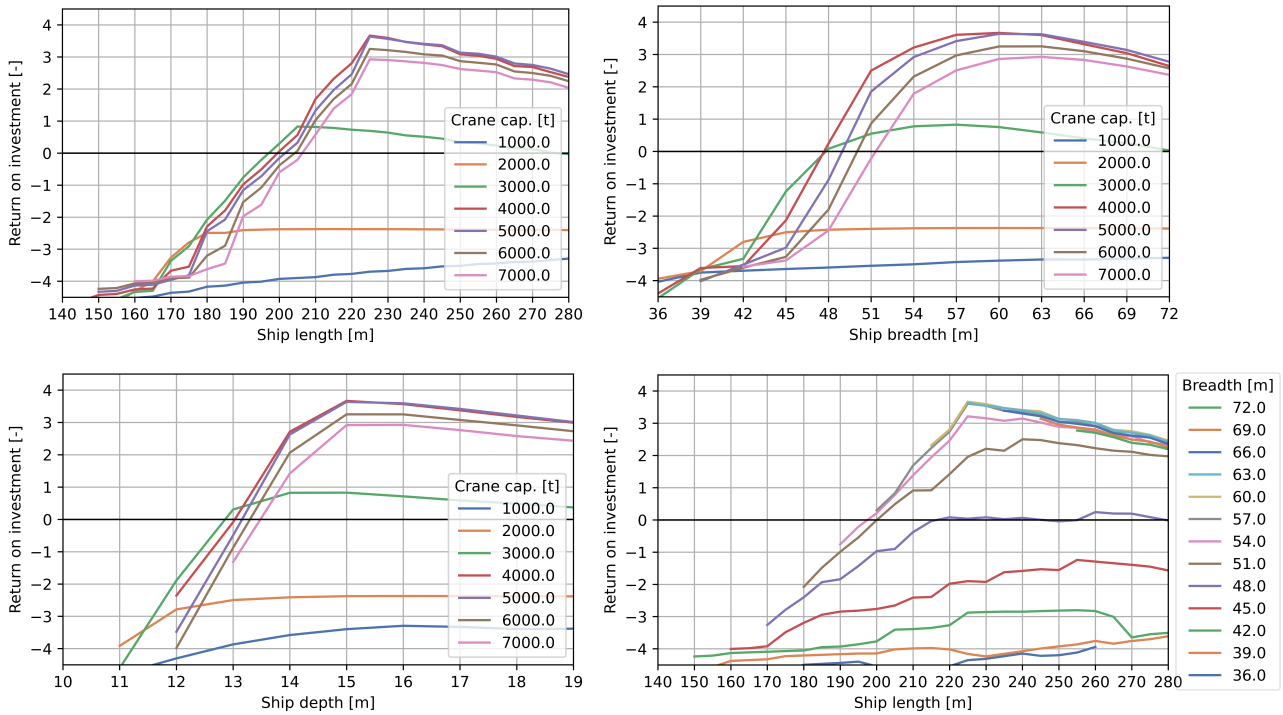

Figure 5.6: Multivariate visualization of the results for a 1,000ft bound market.

The results show that configurations with crane capacities of 1,000 and 2,000 tonnes consistently yield a negative ROI. This is primarily due to the limited turbine size they can handle. For example, vessels with these crane capacities would only be capable of lifting turbines up to 5 and 11 MW, respectively. The market projection in Figure 5.4 shows that there would not be many contracts for 5 MW turbines within the timeframe of the simulation. To install 11 MW turbines, sufficient stability is required to lift the complete assembly, requiring larger vessels with enough breadth. Furthermore, enough length should be available to accommodate the components, particularly the blades. Consequently, such a vessel would likely be substantial in size, albeit with a small crane. However, due to the relatively low crane capacity, this relatively large vessel would perform worse compared to a similar-sized vessel equipped with a larger crane capacity. The plots also reveal that a crane capacity of 3,000 tonnes is

the best-performing option up to a certain ship size, although the ROI remains relatively low. This is primarily because this ship size, particularly in terms of breadth, does not provide sufficient stability for installation of the larger turbines prevalent in the market. As a result, the performance of the line representing a 3,000-tonnes crane capacity intersects with the line representing a 4,000-tonnes crane capacity, which is the best-performing crane capacity for all ranges of ship parameters beyond this point. At a certain point the performance is similar to 5,000 tonnes. This is exactly at the same ship parameter values that were found to be optimal. Crane capacities exceeding 4,000 or 5,000 tonnes display worse performance, due to the fact that the mass of the largest turbines in the market is not that high.

In the plot depicting the ship length and ship breadth, the L/B feasibility limit, within the range of 3.5 and 9.5, is clearly visible. It stands out that the lines in the upper right corner of the plot are closely clustered, indicating comparable ROI for these combinations of length and breadth. This plot indicates that ship configurations that are relatively long and wide are favorable. However, there are clearly some combinations of length and breadth that show the best financial performance.

In all previous plots, the optimum ship parameters based on one or two ship variables were observable. The lines showed the Pareto fronts, which means that they only indicated the ship parameter value of the configurations for which the ROI is maximum. However, there are many ship configurations with the same value for a ship parameter with a lower ROI. Combining the findings of all line plots, it is possible to select the best-performing configuration and those that perform within a margin of the ROI. To ensure the existence of these ship configurations, the output data from *Blended Design* should be checked. Another way to display all unique ship configurations is by creating a parallel coordinates plot. These plots are commonly used for visualizing multivariate data and are a great way to visualize all ship configurations. A parallel coordinates plot for the financial performance in a 1,000 ft bound market is shown in Figure 5.7. The continuous line highlights the ship configuration among 38,219 with the highest ROI. Besides that, 11 unique configurations perform within 2.5 percent of the best configuration. These are represented with dotted lines.

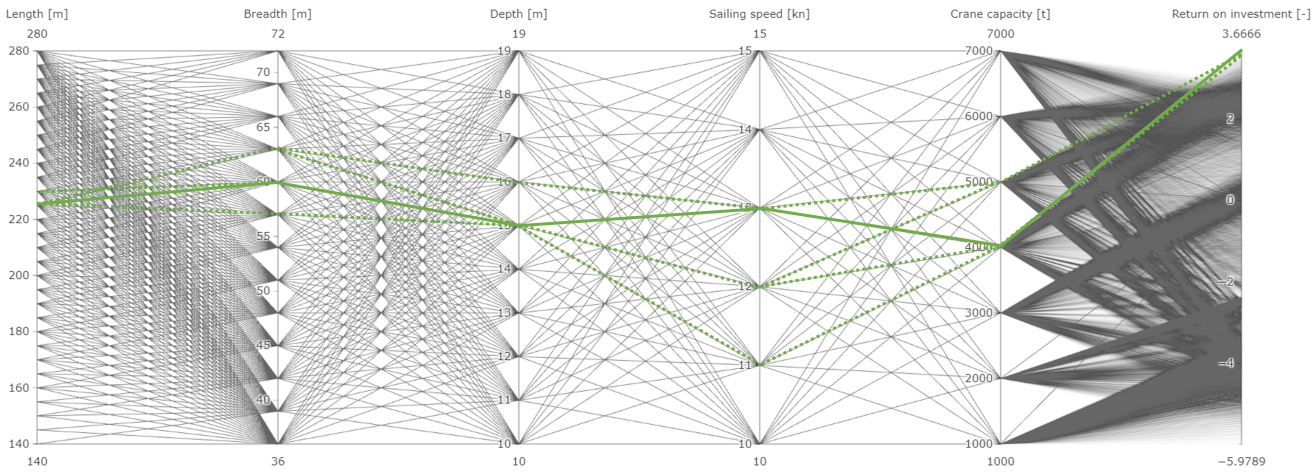

Figure 5.7: Parallel coordinates plot of the financial performance in a 1,000ft bound market.

5.2.3. Influence of distance to port

The previous calculations were conducted with a distance to port of 140 nautical miles (NM). This distance was selected based on insights from literature, displayed in Figure 1.3 of Chapter

1. This chosen distance roughly corresponds to the anticipated maximum distance to shore for OWFs in 2026. The objective of the following section is to explore the impact of varying distance ranges, both shorter and longer than the 140 NM. Therefore, calculations have been performed for distances of 35 and 350 NM. The short distance is based on current global maximum distances to OWFs, as visualized in Figure 1.3. The long distance of 350 NM is ten times that distance. The results of the calculations are presented in the plots below.

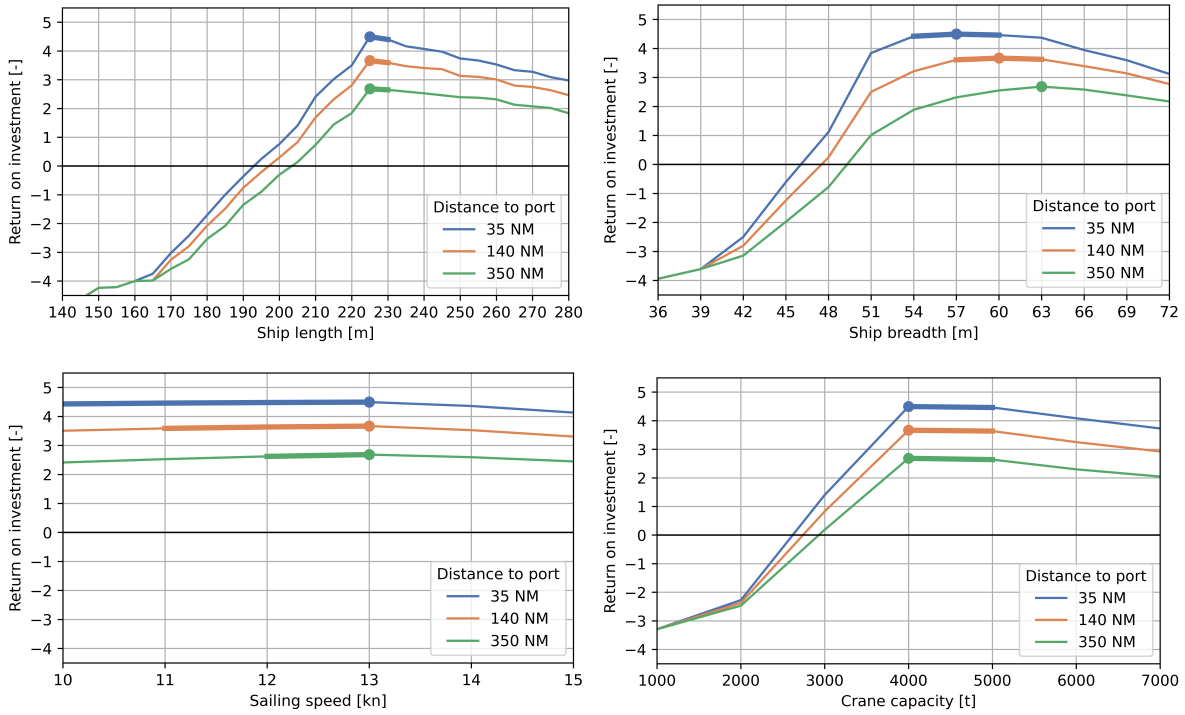

Figure 5.8: Visualization of the results of a 1,000ft bound market with three distances to port.

The results show that ROI decreases with increasing distances to port. This is mainly because the sailing time increases, while the number of turbines that can be installed does not necessarily increase. As a result, the revenue remains roughly the same while costs increase. The general trend of all lines remains consistent. As distance to port increases, the optimal ship length remains unchanged. However, the optimal breadth clearly shifts towards larger values as sailing distances increases. Therefore, it can be concluded that that bigger ships perform better as distance to port increases, likely due to the increased cargo capacity for larger vessels. The optimal crane capacity does not change with increasing sailing distance.

The lines for sailing speed for different distances show a similar trajectory. The optimal sailing speed is the same for all distances. Initially, it was expected that the optimal sailing speed would increase for longer sailing distances. However, this is not the case, but the optimal speed range narrows as the distance increases.

Increasing the speed would lead to an increase in the resistance of a ship configuration, requiring more installed power. This would, in turn, increase the lightship weight. Additionally, more fuel is required, which also decreases the available deadweight for cargo. An increase in speed would eventually result in higher costs per year. On the other hand, yearly income would increase because higher sailing speeds enable more installation cycles per year. However, examining the the operational cycle of *Moonshot* reveals that sailing time only constitutes a relatively small portion of the total time of an operational cycle. Installation takes around 20

hours per turbine, while sailing to the OWF at a sailing speed of 12 knots takes approximately 3, 12, or 29 hours for sailing distances of 35, 140, or 350 NM respectively. Hence, the differences in the the optimal sailing speeds are not very pronounced. Increasing the cargo carrying capacity appears to be more beneficial as it would allow for the transportation and installation of more turbines per cycle.

5.2.4. Splitting the turbine towers

In accordance with the findings and assumptions outlined in Section 6, the turbine towers are transported as one part. The towers are heavy and very tall, resulting in a high VCG. As discussed in Section 4.3, the carrying capacity of a ship configuration can be constrained by five different limiting factors: crane capacity, deck area, deadweight, transit stability, and lifting stability. The distribution of these limiting factors, dictating the number of turbines that could be carried, has been analyzed to understand what drives the carrying capacity of the *Moonshot* design. A breakdown of the limiting factors for all feasible ship configurations is depicted in Figure 5.9. In Figure 5.10 a distinction is made between turbine sizes to visualize how the limiting factors are affected with increasing turbine sizes.

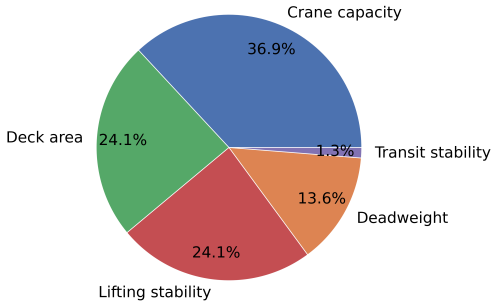

Figure 5.9: Distribution of limiting factors for feasible ship configurations.

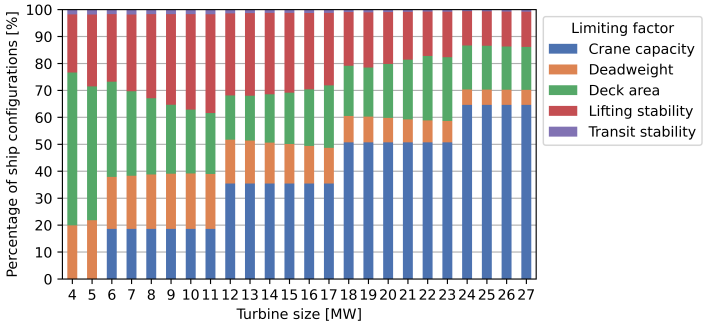

Figure 5.10: Distribution of limiting factors for feasible ship configurations, grouped per turbine size.

In a large portion of ship configurations, the limiting factor is the crane capacity. This is because all configurations in the design space have crane capacities from 1,000 to 7,000 tonnes. With larger turbines being more heavy, crane capacity becomes increasingly limiting. Besides that, the carrying capacity of the configurations is predominantly limited by the available deck area. Then, lifting stability is the most common limiting factor, particularly in the 8 to 20 MW range, impacting ore configurations than deck area limitations. For smaller turbines, deadweight plays a role in limiting the carrying capacity. However, as turbines become bigger this impact decreases. Interestingly. Transit stability is in only a small number of cases the main limiting factor for carrying capacity.

The fact that a large amount of configurations is limited by lifting stability suggests that the deck area or deadweight, and thus potential of a lot of ship configuration is not fully used. Therefore, it could be beneficial to explore ways for reducing the share of lifting stability. The primary reason for lifting stability limiting the carrying capacity is related to the high VCG of the heavy turbine towers. This led to the decision to investigate the effects of transporting turbine towers as two smaller parts, rather than a single large component. This approach would lower the VCG of the turbine tower components and the overall VCG of the deck cargo components, potentially improving the carrying capacity of the ship configurations. However, there are some downsides. Firstly, it would increase the required deck space to turbine components. Secondly, more lifts would have to be performed during loading and installation of

the towers, which would double loading and installation times for tower parts. Additionally, as the number of lifts increases, so does the associated risk.

For the analysis, the tower is divided at the VCG, which is located at around 41 percent of the tower height. Details about the VCG can be found in Section 3.4.2. Splitting the tower at the VCG would result in two parts with equal mass but different height. The VCG of the two parts was assumed to be also at 41 percent of their respective heights. The following figures show how the limiting factors are distributed across all feasible ship configurations when the towers are transported as two parts.

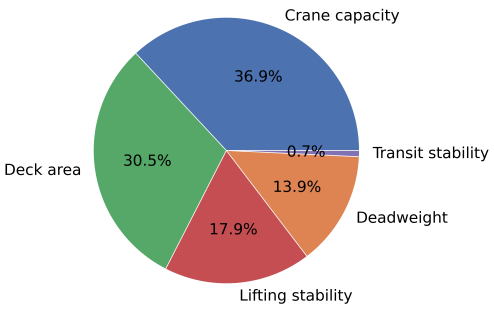

Figure 5.11: Distribution of limiting factors for feasible ship configurations with towers carried in two parts.

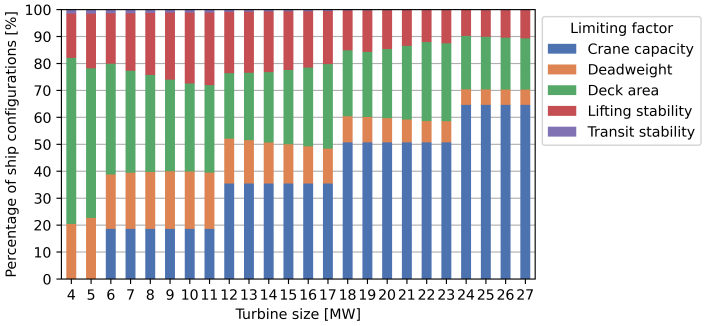

Figure 5.12: Distribution of limiting factors for feasible ship configurations with towers carried in two parts, grouped per turbine size.

The plots indicate that the stability during installation is a less dominant limiting factor for carrying capacity when the towers are divided into two parts. The share of the deck area limiting factor among all configurations has significantly been increased, suggesting that the carrying capacity of the configurations is used more efficiently. The difference in carrying capacity of a configuration for the two approaches is visualized in Figure 5.13. The two plots depict the number of turbines that can be transported according to the five constraints for every turbine size. It also shows the main limiting factor for every turbine size and the resulting capacity.

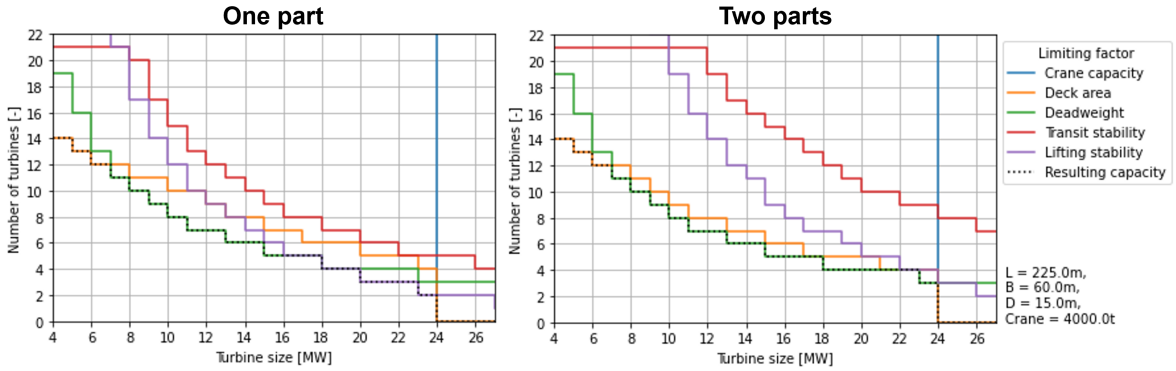

Figure 5.13: Visualization of limiting factors and number of turbines for the two tower strategies.

To assess the benefits of the transportation strategy, a financial performance analysis was conducted. The objective is to determine whether the advantages of transporting the towers as two parts outweigh the negative consequences.

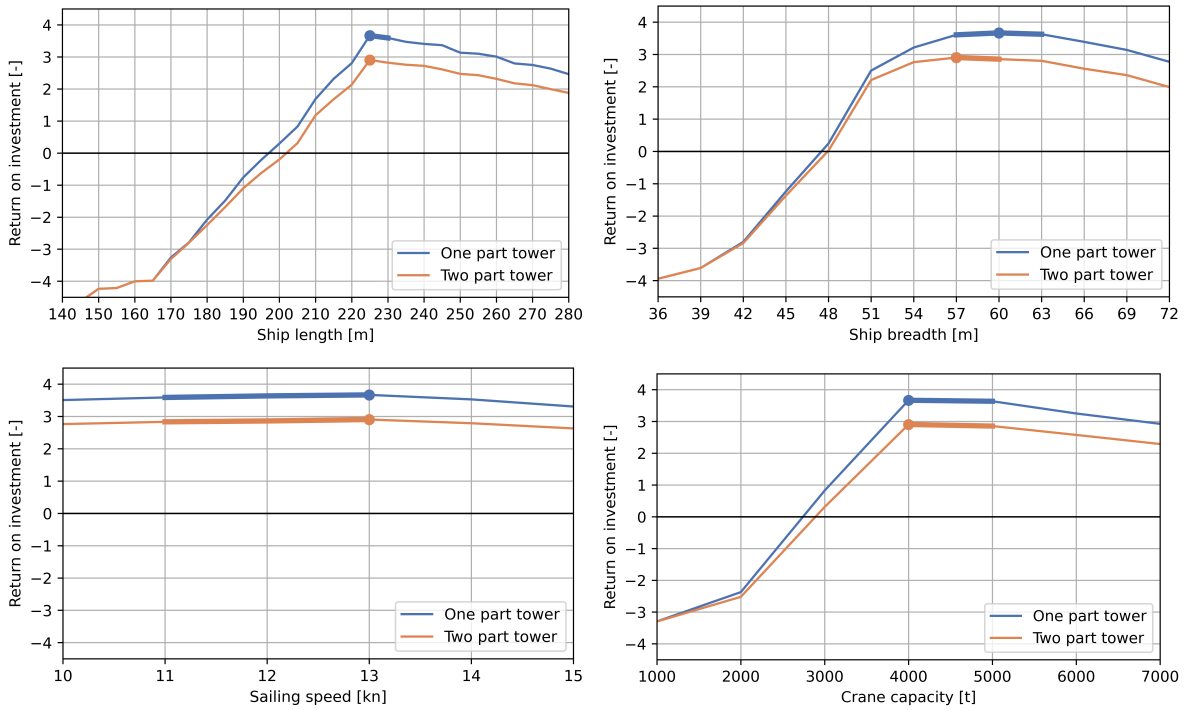

Figure 5.14: Visualization of the results for two different tower transportation strategies in a 1,000ft bound market. The distance to port is 140 NM.

The results show that the ROI is lower when the towers are divided into two parts instead of being transported as single components. Notably, the optimal breadth differs for both strategies. Analysis of the results revealed that the configuration with a breadth of 57.0 meters is cheaper to build and operate, while the difference between revenue is not very substantial compared to a breadth of 60.0 meters. The rest of the ship parameters remain unchanged. The strategy does not affect optimal crane capacity since the overall mass of the assembled turbine remains the same. Therefore, crane capacity cannot be reduced when the tower is split into two parts. Based on this performance analysis, it is concluded that there is no financial benefit in transporting the towers as two parts.

5.3. Seakeeping performance

In thie following section, the seakeeping performance of all ship configurations will be analyzed. The seakeeping performance will be calculated as the MPE motion response, as explained earlier. The MPE motion response considers the maximum observations for each case, essentially calculating the MPE response for every wave heading and selecting the values for which the MPE displacement is maximum in the x-, y-, and z-directions. The outcomes have been combined in one plot to visualize the relation between ship parameters and the MPE responses. Figures show the Pareto front of the minimum observed values for each ship parameter value. The influence of various ship parameters will be investigated, and optimal design configurations will be determined. The calculations were performed for a significant wave height of 2.5 meters, according to the assumptions in Section 4.2.5 of Chapter 4, and under a weathervaning assumption.

5.3.1. Local displacements while weathervaning

The following subsection will explore the effect of ship parameters on the motion behavior during weathervaning. The plots within this section depict MPE displacement in each of the three motion directions.

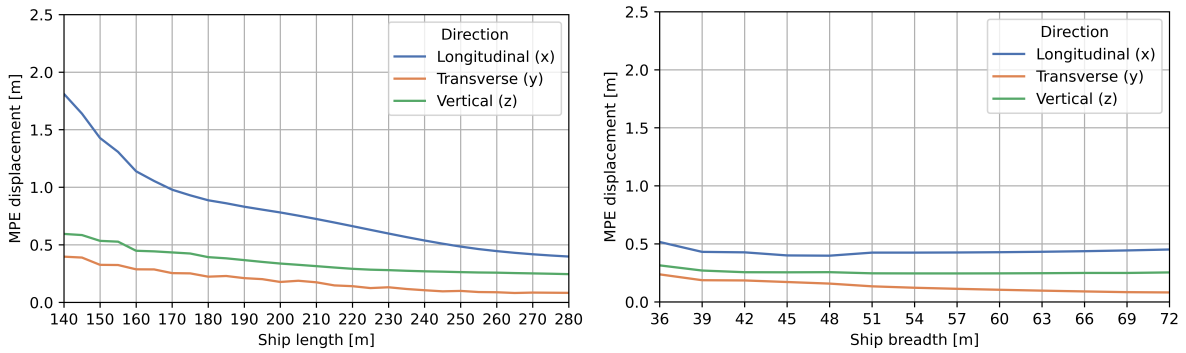

Figure 5.15: Visualization of the MPE displacements during weathervaning.

The results shows that the longitudinal MPE displacement is higher than the MPE displacement in the other two directions. This is due to the weathervaning environment, in which waves approach the bow of the vessel with a maximum offset of 30 degrees to each side. The main contributor to the longitudinal displacement is the pitch motion, which will be relatively high because of the wave direction. The length of a ship configuration dictates the pitch angles. For longer ship configurations, the pitch motion will be less. This is clearly visible in the results. The results also show that increasing the breadth does not notably influence the MPE longitudinal displacement.

In the transverse direction, the main contributor to the motion-induced displacement is the roll motion. Nevertheless, roll motion is relatively low due to both the weathervaning and the method used to determine the RAOs. The method neglects coupling effect between motions, meaning that pitch motion does not, for example, induce roll motions. While this would occur in reality, the uncoupling assumption, along with the simplicity of the RAO estimation method, results in little to no roll motion when weahtervaning. When waves are approaching from an angle of 150 degrees in the weathervaning scenario, the roll motion would be maximum. For longer configurations, the hydrodynamic damping (b_{44}) increases, while the excitation moment (F_4) decreases. This combination eventually results in an RAO with lower amplitudes for increased ship lengths. The same behavior is observed for increasing ship breadths.

In the vertical direction, heave motion in combination with pitch and roll contributes to the motion induced-displacement. The results show that vertical motion decreases for longer ship configurations. This could be because of the fact that the heave motion RAO shifts to lower wave frequencies for longer ships. This results in lower RAOs values at the same wave frequency for longer vessels. Furthermore, the pitch and roll RAO also contribute to the reduction in motions for increasing ship lengths. When looking at the influence of ship breadth on the MPE vertical displacement, a relatively constant line is observed. This is because the heave motion is not significantly influenced by ship breadth with the used calculation method. In addition, due to decoupled motions and the weathervaning conditions, the roll motion is very little influenced by increased breadth.

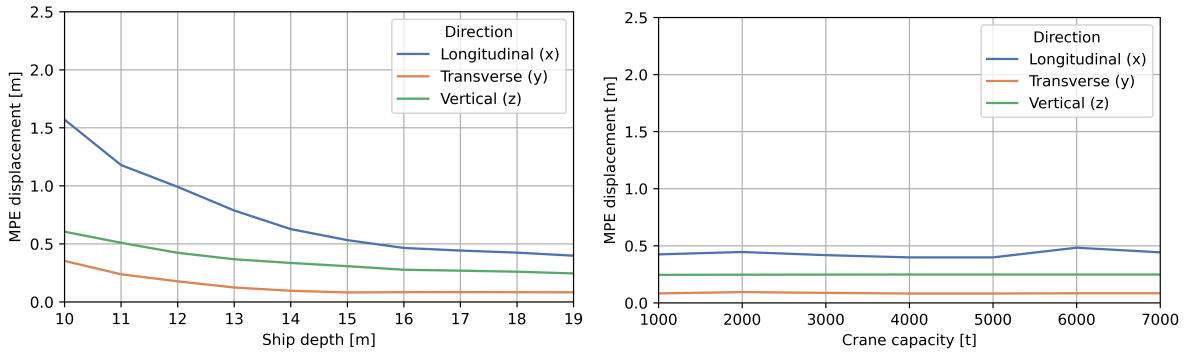

Figure 5.16: Visualization of the MPE displacements during weathervaning.

The influence of depth on the motion behavior of the configurations is not entirely straightforward. As depth increases, so does the maximum draft of a configuration, leading to an increase in displacement. This affects the motion behavior. However, an increase in draft leads also results in a decrease in the sectional hydrodynamic damping (A) and the effective wave number (k), influencing the forcing functions for heave (F_3) and pitch (F_5). This in turn affects the heave and pitch RAOs. Furthermore, increased depth and draft can also affects the ship's stability in multiple ways. On one hand, the draft affects the $\overline{GM_t}$ of a ship configuration, thereby affecting the stability and the behavior of the roll RAO. On the other hand, an increase in depth at the same breadth corresponds to a decrease in B/D ratio. This ratio is very important to establish the GZ curve, which ultimately determines the transverse stability of a configuration. Lower B/D ratios often result in poor stability. Stability of the ship configurations eventually dictates the maximum turbine size they can transport and install. This in turn determines the location of the point in which the local motions are calculated. In general, it can be concluded that an increase in depth results in a decrease of MPE displacement in all directions. This is also reflected in the figure above.

Crane capacity has a limited influence on motion behavior, with the lines for all three directions remaining relatively constant. This is mainly because the ship configurations with the best motion behavior are independent of crane capacity. For example, the best configurations for longitudinal motions are the ones with a low to moderate breadth, in combination with the highest depth. However, because of the combination of breadth and depth, these configurations have poor stability. As a result, these configurations can only handle the smallest turbine sizes in the market. this in turn locates point P, in which the local motions are calculated, closest to the CoG of the vessel. Subsequently, the longitudinal motions are very low. In transverse direction, the first 'best' configurations featuring crane capacities of 1,000 and 2,000 tonnes are very large ships with the largest possible length and breadth. Beyond these, the configurations with the best performance have a resemblance with the ones found for longitudinal motion. These configurations have a breadth and depth that limits their capacity of carrying larger turbines than the smallest turbine size.

The model behavior explained above is obviously not an elegant way to design a vessel, but the model does achieve the objective of findings the configurations with the best seakeeping behavior. This model behavior, while effective, can be considered undesired and should be taken into account when evaluating motion behavior or optimizing a vessel on motion performance.

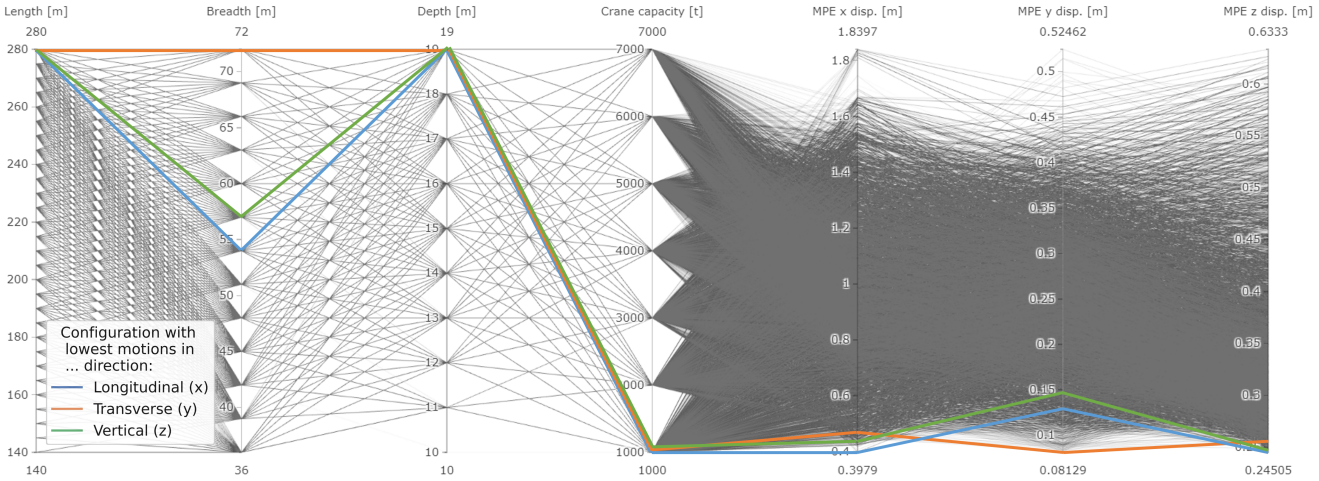

Figure 5.17: Parallel coordinates plot of motion performance.

Figure 5.17 presents a parallel coordinates plot of the motion performance, showing all feasible ship configurations within the design space with their MPE displacements in all three directions. The motions are independent of sailing speed, because the motion behavior is only assessed during installation. Which means that the ship is stationary and ship speed is zero. Therefore, sailing speed is not displayed in the parallel coordinates plot.

Three combinations of ship parameters have been highlighted. These three configurations would have the lowest MPE displacement in one of the three directions. These three optimal ships would be very large and equipped with the smallest crane possible. The model selects these configurations as the best ones, because it can only lift the smallest turbines, with point P for local motion calculation closest to the CoG of the vessel. When comparing the findings from financial performance with the best configurations in terms of motion performance, a large gap is observed between the optimal ship configurations for *Moonshot* is observed. This gap will be addressed later.

5.3.2. Local accelerations while weathervaning

In addition to evaluating displacements during weathervaning, accelerations were also calculated for all configurations to assess the acceleration performance. Just as the MPE dispalcements, the MPE accelerations were calculated in point P for three directions. These three components were then combined into a resultant MPE acceleration vector using Equation 5.1.

$$\text{MPE } \mathbf{a} = \sqrt{(\text{MPE } a_x)^2 + (\text{MPE } a_y)^2 + (\text{MPE } a_z)^2} \tag{5.1}$$

Figure 5.18 depicts the resultant MPE acceleration in relation to the ship displacement of all configurations. Unlike the smooth lines seen in all the previously seen plots, this graph shows more jagged lines. This is because many ship configurations within the design space have displacements that are close to each other, but they have different crane capacities, loading to variations in acceleration behavior. The crane capacity defines the maximum turbine size a vessel can install throughout its operational life. Lower crane capacities result in a smaller maximum turbine sizes, which, by definition, results in a lower hub height. Subsequently, point P in which the local MPE accelerations are calculated will be closer to the ship's CoG.

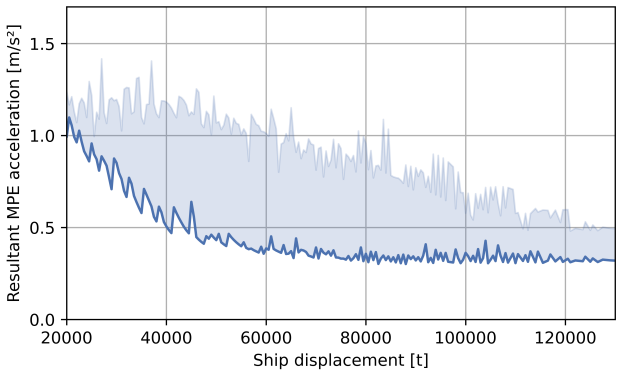

Figure 5.18: Visualization of the MPE acceleration vector results.

To prevent damage to wind turbines, suppliers specify limits on acceleration in the nacelle during transportation and installation. The acceleration limit is typically set at 0.5g [83], which is approximately 4.9 m/s². As demonstrated in the figure, the MPE accelerations for all configurations within the design space remain well below this specified limit. Consequently, accelerations in the nacelle are not considered a major concern during installation. Accordingly, this aspect will not be further explored in this research. However, it is important to keep in mind that the actual local accelerations might be slightly higher, due to the inaccuracies in the calculation methods in SAM. Also, in a next design phase, it is important to also investigate local accelerations that occur on the resulting *Moonshot* concept during transit.

5.4. Seakeeping performance meets financial performance

As previously highlighted, conflicting optimal ship configurations emerge when optimizing for either financial performance or seakeeping performance. To reconcile this discrepancy between the two objectives, a financial penalty will be imposed on configurations exhibiting inferior seakeeping behavior. This penalty will take the form of additional costs for motion compensation, which is a supplement to the base cost for the main crane. The unit of this metric is €/(t·m), incorporates both the crane capacity and the cumulative MPE displacements in longitudinal, transverse, and vertical direction, quantified in meters. While this metric might not be documented in existing literature, it aligns well with practical considerations. It is reasonable to assume that cost of lifting equipment would increase with higher motion compensation requirements. Moreover, including crane capacity in the metric is logical since motion compensation systems for higher crane capacity are likely to be more complex and larger, inherently resulting in higher costs.

As this metric is not documented in existing literature, there is no reference for quantifying the cost of motion compensation. Consequently, a range with different cost levels has been assumed. This range spans from €0 to €10,000/(t·m). The resulting ROI for these different cost levels is depicted in the following figures.

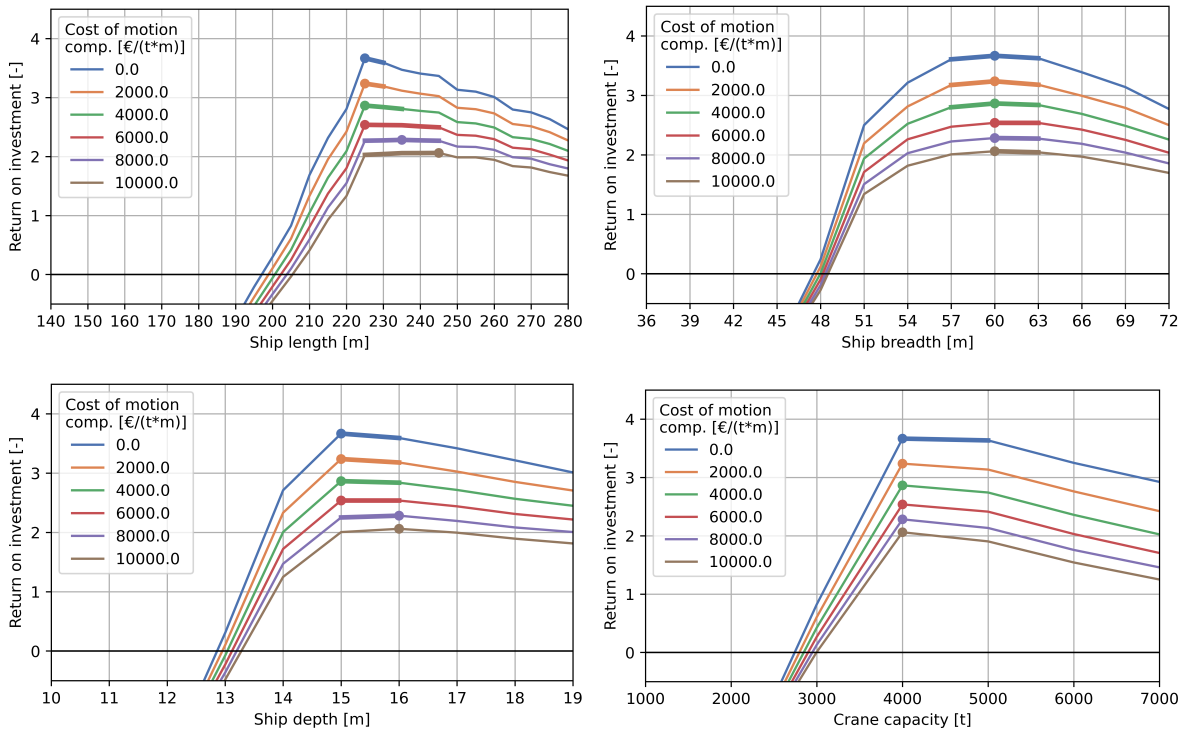

Figure 5.19: Visualization of the financial results with motion performance penalty in a 1,000ft bound market with an operational H_s limit of 2.5 meters.

As expected, the results demonstrate a decrease in ROI as the cost for motion compensation increases. The optimal ship length for different cost levels remains the same up to €6,000/(t·m). Additionally, the optimal range for ship length widens because of the flatter lines beyond the optimal length. For the highest cost levels, the optimal ship length gradually shifts towards longer configurations. This shift aligns with the findings from previous sections, where motion-induced displacements decreased as ship length increased. The shift in optimal length indicates that, at a certain point, the higher costs associated with investing in and operating a longer ship surpasses the increased cost of motion compensation of shorter vessels.

In terms of ship breadth, noticeable variations in ROI are observed for different cost levels for ship breadths exceeding 51.0 meters. The breadth that yields the maximum ROI remains consistent across all cost levels, Only a variation in optimal breadth ranges can be seen.

Regarding ship depth, a similar trend as ship length is observed. The optimal point for ship depth also shifts towards larger values at the highest cost level. Furthermore, the results show that the lines corresponding to higher cost levels are more flat and the optimum becomes less pronounced. The optimal crane capacity is 4,000 tonnes for all cost levels. The trajectory of the lines also remains consistent with the zero cost level. However, what stands out is that the relative differences in ROI for increasing cost levels tends to decrease, resulting in smaller distances between the lines.

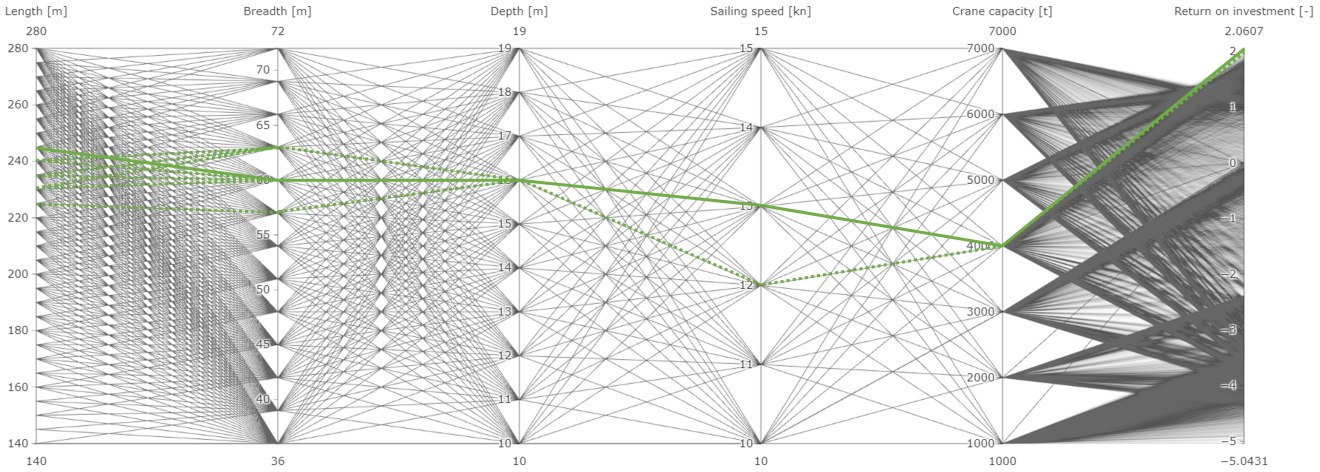

Figure 5.20: Parallel coordinates plot of the financial performance at a motion compensation cost of €10,000/(t·m).

Above, the parallel coordinates plot for all combinations of ship variables at the highest cost level for motion compensation of €10,000/(t·m) is depicted. The continuous line highlights the ship configuration with the highest ROI. Besides that, there are 13 other configurations that perform within 2.5 percent of the best configuration. These are displayed with dotted lines. At this cost level, the best configuration would be slightly longer than the optimal configuration obtained when solely considering financial performance.

5.5. Optimal design ranges for Moonshot

Considering all findings in the previous sections, optimum design ranges for the ship design have been established. These findings for different scenarios are summarized in the table below. Based on the results of all these scenarios, initial design parameters for *Moonshot* can be determined. The initial design parameters can be chosen according to client preferences or based on a designer's perspective. The initial design parameters, as chosen by the author, are displayed in the last row of the table. Eventually, the initial design parameters can be used in the next phase of designing *Moonshot*.

Table 5.2: Summary of optimal design ranges for *Moonshot*.

Category	Length [m]	Breadth [m]	Depth [m]	Sailing speed [kn]	Crane capacity [t]
Financial performance					
16MW bound market	210 - 215	57 - 60	14 - 15	12 - 14	4,000
22MW bound market	225 - 230	60 - 63	15	11 - 13	4,000
1,000ft bound market	225 - 230	57 - 63	15 - 16	11 - 13	4,000 - 5,000
Unbound market	245 - 250	60 - 69	16 - 17	11 - 13	5,000
Distance to port^{+}					
35 NM	225 - 230	54 - 60	15	10 - 13	4,000 - 5,000
140 NM	225 - 230	57 - 63	15 - 16	11 - 13	4,000 - 5,000
350 NM	225 - 230	63	16	12 - 13	4,000 - 5,000
Seakeeping performance$^{+,\circ}$					
Weathervaning x-disp.	280	54	19	11 - 13	1,000
Weathervaning y-disp.	280	72	19	11 - 13	1,000
Weathervaning z-disp.	280	57	19	11 - 13	1,000
Motion compensation*$^{,\circ}$					
€2,000/(t·m)	225 - 230	57 - 63	15 - 16	11 - 13	4,000
€6,000/(t·m)	225 - 245	60 - 63	15 - 16	11 - 13	4,000
€10,000/(t·m)	225 - 245	60 - 63	16	11 - 13	4,000
Initial design parameters	**230**	**63**	**16**	**12**	**4,000**

* in a 1,000ft bound market with a 140 NM distance between port and OWF.
$^{\circ}$ for a maximum significant wave height of 2.5 meters.
$^{+}$ in a 1,000ft bound market scenario.

The seakeeping results, as well as the financial outcomes including motion compensation costs, have been computed for a specified limit of 2.5 meters significant wave height. Further analysis has been conducted to assess the impact of changing the operational H_s limit to 1.5 and 3.5 meters on the main parameters. The findings are detailed in Appendix K.

5.6. Chapter conclusion

In this chapter, the design space of *Moonshot* has been explored. Over 38,000 unique ship configurations have been evaluated on their performance in different market scenarios. Firstly, the financial performance has been addressed, including how the main particulars would affect the performance. Thereafter, all configurations were evaluated on their seakeeping performance. Most probable extreme (MPE) displacements and accelerations were calculated, revealing that accelerations were well within the limits prescribed for wind turbines. The MPE displacements varied a lot between different ship configurations. Optimal ship configurations with minimal motions were found. However, the results revealed a large disparity between the optimal ship configurations for financial performance and seakeeping performance. To address the disparity, a penalty was introduced for vessels with poor seakeeping behavior. The penalty involves cost for motion compensation, which is an amount of euros per tonne crane capacity multiplied by the cumulative MPE displacements. By applying this penalty mechanism, configurations with poor motion behavior but good financial performance automatically get penalized.

Ultimately, optimal design ranges for the ship parameters were determined for all scenarios. These ranges will serve as a basis for determining the initial design parameters for the next stage in the design of *Moonshot*. These design parameters, in combination with the results from the seakeeping analysis, considering a specified workability limit of up to 2.5 meters significant wave height, can be supplied to mission equipment manufacturers. This data allows them to design the appropriate lifting equipment in alignment with the optimal design of *Moonshot*.

(This page intentionally left blank)

6

Benchmarking the design

In the preceding chapters, the *Moonshot* wind turbine installation concept has been developed and its performance was evaluated using *Blended Design*. Also, optimal ship parameters were established for both financial and seakeeping performance. However, a crucial question remains: *"How does the performance of the proposed Moonshot concept design compare to other vessels for future offshore wind turbine installation?"*. In this chapter, the aim is to address this question through benchmarking.

6.1. Strategy for benchmarking

To benchmark the design, the strategy is to create a version of *Moonshot* that competes directly with the largest jack-up design available in the market, the *NG-20000X* design [102] from *GustoMSC*. This jack-up has a capacity of five to six 13 to 16 MW turbines or four 20 MW turbines [103]. A visualization of the jack-up is shown in Figure 6.1.

Figure 6.1: Render of an *NG-20000X* jack-up, currently under construction for *Havfram*. From [104].

To compare the performance of the *Moonshot* concept with the *NG-20000X*, the *Blended Design* tool will be used to create a dedicated variant of *Moonshot* that will exclusively install 20 MW turbines. This enables to make a fair performance comparison with the *NG-20000X* jack-up. Moreover, other installation solutions will also be included in the comparison such as SSCVs and *Huisman*'s *WIV* concept. Concluding, the objective is to identify the optimal configuration for a 20 MW *Moonshot* and evaluate its performance in relation to installation solutions.

For this analysis, the same assumptions for seakeeping were used as in the evaluation earlier in this report. A maximum significant wave height (H_s) of 2.5 meters and ability to weath-

ervane. The input parameters for *Blended Design* are listed in Table 6.1. In total, 1,532,160 ship configurations were investigated, of which 766,001 were found to be feasible. The run time with a single computer was approximately 21 hours.

Table 6.1: Input for *Blended Design* to create the design space for benchmarking.

Particular		Start	End	Step size	#
Length	[m]	179.2	282.8	2.8	38
Breadth	[m]	50.4	71.4	1.4	16
Depth	[m]	12.6	20.3	0.7	12
Sailing speed	[kn]	10.0	15.0	1.0	6
Crane capacity	[t]	1,000	5,000	1,000	5
Block coefficient	[-]	0.75	0.81	0.01	7

6.2. Optimal financial performance

The first step is to explore the optimum design ranges for a 20 MW *Moonshot* in terms of financial performance. The following graphs display the relative ROI within a market exclusively featuring 20 MW turbines. The ROI values are not displayed because the installation reward per MW is unknown, and does not really matter in this analysis. As the focus is on finding the best-performing configurations regardless of absolute ROI values.

The configurations were analyzed for two different cost scenarios for motion compensation. The actual cost levels will most probably fall somewhere within the range of 0 to 10,000 €/(t·m). Consequently, the optimal design configuration is expected to lie between the optimal design points corresponding to these two cost levels.

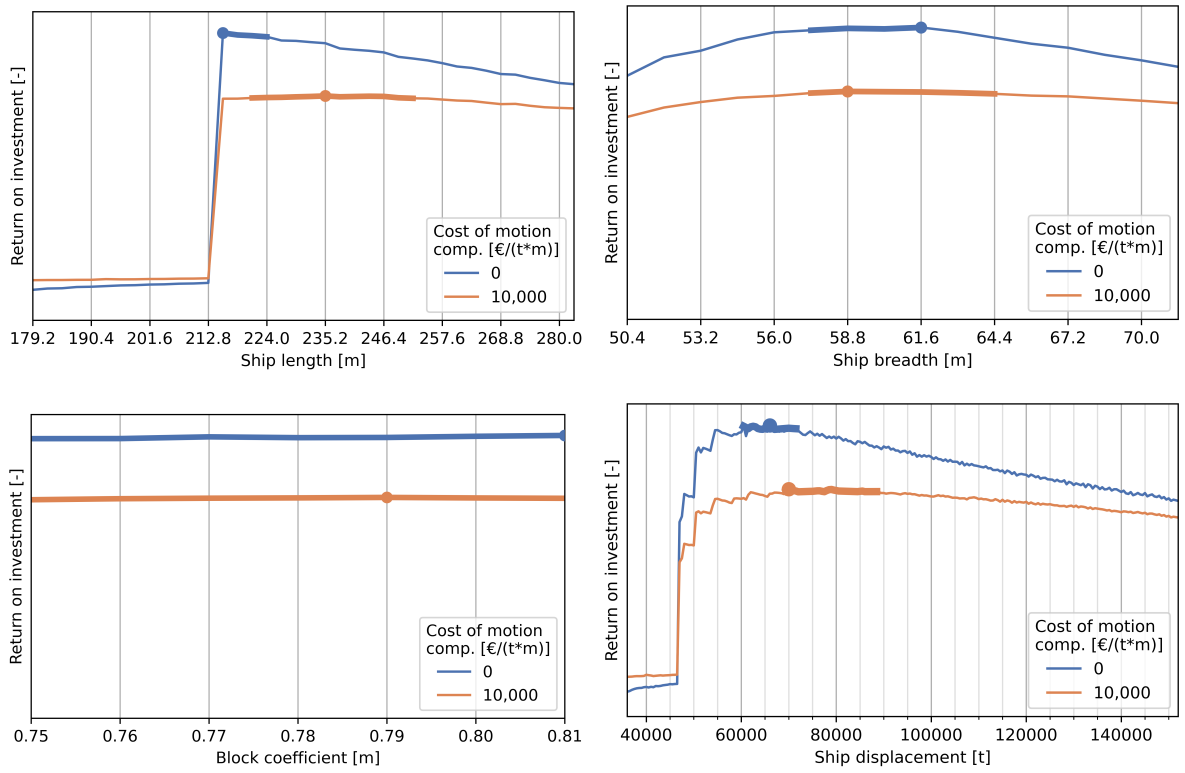

Figure 6.2: Visualization of the financial performance results for the 20 MW *Moonshot*.

It is evident that the optimal crane capacity is around 4,000 tonnes, given the mass of 20 MW turbines. The mass of such a turbine would be around 3,250 tonnes. Therefore, a crane

capacity of 4,000 tonnes would be the most suitable choice, as other crane capacities are either too small or too high. In terms of ship length, anything below 215.6 meters results in a negative ROI. This is due to the required deck length for carry the blades. If the ship is too short, it cannot transport any turbine parts, rendering it enviable. For lengths exceeding 215.6 meters, the ROI gradually declines. The lines indicate that the decrease in ROI is less steep at a cost level of 10,000 €/(t·m), resulting in a broader optimal length range. Regarding depth, the results are not presented here as the plot closely resembles that for breadth. At the higher motion compensation cost level, the optimal depth is higher compared to the scenario with zero penalty. However, an overlap between the optimal ranges occurs at 15.4 meters. The lines for sailing speed are relatively flat. Therefore, the optimal sailing speed would be somewhere between 11 to 13 knots. The results show that the block coefficient does not affect the ROI. In these results, the ship displacement was also visualized, showing a clear optimum. For a zero-cost level, the optimal displacement is around 66,000 tonnes, with a range extending from 60,000 to 72,000 tonnes. At a cost level of €10,000 the range is much wider, spanning from 69,000 to 88,000 tonnes. This is due to the earlier findings that larger ships provide better seakeeping performance. There is an overlap between the optimal design displacements for the two costs levels for motion compensation. This overlap spans from a displacement of 69,000 to 72,000 tonnes. The optimal displacement of the final 20 MW *Moonshot* would thus fall within this range.

6.3. Optimal seakeeping performance

In the previous section, design ranges have been identified for a 20 MW *Moonshot* configuration with optimal financial performance. Now, optimal seakeeping performance will be assessed. The approach will be different to the earlier seakeeping assessment in Chapter 5. Given the established optimal displacement of around 70,000 tonnes from the financial analysis, this analysis will maintain a fixed displacement while varying other ship parameters to identify the most suitable ones for the best seakeeping performance. These calculations were performed for a set operational H_s limit of 2.5 meters while weathervaning. The results are presented in the following graphs, which represent the sum of the MPE displacement in the directions. For guidance on interpreting these plots, please refer to Figure 5.1 in the previous chapter.

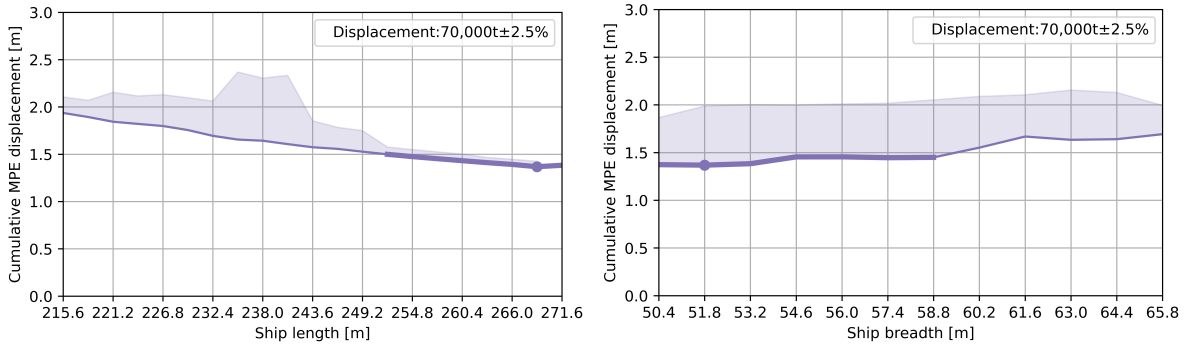

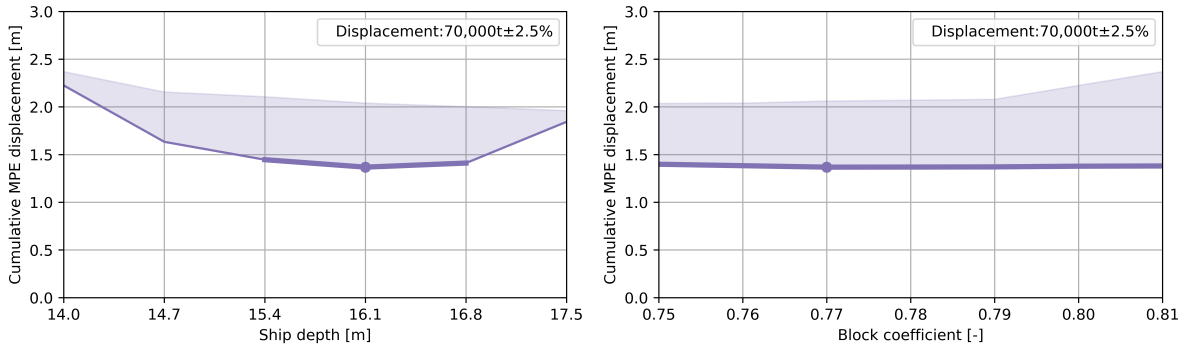

Figure 6.3: Visualization of the seakeeping performance results for the 20 MW *Moonshot* with fixed displacement.

Comparing these results with those from Section 5.3 in Chapter 5, it can be observed that some of these plots show different and more interesting behavior due to the fixed turbine capacity of 20 MW and displacement. For instance, a distinct optimum ship depth can be observed at 16.1 meters depth. Also, the cumulative MPE motion-induced displacement decreases as ship length increases, which is a consequence of the fact that longitudinal motions are dominant, given the weathervaning assumption. As seen in the previous chapter, longer ships experience less longitudinal displacements. Conversely, the results above show that smaller ship breadths result in lower MPE displacements. This is interesting behavior compared to the findings from the previous chapter on seakeeping performance. The observed increase in cumulative MPE displacement for larger ship breadths can be attributed to the displacement constraint; if the ship breadth increases, the associated ship length would automatically be lower. This impacts the longitudinal displacement, which is the main contributor to the cumulative displacement. The results also show that seakeeping behavior is not affected by the block coefficient. Sailing speed does not matter for this seakeeping analysis because the calculated behavior is during installation. Therefore, sailing speed would only influence the weight and CoG of the ship as a result of fuel and machinery weight.

6.4. Optimal design parameters for the 20 MW *Moonshot*

The optimal design ranges of a 20 MW *Moonshot* are summarized in Table 6.2. The values in the last row represent the determined optimal ship parameters for the 20 MW *Moonshot*.

Table 6.2: Summary of optimal design ranges for the 20 MW *Moonshot*.

Category	Length [m]	Breadth [m]	Depth [m]	Block coefficient [-]	Sailing speed [kn]	Crane capacity [t]
Financial performance						
Penalty €0/(t·m)	215.6 - 224.0	57.4 - 61.6	14.0 - 15.4	0.75 - 0.81	10 - 13	4,000
Penalty €10,000/(t·m)	221.2 - 252.0	57.4 - 64.4	15.4 - 16.8	0.75 - 0.81	11 - 13	4,000
Seakeeping						
Weathervaning H_s=2.5	252.0 - 271.6	50.4 - 58.8	15.4 - 16.8	0.75 - 0.81	10 - 15	4,000
20 MW Moonshot	**252.0**	**58.8**	**16.8**	**0.79**	**13**	**4,000**

6.5. Comparing *Moonshot* with other solutions

The performance of the 20 MW *Moonshot* configuration can now be compared with the *NG-20000X* jack-up, SSCV, and *Huisman*'s *WIV* concept. All solutions will be evaluated on several key metrics such as day rate, number of installed turbines in one year, and installation cost per MW. For the *Moonshot* variant these metrics can be derived from the output of *Blended Design*. The metrics for the other solutions need to be calculated manually. Several assumption were made for this:

1. The number of operational days per year is 300. The remaining 65 days are allocated for repairs, maintenance, and relocation of the vessel;
2. Day rates are paid for every operational day, even when waiting on weather. This is common practice [105];
3. The distance between the marshalling port and OWF location is 140 NM.
4. SSCVs and the *WIV* cannot enter marshalling ports and require feeder systems. Therefore, they are assumed to sail to the OWF location and back to port once, while staying the rest of the year at sea;
5. Turbine component transfer from the feeder to the installation vessel is assumed not to occur simultaneously with assembly or installation. It is deemed to be too risky to have multiple lifting operations going on at the same time on a vessel;
6. Towers for the *WIV* concept are transported horizontally by feeder vessels. Therefore, they can be fed as single components. Transporting towers horizontally is, however, questionable (as described earlier in section of Chapter 3);
7. Towers for the SSCVs are transported vertically. Because of the characteristics of feeder barges or vessel, it is assumed that they are transported in two separate parts.

The sailing speed of the *NG-20000X* not known, so this is estimated to be around 11 knots. This is in accordance with other WTIVs (Appendix B). The day rate of a *NG-20000X* is also unknown. Recently, an article was published about *Cadeler* signing an installation contract with a day rate around €375,000 per day [106] for a project in 2026. The contract is for only 11 MW turbines and a smaller jack-up than the *NG-20000X* will be deployed. Therefore, the day rate of a *NG-20000X* jack-up is assumed to be in the same range. It could very well be that it would be even higher, as this jack-up will be larger and capable of handling larger turbines. The H_s limit of jack-ups is typically 1.5 to 2.0 meters (Table 1.2 in Chapter 1). This corresponds to an operability of 60 percent in the North Sea. The assumed operational cycle of the jack-up is shown in Appendix I. The following equations are used to calculate the key metrics for the jack-up design.

$$\begin{aligned} t_{roundtrip} = {} & t_{jack.up} + t_{harbour.ops} \cdot N_{WTG} + t_{jack.down} \\ & + 2 \cdot t_{sailing} \\ & + (t_{jack.up} + t_{installation} + t_{jack.down}) \cdot N_{WTG} \end{aligned} \tag{6.1}$$

$$\text{Turbines/year [-]} = \frac{\text{Workability} \cdot \text{Oper. days} \cdot 24}{t_{roundtrip} \cdot N_{WTG}} \tag{6.2}$$

$$\text{Installation costs [€/MW]} = \frac{\text{Day rate [€/day]}}{24} \cdot \frac{t_{roundtrip}}{\text{Workability [-]} \cdot N_{WTG} \cdot P_{WTG}} \tag{6.3}$$

According to literature, the day rate of an SSCV could be up to €500,000 per day [28]. However, [105] indicated that day rates for SSCVs could be up to €1,000,000 per day. Therefore, for this analysis the day rate of the SSCV was assumed to be €750,000. This day rate was also adopted for the *WIV*. For smooth operations without too much waiting time, it was assumed that at least two feeder vessels would have to be deployed. The day rate per feeder vessel would probably be around €50,000 per day [28]. This was found to also be in accordance with internal knowledge within *UDSBV* [105]. The feeder vessels are assumed to be gearless, so for loading of the components in the marshalling port, a large harbour crane would be required. Therefore, the rent of this crane needs also to be incorporated in the installation costs. The rent of a 2,500-tonne crane was assumed to be around €32,000 per day. This number was calculated with the cost per tonne for an offshore crane, as included in *Blended*

Design. The operational cycles for both the SSCV and *WIV* concept are attached in Appendix H. The following equations are used to calculate the desired metrics for the SSCV and the *WIV* concept.

$$t_{per.turbine} = t_{offshore.loading} + t_{installation} \tag{6.4}$$

$$\text{Turbines/year [-]} = \frac{\text{Workability} \cdot \text{Oper. days} \cdot 24 - 2 \cdot t_{sailing}}{t_{per.turbine}} \tag{6.5}$$

$$\text{Installation costs [€/MW]} = \frac{\text{Day rate [€/day]} \cdot \text{Oper. days}}{\text{Turbines/year [-]} \cdot P_{WTG}} \tag{6.6}$$

Table 6.3 presents a comparison of main particulars for the various installation solutions. The calculated key metrics are also included in the table. It is important to note that these results are subject to the associated assumptions. Therefore, absolute results from the table should be interpreted with caution.

Table 6.3: Comparison of different installation solutions to benchmark *Moonshot*.

Parameter	Unit	NG-20000X	SSCV	*Huisman*'s *WIV* concept	20 MW *Moonshot*
Sailing speed	[kn]	11	10	12	13
Cargo capacity (20 MW turbines)	[-]	4	-	-	5
Workability	[-]	0.6	0.6^{+}	0.6^{+}	0.78
Day rate installation vessel	[€/day]	375,000	750,000	750,000	260,000*
Day rate feeder vessels	[€/day]	-	2x 50,000	2x 50,000	-
Day rate harbour crane	[€/day]	-	32,000	32,000	-
Installed turbines per year	[-]	110	165	179	180
Cost per installed MW	**[€/MW]**	**50,900**	**80,100**	**73,900**	**21,500***

$^{+}$ The actual workability of the installation vessel is higher. However, it is assumed that the workability is dictated by the offshore transfer from the feeder barges or vessels.

$*$ Profit margins are not included in the day rates and installation cost per MW for *Moonshot*, whereas for the other solution it is included.

According to *Blended Design calculations*, the day rate for the established 20 MW *Moonshot* would be between €225,000 and €260,000 per day, depending on the cost for motion compensation, which would be notably lower than the day rates for the other solutions. However, it is important to consider that the day rate alone does not provide insight into the overall efficiency of the solution. Therefore, the number of turbines and cost per installed MW are also included. The analysis reveals that the number of installed turbines per year is higher for the other solutions, indicating that *Moonshot* would be a more efficient solution. This is also reflected in the cost per installed MW, which is at 19,000 to 21,500 €/MW significantly lower than all other solutions. These findings highlight the cost-efficiency of *Moonshot*.

As mentioned in the table, the day rates listed in the table for the other solutions include profit margins, representing the cost to rent the vessel for a day. However, the calculated day rate for *Moonshot* by *Blended Design* only covers all vessel costs, such as CAPEX, OPEX, and VOYEX, without accounting for profit margins. Consequently, the day rate would automatically be lower than for the other solutions. This difference in calculation has a direct impact on the cost per installed MW. Therefore, it is tricky to one-on-one compare the number of the other solutions with the numbers for *Moonshot*.

To better understand how an increase in the day rate of *Moonshot* due to profits and other margins would impact these calculations, consider a scenario in which the day rate of the 20 MW *Moonshot* would be 50 percent higher. In this case, the day rate would increase to approximately €390,000 per day. Despite the substantial increase, the cost per installed MW for

Moonshot would be 33,000 €/MW. This would still be significantly lower than the other installation solutions, ensuring its competitiveness.

The results of the benchmarking show the potential of *Moonshot* in comparison to other solutions as a competitive and cost-efficient offshore wind turbine installation solution. Above all, the *Moonshot* concept is not constrained by seabed conditions or water depth, which one of the primary motivations for its development as an alternative to traditional jack-up designs. These findings encourage further exploration of the technical feasibility of *Moonshot*.

6.6. Visualization of *Moonshot*

Figure 6.4 shows a visualization of the 20 MW *Moonshot* with the *Zephyr* crane concept from *Huisman*. Additional artist impressions, including renders of the intended installation process, are presented in Appendix M.

Figure 6.4: Artist impression of the 20 MW *Moonshot*

6.7. Chapter conclusion

In this chapter, the *Moonshot* concept was benchmarked against other wind turbine installation alternatives. A variant of *Moonshot* was created to directly compete with the largest self-propelled jack-up design, the *NG-20000X*. A *Moonshot* configuration was developed using *Blended Design*, specifically designed for the transportation and installation of 20 MW turbines. This approach enabled a fair comparison between *Moonshot* and its direct competitor. While creating the 20 MW *Moonshot* design, an evaluation was conducted on financial and seakeeping performance. Eventually, optimal design parameters for the 20 MW *Moonshot* were determined. Subsequently, the resulting 20 MW *Moonshot* design was compared to the *NG-20000X* jack-up, an SSCV, and *Huisman*'s *WIV* concept, considering operational cycles, day rates, the number of installed 20 MW turbines per operational year, and cost per installed MW. Benchmarking revealed that *Moonshot* is a more efficient and cost-effective solution, capable of installing a larger number of turbines per year at a considerably lower cost per MW compared to other solutions. The results of the benchmarking show the potential of *Moonshot* in comparison to other solutions as a competitive and cost-efficient offshore wind turbine installation solution. Above all, *Moonshot* is not constrained by seabed conditions or water depth, addressing the main bottleneck of jack-up vessels.

(This page intentionally left blank)

7

Conclusion

The objective of this research was to explore the feasibility of a floating monohull vessel,*Moonshot*, for installation of offshore wind turbines and to optimize it for future offshore wind markets. The main research question of this research was as follows:

"What should optimal design parameters be for the innovative Moonshot concept, a floating monohull vessel for offshore wind turbine installation, taking into account financial and seakeeping performance, while considering the uncertainties and evolving requirements of the offshore wind market?"

To answer the main research question of this research, the sub-questions and the answers to them will be addressed in the following part.

What are state-of-the-art ship design strategies and how can they cope with innovation and the uncertainty of the offshore wind market and requirements for future offshore wind installation vessels?
A lot of different ship design strategies are available and described in literature. The main strategies are: point-based design, set-based design and Systems Engineering, system-based and optimization-based design. The approach and goal of each strategy has been reviewed, along with their respective advantages and disadvantages. All strategies were evaluated on aspects that apply to the development for *Moonshot*. These consider innovation, optimization with a parametric model, and flexibility in dealing with changing requirements or market uncertainty. No design strategy was found to be particularly suitable for the development of *Moonshot*. In response to this, two strategies by *UDSBV* have been introduced and explained in detail. These methods are: *Controlled Innovation* and *Blended Design*. An evaluation of the capabilities of these strategies was also conducted. The analysis showed that a combination of the two strategies would be highly suitable for the design process of *Moonshot*. The main characteristic of the *Controlled Innovation* process is that it enables the design of major innovations, while *Blended Design*'s strength is that it can account for uncertain markets and evaluate the performance of a wide range of design variations. However, *Blended Design* requires modifications to tailor it to the specific needs of *Moonshot*.

How can the Moonshot idea for turbine installation from a floating monohull be developed into a viable ship concept using UDSBV's Controlled Innovation process?
A combination of *Controlled Innovation* and *Blended Design* emerged as the most appropriate design strategy for the development of *Moonshot*. Initially, it was unclear which parts of the design process would be best suited for *Controlled Innovation* and where *Blended Design* should

be used. To address this, *Controlled Innovation* was employed to establish the high-level objective and functions of the design. Subsequently, the underlying design aspects associated with the functions were identified. Following a systematic approach, the design aspects have been evaluated on uncertainty of their requirements and the consequence on the design. n. In this way, high-risk design aspects, requiring extra focus or knowledge generation, were identified. Eventually, a differentiation between those design aspects has been made whether they could be covered in development packages, which are part of the *Controlled Innovation* process, or that a design aspect should be covered in *Blended Design*. Three designs aspects that needed knowledge generation within development packages were identified, including the lifting equipment, turbine component properties, and optimal deck layout. Requirements of other high-risk design aspects were found to be best addressed with *Blended Design*.

The conclusion of the development package about lifting equipment was that a combination of a free-hanging and guided lift solution, such as *Huisman*'s *Zephyr* crane concept, would be the preferred solution for *Moonshot*. In the second development package, correlations between size and mass properties of wind turbine components were investigated with data on wind turbine models and literature. Correlations between most of the parameters were found. Based on the data points, fitting curves were established. These curves were used for extrapolation to estimate the size and mass properties of next-generation wind turbine components. Also, CoG locations of wind turbine components were identified. The third development package explored various deck layouts. The third development package explored various deck layouts. Following an extensive analysis of different options on various criteria, the research concluded that the most favorable deck layout would have the lifting equipment and assembly location on the side of the vessel, with installation of the turbine over the side.

What modifications to Blended Design are needed to properly explore the design space for Moonshot and evaluate financial and seakeeping performance?
The existing *Blended Design* model lacks the ability to assess seakeeping behavior. The model is also unsuitable for wind turbine installation vessels. As a result, several modifications were made to the model to address these limitations. All changes to the existing model and revised assumptions have been discussed, such as the addition of a wind turbine deck cargo module.

The most substantial addition was the seakeeping analysis module (SAM). An approach for determining the response maxima for a set operational limit has been devised. The approach involved calculating the RAOs in six degrees of freedom for all ship configurations in the design space. Various methods were explored, such as the semi-analytical method proposed by Jensen et al. [88] for calculation of the heave, roll, and pitch RAOs. The resulting RAOs from this method were validated with RAOs from hydrodynamic analysis software. Various ways to validate the results were used, such as a visual comparison, comparison of the areas under the RAO curves, and the standard deviation of the response spectrum for different wave heading angles and three different wave periods. The validation showed that the method by Jensen et al. produces results in the correct order of magnitude and could be applicable to predict the relative merits of ship configurations within the design space. In addition, an attempt was made to calculate the RAOs for the remaining degrees of freedom, drawing upon a method by Matsui et al. [90]. Unfortunately, this method did not yield satisfactory results. Therefore, it was decided to only incorporate the three RAOs from the method by Jensen et al. in the module.

The output from SAM was further validated by comparing the results with those obtained from hydrodynamic software. Local response maxima for different wave periods in both omnidirectional and weathervaning conditions were calculated. The validation demonstrated that SAM provided accurate results for weathervaning conditions but was not suitable for use in an omnidirectional wave environment.

How would the main particulars of the Moonshot design influence its financial and seakeeping performance in various future offshore wind market scenarios?
Different future wind market scenarios were simulated using *Blended Design*. Subsequently, the financial performance of over 38,000 unique ship configurations was evaluated within these market scenarios. Following that, all configurations were evaluated on their seakeeping performance. Most probable extreme (MPE) displacements and accelerations were calculated, revealing that accelerations of all ship configurations were well within the limits prescribed for wind turbines. The MPE displacements varied a lot between different ship configurations. Optimal ship configurations with minimal motions were found. However, the results revealed a large disparity between the optimal ship configurations in terms of financial and seakeeping performance. To address this disparity, a penalty was introduced for vessels with poor seakeeping behavior. The penalty involved a cost for motion compensation, which is an amount of euros per tonne crane capacity multiplied by the cumulative MPE displacements [€/($t \cdot m$)]. By applying this penalty mechanism, configurations with poor motion behavior but good financial performance automatically get penalized. The exact cost for motion compensation remains uncertain; therefore, various cost levels were introduced. This approach led to new optimal ship configurations that varied depending on the costs levels. Ultimately, optimal design ranges for the ship parameters were determined across all scenarios. These ranges will serve as a basis for determining the initial design parameters for the next stage in the design of *Moonshot*.

How does the performance of the proposed Moonshot concept design compare to other vessels for future offshore wind turbine installation?
The answer to the previous sub-question revealed that *Moonshot* could potentially be a viable concept for future wind turbine installation with a floating monohull. However, this evaluation did not provide insights into how well *Moonshot* would compare to other installation solutions. Consequently, the *Moonshot* concept was benchmarked against other wind turbine installation alternatives. A variant of *Moonshot* was created to directly compete with the largest self-propelled jack-up design, the *NG-20000X*. A *Moonshot* configuration was developed using *Blended Design*, specifically designed for the transportation and installation of 20 MW turbines. This approach enabled a fair comparison between *Moonshot* and its direct competitor. While creating the 20 MW *Moonshot* design, an evaluation was conducted on financial and seakeeping performance. Eventually, optimal design parameters for the 20 MW *Moonshot* were determined. Subsequently, the resulting 20 MW *Moonshot* design was compared to the *NG-20000X* jack-up, an SSCV, and *Huisman*'s *WIV* concept, considering operational cycles, day rates, number of installed 20 MW turbines per operational year, and cost per installed MW.

Benchmarking revealed that *Moonshot* is a more efficient and cost-effective solution, capable of installing a larger number of turbines per year at a considerably lower cost per MW compared to other solutions. The results of the benchmarking show the potential of *Moonshot* in comparison to other solutions as a competitive and cost-efficient offshore wind turbine installation solution. Above all, *Moonshot* is not constrained by seabed conditions or water depth, addressing the main bottleneck of jack-up vessels.

(This page intentionally left blank)

8

Discussion

This research shows the potential for *Moonshot*, a floating monohull solution for wind turbine installation. Further research is required to advance the concept into a feasible ship design, which will hopefully disrupt the wind turbine installation and accelerate the energy transition.

Mission equipment

During the development of the *Moonshot* concept, several assumptions were made regarding mission equipment, including the crane concept. Additionally, workability for the ship concept was established, based on a set requirement for the maximum significant wave height. The next step in the development of *Moonshot* would involve engaging equipment designers, such as *Huisman*, to collaborate on refining the operational requirements for *Moonshot* and elaborate more on the logistical process on board and the required equipment and tools. In this way, they can design the right equipment solutions for the design. This would result in more detailed specifications and information about the mission equipment. These details could then be used to validate the initial assumptions or update *Blended Design* to assess potential changes in the model and optimal ship design parameters.

Converge towards a feasible solution

While this research suggests that the concept of *Moonshot* could be a promising solution, it is essential to acknowledge that various unknowns and challenges still exist and require more detailed analysis, particularly concerning mission equipment. When information about the mission equipment is more clear, *Moonshot* could be evolved further. This involves refining the design iteratively, based on the established initial ship parameters obtained from *Blended Design*. The aim is to work towards a complete and feasible ship design. Once a complete concept design is finished, it will be possible to validate the scaling factors and functions within *Blended Design* for this specific ship type, thereby enhancing the accuracy of results in future *Moonshot* design assessments.

Environmental performance and alternative fuels

Environmental performance was not the primary focus of this research on the concept development of *Moonshot*. However, a brief analysis was conducted the environmental performance of configurations falling within the optimal displacement range for financial performance from Chapter 6. This analysis is not included in the thesis but is presented in Appendix L due to being beyond the scope of this research. However, as the industry is looking into greener solutions for ships, environmental considerations will play a more and more significant role. Also, the anticipation of future CO_2 taxes highlights the importance of emissions reduction. There-

fore, it is recommended to further analyze the feasibility of using alternative fuels in *Moonshot*, assessing their impact on financial performance and, possibly, optimal ship dimensions.

Response amplitude operators
This research explored two methods for rapid determination of a ship's RAOs. Only one of the two yielded satisfactory results, resulting in the incorporation of calculations for only three of the six RAOs within the seakeeping assessment module in *Blended Design*. Further research efforts may focus on refining the other method or developing a new approach for fast determination of the surge, sway, and yaw RAOs.

Improving the seakeeping analysis module
Validation of the seakeeping analysis module showed that the applicability of the module is limited to weathervaning conditions, as omnidirectional environments do no generate sensible results. If the determination of the RAOs would be improved, this could also improve the applicability of the seakeeping module. Additionally, the results of the seakeeping module were validated using only one ship design. The recommendation is to validate the results of the calculations for other ship sizes too, using hydrodynamic analysis software.

Floating wind
While this research primarily focused on wind turbine installation on bottom-fixed foundations, it is worth investigating whether *Moonshot* would also be suitable for turbine installation on floating foundations. Especially with floating-to-floating installation, the motion challenges would be a lot bigger. It should be investigated whether this would be possible with the developed *Moonshot* concept or how it would affect the design to make it work.

Operational regions
The seakeeping performance analysis of *Moonshot* was performed based on the wave scatter diagram of only one region, the North Sea. It could be interesting to explore how *Moonshot* would perform in other regions and if it would affect the optimal ship parameters. The seakeeping assessment module in *Blended Design* is set-up in such a way that it would be fairly easy to calculate the seakeeping performance for other regions. The Weibull parameters and Log-Normal distribution parameters to determine wave scatter diagrams nautic zones can be found in DNV-RP-C205 [82]. These parameters can then be adjusted in the input of the seakeeping module, changing the wave scatter diagram, workability, and seakeeping results.

Improving *Blended Design*
The original code for *Blended Design* was written as part of a graduation project. Thereafter, the code was reorganized and used for another graduation project, adding new code for a new vessel type. This resulted in some code quality issues. In addition, all functions and code were documented well. As a result, a lot went into understanding all elements of the code and making sure that everything worked properly before adding new code. I now have written documentation about all parts and functions of the code, making sure that other *UDSBV* employees or new graduates do not have to spend a lot of time in understanding the code. During this process, bugs, not properly working parts, and out-dated or incomplete assumptions were found. Time was also invested in enhancing the code's structure and modularization, to make it easier to fit the new modules for wind turbine installation and *Moonshot*. While substantial progress has been made in this regard, refining the *Blended Design* code is an ongoing task. There is still work to be done to improve the tool and to ease implementation of other ship types, making the tool more flexible and robust.

References

[1] United Nations. *Causes and Effects of Climate Change*. n.d. URL: https://www.un.org/en/climatechange/science/causes-effects-climate-change (visited on 02/17/2023).

[2] U.S. Energy Information Administration. *Wind explained - Wind energy and the environment*. 2022. URL: https://www.eia.gov/energyexplained/wind/wind-energy-and-the-environment.php (visited on 02/17/2023).

[3] K. E. Thomsen. "Chapter 1 - What is an Offshore Wind Farm?" In: *Offshore Wind*. Elsevier, 2012, pp. 1–7. ISBN: 9780123859365. DOI: https://doi.org/10.1016/B978-0-12-385936-5.00001-1.

[4] P. Van der Male. *Lecture notes of OE44005 Introduction to Offshore Engineering*. Delft University of Technology, 2021.

[5] D. L. Chandler. *This algorithm can make all the world's wind farms produce more electricity*. 2022. URL: https://www.weforum.org/agenda/2022/08/new-method-wind-farms-energy-output/ (visited on 02/20/2023).

[6] G. Nikitas, S. Bhattacharya, and N. Vimalan. "Chapter 16 - Wind Energy". In: *Future energy (Third edition)*. Ed. by T. Letcher. Elsevier, 2020, pp. 331–355. ISBN: 9780081028865. DOI: https://doi.org/10.1016/B978-0-08-102886-5.00016-5.

[7] Corporate Finance Institute. *Levelized Cost of Energy (LCOE)*. 2022. URL: https://corporatefinanceinstitute.com/resources/valuation/levelized-cost-of-energy-lcoe/ (visited on 02/21/2023).

[8] International Energy Agency. *Projected Costs of Generating Electricity*. pg 14. 2020. URL: https://iea.blob.core.windows.net/assets/ae17da3d-e8a5-4163-a3ec-2e6fb0b5677d/Projected-Costs-of-Generating-Electricity-2020.pdf (visited on 02/22/2023).

[9] P.E. Morthorst and L. Kitzing. "Chapter 2 - Economics of building and operating offshore wind farms". In: *Offshore Wind Farms - Technologies, Design & Operation*. Ed. by C. Ng and L. Ran. Woodhead Publishing, 2016, pp. 9–27. ISBN: 9780081007792. DOI: https://doi.org/10.1016/B978-0-08-100779-2.00002-7.

[10] C. Maienza et al. "A Comparative Analysis of Construction Costs of Onshore and Shallow- and Deep-Water Offshore Wind Farms: IN-VENTO 2018". In: *Proceedings of the XV Conference of the Italian Association for Wind Engineering* (2019), pp. 440–453. DOI: 10.1007/978-3-030-12815-9_35.

[11] F. Kuhn et al. *How to succeed in the expanding global offshore wind market*. McKinsey & Company, 2022.

[12] M. Bošnjaković et al. "Wind Turbine Technology Trends". In: *Applied Sciences* 12.17 (2022). 8653. ISSN: 2076-3417. DOI: https://doi.org/10.3390/app12178653.

[13] J.S. Hill. *Massive 20MW turbines proposed for world's first subsidy-free floating wind farm*. 2022. URL: https://reneweconomy.com.au/massive-20mw-turbines-proposed-for-worlds-first-subsidy-free-floating-wind-farm/#:~:text=Massive%2020MW%20turbines%20proposed%20for%20world's%20first%20subsidy%2Dfree%20floating%20wind%20farm,-Joshua%20S%20Hill&text=Source%3A%20BayWa.&text=German%20renewable%20energy%20developer%20BayWa,off%20the%20coast%20of%20Portugal (visited on 01/06/2023).

[14] Vestas. *V236-15.0 MW*. n.d. URL: https://www.vestas.com/en/products/offshore/V236-15MW (visited on 02/28/2023).

[15] Van Oord. *Van Oord orders mega ship to install 20 MW offshore wind foundations and turbines*. 2021. URL: https://www.vanoord.com/en/updates/van-oord-orders-mega-ship (visited on 01/04/2023).

[16] National Renewable Energy Laboratory. *Definition of the IEA Wind 15-Megawatt Offshore Reference Wind Turbine*. 2020. URL: https://www.nrel.gov/docs/fy20osti/75698.pdf (visited on 02/28/2023).

[17] INNOSEA (INS). *D.4.2 – Design Brief: Specifications of a generic wind turbine*. 190927-FLT-WP4$_D - 4 - 2_V2$. 2019. URL: https://flotantproject.eu/wp-content/uploads/2020/04/190927_FLT-D.4.2-Specification_Turbine_V2.pdf (visited on 02/28/2023).

[18] C.E. Silva de Souza and E.E. Bachynski-Polić. "Design, structural modeling, control, and performance of 20 MW spar floating wind turbines". In: *Marine Structures* 84 (2022). 103182. ISSN: 0951-8339. DOI: https://doi.org/10.1016/j.marstruc.2022.103182.

[19] I. Komusanac et al. *Wind energy in Europe*. WindEurope, 2021. URL: https://www.windenergyhamburg.com/fileadmin/windenergy/2022/pdf/we22_wind-europe-stats2020.pdf (visited on 01/06/2023).

[20] WindEurope. *Offshore wind in Europe*. 2020. URL: https://windeurope.org/wp-content/uploads/files/aboutwind/statistics/WindEurope-Annual-Offshore-Statistics-2019.pdf (visited on 02/28/2023).

[21] Renewable Consulting Group & Norwegian Energy Partners. *Global Offshore Wind: Annual Market Report 2022*. 2022. (Visited on 02/24/2023).

[22] Fowind. *Supply chain, Port infrastructure and Logistics study*. Facilitating Offshore Wind in India (FOWIND), 2016. URL: https://www.gwec.net/wp-content/uploads/vip/Fowind-study-report_29-06-2016_pages_JWG-update_v2.pdf.

[23] S.B. Parkison and W. Kempton. "Marshaling ports required to meet US policy targets for offshore wind power". In: *Energy Policy* 163 (2022). 112817. ISSN: 0301-4215. DOI: https://doi.org/10.1016/j.enpol.2022.112817.

[24] I.F.A. Vis and E. Ursavas. "Assessment approaches to logistics for offshore wind energy installation". In: *Sustainable Energy Technologies and Assessments* 14 (2016), pp. 80–91. ISSN: 2213-1388. DOI: https://doi.org/10.1016/j.seta.2016.02.001.

[25] M. Asgarpour. "Chapter 17 - Assembly, transportation, installation and commissioning of offshore wind farms". In: *Offshore Wind Farms - Technologies, Design & Operation*. Ed. by C. Ng and L. Ran. Woodhead Publishing, 2016, pp. 527–541. ISBN: 9780081007792. DOI: https://doi.org/10.1016/B978-0-08-100779-2.00017-9.

[26] D. Foxwell. *Warning issued that offshore wind won't have enough foundation installation vessels*. Riviera. 2022. URL: https://www.rivieramm.com/news-content-hub/news-content-hub/warning-issued-that-offshore-wind-sector-wont-have-enough-foundation-installation-vessels-71561 (visited on 03/02/2023).

[27] Siemens Gamesa. *How it all comes together at sea: installing an offshore wind farm*. 2020. URL: https://www.youtube.com/watch?v=mDvS7tizetg&ab_channel=SiemensGamesa (visited on 03/02/2023).

[28] Z. Jiang. "Installation of offshore wind turbines: A technical review". In: *Renewable and Sustainable Energy Reviews* 139 (2021). 110576. ISSN: 1364-0321. DOI: https://doi.org/10.1016/j.rser.2020.110576.

[29] M. Richmond et al. "Multi-Criteria Decision Analysis for Benchmarking Human-Free Lifting Solutions in the Offshore Wind Energy Environment". In: *Energies* 11 (2018). 1175. DOI: https://doi.org/10.3390/en11051175.

[30] EnergyFacts.eu. *Revolutionary Construction Methodology for Arcadis Ost 1 Offshore Wind Farm*. 2019. URL: https://www.energyfacts.eu/revolutionary-construction-methodology-for-arcadis-ost-1-offshore-wind-farm/ (visited on 04/06/2023).

[31] M.J. Kaiser and B. Snyder. *Offshore Wind Energy Installation and Decommissioning Cost Estimation in the U.S. Outer Continental Shelf*. Herndon, VA: U.S. Dept. of the Interior, Bureau of Ocean Energy Management, Regulation and Enforcement, 2011. 340 pp.

[32] S.A. Herman. *Offshore Wind Farms - Analysis of Transport and Installation Costs*. ECN-I–02-002. 2002.

[33] E. Uraz. "Offshore Wind Turbine Transportation & Installation Analyses. Planning Optimal Marine Operations for Offshore Wind Projects". MSc thesis. Visby, Sweden: Gotland University, 2011.

[34] Iberdrola. *Wikinger Offshore Wind Farm*. n.d. URL: https://www.iberdrola.com/about-us/what-we-do/offshore-wind-energy/wikinger-offshore-wind-farm (visited on 03/02/2023).

[35] H. Díaz and C. Guedes Soares. "Approach for Installation and Logistics of a Floating Offshore Wind Farm". In: *Journal of Marine Science and Engineering* 11.1 (2023). 53. DOI: https://doi.org/10.3390/jmse11010053.

[36] S. Killoh. *Heerema installs first wind turbine using novel RNA method*. Heerema. 2022. URL: https://www.heerema.com/news/heerema-installs-first-wind-turbine-using-novel-rna-method (visited on 03/07/2023).

[37] Heerema. *Parkwind, Heerema Marine Contractors en MHI Vestas kondigen een revolutionaire bouwmethode aan voor Arcadis Ost 1*. 2019. URL: https://heerema-production-content.s3.amazonaws.com/HMC/Press%20Releases%20pdf/2019-11-26%20-%20Persbericht%20Parkwind_Heerema_MHI%20Vestas.pdf (visited on 04/06/2023).

[38] R. Robinson and I. Furtado. "Alternatives to Conventional Offshore Fixed Wind Installation". In: *Offshore Technology Conference* (2022). DOI: https://doi.org/10.4043/31986-MS.

[39] G.B. Thennarasu and H.K.A. Muralidharan. "Transportation Excellence for Wind Turbine Nacelle. Planning Optimal Marine Operations for Offshore Wind Projects". MSc thesis. Stockholm, Sweden: Royal Institute of Technology (KTH), 2012.

[40] A. Attari et al. *D3.1 - WP Framework/Industry Challenges Report – Novel vessels and equipment*. LEANWIND - Logistic Efficiencies and Naval architecture for Wind Installations with Novel Developments, 2014.

[41] A.F. Haselsteiner et al. “Lifting Wind Turbine Components From a Floating Vessel: A Review on Current Solutions and Open Problems”. In: *Journal of Offshore Mechanics and Arctic Engineering* 141.5 (2019). 050801. DOI: https://doi.org/10.1115/1.4042385.

[42] C. Streatfeild et al. *Guidelines for the Selection and Operation of Jack-ups in the Marine Renewable Energy Industry*. London, United Kingdom: RenewableUK, 2013.

[43] Riviera Newsletters. *Interview with Nick Wessels (Ulstein Design & Solutions BV) in Concept quickens installation of offshore turbines*. Riviera. 2010. URL: https://www.rivieramm.com/news-content-hub/news-content-hub/concept-quickens-installation-of-offshore-turbines-45123 (visited on 03/06/2023).

[44] Saipem. *Hywind*. n.d. URL: https://www.saipem.com/en/projects/hywind (visited on 03/07/2023).

[45] Heerema Marine Contractors. *Sleipnir*. 2020. URL: https://www.heerema.com/heerema-marine-contractors/fleet/sleipnir (visited on 03/07/2023).

[46] S. Djupevåg Eri. “Analysis of Operability in Installing Heavy Subsea Modules”. MSc thesis. Stavanger, Norway: University of Stavanger, 2015.

[47] E. Schouten. “Monohull versus Semi-submersible for offshore heavy lift crane operations”. MSc thesis. Delft, The Netherlands: Delft University of Technology, 2018.

[48] G. Hoogendoorn. “Design in principle for flexible fully assembled wind turbine installation”. MSc thesis. Delft, The Netherlands: Delft University of Technology, 2020.

[49] J.J. Zwaginga. “Exploring Market Uncertainty in Early Ship Design”. MSc thesis. Delft, The Netherlands: Delft University of Technology, 2020.

[50] C. van Lynden. “Offshore Wind Installation Vessels”. MSc thesis. Delft, The Netherlands: Delft University of Technology, 2021.

[51] R. Krishnakanth. “Concept design of an installation vessel to install fully assembled next generation offshore wind energy turbines”. MSc thesis. Delft, The Netherlands: Delft University of Technology, 2014.

[52] T.M. van Bruinessen. “Towards controlled innovation of complex projects. A social-technological approach to describing ship design”. PhD dissertation. Delft University of Technology, 2016. ISBN: 978946186637.

[53] S.O. Erikstad and B. Lagemann. “Design Methodology State-of-the-Art Report”. In: *International Marine Design Conference* (2022). DOI: https://doi.org/10.5957/IMDC-2022-301.

[54] J.J. Garcia Agis et al. “Overspecifed vessel design solutions in multi□stakeholder design problems”. In: *Research in Engineering Design* 30.4 (2019). DOI: https://doi.org/10.1007/s00163-019-00319-3.

[55] N. Wessels. *Securing your future in offshore wind*. Ulstein. 2019. URL: https://ulstein.com/news/securing-your-future-in-offshore-wind (visited on 03/14/2023).

[56] R. Garcia and R. Calantone. “A critical look at technological innovation typology and innovativeness terminology: A literature review”. In: *Journal of Product Innovation Management* 19 (2002), pp. 110–132. DOI: https://doi.org/10.1016/S0737-6782(01)00132-1.

[57] R. Ottinger. *Create Sustainable Success with the 4 Types of Innovation*. 2021. URL: https://www.freshconsulting.com/insights/blog/the-4-types-of-innovation/ (visited on 05/03/2023).

[58] T.M. Van Bruinessen, F.E.H.M. Smulders, and J.J. Hopman. “Towards a different view on ship design: The development of ships observed through a social-technological perspective”. In: *IPDMC 2013: 20th International Product Development Management Conference* (2013). URL: http://resolver.tudelft.nl/uuid:7a4e7435-2916-45c1-89f9-7d2842662621.

[59] D. Andrews and S. Erikstad. “State of the art report on design methodology”. In: *IMDC 2015 - 12th International Marine Design Conference* (2015), pp. 90–105.

[60] D. Andrews et al. “State of the art report on design methodology”. In: *IMDC 2018: 13th International Marine Design Conference* 2 (2018), pp. 3–16.

[61] V.P.M. Peeten. “Evaluating Emissions of Offshore Transportation Vessels”. MSc thesis. Delft, The Netherlands: Delft University of Technology, 2022.

[62] J.J. Zwaginga, J.D. Stroo, and A.A. Kana. “Exploring market uncertainty in early ship design”. In: *International Journal of Naval Architecture and Ocean Engineering* 13 (2021), pp. 352–366. ISSN: 2092-6782. DOI: https://doi.org/10.1016/j.ijnaoe.2021.04.003.

[63] J. Kamp. “Conceptual Design Analysis of an 8,000mt Crane for HMC’s NSCV”. MSc thesis. Delft, The Netherlands: Delft University of Technology, 2013.

[64] . *Maintenance of large offshore wind turbine generators*. Offshore Wind Logistics B.V. 2020. URL: https://projecten.topsectorenergie.nl/storage/app/uploads/public/5ed/8fc/131/5ed8fc1310c19913517687.pdf (visited on 05/31/2023).

[65] R.F. Dam. *The MAYA Principle: Design for the Future, but Balance it with Your Users’ Present*. Interaction Design Foundation. 2021. URL: https://www.interaction-design.org/literature/article/design-for-the-future-but-balance-it-with-your-users-present (visited on 05/31/2023).

[66] S. Cheusheva. *How to do Spearman correlation in Excel*. 2023. URL: https://www.ablebits.com/office-addins-blog/spearman-rank-correlation-excel/ (visited on 05/02/2023).

[67] R.N. Forthofer, E.S. Lee, and M. Hernandez. “Chapter 3 - Descriptive Methods”. In: *Biostatistics: A Guide to Design, Analysis, and Discovery*. Elsevier, 2007, pp. 21–69. ISBN: 9780123694928.

[68] . *Correlation (Pearson, Kendall, Spearman)*. Statistics Solutions. n.d. URL: https://www.statisticssolutions.com/free-resources/directory-of-statistical-analyses/correlation-pearson-kendall-spearman/ (visited on 05/03/2023).

[69] N.Y. Sergiienko et al. “Review of scaling laws applied to floating offshore wind turbines”. In: *Renewable and Sustainable Energy Reviews* 162.112477 (2022), pp. 160–175. ISSN: 1364-0321. DOI: https://doi.org/10.1016/j.rser.2022.112477.

[70] H. Canet, P. Bortolotti, and C. Bottasso. “On the scaling of wind turbine rotors”. In: *Wind Energy Science* 6 (2021), pp. 601–626. DOI: https://doi.org/10.5194/wes-6-601-2021.

[71] F. Mølholt Jensen and K. Branner. “Chapter 3 - Introduction to wind turbine blade design”. In: *Woodhead Publishing Series in Energy*. Ed. by P. Brøndsted and R. Nijssen. Woodhead Publishing, 2013, pp. 3–28. ISBN: 9780857094261. DOI: https://doi.org/10.1533/9780857097286.1.3.

[72] P. Jamieson. “Chapter 4 - Upscaling of Wind Turbine Systems”. In: *Innovation in Wind Turbine Design*. John Wiley & Sons Ltd, 2018, pp. 97–126. ISBN: 9781119137900. DOI: https://doi.org/10.1002/9781119137924.ch4.

[73] M.D. Madvar et al. “Forecasting of wind energy technology domains based on the technology life cycle approach”. In: *Energy Reports* 5 (2019), pp. 1236–1248. ISSN: 2352-4847. DOI: https://doi.org/10.1016/j.egyr.2019.08.069.

[74] A. Hayes et al. “Structural Optimization of a Direct-Drive Wind Turbine Generator Inspired by Additive Manufacturing”. In: *Procedia Manufacturing* 26 (2018), pp. 740–752. ISSN: 2351-9789. DOI: https://doi.org/10.1016/j.promfg.2018.07.084.

[75] E. Osmanbasic. *The Future of Wind Turbines: Comparing Direct Drive and Gearbox*. Engineering.com. 2020. URL: https://www.engineering.com/story/the-future-of-wind-turbines-comparing-direct-drive-and-gearbox (visited on 05/26/2023).

[76] S. Bhattacharya. “Appendix C: Tower Idealisation”. In: *Design of Foundations for Offshore Wind Turbines*. John Wiley & Sons Ltd, 2019. ISBN: 9781119128120. DOI: https://doi.org/10.1002/9781119128137. URL: https://www.oreilly.com/library/view/design-of-foundations/9781119128120/b03.xhtml.

[77] J. Nørkaer Sørensen. “On the Calculation of Trajectories for Blades Detached from Horizontal Axis Wind Turbines”. In: *Wind Engineering* 8.3 (1984), pp. 160–175. URL: https://www.jstor.org/stable/43749983.

[78] N. Sharpley. *How can the industry prepare for the logistics of offshore wind?* Windpower engineering & development. 2015. URL: https://www.windpowerengineering.com/how-can-the-industry-prepare-for-the-logistics-of-offshore-wind/ (visited on 06/01/2023).

[79] . *Maritime Engineering*. DEKC Maritime. n.d. URL: https://www.dekc-maritime.com/ (visited on 06/01/2023).

[80] . *Blade Lifting Yokes*. ENABL. n.d. URL: https://enabl-wind.com/products/all-equipment/blade-lifting-yokes-offshore/ (visited on 06/02/2023).

[81] DNV. *Sesam modules for floating structures*. n.d. URL: https://www.dnv.com/services/sesam-modules-for-floating-structures-2411 (visited on 06/06/2023).

[82] *Recommended practice: Environmental Conditions and Environmental Loads*. DNV-RP-C205. Høvik, Norway: Det Norske Veritas AS, 2017.

[83] BVG Associates. *Guide to an offshore wind farm - Updated and extended*. Published on behalf of The Crown Estate and the Offshore Renewable Energy Catapult. 2019.

[84] P. Naaijen and P. Wellens. *Lecture slides: MT44021 2022-2023 - Motions & Loading of structures in Waves*. Delft University of Technology, 2022.

[85] F. Pacuraru, L. Domnisoru, and S. Pacuraru. “On the Comparative Seakeeping Analysis of the Full Scale KCS by Several Hydrodynamic Approaches”. In: *Journal of Marine Science and Engineering* 8.12 (2020). DOI: https://doi.org/10.3390/jmse8120962.

[86] J. Parunov et al. “Benchmark study of global linear wave loads on a container ship with forward speed”. In: *Marine Structures* 84.103162 (2022). ISSN: 0951-8339. DOI: https://doi.org/10.1016/j.marstruc.2022.103162.

[87] C. Zhao and M. Ma. “A Hybrid 2.5-Dimensional High-Speed Strip Theory Method and Its Application to Apply Pressure Loads to 3-Dimensional Full Ship Finite Element Models”. In: *Journal of Ship Production and Design* 32.4 (2016), pp. 216–225. ISSN: 2158-2866. DOI: https://doi.org/10.5957/JSPD.32.4.150010.

[88] J.J. Jensen, A.E. Mansour, and A.S. Olsen. “Estimation of ship motions using closed-form expressions”. In: *Ocean Engineering* 31 (2004), pp. 61–85. ISSN: 0029-8018. DOI: https://doi.org/10.1016/S0029-8018(03)00108-2.

[89] R. Nabergoj. *Fondamenti di Tenuta della Nave al Mare*. 2010, p. 100.

[90] S. Matsui et al. “Development of Simplified Formula for Froude-Krylov Force of 6-DOFs Acting on Monohull Ship”. In: *Journal of the Japan Society of Naval Architects and Ocean Engineers* 32 (2021), pp. 9–19. ISSN: 1880-3717. DOI: https://doi.org/10.2534/jjasnaoe.32.9.

[91] O.M. Faltinsen. *Sea loads on ships and offshore structures*. 1st ed. Cambridge, United Kingdom: Cambridge University Press, 1993. ISBN: 0521458706.

[92] L.H. Holthuijsen. “Statistics”. In: *CT5316 - Waves in oceanic and coastal waters*. 2004, p. 25.

[93] J.M.J. Journée and W.W. Massie. *Offshore Hydromechanics*. Delft University of Technology, 2001.

[94] W.J. Pierson and L. Moskowitz. “A proposed spectral form for fully developed wind seas based on the similarity theory of S. A. Kitaigorodskii”. In: *Journal of Geophysical Research* 69.24 (1964), pp. 5181–5190. DOI: https://doi.org/10.1029/JZ069i024p05181.

[95] M. Marghany. “Quantum description of sea surface”. In: *Synthetic Aperture Radar Imaging Mechanism for Oil Spills*. Elsevier, 2020, pp. 93–110. ISBN: 9780128181119. DOI: https://doi.org/10.1016/C2018-0-02617-1.

[96] K. Hasselmann et al. *Measurements of wind-wave growth and swell decay during the joint North Sea wave project (JONSWAP)*. Ergänzungsheft zur Deutschen Hydrographischen Zeitschrift, Reihe A, Nr. 12, 1973.

[97] R. Bhattacharya. *Dynamics of Marine Vehicles*. John Wiley & Sons Ltd, 1978. ISBN: 9780471072065.

[98] DNV. *Sesam User manual - Postprocessor for Statistical Response Calculations*. Det Norske Veritas AS, 2021.

[99] M. Shields et al. “Impacts of turbine and plant upsizing on the levelized cost of energy for offshore wind”. In: *Applied Energy* 298.117189 (2021). ISSN: 0306-2619. DOI: https://doi.org/10.1016/j.apenergy.2021.117189.

[100] H. Rijntalder. *Recommended maximum height for offshore windturbines*. Pondera consult. 2023. URL: https://ponderaconsult.com/en/ponderacontent/recommended_maximum_height_for_offshore_windturbines/#:~:text=A%20workgroup%20on%20the%20issue,the%20developments%20of%20wind%20turbines. (visited on 08/01/2023).

[101] Netherlands Wind Energy Association. *Windmolens op zee niet hoger dan 1000 voet (Dutch)*. 2023. URL: https://www.nwea.nl/windmolens-op-zee-niet-hoger-dan-1000-voet/ (visited on 08/01/2023).

[102] GustoMSC. *NG-20000X brochure*. n.d. URL: https://www.nov.com/-/media/nov/files/products/rig/marine-and-construction/ng-20000x/ng-20000x-brochure.pdf (visited on 09/01/2023).

[103] 4C Offshore. *NG-20000X*. n.d. URL: https://www.4coffshore.com/vessels/vessel-ng-20000x-vid2304.html (visited on 09/01/2023).

[104] A. Durakovic. *First Havfram Hybrid Mega Jack-Up Now Under Construction*. OffshoreWIND.biz. 2022. URL: https://www.offshorewind.biz/2022/12/12/first-havfram-hybrid-mega-jack-up-now-under-construction/ (visited on 09/04/2023).

[105] J.D. Stroo. *Personal communication*. Ulstein Design & Solutions B.V. 2023.

[106] A. Ajdin. *Cadeler scores Siemens Gamesa contract for wind turbine installation off Denmark*. Splash247.com. 2023. URL: https://splash247.com/cadeler-scores-siemens-gamesa-contract-for-wind-turbine-installation-off-denmark/ (visited on 09/01/2023).

[107] International Energy Agency. *Net Zero by 2050 - A Roadmap for the Global Energy Sector*. page 47 for figure. 2021. URL: https://iea.blob.core.windows.net/assets/deebef5d-0c34-4539-9d0c-10b13d840027/NetZeroby2050-ARoadmapfortheGlobalEnergySector_CORR.pdf (visited on 02/17/2023).

[108] International Energy Agency. *Wind Electricity - Technology deep dive*. 2022. URL: https://www.iea.org/reports/wind-electricity (visited on 02/17/2023).

[109] V. N. Dinh and E. McKeogh. "Offshore Wind Energy: Technology Opportunities and Challenges: Energy and Geotechnics". In: *Proceedings of the 1st Vietnam Symposium on Advances in Offshore Engineering* (2019), pp. 3–22. DOI: 10.1007/978-981-13-2306-5_1.

[110] P. Hevia-Koch and H. Klinge Jacobsen. "Comparing offshore and onshore wind development considering acceptance costs". In: *Energy Policy* 125 (2019), pp. 9–19. ISSN: 0301-4215. DOI: https://doi.org/10.1016/j.enpol.2018.10.019.

[111] Office of Energy Efficiency & Renewable Energy. *Wind Turbines: the bigger, the better*. 2022. URL: https://www.energy.gov/eere/articles/wind-turbines-bigger-better#:~:text=In%202021%2C%20there%20was%20an,ultimately%20leading%20to%20lower%20costs. (visited on 02/17/2023).

[112] Nationalgrid. *What is offshore wind power?* 2022. URL: https://www.nationalgrid.com/stories/energy-explained/what-offshore-wind-power (visited on 02/20/2023).

[113] Power Technology. *Borssele III and IV Offshore Wind Farm*. 2021. URL: https://www.power-technology.com/projects/borssele-iii-iv-offshore-wind-farm/ (visited on 04/03/2023).

[114] N. Nilaj et al. "Power Generation from Wind Turbines". In: *NCORE-2008* (2008). ISSN: 0301-4215. DOI: https://doi.org/10.1016/j.enpol.2018.10.019.

[115] J.F. Manwell, J.G. McGowann, and A.L. Rogers. *Wind Energy Explained - Theory Design and Application*. Chichester, United Kingdom: Wiley, 2009. ISBN: 9780470015001.

[116] Office of Energy Efficiency & Renewable Energy. *Advanced Wind Turbine Drivetrain Trends and Opportunities*. 2019. URL: https://www.energy.gov/eere/articles/advanced-wind-turbine-drivetrain-trends-and-opportunities#:~:text=Most%20wind%20turbine%20drivetrains%20currently,minute)%20needed%20to%20generate%20electricity (visited on 02/20/2023).

[117] Wind & Water works. *Export and inter-array cable installation*. n.d. URL: https://www.windandwaterworks.nl/cases/export-and-inter-array-cable-installation (visited on 02/20/2023).

[118] N. Srinil. “Chapter 13 - Cabling to connect offshore wind turbines to onshore facilities”. In: *Offshore Wind Farms - Technologies, Design & Operation*. Ed. by C. Ng and L. Ran. Woodhead Publishing, 2016, pp. 419–440. ISBN: 9780081007792. DOI: https://doi.org/10.1016/B978-0-08-100779-2.00013-1.

[119] M. Stark and M. Bermudez-Neubauer. *Changing the Scale of Offshore Wind - Examining Mega-Projects in the United Kingdom*. 2013. URL: https://www.accenture.com/t20150624t211115__w__/us-en/_acnmedia/accenture/conversion-assets/dotcom/documents/global/pdf/industries_10/accenture-changing-scale-offshore-wind.pdf (visited on 02/21/2023).

[120] S. Wood. *Aging offshore wind turbines could stunt growth of renewable energy sector*. 2021. URL: https://www.sciencedaily.com/releases/2021/02/210216114930.htm (visited on 02/21/2023).

[121] L. Rodríguez. *What is LCOE and why is it important?* 2022. URL: https://ratedpower.com/blog/lcoe/#:~:text=If%20the%20LCOE%20is%20lower,project%20will%20likely%20be%20unprofitable. (visited on 02/21/2023).

[122] S. Shah. *LCOE and its limitations*. 2020. URL: https://www.energyforgrowth.org/wp-content/uploads/2020/01/LCOE-and-its-Limitations.pdf (visited on 02/21/2023).

[123] International Renewable Energy Agency. *Future of Wind - Deployment, Investment, Technology, Grid Integration and Socio-economic Aspects*. 2019. URL: https://www.irena.org/-/media/Files/IRENA/Agency/Publication/2019/Oct/IRENA_Future_of_wind_2019_summ_EN.PDF (visited on 02/22/2023).

[124] Catapult Offshore Renewable Energy. “Operations & Maintenance the Key to Cost Reduction”. In: *Circuit* (2016), p. 7. URL: https://ore.catapult.org.uk/wp-content/uploads/2020/10/Circuit-8-WEB-small.pdf (visited on 02/22/2023).

[125] Leanwind. *Driving Cost Reductions in Offshore Wind*. 2017. URL: https://windeurope.org/wp-content/uploads/files/about-wind/reports/LEANWIND-Driving-cost-reductions-in-offshore.pdf (visited on 02/22/2023).

[126] T. Adedipe and M. Shafiee. “An economic assessment framework for decommissioning of offshore wind farms using a cost breakdown structure”. In: *The International Journal of Life Cycle Assessment* 26 (2021), pp. 344–370. DOI: https://doi.org/10.1007/s11367-020-01793-x.

[127] Y. Liang et al. “Levelised cost of energy analysis for offshore wind farms – A case study of the New York State development”. In: *Ocean Engineering* 239 (2021). 109923. ISSN: 0029-8018. DOI: https://doi.org/10.1016/j.oceaneng.2021.109923.

[128] Trinomics. *Final Report Cost of Energy - Energy costs, taxes and the impact of government interventions on investments*. 2020. URL: https://energy.ec.europa.eu/system/files/2020-10/final_report_levelised_costs_0.pdf (visited on 02/22/2023).

[129] S. Livaniou et al. *D3.2 - Key design parameters and criteria related to installation and maintenance vessels design; their layouts, crane operations and access systems*. LEANWIND - Logistic Efficiencies and Naval architecture for Wind Installations with Novel Developments, 2015.

[130] R. Auckland. “Offshore Wind Jack-ups: Supply & Demand 2017-2026”. In: *4COffshore* (2017).

[131] *Ships and marine technology — Offshore wind energy — Port and marine operations*. ISO 29400:2020(EN). Geneva, Switzerland: International Organization for Standardization, 2020.

[132] Wind power NL. *Fugro supports Heerema's turbine installations with innovative camera technology*. 2023. URL: https://windpowernl.com/2023/02/02/fugro-supports-heeremas-turbine-installations-with-innovative-camera-technology/ (visited on 03/07/2023).

[133] K. Van Dokkum. *Ship Knowledge*. 7th ed. Enkhuizen, The Netherlands: DOKMAR, 2011. ISBN: 9789071500183.

[134] Wind Energy The Facts. *Installation*. n.d. URL: https://www.wind-energy-the-facts.org/installation.html (visited on 03/06/2023).

[135] Royal Wagenborg. *300T Sheerleg*. 2019. URL: https://www.wagenborg.com/media/1098/2019-triton.pdf (visited on 03/06/2023).

[136] Marine Insight. *Hyundai-10000, The World's Biggest Shear-leg Floating Crane In Operation*. 2015. URL: https://www.marineinsight.com/shipping-news/hyundai-10000-the-worlds-biggest-shear-leg-floating-crane-in-operation/ (visited on 03/06/2023).

[137] Scaldis. *Transport and Installation of two 5MW Wind Turbine Generators for the Beatrice Demonstrator Project*. n.d. URL: https://www.scaldis-smc.com/en/projects/groen-2007-jul-beatrice/ (visited on 03/06/2023).

[138] Ocean Energy Resources. *Aegir installs first offshore wind turbine*. 2018. URL: https://ocean-energyresources.com/2018/10/01/aegir-installs-first-offshore-wind-turbine/ (visited on 03/07/2023).

[139] OffshoreWIND.biz. *Aegir Installs DOT at Princess Amalia*. 2018. URL: https://www.offshorewind.biz/2018/10/01/aegir-installs-dot-at-princess-amalia/ (visited on 03/07/2023).

[140] van Oord. *Van Oord orders mega ship to install 20 MW offshore wind foundations and turbines*. 2021. URL: https://www.vanoord.com/en/updates/van-oord-orders-mega-ship/ (visited on 03/08/2023).

[141] Van Oord. *Offshore installation vessel - Boreas*. 2021. URL: https://vanoord.de/wp-content/uploads/2022/03/Equipment-leaflet-Offshore-installation-vessel-Boreas-draft.pdf (visited on 03/08/2023).

[142] Seaway7. *Seaway Ventus*. 2022. URL: https://www.seaway7.com/wp-content/uploads/2022/10/Seaway_Ventus.pdf (visited on 03/08/2023).

[143] Cadeler. *Investor Presentation - X-Class vessels*. 2021. URL: https://www.cadeler.com/media/1638/investor_presentation_x-class.pdf (visited on 03/08/2023).

[144] Seajacks. *Siren*. 2022. URL: https://new.eneti-inc.com/wp-content/uploads/2022/12/Seajacks-SIREN-Spec-Sheet-2022.pdf (visited on 03/08/2023).

[145] Cadeler. *X-class vessels: Building our green future*. n.d. URL: https://www.cadeler.com/en/vessels/x-class-vessels/ (visited on 03/08/2023).

[146] Cadeler. *Investor Presentation*. 2022. URL: https://www.cadeler.com/media/1832/investor_presentation_interimreport_2022_final.pdf (visited on 03/08/2023).

[147] Cadeler. *Our vessels - designed for the future of offshore wind*. n.d. URL: https://www.cadeler.com/en/vessels/ (visited on 03/08/2023).

[148] Van Oord. *After major upgrade, Aeolus starts work on Belgium's largest offshore wind farm*. 2018. URL: https://www.vanoord.com/en/updates/after-major-upgrade-aeolus-starts-work-belgiums-largest-offshore-wind-farm/ (visited on 03/08/2023).

[149] OffshoreWIND.biz. *Aeolus Completes Sea Trials, Set for Norther OWF Works*. 2018. URL: https://www.offshorewind.biz/2018/07/10/aeolus-completes-sea-trials-set-for-norther-owf-works/ (visited on 03/08/2023).

[150] A. Buljan. *Van Oord's Aeolus Ready for 15 MW Wind Turbines with Crane Upgrade No. 2*. OffshoreWIND.biz. 2023. URL: https://www.offshorewind.biz/2023/01/20/van-oords-aeolus-ready-for-15-mw-wind-turbines-with-crane-upgrade-no-2/ (visited on 03/08/2023).

[151] Heavy Lift News. *DEME Offshore's Sea Installer to be Upgraded with 1600t Huisman Crane*. 2021. URL: https://www.heavyliftnews.com/deme-offshores-sea-installer-to-be-upgraded-with-1600t-huisman-crane/ (visited on 03/08/2023).

[152] A. Durakovic. *Sea Installer Undergoing Crane Replacement, Next Stop USA*. OffshoreWIND.biz. 2023. URL: https://www.offshorewind.biz/2023/02/22/sea-installer-undergoing-crane-replacement-next-stop-usa/ (visited on 03/08/2023).

[153] Cadeler. *Our O-class vessels: Designed for the future of offshore wind*. n.d. URL: https://www.cadeler.com/en/vessels/o-class-vessels/ (visited on 03/08/2023).

[154] 4COffshore. *Wind Osprey*. n.d. URL: https://www.4coffshore.com/vessels/vessel-wind-osprey-vid257.html (visited on 03/08/2023).

[155] M. Buitendijk. *Pacific Osprey's sets sail with upgraded crane*. SWZ|Maritime. 2020. URL: https://swzmaritime.nl/news/2020/06/05/pacific-ospreys-sets-sail-with-upgraded-crane/ (visited on 03/08/2023).

[156] Ulstein. *Windlifter*. n.d. URL: https://ulstein.com/equipment/ulstein-windlifter (visited on 03/09/2023).

[157] F. van Heerd. *Wind Turbine Shuttle*. Huisman. n.d. URL: https://www.kivi.nl/uploads/media/5644bee53d3b1/Huisman-Wind_Turbine_Shuttle.pdf (visited on 03/09/2023).

[158] M. Buitendijk. *Huisman launches floating installation of wind turbines with Windfarm Installation Vessel*. SWZ|Maritime. 2022. URL: https://swzmaritime.nl/news/2022/04/22/huisman-launches-floating-installation-of-wind-turbines-with-windfarm-installation-vessel/ (visited on 03/09/2023).

[159] A. Memija. *US and German Firms Unveil Jones Act-Compliant Offshore Wind Farm Installation Solution*. OffshoreWIND.biz. 2022. URL: https://www.offshorewind.biz/2022/09/27/us-and-german-firms-unveil-jones-act-compliant-offshore-wind-farm-installation-solution/ (visited on 03/09/2023).

[160] J. Gelling. *Lecture slides: AMV MT-44095 2021-2022 - Passive Static Lift Multihulls*. Delft University of Technology, 2022.

[161] Huisman. *Huisman product brochure - Wind Turbine Shuttle*. 2020. URL: https://www.huismanequipment.com/documenten/brochures_2020_sept/brochure_wind_turbine_shuttle_web.pdf (visited on 03/09/2023).

[162] Huisman. *Radical change in installing floating windfarms*. Floating Wind Solutions 2022. 2022. URL: https://floatingwindsolutions.com/wp-content/uploads/2022/03/HUISMAN_JOOPROODENBURG_fnlJRO-Presentation-2022-03-03.pdf (visited on 03/09/2023).

[163] Huismam. *Windfarm Installation Vessel*. n.d. URL: https://www.huismanequipment.com/en/products/renewables/offshore_wind/windfarm-installation-vessel (visited on 03/09/2023).

[164] ONP Management GmbH. *Customs Issues Comprehensive Offshore Wind Jones Act Ruling*. The Maritime Economy publications. 2022. URL: https://www.winston.com/en/maritime-fedwatch/customs-issues-comprehensive-offshore-wind-jones-act-ruling.html#:~:text=The%20Jones%20Act%20is%20an,to%20qualified%20U.S.%2Dflag%20vessels. (visited on 03/09/2023).

[165] C. Papavizas. *Feederdock: Game-changing, Jones Act compliant offshore wind installation solution.* Winston & Strawn LLP. 2022. URL: https://www.maritimeeconomy.com/post-details.php?post_id=aG5ubg==&post_name=Feederdock%20Gamechanging%20Jones%20Act%20compliant%20offshore%20wind%20installation%20solution.&segment_name=Ocean%20%20Offshore%20Energy (visited on 03/09/2023).

[166] Maersk Supply Service. *Wind Installation Vessel - Maersk Supply Service's pioneering new design*. 2022. URL: https://www.maersksupplyservice.com/offshore-wind/ (visited on 03/20/2023).

[167] D.J. Singer, N. Doerry, and M.E. Buckley. "What is set□based design?" In: *Naval Engineers Journal* 121.4 (2009), pp. 31–43. DOI: https://doi.org/10.1111/j.1559-3584.2009.00226.x.

[168] J. Harvey Evans. "Basic design concepts". In: *Journal of the American Society for Naval Engineers* (1959). DOI: https://doi.org/10.1111/j.1559-3584.1959.tb01836.x.

[169] M. Frye. "Applying Set Based Methodology in Submarine Concept Design". MSc thesis. Cambridge, Massachusetts, USA: Massachusetts Institute of Technology, 2010.

[170] M. Fernandez, F. Mistree, and J. Allen. "A Decision Support Framework for Distributed Collaborative Design and Manufacture". In: *9th AIAA/ISSMO Symposium on Multidisciplinary Analysis and Optimization* (2002). DOI: https://doi.org/10.2514/6.2002-5496.

[171] T. Lamb. *Ship Design and Construction*. Vol. 1. Jersey City, NJ, USA: The Society of Naval Architects and Marine Engineers, 2003. ISBN: 0939773406.

[172] B. Toche, R. Pellerin, and C. Fortin. "Set-based design: a review and new directions". In: *Design Science* 6 (2020). DOI: https://doi.org/10.1017/dsj.2020.16.

[173] H.M. Rocha, H.L.M. Quintella, and U.R. De Oliveira. "Product development process maturity leverage through the use of set-based concurrent engineering process". In: *XIX International Conference on Industrial Engineering and Operations Management, ICIEOM 2013* (2013). DOI: https://doi.org/10.13140/2.1.3130.8165.

[174] A. Akaberi. "Set-based concurrent engineering process: Contextualization, industry analysis and business game development". MSc thesis. Milan, Italy: Politecnico di Milano, 2011.

[175] A. Kossiakoff et al. *Systems Engineering Principles and Practice*. 2nd ed. Hoboken, New Jersey, USA: Wiley, 2011. ISBN: 9781118001028.

[176] L. Bretz, L. Kaiser, and R. Dumitrescu. "An analysis of barriers for the introduction of Systems Engineering". In: *Procedia CIRP* 84 (2019), pp. 783–789. ISSN: 2212-8271. DOI: https://doi.org/10.1016/j.procir.2019.04.178.

[177] M.J. Pennock and J.P. Wade. "The Top 10 Illusions of Systems Engineering: A Research Agenda". In: *Procedia Computer Science* 44 (2015), pp. 147–154. ISSN: 1877-0509. DOI: https://doi.org/10.1016/j.procs.2015.03.033.

[178] T.M. Van Bruinessen, J.J. Hopman, and F.E.H.M. Smulders. “Towards a different view on ship design: The development of ships observed through a social-technological perspective”. In: *ASME 2013: 32nd International Conference on Ocean, Offshore and Arctic Engineering* (2013). URL: http://doi.org/10.1115/OMAE2013-11585.

[179] S. Erikstad and K. Levander. “System Based Design of Offshore Support Vessels”. In: *IMDC12 - The 11th International Marine Design Conference* (2012), pp. 397–412.

[180] A. Papanikolaou. “Holistic Approach to Ship Design”. In: *Journal of Marine Science and Engineering* 10.11 (2022). DOI: https://doi.org/10.3390/jmse10111717.

[181] E. De Vries. *Haliade-X uncovered: GE aims for 14MW*. Windpower Monthly. 2019. URL: https://www.windpowermonthly.com/article/1577816/haliade-x-uncovered-ge-aims-14mw#:~:text=The%20Haliade%2DX%27s%20600%2Dtonne,MW)%20for%20a%2012MW%20rating. (visited on 05/01/2023).

[182] Vestas Wind Systems A/S. *Catalog: Offshore V164-8.0 MW/V112-3.3 MW*. 2013. URL: https://pdf.archiexpo.com/pdf/vestas/offshore-v164-80-mw-v112-33-mw/88087-243525.html (visited on 05/01/2023).

[183] Alstom Wind. *Catalog: Haliade 150-6MW*. 2014. URL: https://pdf.archiexpo.com/pdf/alstom/haliade-150-6mw/88574-242448.html (visited on 05/01/2023).

[184] *MHI Vestas Offshore V164-9.5 MW*. Wind turbine models. n.d. URL: https://en.wind-turbine-models.com/turbines/1605-mhi-vestas-offshore-v164-9.5-mw (visited on 05/01/2023).

[185] Siemens AG. *Catalog: SWT-7.0-154*. 2015. URL: https://pdf.archiexpo.com/pdf/siemens-gamesa/swt-70-154/88089-249551.html (visited on 05/01/2023).

[186] MingYang Smart Energy. *Catalog: MySE6.0MW Product Line*. n.d. URL: http://www.myse.com.cn/uploadfiles/2020/11/20201110085734953.pdf (visited on 05/01/2023).

[187] *MingYang MySE7.0-158*. Wind turbine models. n.d. URL: https://en.wind-turbine-models.com/turbines/1910-mingyang-myse7.0-158 (visited on 05/01/2023).

[188] *MingYang MySE5.5-155*. Wind turbine models. n.d. URL: https://en.wind-turbine-models.com/turbines/1919-mingyang-myse5.5-155 (visited on 05/01/2023).

[189] *Vestas Offshore V112-3.3 MW*. Wind turbine models. n.d. URL: https://en.wind-turbine-models.com/turbines/1463-mhi-vestas-offshore-v112-3.3-mw (visited on 05/01/2023).

[190] Siemens Gamesa. *The SG 14-222 DD*. n.d. URL: https://www.siemensgamesa.com/-/media/siemensgamesa/downloads/en/products-and-services/offshore/brochures/siemens-gamesa-offshore-wind-turbine-brouchure-sg-14-222-dd.pdf (visited on 05/01/2023).

[191] Siemens Gamesa. *The SG 8.0-167 DD*. n.d. URL: https://www.siemensgamesa.com/-/media/siemensgamesa/downloads/en/products-and-services/offshore/brochures/siemens-gamesa-offshore-wind-turbine-brochure-sg-8-0-167.pdf (visited on 05/01/2023).

[192] Siemens AG. *Catalog: SWT-6.0-154*. n.d. URL: https://pdf.archiexpo.com/pdf/siemens-gamesa/swt-60-154/88089-271887.html (visited on 05/01/2023).

[193] Vestas Wind Systems A/S. *Catalog: V236-15.0MW*. 2023. URL: https://nozebra.ipapercms.dk/Vestas/Communication/Productbrochure/OffshoreProductBrochure/v236-150-mw-brochure/?page=6 (visited on 05/01/2023).

[194] Vestas American Wind Technology. *V164-10.0 MW*. URL: https://us.vestas.com/en-us/products/offshore/V164-10-0-MW (visited on 05/01/2023).

[195] Vestas American Wind Technology. *V174-9.5 MW*. URL: https://us.vestas.com/en-us/products/offshore/v174-9-5-mw- (visited on 05/01/2023).

[196] J. Jonkman et al. *Definition of a 5-MW Reference Wind Turbine for Offshore System Development*. NREL/TP-500-38060. National Renewable Energy Laboratory, 2009.

[197] C. Desmond. *Summary description of LEANWIND 8 MW reference turbine*. LEANWIND - Logistic Efficiencies and Naval architecture for Wind Installations with Novel Developments, 2015.

[198] P. Bortolotti et al. *IEA Wind Task 37 on Systems Engineering in Wind Energy WP2.1 Reference Wind Turbines*. 2019.

[199] C.E. Silva de Souza et al. *Definition of the INO WINDMOOR 12 MW base case floating wind turbine*. OC2020 A-044. SINTEF, 2021.

[200] Do Thanh Sen and Tran Canh Vinh. "Determination of Added Mass and Inertia Moment of Marine Ships Moving in 6 Degrees of Freedom". In: *International Journal of Transportation Engineering and Technology* 2.1 (2016), pp. 8–14. DOI: https://doi.org/10.11648/j.ijtet.20160201.12.

[201] J.J. Serraris. "Time domain analysis for DP simulations". In: *28th International Conference on Ocean, Offshore and Arctic Engineering (OMAE2009)* (2009), pp. 595–605. DOI: https://doi.org/10.1115/OMAE2009-79587.

[202] Thor .I. Fossen. *Handbook of marine craft hydrodynamics and motion control*. 1st ed. Chichester, United Kingdom: John Wiley & Sons Ltd, 2011. ISBN: 9781119991496.

[203] E. Czermański et al. "Implementation of the Energy Efficiency Existing Ship Index: An important but costly step towards ocean protection". In: *Marine Policy* 145.105259 (2022). ISSN: 0308-597X. DOI: https://doi.org/10.1016/j.marpol.2022.105259.

A

Offshore wind

A.1. Wind energy

Wind is a clean and renewable energy source, with wind turbines producing no emissions that pollute the air [2]. The *International Energy Agency* (2021) forecasts that global electricity generation will almost double over the next three decades, spanning from 2020 to 2050, based on a so-called Announced Pledges Scenario (APS) [107]. In this scenario, low-emission energy sources would provide all of the increase. By 2050, it is anticipated that wind and solar power would together account for almost half of the electricity supply. The increase in contribution of wind energy is clearly visible in Figure A.1.

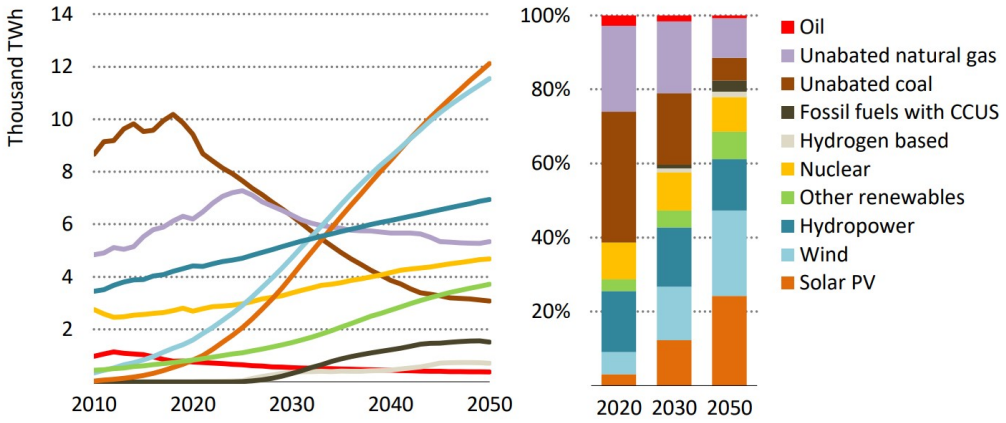

Figure A.1: Global electricity generation by source, from [107].

In 2021, the total installed wind power capacity was 830 gigawatts, with onshore systems making up 93 percent of the total, while offshore wind farms covered the remaining 7 percent [108]. While onshore wind currently dominates the wind energy market, offshore wind is expected to expand its share in the coming years. As more wind is being deployed, the available sites on land become scarce. Onshore wind energy is currently nearing the development limit in some countries, due to visual impact and noise. This makes it difficult to find new sites for future growth [109]. In addition, wind conditions on the remaining land areas are becoming less favorable due to obstructions, resulting in lower capacity factors [110].

The capacity factor expresses the average annual power output divided by the rated power of a turbine. A higher capacity factor means that fewer turbines are needed to generate the

same amount of energy, ultimately leading to lower costs [111]. Offshore locations offer several advantages, including less physical obstructions to block the wind flow, more consistent wind conditions, and the potential to build much larger turbines compared to the onshore wind turbines, resulting in higher power outputs [4]. These factors contribute to a higher capacity of the wind turbine, making the offshore wind environment attractive for wind energy expansion.

A.2. Offshore wind farms

Offshore wind energy is harvested by means of offshore wind farms (OWFs). An OWF can be defined as a power plant that contains all the required facilities to capture the kinetic energy from wind, transform it to electric energy, and supply it to the main electricity network on the mainland [6]. Besides the advantage of more favorable wind conditions and higher capacity factors, another advantage of OWFs is the distance from local population. In this way, the effects of visual impact and worries about noise from rotation of the blades are mitigated [112].

Wind farms typically consists of dozens or even hundreds of turbines [5]. In an OWF, wind turbines are typically placed in a grid pattern. To minimize aerodynamic losses between turbines caused by wake effects from neighbouring turbines, turbine spacing is typically (by rule of thumb) 7 to 10 times the rotor diameter (D) in the governing direction of the wind. In lateral direction the spacing could be smaller [4]. As a result, offshore wind farms can occupy quite a large area compared to the small footprint of a single turbine. Typically, an OWF has an area of ten to hundreds of square kilometers, depending on the size and number of turbines. For instance, the *Borselle III and IV* wind farms are spread across a 146 km² area, compromising 77 9.5 MW turbines [113]. The design of an OWF is not primarily focused on the optimal performance of a single wind turbine, but aims at maximizing the power output of the energy plant as a whole [4].

A.2.1. Electrical energy generation

The vital part of an OWF is the conversion from kinetic energy from the wind into electrical energy. To achieve this, horizontal-axis wind turbines (HAWTs) are typically used. This type of wind turbine consists of the following three main components [3]:

- Tower, which is basically a big steel tube (or more tubes bolted together);
- Nacelle, which is fitted on top of the tower and is the generator housing;
- Rotor, consists of three rotor blades connected to the hub on the nacelle.

Figure A.2 provides a visual representation of the main components of an offshore wind turbine.

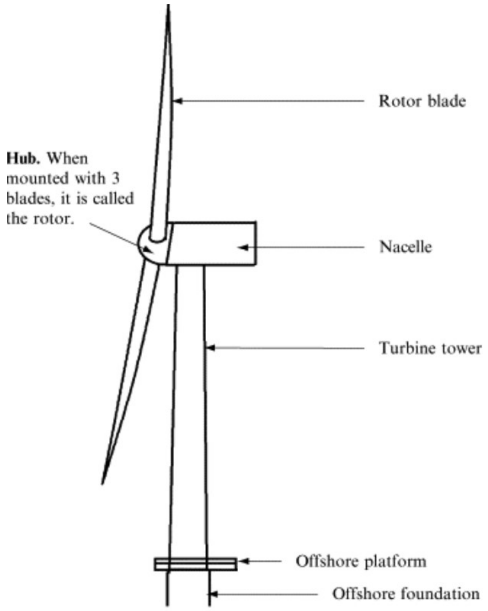

Figure A.2: Anatomy of an offshore wind turbine, from [3].

The working principle of wind turbines involves converting the kinetic energy from wind into mechanical energy, which is then used to generate electricity. The blades of a wind turbine are shaped like an airfoil. When the wind blows, air is travelling over the blades, creating lift. The lift force acts perpendicular to the direction of the wind flow, causing a rotational motion of the rotor. As the rotor rotates, torque is transmitted to the main shaft of the turbine [114] [115]. The main shaft is typically connected to a gearbox, which increases the speed of rotation [116] and drives a generator inside the nacelle. It is also possible to omit the gearbox and use a direct-drive configuration [75]. Ultimately, the generator produces electricity. The available power in wind can be described with Equation A.2.1 [115].

$$P = \frac{1}{2}\rho_a A U_w^3 = \frac{1}{8}\rho_a \pi D_{rotor}^2 U_w^3 \tag{A.1}$$

where:

P = Available power in wind [W]
ρ_a = Density of air [kg/m^3]
D_{rotor} = Rotor diameter [m]
U_w = Wind speed [m/s]

As the formula shows, the power output is a cube function of the wind velocity. Consequently, doubling wind speeds would results in eight times the power. This underscores the push towards offshore wind, where wind speeds are generally higher. Additionally, wind speeds increase with greater heights. Therefore it is beneficial to increase the height of the tower and produce larger turbines.

A.2.2. Electrical energy transportation

Besides electrical energy generation, another function of an OWF is to transport the generated energy to the mainland, where it can be used. Therefore, apart from the wind turbines, the main components of an OWF include cables and substations. The electric power produced by each individual wind turbine is transported through a network of inter-array cables on the seabed to an offshore substation [117]. At the offshore substation, the voltage is stabilized and

maximized before it is transported to the mainland via an export cable [6]. The export cable is connected to an onshore substation, which integrates the electrical energy from offshore into the main electricity grid on land, transporting it to consumers [118]. The layout of a typical OWF and the electrical energy transportation is shown in Figure A.3.

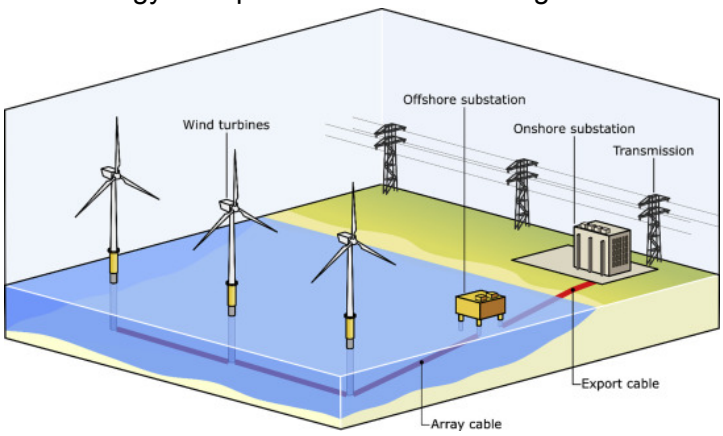

Figure A.3: Schematic of typical offshore wind farm, showing the energy transportation to shore, from [6].

A.3. Life cycle

To get a better understanding of OWFs and their development, it is essential to gain insight into the life cycle. Typically, an offshore wind project is composed of three different phases: investment, operation, and decommissioning [119]. The investment phase can take up to almost a decade and is divided into three parts [28], [119]. Figure A.4 illustrates the five main phases in the life cycle of an OWF. The Installation & Commissioning phase is primary focus of this research and is highlighted in green.

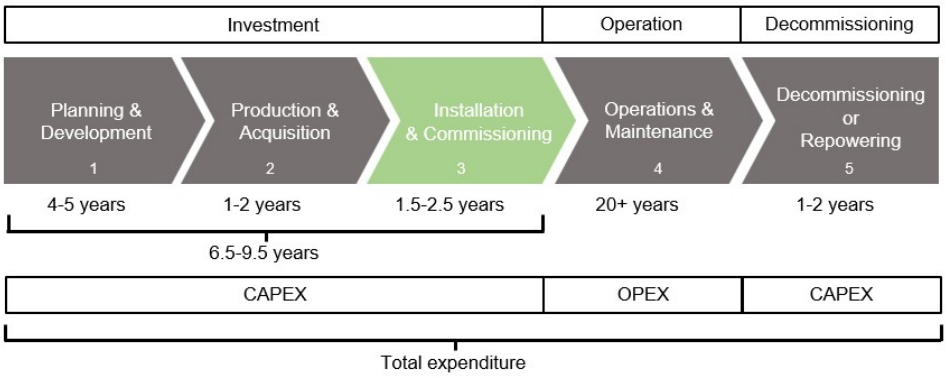

Figure A.4: Life cycle of an offshore wind farm, adapted from [6] and [28].

Below, each of the phases will be elaborated:

1. **Planning & Development** - During this phase, potential sites for the OWF are identified. Once a site is selected, it is leased to developers and the development will start. The majority of time is spent on planning, obtaining planning consent, and securing permits. Prior to site selection, multiple site investigations and surveys must be conducted. Also, extensive research is carried out regarding financing, wind farm design, and preparations for the production phase. This phase canaccount for up to 10 percent of the total Capital Expenditure (CAPEX) of an OWF. Risks in this phase include the need for costly surveys and regulatory uncertainties [6], [119], [28];

2. **Production & Acquisition** - After all permits and planning consents are in place, the second phase begins. This phase involves the manufacturing and acquisition of OWF components, including wind turbines and foundations. This phase accounts for the largest share in total CAPEX (50 to 80 percent) [119];
3. **Installation & Commissioning** - The third phase involves the installation of OWF components, including foundations, wind turbines, cables, and the offshore substation. *Accenture* [119], a consultancy firm, points out that the main risks in this phase are the limited vessel supply and lack of bespoke vessels for wind farm installation, such as foundation installation and wind turbine installation vessels. Inefficient logistics also pose a risk during this phase. In total, this phase takes up to 15 percent of total CAPEX. This research focuses primarily on this third phase of the OWF's life cycle.
4. **Operations & Maintenance (O&M)** - Once the OWF is in place and fully operational, it is expected to produce electricity for approximately 20 to 25 years [120]. During this phase, measures are taken to ensure that the turbines continue producing electricity, minimizing downtime, and prolong the lifespan of the wind farm. To achieve this, regular inspection and maintenance activities are carried out. The personnel and equipment required for these activities are transferred by Service Operation Vessels (SOVs), Crew Transfer Vessels (CTVs), or small daughter crafts;
5. **Decommissioning or Repowering** - When an OWF reaches the end of its operational life after 20+ years, it enters the fifth and final phase of its life cycle. There are two options for this phase. The first is decommissioning, which means complete dismantling and removal of the OWF. The second option is repowering, which entails updating or replacing the wind turbines with newer ones. After that, a new life cycle can begin.

A.4. Economics of offshore wind farms

The energy policy and investments of a country are often influenced by economic factors. When considering the development of an OWF, it is important to have an understanding of the economics of such projects. As mentioned earlier, this includes the breakdown of CAPEX and operational expenditure (OPEX) for the various stages of the project's life cycle. Furthermore, this section conducts a more detailed analysis of the investment costs, identifies key drivers of decision-making, and explores ways to increase the financial viability of OWFs. Ultimately, this information can be used to ensure that the market for offshore wind energy remains competitive with other electricity sources.

A.4.1. Levelized cost of energy

One very important metric for determining whether to move forward with an energy project and comparing competitiveness between different projects is the Levelized cost of energy (LCOE). LCOE is a measure of the average net present cost of energy generation over its assumed lifetime. It allows to compare different power-generating technologies with unequal life span, risk, return, and capacity [7]. In relation to the electricity price the LCOE is also an indicator of profitability. If the LCOE is higher than the electricity price, the project will likely not be profitable [121]. The LCOE is calculated with Equation A.2.

$$LCOE = \frac{Sum\ of\ cost\ over\ lifetime}{Sum\ of\ energy\ produced\ over\ lifetime} = \frac{\sum_{t=1}^{n} \frac{I_t + M_t + F_t + D_t}{(1+r)^t}}{\sum_{t=1}^{n} \frac{E_t}{(1+r)^t}} \tag{A.2}$$

where:

$LCOE$ = Levelized cost of energy [$EUR\ MWh^{-1}$]
I_t = Investment expenditure in year t [EUR]
M_t = Operations and maintenance expenditure (O&M) in year t [EUR]
F_t = Fuel expenditure in year t [EUR]
D_t = Decommissioning cost in year t [EUR]
E_t = Energy generation in year t [MWh]
r = Discount rate [$-$]
n = Lifetime of structure [$-$]

While LCOE is a great way to compare different power-generating technologies, it has a few drawbacks. For example, in a LCOE calculation costs are simplified. It does not use all costs associated with an actual financial decision [122]. LCOE also ignores context such as risks, uncertainty about future fuel prices, compliance with regulations, policies, inter-regional electricity trade, and system reliability [4].

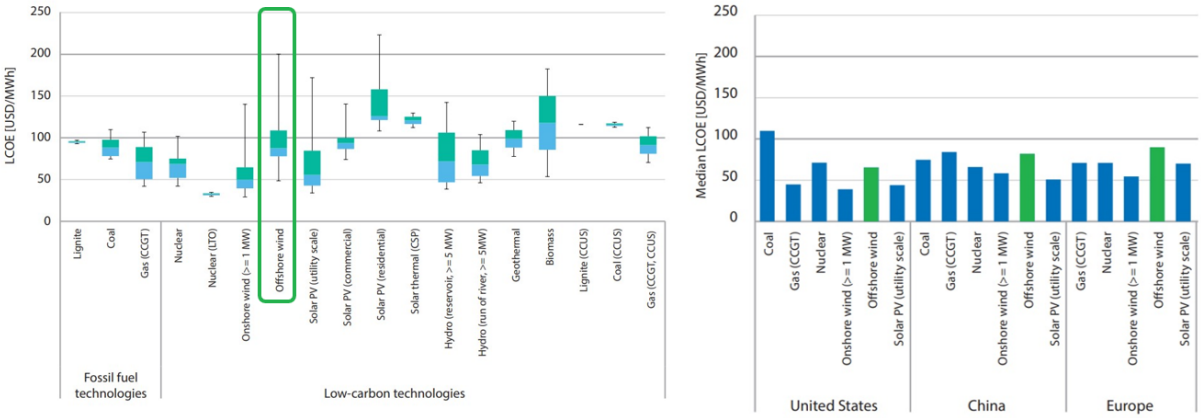

Figure A.5: *IEA* 2020 LCOE comparison by technology (left) and median LCOE comparison by region for different technologies (right), adapted from [8].
Note: values at 7% discount rate.

Figure A.5 shows on the left a box plot of the LCOE for different energy-generating technologies. As displayed, the LCOE of offshore wind is significantly higher than the LCOE of onshore wind. The LCOE is also higher than for fossil fuel technologies. The right plot of Figure A.5 shows a comparison of the median LCOE for different technologies per region. In this figure, differences in LCOE are clearly visible between regions. The LCOE comparison emphasizes the need to reduce the LCOE of offshore wind to enhance the competitiveness in relation to fossil fuel technologies and other low-carbon technologies.

A.4.2. Decreasing the LCOE

From Equation A.2, various ways to reduce the LCOE can be identified. These are stated below:

- **Increasing electricity production** - Electricity production is highly dependent on the capacity factor. To increase the electricity production and capacity factor, technological advancements are ongoing towards larger turbines, increased hub height, and larger rotor diameters. For instance, the global weighted average capacity factor of offshore wind was 43 percent in 2018 and is expected to reach 36 to 58 percent by 2030 and 43 to 60 percent by 2050 [123];
- **Decreasing O&M expenditures** - O&M expenses can account for up to 25 percent of the overall costs [124]. Reducing these costs can make a significant difference. This can be

achieved by means of more efficient maintenance scheduling and improved condition monitoring systems [125]. A lot of research is going on into predictive maintenance and optimized scheduling. In addition, research is currently being done on the effect of weather conditions and improved operability on the transfer of maintenance personnel to decrease costs and improve efficiency;

- **Decreasing decommissioning cost** - Decommissioning of OWFs is a relative new practice in the industry. At this moment, there has been limited research on the economic analysis of decommissioning of OWFs to identify its key cost drivers [126];
- **Increasing lifetime** - An LCOE analysis by means of a case study, performed by Liang et al. [127], indicated that when an OWF has a short lifetime (around 5 years), the LCOE would be extremely high. The energy production could then not cover the development cost. However, for longer lifetimes (20+ years), the LCOE decreases and eventually converges. Therefore, the influence of further increase of the lifetime is not so high. Nowadays, offshore wind projects are designed for 20 to 25 years (Section A.3), making further extensions of the lifetime less useful;
- **Decreasing discount rate** - The discount rate is related to financing costs of an offshore wind project and reflects the average cost of capital. A way to reduce the discount rate is by reducing the project risks [83]. The discount rate is highly project dependent [128];
- **Decreasing investment expenditure** - The investment expenditure is composed of various components, as shown in Figure A.4. There are various ways to decrease the investment expenditure such as technology changes during manufacturing or installation [83]. In addition, cost reduction can be achieved through economies of scale, which often leads to the design and construction of larger turbines [9].

Figure A.6 displays the capital cost breakdown for bottom-fixed (shallow water) and floating (deep water) offshore wind projects. It demonstrates that assembly and installation costs take up approximately 11 to 20 percent of the total capital cost. To enhance the competitiveness of offshore wind energy and reduce the LCOE, it is crucial to minimize costs associated to the third phase in the life cycle (Figure A.4) of an OWF by means of reducing the installation cost. This can be achieved by deploying more cost-effective and efficient WTIVs.

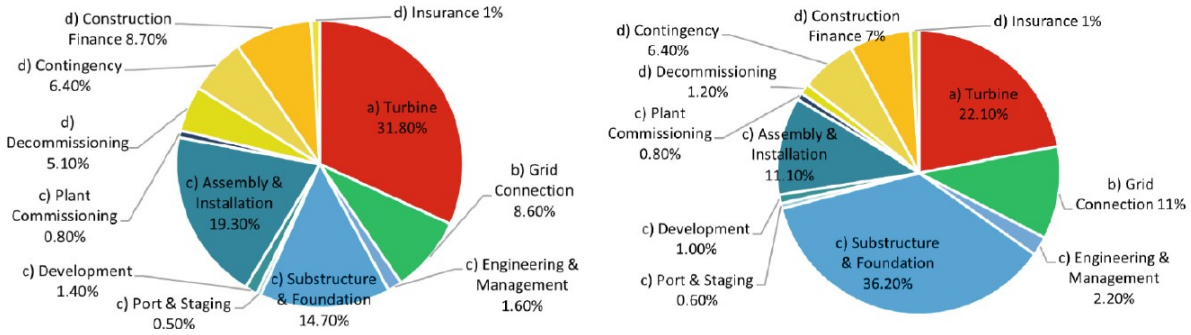

Figure A.6: Capital cost breakdown for bottom-fixed (left) and floating (right) offshore wind farms, from [10].

(This page intentionally left blank)

B

Wind turbine installation solutions

B.1. Existing solutions

This section introduces the current offshore wind installation fleet and its vessels, categorizing them into two main ship types: jack-up vessels and floating vessels. The floating vessels can further be subdivided in three sub-types: semi-submersible, sheerleg, and monohull vessels.

B.1.1. Jack-up vessels

Currently, jack-up vessels are predominantly used for wind turbine T&I [25]. A jack-up is defined as: "*A non-propelled or self-propelled marine vessel that is fitted with legs and a jacking system that provides the vessels with the capability to elevate the hull above the surface of the sea.*" [42]. Jack-ups consist of a buoyant hull and a number of legs, ranging from four to six. Jack-ups move to the location, self-propelled or by towing, with the legs raised. On position, the legs are lowered onto the seabed for preloading. During preloading, the weight of the vessel and additional ballast water are used to penetrate the seabed, avoiding further penetration during operations. After preloading, the hull is elevated out of the water by the jacking system [40]. Because jack-ups are raised above sea level they provide a stable base for lifting operations and eliminate vessel and crane displacements due to waves and surges [40].

On average, the transit speed is 4 to 8 knots for a jack-up barge, depending on the tug power. The transit speed for a self-propelled jack-up vessel is 8 to 12 knots [31]. This type of jack-ups was mostly used in the last decade [28]. Jacking speeds range from 0.35 to 2.4 meters per minute [33]. As a result, lowering and raising the legs can take up a considerable amount of time. Especially when considering that the jacking process must to be done at every wind turbine location and in port for loading of the components. This is visualized in Figure B.1. Another drawback is that weather should not be too bad to be able to jack-up the vessel, which limits the operability of the vessel. Therefore, this type of vessel is limited by metocean conditions [129]. In addition, before deploying a jack-up vessel, a survey of the seabed is required. This must be done by dedicated survey vessels. Therefore, installation of wind turbines by jack-up vessels requires a complete support fleet [43]. This is often overlooked and increases the cost of using a jack-up. Also, the use of jack-up vessels is limited by the length of the jacking legs [40]. Asgarpour [25] noticed that for deeper waters and growing turbine sizes, new customized vessels will be required.

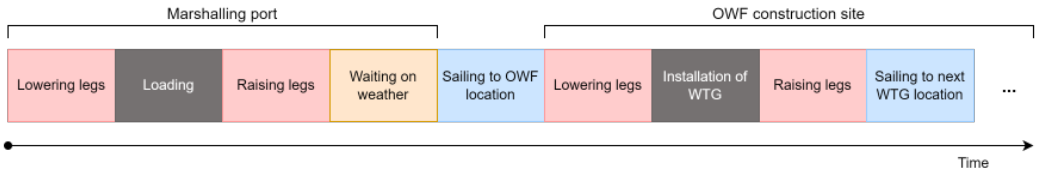

Figure B.1: Timeline showing the T&I process for a jack-up vessel. The timeline is not to scale. The installation bottleneck is shown in red.

Data on the current wind installation fleet has been extracted from *4C Offshore*s wind vessel database (March 10, 2023). The data reveals that the wind installation fleet currently consists of 81 operational jack-ups. The 1st generation of jack-ups are general-purpose jack-ups from the oil and gas industry or converted vessels for wind installation. After that, 2nd generation jack-ups were introduced, which were designed specifically for wind installation. 3rd and 4th generation [55] refers to later generations of jack-ups, that have improved capabilities and are capable of transporting and installing bigger turbines. This shows mainly in their main crane capacity. The distinction between generations is clearly visible in Figure B.2. The older generations are mostly deployed for smaller construction or O&M work due to their inability to handle larger turbine [130].

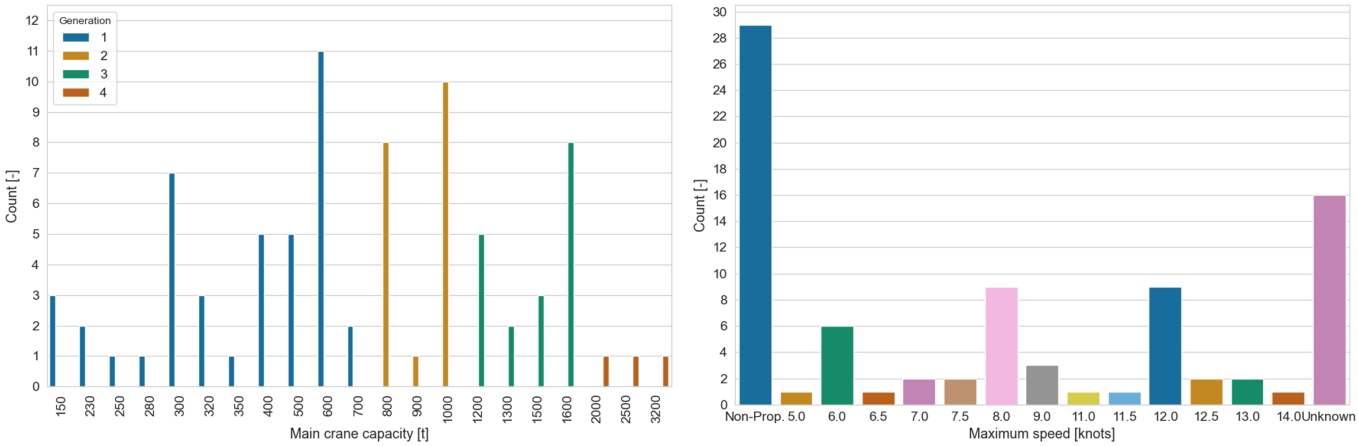

Figure B.2: Main crane capacity and maximum speed of jack-up fleet, own analysis of *4C Offshore* fleet data.

All relevant findings from the analysis of *4C Offshore* data are presented in Figures B.2 and B.3. Almost 30 of the 81 jack-ups in the fleet are non-propelled. These are mostly part of the older generations. The maximum speed of self-propelled jack-up is predominantly between 8 to 12 knots. Most of the jack-ups have a maximum operational water depth of 50 to 60 meters. A few vessels are capable of up working in depth up to 85 meters. The maximum lifting height of most of the vessels is unknown. However, based on the available data, it can be concluded that the lifting height for the older generations is already too low for the installation of current wind turbines. The lifting height for the most recent vessels is up to 170 meters above main deck.

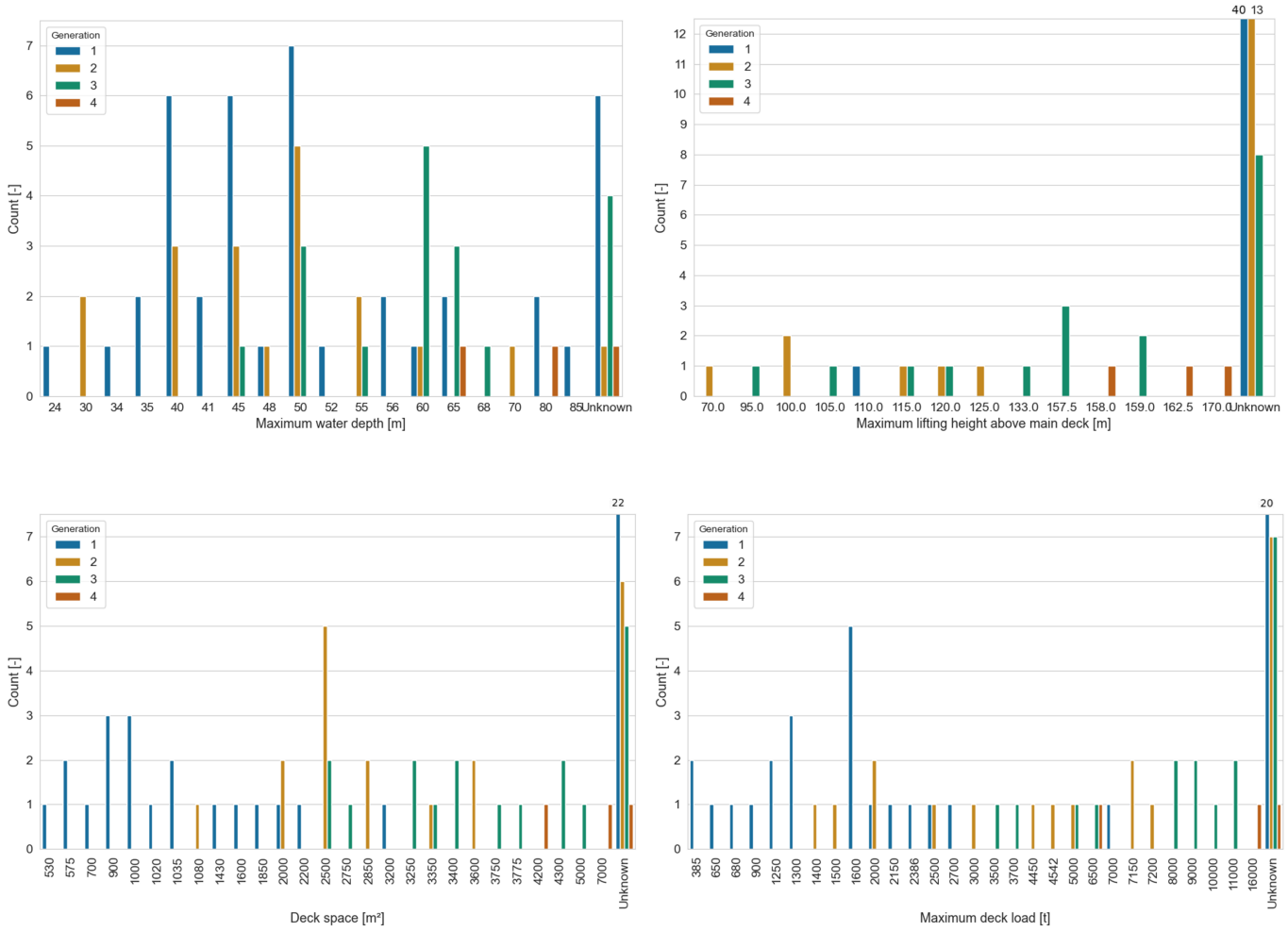

Figure B.3: Visualization of relevant findings of the current jack-up fleet, own analysis of *4C Offshore* fleet data.

The most advanced jack-ups (3rd and 4th generation) have accommodation capabilities of 80 to 150 persons. In the given range for total number of accommodation, the majority is clustered around 100 persons. The dynamic positioning (DP) capability class is DP2 for the majority of the 3rd and 4th generation jack-ups in the database.

B.1.2. Floating vessels

In addition to jack-up vessels, floating vessels are also employed for offshore wind turbine installation. Floating vessels can be classified into semi-submersible, sheerleg, and monohull vessels.

Semi-submersible vessels

A semi-submersible vessel is defined as: "*A floating structure normally consisting of a deck structure with a number of widely spaced, large cross-section, supporting columns connected to submerged pontoons.*" [131]. Semi-submersible vessels are mainly used in the offshore oil and gas industry. One of the applications is as a heavy-lift vessel [129]. An impression of semi-submersible crane vessels (SSCVs) is shown in Figure B.4.

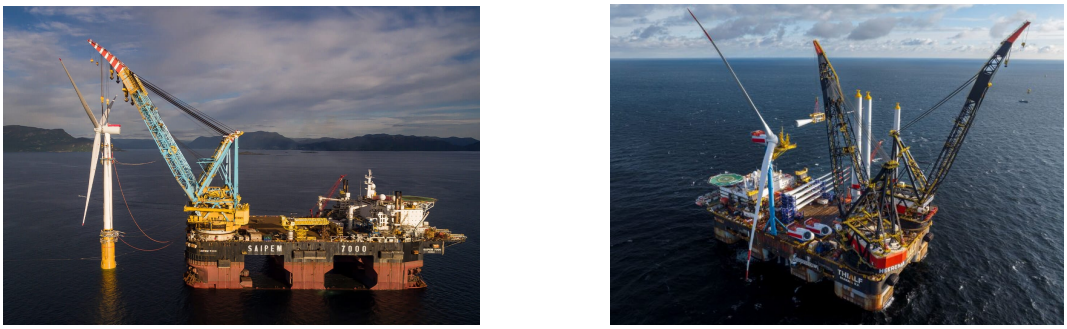

Figure B.4: *Saipem 7000* [44] (left) and *Thialf* [132] (right) installing wind turbines.

SSCVs are equipped with thrusters but have a relatively slow transit speed, averaging around 10 knots [49]. They are primarily designed for heavy-lifting operations. At the installation location, the vessel is ballasted, increasing draft and displacement. In this way the vessel provides a stable platform for heavy lifts. In ballasted condition only the columns penetrate the waterline, resulting in a small waterplane area and improved motion behavior in harsher environments [133]. SSCVs are typically equipped with one or two large cranes that can (simultaneously) lift very heavy loads, ranging from several thousands to 20,000 tonnes [45]. SSCVs are sometimes used for offshore wind applications, particularly for the installation of foundations or substations.

SSCVs have also been used for installation of wind turbines. For example, in 2017 SSCV *Saipem 7000* installed five fully preassembled 6 MW wind turbines for the *Hywind* project [44]. These turbines were transported fully preassembled, while suspended in the cranes. In addition, in 2022 *Thialf* installed 9.5 MW turbines for the *Arcadis Ost 1* project, using the RNA method. A major drawback of this vessel type is that the day rates of are high [28]. Therefore, the use of SSCVs is not cost-efficient, because their capabilities and costs exceed what is required for offshore wind turbine installation [31].

Another limitation of SSCVs is the disability to transport turbine components, despite having substantial deck area. The problem is their large draft. Typically, SSCVs have a transit draft of 10 to 12 meters. Their maximum draft, during lifting operations, ranges from 25 to 32 meters [44], [45]. The water depth at marshalling ports is typically not larger than 9 to 13 meters [23]. As a result, SSCVs are not able to enter the marshalling port and load the turbine components. Consequently, this type of vessel requires a feeder system, introducing additional challenges and drawbacks to the installation process. Figure B.5 shows a timeline with the T&I process. The bottleneck is marked red.

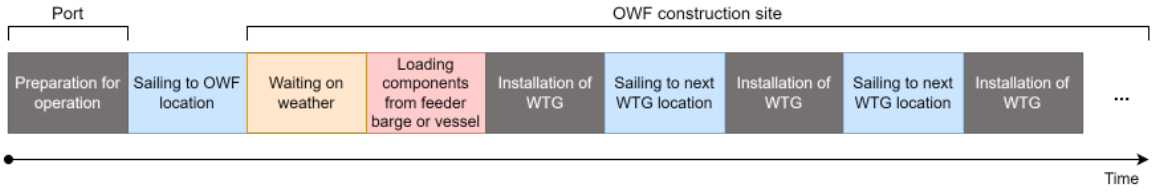

Figure B.5: Timeline showing the T&I process for an SSCV. The timeline is not to scale. The installation bottleneck is shown in red.

Sheerleg

A sheerleg is defined as: "*A barge-shaped crane vessel, which is not capable of rotating the crane independently from the hull.*" [129]. An impression of a sheerleg is shown in Figure B.6.

Figure B.6: Sheerleg crane *Rambiz* lifting a 5 MW turbine, from [134].

Sheerleg cranes have a high lifting capacity, ranging form 300 to 10,000 tonnes [135], [136], and are widely used in offshore oil and gas construction projects. They are also sometimes applied in offshore wind projects [129]. Sheerlegs are used to install substations onto their jackets. Also, they are very rarely used for wind turbine installation [31]. For example, sheerleg *Rambiz* transported and installed two 5 MW turbines for the *Beatrice Demonstrator* project in 2007 [137]. Sheerlegs do not have free cargo deck space, which requires them to sail with the cargo suspended in the crane or use a feeder system. Due to the barge-shaped hull, this type of vessel can only operate in low sea states and has a very low transit speed [49]. As a result, it is not attractive to use. Figure B.7 shows a timeline of the T&I process with a sheerleg.

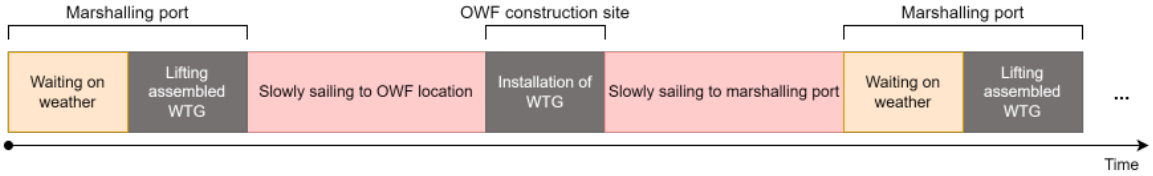

Figure B.7: Timeline showing the T&I process for a sheerleg. The timeline is not to scale. The bottleneck is shown in red.

Monohull vessels

Monohull vessels are defined as: "*A ship with only one hull, as opposed to a catamaran or multihull.*". Floating monohulls are self-propelled and can be fitted with a heavy-lift crane. There are various floating monohull crane vessels in the market. This vessel type is currently mainly used in the offshore wind market for foundation installation [28]. An example of a floating monohull heavy-lift vessel is shown in Figure B.8.

Figure B.8: *Aegir* installing a wind turbine, from [138].

One advantage of monohulls is that they are capable of higher transit speeds up to 15 knots [49]. Unlike jack-ups, this type of vessel is floating during installation activities, and is

therefore not restricted by water depth or soil conditions. Since it does not have to lower and raise legs, it saves a considerable amount of time to use a monohull in comparison to jack-ups. Monohull vessels normally have a large open deck and are therefore capable of carrying a lot of cargo. Also, day rates are lower than the other mentioned vessel types [28].

However, floating monohull vessels are more susceptible to motions as a result of waves. In literature, only one instance of a floating monohull crane vessel installing a turbine was found. In 2018, monohull crane vessel *Aegir* installed a turbine for a trial at the Princess Amalia OWF. In the trial, the installation was conducted via a Slip Joint connection, which involves that the turbine is slid over the monopile without using grout or bolts. *Aegir* transported the fully-assembled and installed it at the offshore site while floating on DP. Since the turbine was preassembled onshore and the installation was done floating, the installation time was only one hour. This is significantly less than usual installation [139], [138]. It should be noted that the turbine in this instance was not particularly large. The challenge is expected to be more substantial for larger future-turbines. Figure B.9 shows a timeline of the installation process of the *Aegir* and a theoretical example with a floating monohull crane vessel installing wind turbines with the single-blade method (method 1 or 2).

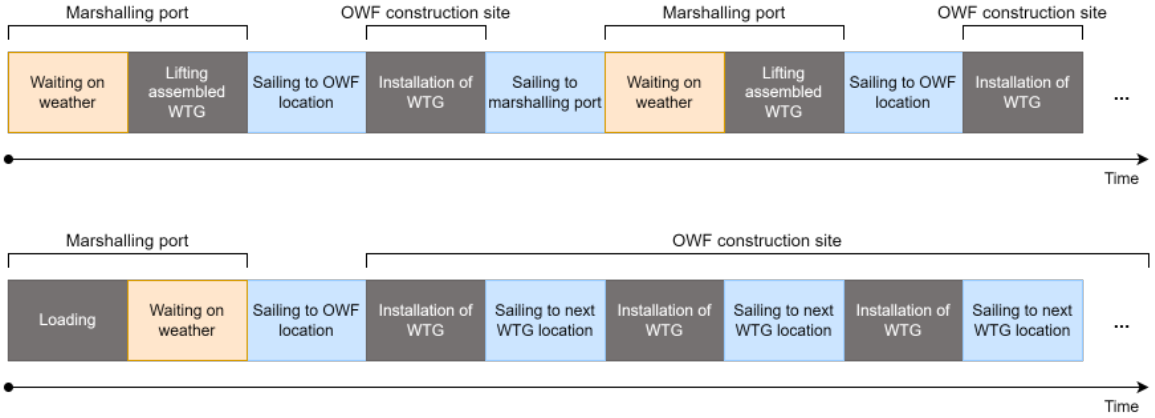

Figure B.9: Timelines showing the T&I process for *Aegir* (top) and a floating monohull using installation method 2 (bottom). The timelines are not to scale.

B.2. Gap between offshore wind market and current installation fleet

A gap exists when looking at the current ways of installing offshore wind turbines and the emerging trends in the offshore wind market. The dominant vessel type for turbine installation today is the jack-up vessel. However, jack-ups are expensive, because of the jacking system. Additionally, the time-consuming process of lowering and raising the legs, as well as the dependency on seabed conditions, and the requirement for support vessels for seabed surveys, make jack-up vessel less cost-effective. This is conflicting with the need to reduce the LCOE to make offshore wind more attractive and competitive. The existing jack-up fleet is capable of water depths of 50 to 60 meters, with a few vessels capable of operating in water depths of up to 80 meters. Considering the development of water depths in recent years and the future, it is clear that the limits of the current vessels will quickly be reached. Furthermore, examining the capabilities of current jack-up vessels, shows that their lifting height would be insufficient for larger turbines. This is displayed in Figure B.10. SSCVs and sheerlegs are not limited by water depth but are also not cost-efficient for installation of offshore wind turbines. Floating monohull vessels have the potential to offer a solution for wind turbine installation, but they

have only been used once for this purpose with a relatively small turbine.

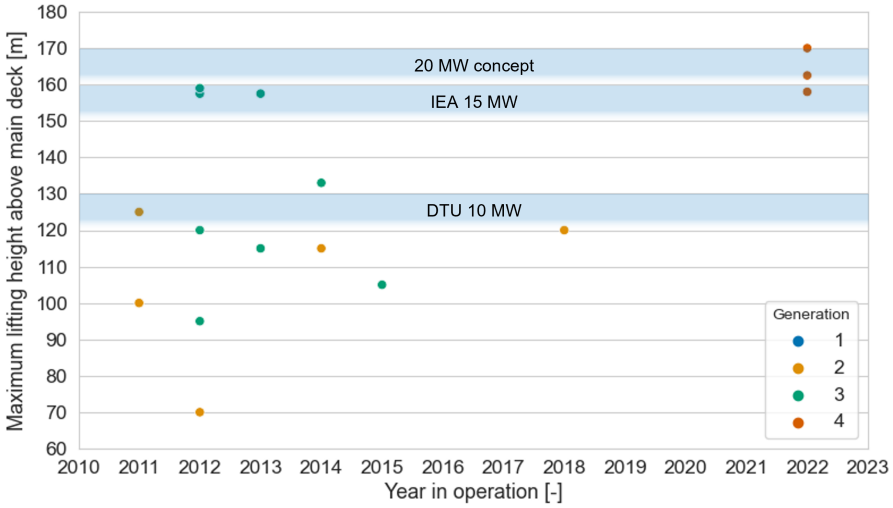

Figure B.10: Scatter plot displaying the lifting height of jack-up vessels and the required lifting height for various wind turbine sizes, own analysis of *4C Offshore* fleet data.

Vessel operators and designers are aware of the challenges and have addressed them in different ways, such as: ordering new vessels, upgrading existing vessels and developing new wind turbine installation concepts. These pathways will be addressed in the following subsections.

B.2.1. Ordering new vessels

Several new wind turbine installation vessels are currently being built or have been ordered. At this moment, around 30 WTIVs are on order or under construction (*4C Offshore*, March 2023). All of them are jack-up vessels. A small selection of vessels under construction, owned by renowned WTIV operators, will be discussed below.

Boreas - Van Oord

One of the new vessels currently under construction is the *Boreas* for *Van Oord*. The ship with a length and breadth of 175.1 and 63 meters is currently being built in China and is expected to enter market in 2024. The jack-up will be able to operate on methanol and could be capable of installing wind turbines with a capacity up to 20 MW. The vessel will have a deck of 7,150 m² and will be equipped with a crane with 3,200 tonnes lifting capacity. With its four legs of 126 meters it will be capable of operating in water depths of up to 70 meters. The transit speed of this jack-up is around 12 knots [140], [141].

Seaway Ventus - Seaway 7

The jack-up *Seaway Ventus* with a *GustoMSC NG-14000XL-G* design is currently being built and is expected to join the *Seaway7* fleet in 2023. The vessel will have a length of 142 meters and breadth of 50 meters. It will have a deck space of 4,600 m² and capacity of 9,800 tonnes. With its four 109 meter long legs it can work in water depths of up 65 meters. This vessel will be equipped with a novel telescopic heavy-lift crane with a capacity of 1,600 (extended boom) to 2,500 tonnes (retracted boom) and a maximum lifting height of 142.5 (retracted boom) to 182 meters (extended boom) above sea level (with a 15 meter air gap). The transit speed is around 10 knots with an empty deck [142].

Siren - Seajacks

Seajacks has ordered two jack-ups of the type *GustoMSC NG16000X*, which will be named *Siren* and *Nessie*. They vessel will be launched in 2024 and 2025. They will have a length of 148 meters and breadth of 56 meters. With the 109 meter legs it will be capable of working at water depths of 65 meters and a significant wave height of 2.0 meters [143]. The main crane will have a capacity of 2,600 tonnes. The deck space is 5,400 m². The loaded service speed will be 9.5 knots [144].

X-class and F-class - Cadeler

Cadeler has ordered two new jack-ups of the *X-class*. These vessels will be ready in 2024 and 2025 [145]. They will feature a main crane capacity of 2,600 tonnes and a hook height of over 200 meters above deck [146]. She will have a deck space of 5,600 m². The vessels will be able to transport and install seven 15 MW turbine or five 20 MW turbines per trip [145]. The maximum operational water depth will be around 70 to 80 meters [143].

Cadeler has also ordered two *F-class* jack-up vessels, which will be ready in 2026. These jack-ups will be almost similar to the two *X-class* vessels, but will enable to handle next-generation foundations. Therefore, the main difference is in the main crane capacity, which will be over 2,600 tonnes [147]. These vessels could also be used for wind turbine installation.

B.2.2. Upgrading existing vessels

Another way of dealing with the gap between the current wind turbine installation fleet and the (future) market is to upgrade existing vessels. A selection of recent or planned upgrades on existing wind turbine installation vessels will be discussed below.

Aeolus - Van Oord

In 2014 jack-up vessel *Aeolus* was built for *Van Oord*. Initially she had a main crane with a lifting capacity of 900 tonnes. Modifications were made to the vessel in 2018. The crane capacity was increased to 1,600 tonnes. Also, the vessel was widened and the deck was reinforced to increase the loading capacity. In addition, the number of onboard accommodations was increased and a helideck was added [148], [149]. Four years later, the company announced that the vessel would be upgraded again to handle 12-15 MW turbines. This time, the crane boom was exchanged for a larger one with a length of 133 meters. The crane upgrade has been completed early 2023 [150].

This vessel shows how fast the market is changing and show the challenges when designing such as vessel for an uncertain future market. This jack-up, which is under ten years of age, had to be upgraded twice to stay competitive in a market where turbines continue to increase in size.

Sea Installer - DEME

Jack-up vessel *Sea Installer* was built in 2012 for *A2Sea*. She was later acquired by *DEME*. In 2023 she received a major crane upgrade with an increase from 900 to 1,600 tonnes. This enables the vessel to handle next-generation offshore wind turbines. DEME also secured an option to upgrade the crane on one of their other wind installation vessels, *Sea Challenger* [151], [152].

Wind Osprey and Wind Orca - Cadeler

Besides the order for new vessels, *Cadeler* will be upgrading their two existing *O-class* jack-

ups *Wind Osprey* and *Wind Orca*. Both vessels are built in 2012 and have a lifting capacity of 1,200 tonnes and a hook height of 132 meters above deck. In 2024, both vessels will be ready to operate with new cranes with a capacity of 1,600 tonnes and a main hook height of 160 meters above main deck [153]. Once updated, they will be able to transport and install three 14 MW next-generation turbines [154]. What stands out is that the *Wind Osprey* had already undergone a crane modification in 2020. The boom of the main crane was extended during that upgrade [155].

B.2.3. Designing new concepts

The last way to bridge the gap between the current wind turbine installation fleet and the evolving market is to design innovative ship concepts or installation methods. A selection of concepts is shown in Figure B.11 and will be discussed below.

Figure B.11: Selection of new concepts, showing *Windlifter* (top left) [156], *WTS* (middle) [157], *WIV* (top right) [158], *PWT* (bottom left) [48] and *Feederdock* (bottom right) [159].

Windlifter

In the 2010s *Ulstein* developed the *Windlifter* concept. The dynamically positioned *Windlifter* is able to transport up to four fully preassembled wind turbines and install them in a single lift without the use of a crane. The installation consists of a rail system and beams suspended from the stern of the ship. The end is fitted around a transition piece. The connection allows the ship to pitch and roll, but the mechanical system compensates for yaw and lateral movement. Therefore, no expensive heave compensation or control systems are needed, making the concept less prone to failure. Installation is subsequently done by a trolley that picks up the wind turbine and rides on rails, that are attached on deck. When at the stern extension, it is lowered onto the transition piece. This vessel can be used for fixed or floating foundations [43].

The *Windlifter* is an elegant and relatively simple solution for transporting and installing wind turbines. The modular system [156] also allows the vessel to be used for other purposes. At the time this concept was developed, however, the wind turbine size was much smaller (5 MW [43]) than what it is now and is expected to be in the future. Wind turbines are and will be much heavier and higher, so it would be a challenge to maintain stability and keep motion behavior during sailing within limits.

Wind Turbine Shuttle

Huisman developed the *Wind Turbine Shuttle (WTS)*. The design focuses on installation efficiency and in that way reduce the installation costs and LCOE. The vessel is a SWATH (Small Waterplane Area Twin Hull) which results in favorable seakeeping behavior. As a result its limiting sea state during installation is 3.5 meters significant wave height [157]. Therefore, it has a high workability. The *WTS* is capable of transporting two fully preassembled wind turbines at a time at a high speed of 14 knots and installing them on dynamic positioning. However, typically SWATHs have a very high friction resistance due to the large wetted surface [160], resulting in less efficiency and higher fuel consumption. The vessel has a lifting capacity of 2x 2,000 tonnes and can handle wind turbines up to 12 MW and has a motion compensation system. Besides, it can also be used for foundation installation and heavy-lifting [161], [157].

Windfarm Installation Vessel by Huisman

Another concept by *Huisman* is the Windfarm Installation Vessel (WIV). The *WIV* is a large semi-submersible vessel with a 3,000-tonne, 3D motion compensated installation tower. It is designed to handle the larger next-generation 20 MW wind turbines, unlike the *WTS*. The *WIV* uses an installation method that is comparable to the RNA method. The separate wind turbine components are assembled on board and only one overboard lift is required. For onboard assembly, this method uses the special assembly tower. The assembly consists of four workstations, which enable simultaneous assembly and installation. The assembly tower first raises the turbine tower, rotates one quarter turn, lifts the nacelle on top, and connects the blades to the hub. The assembled turbine is then lifted, while the tower turns again one quarter, and lifted onto the foundation. Due to the high installation efficiency and onboard assembly of the wind turbine it will be capable of installing wind turbines in just one day. The assembly process is visualized in Figure B.12. Because of the semi-submersible hull, it can be operated in a maximum significant wave height of 3.5 meters, which results in a high workability. The installation efficiency and high workability result in a short installation time, contributing to lowering the LCOE of offshore wind. She would have an empty transit speed of 12 knots [162], [158]. However, due to the semi-submersible hull, components must be supplied by feeder barges or vessels.

Figure B.12: Visualization of the assembly process with the assembly tower, snapshots from [163].

Parallelogram Wind Turbine (PWT) installation vessel

The *PWT* installation vessel was the result of the graduation research by G. Hoogendoorn at *Huisman*. The concept involves a semi-submersible monohull that is capable of installing fully preassembled wind turbines. The wind turbines are fitted on a barge for quick (un)loading of wind turbines without the need for loading individual turbines [48]. This barge exchanging would make it a good solution for US waters, where the Jones Act applies. This states that

installation vessels built outside the US are not allowed to load at a port in the US. Therefore, feeder solutions are needed to supply an installation vessel [164]. The research was mostly focused on having an efficient installation process. As a result, two large heavy-lift cranes are located at the stern, which efficiently install a fully preassembled turbine [48]. The result of the thesis is a very high-level concept design. It is therefore the question if it would really work. For example, the calculated values of the transverse metacentric height ($\overline{GM_t}$) in the stability analysis are very high. High $\overline{GM_t}$ values typically result in high accelerations. It is the question if accelerations at the nacelle would be within the limits to prevent damage to it.

Feederdock

In 2022 the *Feederdock* concept was presented. The *Feederdock* is a U-shaped crane vessel that can dock barges before jacking-up. This jack-up design has especially been designed to be a Jones Act-compliant T&I solution, fit for US markets [159]. The concept has a main crane capacity of 3,000 tonnes and is able to install 25 MW wind turbines [165] via method 1 or method 2 (single-blade). The U-shaped crane vessel can stay at the offshore wind farm location, while being fed by the barges. This will save transit time and costs. However, it looks like components for only one wind turbine can be fitted on a barge [165], meaning that a lot of tugs and barges are needed for feedering. Still, this concept is an elegant Jones Act-compliant solution for US waters. However, since it is a jack-up, it still has all the associated disadvantages. According to *4C Offshore* data and [21], the general trend in the US is to move further offshore and to deeper waters. This could be troublesome for this concept. Also, this concept still has to raise and lower the legs at every wind turbine location, resulting in a not so efficient installation procedure. Therefore, it is the question if this concept will contribute to lowering the LCOE.

At this moment, a U-shaped jack-up with a comparable installation process is actually being built in Singapore for *Maersk Supply Service*. She is expected to be delivered in 2025 to operate in US waters [166]. Although further information about the vessel is not available, its construction is a noteworthy development for the construction of OWFs in US waters.

(This page intentionally left blank)

C

Design strategies

C.1. Point-based design

The point-based design approach refers to the method of solving for a single optimal solution [167]. Point-based design is a linear process that starts with an initial concept or idea and gradually advances towards a greater level of detail. In ship design, this is method is synonymous with the design spiral from J. Evans (1959) [168]. Evans' design spiral is most commonly used to describe the design process for a ship. The design spiral is depicted in Figure C.1. It is most effective for designing or refining the design of ships that have been made many times before. However, it is less suitable for real complex designs. The design spiral approaches the design process by conducting iterative passes through the spiral, sequentially addressing each element and gradually increasing the level of detail with each iteration. Ultimately, this results in a single balanced design that satisfies all requirements [169].

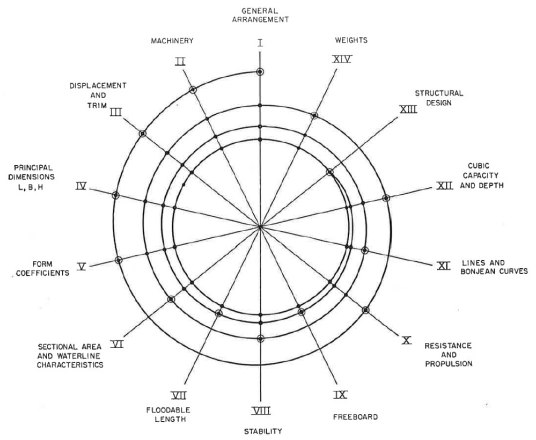

Figure C.1: Traditional design spiral from 1959, from [168].

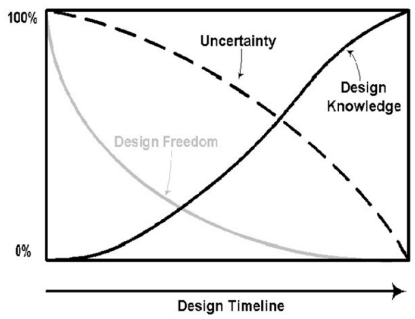

Figure C.2: Relationship between freedom, knowledge, and uncertainty in design during design process, from [170].

While the design spiral is very successful in describing the increasing level of detail during the design process, it is incapable of dealing with changing requirements during the design process [58]. If one of the requirements changes or requirements are added during the process due to new insights, the process may need to start over again. Consequently, it is necessary that all requirements are already known before the design process starts and are fixed during the whole process. However, as shown in C.2, this is often not the case. Another limitation of

point-based design methods is that they produce a feasible design that meets the requirements but it may not necessarily yield a global optimum [167]. There is no way of knowing if it is a good solution, other than from experience. Additionally, point-based design is less suitable for optimization, because one solutions has to be evaluated after another in a standard routine. This can be very time-consuming in the number of single designs that need to be generated to evaluate and find optimal solutions [171], which makes this approach expensive. Furthermore, point-based design is not well-suited as a method for creating innovative ship designs, as it relies on previous designs. As a result of that, the design spiral is only suited for incremental innovation [52].

C.2. Set-based design

Rather than selecting one promising design option and develop that further, set-based design takes into account a wide range of possible options. At the beginning of a set-based design process, which is also sometimes referred to as set-based concurrent design [172], a broad design space with design parameters is defined. These sets remain open to allow for full-exploration of trade-off information [167]. This approach prevents narrowing down to quickly and thereby losing opportunities for innovation [172]. Decision-making at the start of the process is thereby avoided and postponed to a later stage, when design knowledge has already increased. Throughout the process, infeasible or unsuitable options are eliminated, and the sets are gradually narrowed until it converges to a more globally optimum solution. As the sets narrow, the level of detail increases [167]. Figure C.3 provides a schematic of the approach. When requirements change or new ones are added during the process, the risk of having to start all over again is reduced because there may still be options that satisfy the new requirements.

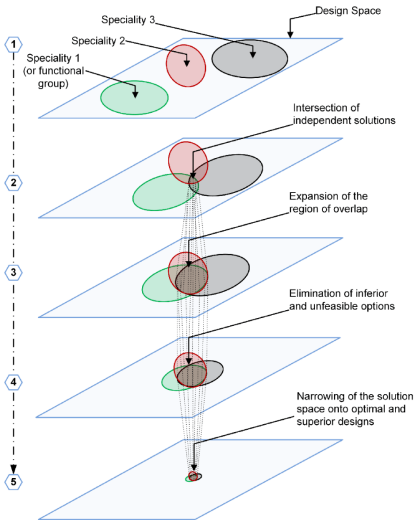

Figure C.3: Set-based design approach, from [172].

Set-based design is better suitable to optimize a design with variable requirements. This could be done by designing multiple alternatives in parallel and eliminating those that are proven to be inferior to others [167]. Set-based design is also better capable to deal with changes in the requirements or errors during the process. When this happens, the sets could be still wide enough to move forward and reach a converged solution without major rework or starting the design over. However, there are disadvantages associated with set-based design. One of them is that developing multiple solutions in parallel requires more resources [173], making it expensive. Also, this method requires coordination of multiple teams and stakeholders who are all working on different aspects of the design. This can be challenging if there are conflicting goals or priorities among the various teams. In addition, if applied incorrectly, set-based design could be inefficient and ineffective, resulting in higher costs, longer lead time and low quality. This approach may be complex than other design methods, especially for teams that are not familiar with the process. Therefore, it is important that everyone understands the process and additional training may be necessary [174].

C.3. Systems engineering

Ships consist of many interconnected and interdependent systems, with their own functions and requirements. This makes ships a complex system. In addition, opposed to vessels built in series, WTIVs are complex-specials: tailor-made high value assets, which are built for a specific client and designated purpose. Therefore, these vessels are generally built in (very) small series or as one-offs [58]. Systems Engineering is a design approach that is often used in the development of complex systems. Unlike set-based design, which explores multiple design options in parallel, Systems Engineering takes a holistic approach to design and consider the entire system and all of its components. By investigating the system, the functional requirements are discovered. The Systems Engineering approached is described by Kossiakoff et al. [175]. The approach can be divided in three main parts, forming the system life cycle model. This is depicted in the figure below.

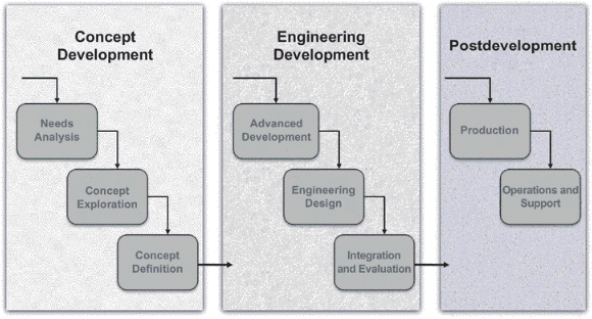

Figure C.4: Systems Engineering life cycle model, from [175].

The *Concept development* stage is the first phase of the formulation and definition of a system concept perceived to best satisfy a valid need. *Engineering development* embodies the translation of the system concept into a validated psychical system design, meeting all requirements. Finally, *Postdevelopment* includes the production, deployment, operation, and maintenance of the system throughout its lifetime. This research focuses on the first stage in the life cycle model. This stage may be further subdivided into three phases, which are also shown in Figure C.5:

1. **Needs Analysis** - Establish that there is a valid need (and market) for a new system and demonstrate its techno-economic feasibility, and define system operation requirements;
2. **Concept Exploration** - Explore feasible concepts and define functional performance requirements;
3. **Concept Definition** - Examine alternative concepts, select the preferred concept on basis of performance, cost, schedule, and risk, and define the system's functional specifications.

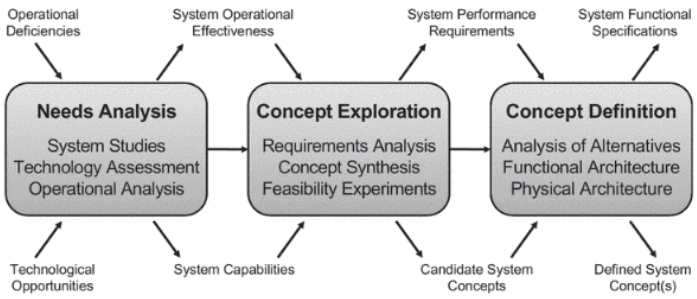

Figure C.5: Concept development phases of system life cycle, from [175].

Systems Engineering offers a holistic approach to design of complex systems, considering the entire system and its components. Collaboration between multiple disciplines and stakeholders ensures optimization. However, this is also the drawback of such an approach. A good communication is very important. A risk in big organizations could be silo thinking, which contradicts the holistic approach [176]. Silo thinking refers to a narrow-minded approach that is limited by one's own expertise, department, or perspective. Today's systems with growing complexity can be challenging to understand. This could make it difficult to identify all the potential interactions between components [177]. There is a risk that some issues may be missed. Also, the Systems Engineering approach follows a very structured process, which can make it less flexible than other design methods. Lastly, it may be hard to organize Systems Engineering in organizations. Complex projects requires specialists, but System Engineering requires both systems-level thinkers and specialists. Therefore, it may be difficult to fill these roles [176].

In addition, Systems Engineering may not be well-suited for innovative design projects. T. M. van Bruinessen et al. [178] showed that innovative solutions have a strong interaction between the required performance, function, and shape of the ship-design and systems it is decomposed in. This means that the systems impact the overall design. As a result, the independent design of different decomposition levels of a system, as proposed by Systems Engineering, appears to be invalid for innovative design projects.

C.4. Systems-based design

Although this system-based approach might sound or look like a variant of Systems Engineering, it is not [53]. System-based design was first introduced in 1991 by K. Lavender. Within this method, the first part of the design spiral has been straightened. This is shown in Figure C.6.

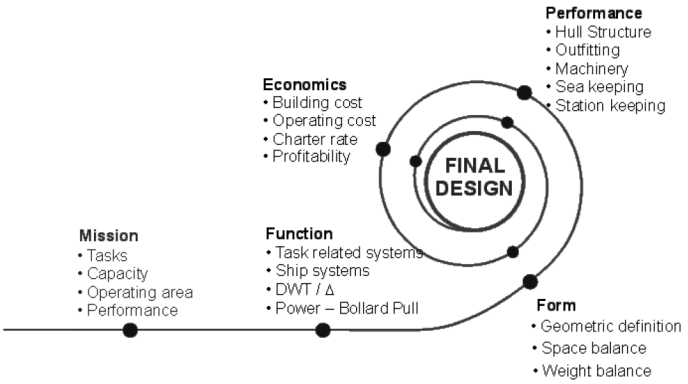

Figure C.6: The system-based design process, from [179].

With straightening the first part of the design spiral this method strives to decrease the number of design iterations. The method starts with the needs and functions ("why and what?") and proceeds, via the form ("how?"), to the performance and economics ("how well?"). By following this step-by-step approach, the naval architect is guided to a technically feasible and economically preferred solution. In order to achieve this, the ship is divided into ship systems and task-related systems. The dimensions, mass and other characteristics of these systems are then estimated using a combination of functional requirements and experience-based functions and coefficients. This knowledge then results into a geometric definition, space and weight balance. With this, modular concept sketches are made [58], [52], [53]. The process can be somewhat compared to a set of *Lego* bricks that could be combined towards many

possible conceptual solutions [53]. In this way, multiple feasible designs are created, which can be used for estimations on performance and economics. Subsequently, the focus can be shifted to the overall conceptual solution and arrangement optimization, based on the system definitions. The system-based design method in ships is often referred to as an inside-out approach because it involves developing and arranging all internal systems and volumes of the ship first, and then wrapping a hull around this assembly [53]. Therefore, this method is a good way to generate a technically feasible design and end up with an economically preferred solution.

However, this method does also have some disadvantages. For instance, in order to estimate the characteristics of the systems experience-based data is used from previously developed vessels, including overall and machinery layouts and trend lines of the existing fleet. As a result of this, the design is limited to known designs on which information is available. As a result, this method does not account for innovation in other parts of the ship design such as individual systems and components or conceptual business cases [52].

C.5. Optimization-based design

Optimization-based design is an approach that aims to find the best possible solution that meets the requirements and expectations of the client and other stakeholders. This method could also be applied in ship design, viewing the design as an optimization problem [53]. Optimization-based design is a design approach that involves formulating the design problem as an optimization problem using mathematical optimization techniques to find the best solution. This approach aims to find the optimal values of design variables that satisfy the requirements and meet the design objectives.

The main challenge with optimization-based design is that the typical ship design problem is too complex. Ship design consists of many interconnections between a large number of design variables and constraints. As a result of that, the large design problem cannot be efficiently and accurately captured within a mathematical optimization model [53]. Efforts have been made to address these challenges in ship design optimization. One example is the HOLISHIP (HOLIstic optimisation of SHIP design and operation for life cycle) project, focusing on multi-objective ship design optimization of various types of ships for a variety of criteria. The project employed various design tools and relied on a core ship database [180]. While the research seems to have made significant progress in the field of optimization-based design, the resulting optimization model is not publicly available.

(This page intentionally left blank)

D

Offshore wind turbines

The created offshore wind turbine database is displayed on the next page. The definitions and units of the used symbols can be found in the Symbols list at the beginning of this report.

Notes and abbreviations

* Tower properties are generally site-dependent.
# Including hub length/weight.

GE = General Electric
SG = Siemens Gamesa
NREL = National Renewable Energy Laboratory
LW = LEANWIND project
DTU = Danmarks Tekniske Universitet
IEA = International Energy Agency
WM = WINDMOOR project

Table D.1: Offshore wind turbine database

				Blade		Nacelle				Hub		Tower*					
Name [-]	**Make or project** [-]	P_{rated} [MW]	D_{rotor} [m]	L_{blade} [m]	M_{blade} [t]	$L_{nacelle}$ + L_{hub} [m]	$B_{nacelle}$ [m]	$H_{nacelle}$ [m]	$M_{nacelle}$ [t]	M_{hub} [t]	D_{hub} [m]	L_{tower} [m]	D_{tower} [m]	M_{tower} [t]	H_{hub} [m]	**Drivetrain** [-]	**Reference** [-]
Haliade-X	GE	14.0	218.2	107.0	55.0	20.6 #	11.0	10.4	600	60		129.1	8	2550	135	Direct drive	[181]
V164-8.0	MHI Vestas	8.0	164.0	80.0	35.0	24.0 #	7.5	7.5	375 #						105/140	Gearbox	[182]
Haliade 150-6	GE	6.0	151.0	73.5											100	Direct drive	[183]
V164-9.5	MHI Vestas	9.5	164.0	80.0	35.0				390						105/140	Gearbox	[184]
SWT-7.0-154	Siemens AG	7.0	154.0	75.0												Direct drive	[185]
MySE8.3-180	MingYang	8.3	178.0	86.5	31.0	10.8 + 5.8	5.5	8.1	276	91						Semi-direct	[186]
MYSE7.0/7.2-158	Mingyang	7.0/7.2	158.0	76.6	36.0	9.5 + 5.8	5.5	9.2	254	93					100	Semi-direct	[187], [186]
MySE6.45-180	MingYang	6.5	178.0	86.5	31.0	10.4 + 5.8	5.5	9.2	247	91						Semi-direct	[186]
MySE5.5-155	MingYang	5.5	158.0	76.6	36.0	9.3 + 5.8	5.5	9.2	230	93					100	Semi-direct	[188], [186]
V112-3.3	MHI Vestas	3.3	112.0	54.7	11.9	12.8	4.0	3.4	157							Gearbox	[182], [189]
SG 14-222	SG	14.0	222.0	108.0					500-600							Direct drive	[190]
SG 8.0-167	SG	8.0	167.0	81.4					480						92	Direct drive	[191]
SWT-6.0-154	Siemens AG	6.0	154.0	75.0								88.0				Direct drive	[192]
V236-15.0	MHI Vestas	15.0	236.0	115.5					575							Gearbox	[193]
V164-10.0	MHI Vestas	10.0	164.0													Gearbox	[194]
V174-9.5	MHI Vestas	9.5	174.0													Gearbox	[195]
	NREL	5.0	126.0	61.5	17.7				240	57		87.6	6	347	90	Gearbox	[196], [197]
	LW	8.0	164.0	80.0	35.0	20.0 + 4	7.5	7.5	285	90	4.0	106.3	7	558	110	Gearbox	[197]
	DTU	10.0	178.3	86.4	41.0				446	105	5.4	115.6	8	987	119	Gearbox	[16], [17]
	IEA	10.0	198.0	96.2	47.7				543	82	5.6	115.6	8	987	119	Direct drive	[198]
	WM	12.0	216.9	105.4	63.0				600	60	6.1	110.2	10		132	Direct drive	[199]
	IEA	15.0	240.0	116.0	65.0				631	191	7.9		10	1528	150	Direct drive	[16]
	Concept	20.0	276.0		77.7				945	253			12	2070	160	Gearbox	[18]
Number of datapoints		23	23	20	15	8	8	8	18	12	5	7	8	7	14	23	

E

Alternative non-feasible deck layouts

In this appendix, additional non-feasible deck layouts are presented. Each layout is accompanied by comments explaining the reasons for considering them non-feasible.

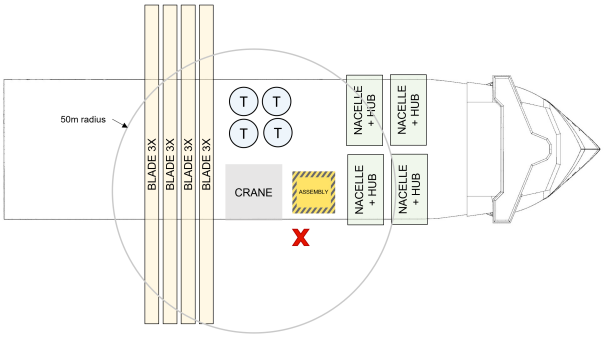

Blades are not allowed to be transported transversely, as explained in Section 6.

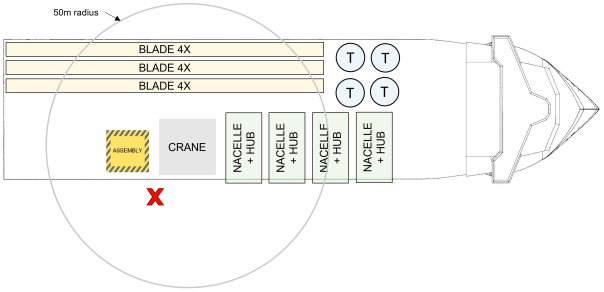

Towers not in reach of crane.

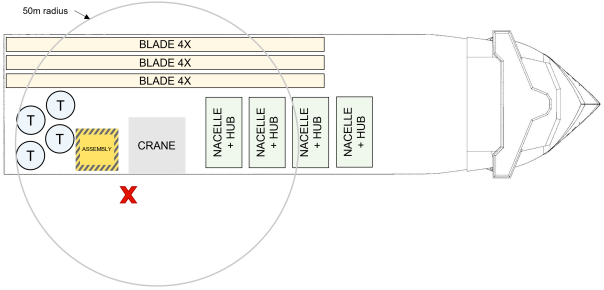

Towers are positioned very close to assembly location. Additionally, the blades need to be lifted and/or rotated over the towers on deck.

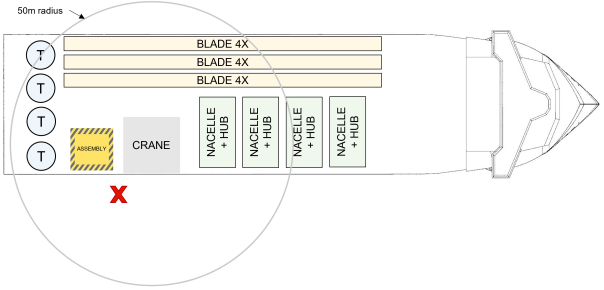

Blades needs to be lifting in proximity of the towers on deck. Also, the fourth tower is beyond the reach of the crane, but could also be positioned between the assembly location and blade racks.

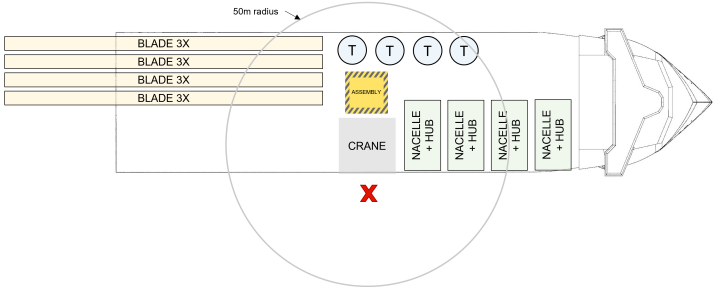

The crane must rotate 180 degrees to position the lifted turbine assembly for installation. Apart from that, the deck layout appears to be good.

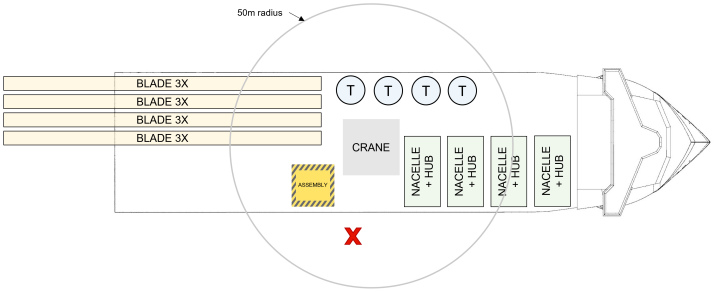

Towers would require lifting over blade racks or nacelles to reach the assembly location.

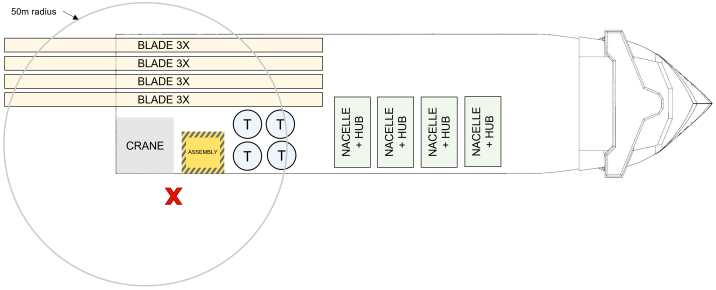

The blades would have to be lifted in proximity of the towers. Nacelles would have to be lifted over the towers. Large part of deck area not in reach of crane.

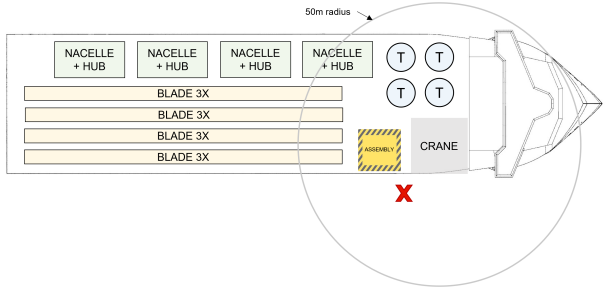

Large part of deck space not in reach of crane. The blades would need to be lifted over tower and nacelle at the assembly location.

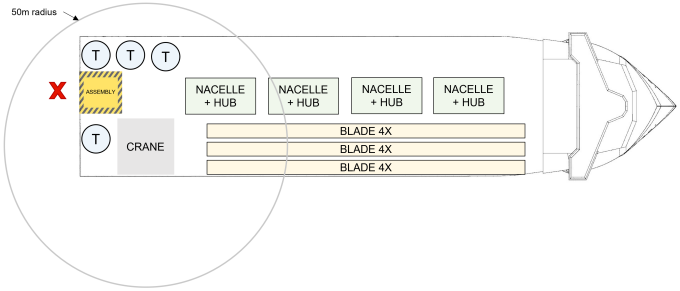

Installation position too far away from crane. Large part of deck outside crane reach.

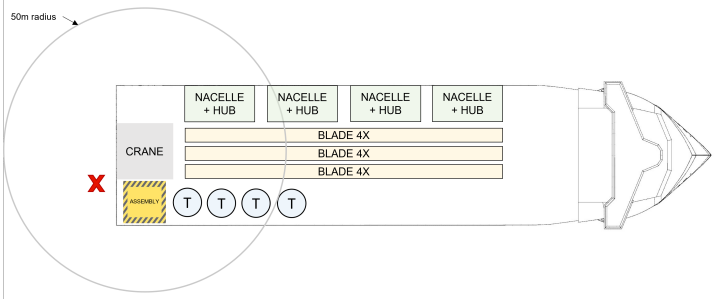

The fourth tower is beyond crane reach. Large part of deck cannot be reached by crane. To assemble the blades, they would need to be positioned above the other towers on deck.

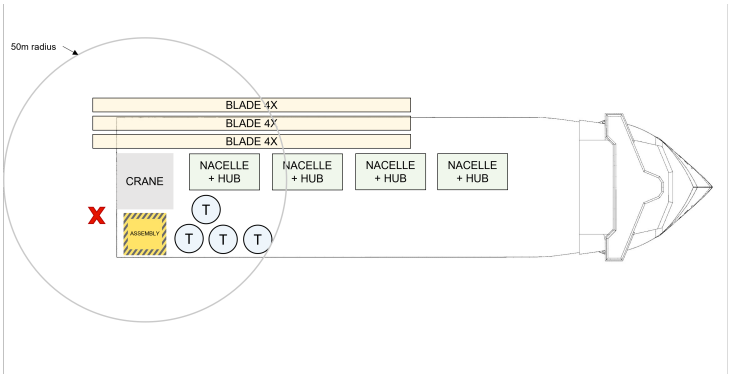

Nacelles require lifting over the towers. Large part of deck beyond crane reach.

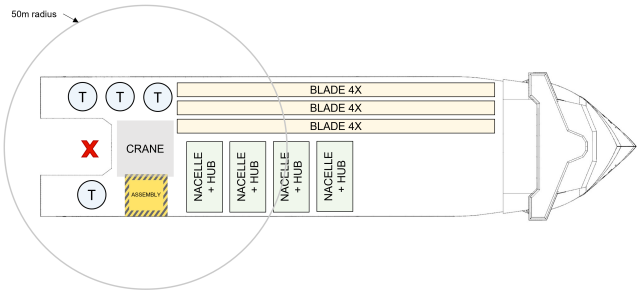

Length of vessel very much determined by length of blades. A large area remains unused.

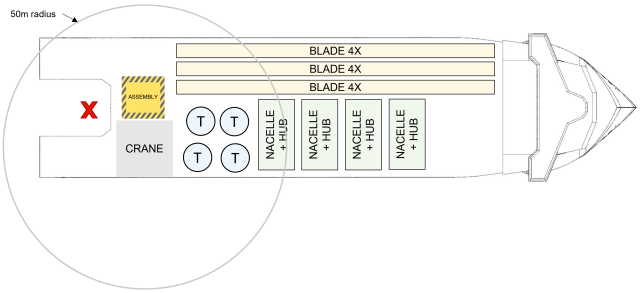

Nacelles would require lifting over the blade racks and crane would extend over the towers lifting the nacelles.

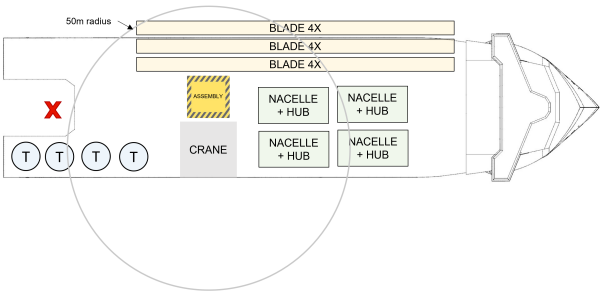

Crane and assembly location too far away from installation location.

(This page intentionally left blank)

F

Validation of CFEs and SAM

The contents of this appendix have been excluded from the repository due to confidentiality reasons.

G

Validation of WTG module

The contents of this appendix have been excluded from the repository due to confidentiality reasons.

H

Wind turbine installation cycles

The contents of this appendix have been excluded from the repository due to confidentiality reasons.

Estimation of installation contract rates

The contents of this appendix have been excluded from the repository due to confidentiality reasons.

J

RAO calculation with simplified formulas for Froude-Krylov force

An alternative method to determine the RAOs, is by estimating all parts of the RAO separately. The paper by Matsui et al. (2021) [90] proposes simple formulas to determine the linear Froude-Krylov forces for the six motions **surge**, **sway**, **heave**, **roll**, **pitch**, and **yaw**. The Froude-Krylov force is one of the main components of the hydrodynamic forces that act on a ship and one of the essential parts of the RAO.

The simplified estimation method requires several input parameters, including: length (L), breadth (B_0), draft (T), block coefficient (C_b), midship coefficient (C_m), waterplane coefficient (C_{wp}), transverse metacentric height ($\overline{GM_t}$), longitudinal center of floatation (LCF), longitudinal center of gravity (LCG), and wave heading angle (β). The LCF and LCG are only required for the calculation of the phase angles, but dueo to an earlier assumption to neglect the phase angles, these inputs are not required. All other input parameters can be determined using *Blended Design*, making this estimation method potentially applicable.

In the paper, the proposed formulas for the Froude-Krylov forces were verified with 77 different ships under various loading conditions. Below, the results from the proposed formula for Froude-Krylov forces are compared with the results from hydrodynamic analysis software (HAS) for a *UDSBV* HX104 hull. These comparisons were conducted for all six degrees of freedom and different wave heading angles.

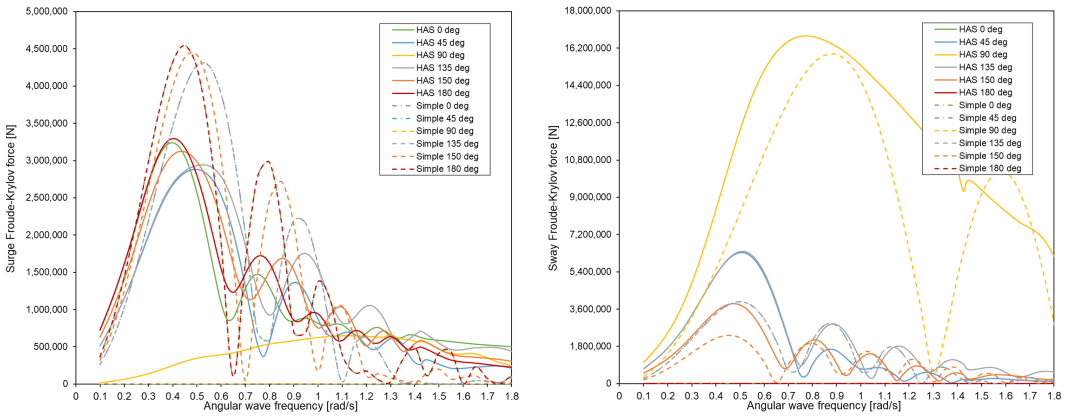

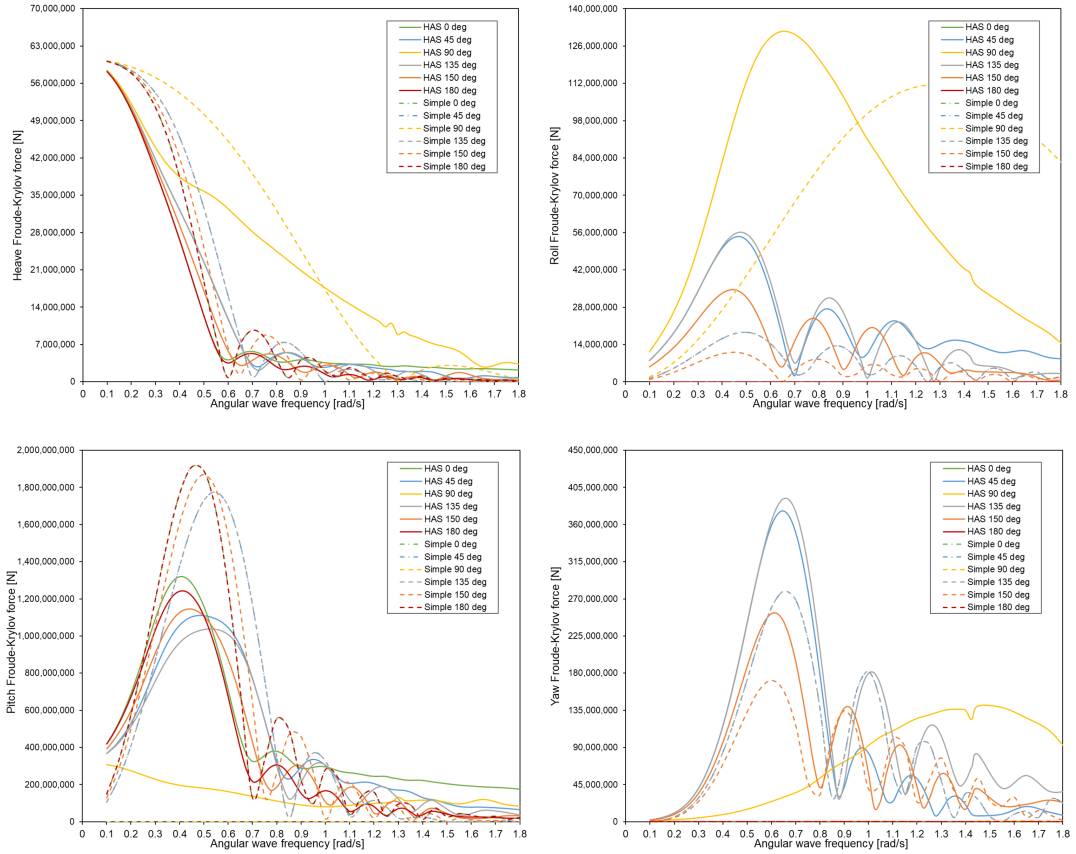

Figure J.1: Froude-Krylov forces for all six degrees of freedom of HX104 as function of wave frequency for different wave heading angles.
Continuous lines represent results from the simplified formulas by Matsui et al.
Dashed lines are results from HAS.

The graphs show that the Froude-Krylov estimated by the simple formulas are in most cases in the same order of magnitude as the results from HAS. Also, the maxima occur at roughly the same wave frequency. However, the simple method overestimates the Froude-Krylov forces for surge at low wave frequencies, and underestimates at higher frequencies. The maxima are at the roughly same wave frequency, but the values for the local maxima and minima are exaggerated. The Froude-Krylov forces for sway are slightly underestimated. For beam seas, the force exhibits deviant behavior because it goes to zero after the first peak, and forms a second peak afterwards. This behavior is not observed in the results from the HAS. For heave there is also some differentiation in beam seas. The methods appears to be unsuitable the Froude-Krylov force for roll motion. It significantly underestimates the forces, and for beam seas, the peak occurs at a completely different wave frequency. Hence, we can already conclude that calculating the RAO for the roll motion via this method will not yield better results than the method by Jensen et al. The Froude-Krylov forces for pitch are overestimated. On the other hand, yaw Froude-Krylov forces from the simple formulas exhibit similar behavior as the results from HAS but tend to be bit underestimated. For surge, sway, and pitch in beam seas, the Froude-Krylov forces are calculated to be zero, while in reality, they are non-zero.

The Froude-Krylov forces and moments are only one part of the wave excitation forces or moments, as displayed in Equation 4.2 of Chapter 4. Also, the other parts of the RAO need to be determined to estimate the RAOs for the six degrees of freedom. Therefore, the remaining challenge is to find the diffraction forces, added mass, damping, and restoring spring terms. An option could be to use 2D-strip theory, but since hull shapes are not included in *Blended*

Design this will not work. Therefore, more simple methods were investigated. Because the RAOs will be calculated without considering coupling effects, only the diagonal terms of the added mass, damping, and restoring spring coefficient matrices will be calculated. Below, simple methods for determining the remaining terms will be explained.

Determination of added mass terms (a)

One method for estimating the six diagonal terms for added mass and the inertia moment of ships was found in literature. A paper by Sen & Vinh [200] describes a method involving the use of an equivalent ellipsoid. The method, as described, only requires the main dimensions of the vessel as input, which makes it particularly suitable for *Blended Design*.

A limitation of this method is that it is only an approximation, since ships are generally not shaped ellipsoids. This method is also not able to determine the added mass for roll a_{44}. Furthermore, the added mass generally differs over the angular wave frequency range. With this method, the added mass is not dependent on the wave frequency. Therefore, the result is only one value for each degree of freedom which is constant over the ranges of frequencies.

Determination of restoring spring terms (c)

Restoring spring terms are only relevant for the heave, roll, and pitch motions. The equations for determining the restoring spring terms, denoted as c_{ii}, are given below.

$$c_{11} = c_{22} = c_{66} = 0$$

$$c_{33} = \rho g A_{wl} \tag{J.1}$$

$$c_{44} = \rho g \nabla \cdot \overline{GM_t} \tag{J.2}$$

$$c_{55} = \rho g \nabla \cdot \overline{GM_L} \tag{J.3}$$

where A_{wl} is the waterplane area and ∇ is the hull volume. $\overline{GM_t}$ and $\overline{GM_L}$ correspond to the transverse and longitudinal metracentric heights, respectively.

Determination of damping terms (b)

Unfortunately, no simple methods were found in literature to estimate the damping terms. Therefore, it has been decided to use the critical damping. The critical damping is calculated for degree of freedom and then it is assumed that the damping would be a fraction of the critical damping. The formula for critical damping is depicted in Equation J.4.

$$b_{cr} = 2\sqrt{(m+a) \cdot c} \tag{J.4}$$

The applied fractions of the critical damping are based on estimations found with the expertise of the hydrodynamic specialist within *UDSBV*. Model decay tests done in the past for one of their vessel designs, the HX104, showed that the damping in heave is very high. Therefore, the fraction for heave is estimated to be around 50% of the critical damping. For pitch, it has been taken as 30 to 40%. The method above does not work for the surge, sway, and yaw motion because these motions do not have a restoring spring term, as depicted in the previous subsection. To determine the critical damping without the need for a restoring spring term, the natural period is needed. In this case, the natural period is based on the stiffness of a DP system, following a similar approach described in a paper by J. Serraris [201]. Combining Equation J.5 with Equation J.4 eventually yields Equation J.6.

$$T_n = 2\pi\sqrt{\frac{m+a}{c}} \tag{J.5}$$

$$b_{cr} = \frac{4\pi(m+a)}{T_n} \tag{J.6}$$

When implementing a feedback control system to regulate the surge, sway, and yaw motions, the natural periods for these motions would be between 100 to 200 seconds [202]. The damping for surge, sway, and yaw is set to be 50 to 70% of the critical damping, based on the paper of J. Serraris [201].

Just as added mass, the damping generally varies over the angular wave frequency range. With the proposed method, damping is not dependent on the wave frequency and is thus constant over the whole frequency range. The results from the damping calculation were validated with results from damping calculation from HAS. The results from the simplified damping determination were found to be in the right order of magnitude.

Determination of diffraction force

While the undisturbed wave forces, also known as Froude-Krylov forces, result from the pressure field generated by the undisturbed wave acting on the floating body, diffraction forces are also part of the wave excitation forces. The diffraction force is a result of the pressure distribution on the submerged surface of the floating body as a result of disturbing the waves and reflecting them.

The computation of diffraction forces involve solving different differential equation from potential theory while considering the appropriate boundary conditions. This is typically done by solving the Laplace equation . The Laplace equation is solved numerically by 3D BEM algorithms, because there is no analytical description of the hull surface. In literature, no alternative methods have been found to estimate the diffraction forces in a simple manner. Consequently, the diffraction forces cannot be determined for this research. Based on this, a preliminary conclusion can be drawn that the proposed method is probably not suitable for determining the RAOs via the Froude-Krylov forces from Matsui et al.

Visual validation of RAOs

While it has been already tentatively concluded that the proposed method is unsuitable, a visual comparison has been conducted between the resulting RAOs obtained from HAS and the simplified method that neglects the diffraction forces. The RAOs (without diffraction forces) for every degree of freedom can be calculated using Equation 4.2 from Chapter 4. The RAO for roll motion cannot be calculated due to the unavailability of a simple method to determine the added mass for roll. Also, the calculated Froude-Krylov force was already found to be significantly inaccurate. Below, the comparison of the RAOs for the remaining five motions is given.

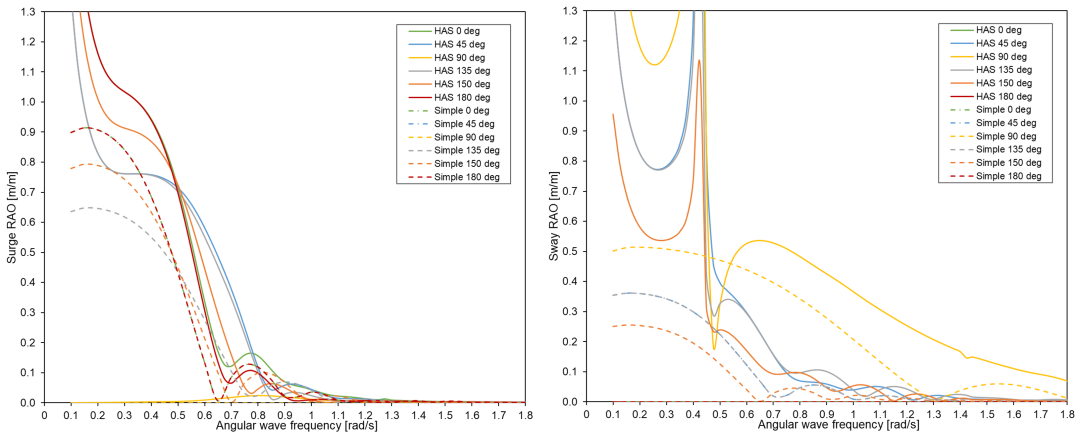

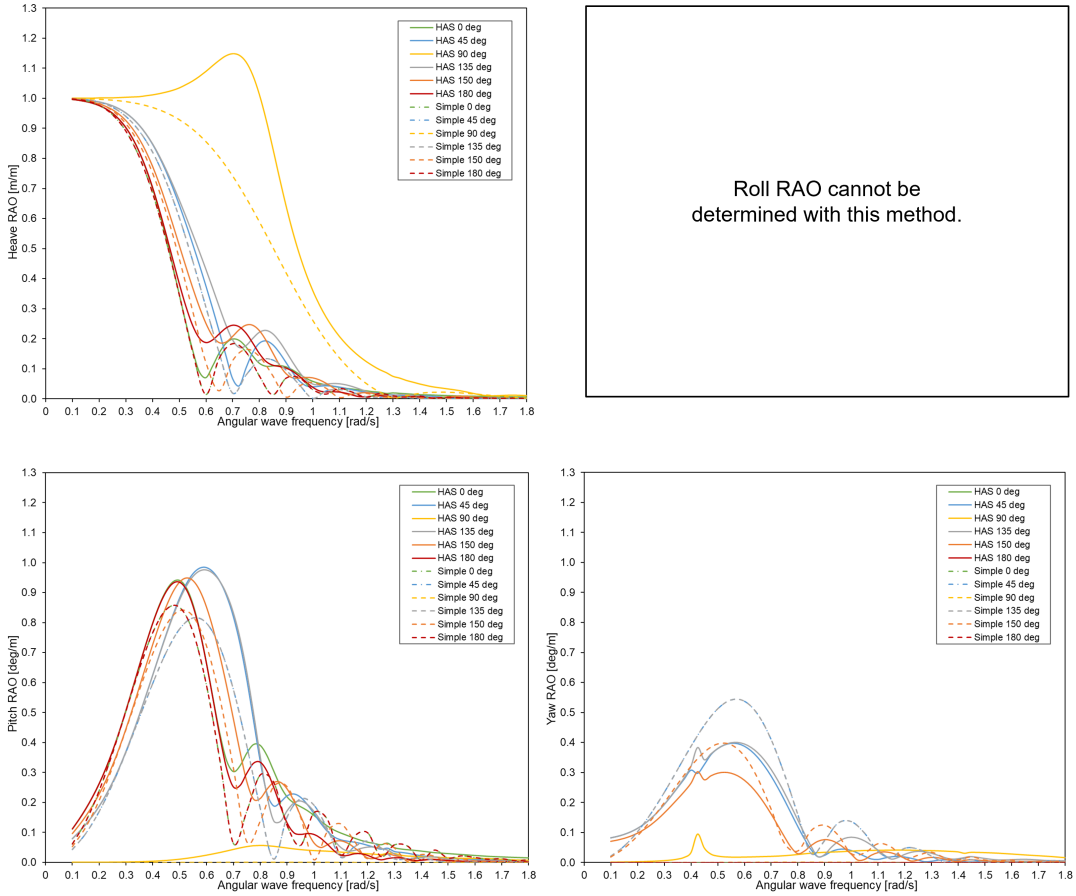

Figure J.2: RAOs for all motions, excluding roll, of HX104 as function of wave frequency for different headings. Continuous lines represent calculated results from the simple method without diffraction forces. Dashed lines are the complete results from HAS.

The locations of the local maxima and minima for the heave and pitch motion RAOs are around the same wave frequency as from HAS, but the values are slightly lower. This could be a result of omitting the diffraction forces. The RAOs, calculated with the simple method, for the surge and yaw motion show nowhere near similar behavior as the RAOs from HAS. Hence, it can be concluded that the assumptions within the simplified formulas for determining all terms of the RAOs and omitting the diffraction forces, is too rigorous to be useful. Based on this, it has been decided to abandon this method and only incorporate the RAOs for heave, roll, and pitch from the CFEs from Jensen at al. in the seakeeping analysis.

From the RAOs from HAS, we can also conclude that the RAO values for the surge, sway, and yaw motions are almost zero for higher wave frequencies. Higher wave frequencies correspond to short wave periods, which are the most common waves periods when looking at the wave scatter diagram of, for example, the North Sea (Figure 4.9). Therefore, the influence of not taking into account the surge, way, and yaw motion RAOs in the seakeeping analysis module is considered to be insignificant.

(This page intentionally left blank)

K

Additional results

All the presented results in this appendix have been calculated under the weathervaning assumption in a 1,000ft bound market with a distance to port of 140 NM. The used wave scatter diagram corresponds to zone 11, which represents the North Sea. For more information, refer to Section 4.2.5 of Chapter 4. The same input for *Blended Design* as in Table 5.1 from Chapter 5 has been used.

K.1. Significant wave height limit of 1.5m

Below, a graph depicting the MPE motion displacements for a range of ship displacements is presented. As expected, the MPE displacements are lower compared to the base case with an operational H_s limit of 2.5 meters.

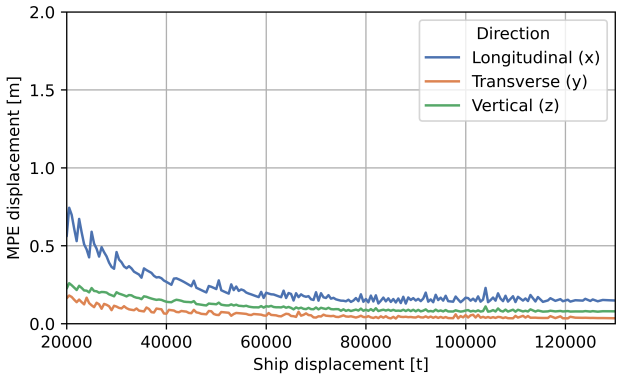

Figure K.1: Visualization of the MPE displacements while weathervaning with a maximum H_s of 1.5 meters.

At a significant wave height of 1.5 meters, the workability would be 60.3 percent. This would consequently impact the time *Moonshot* could install wind turbines. The number of annual installed turbines would be lower and result in a decrease of revenue. On the other hand, the lower motions would lead to reduced potential costs for motion compensation. Therefore, the financial results for different ship parameters, including the motion penalty, are presented in the plots below.

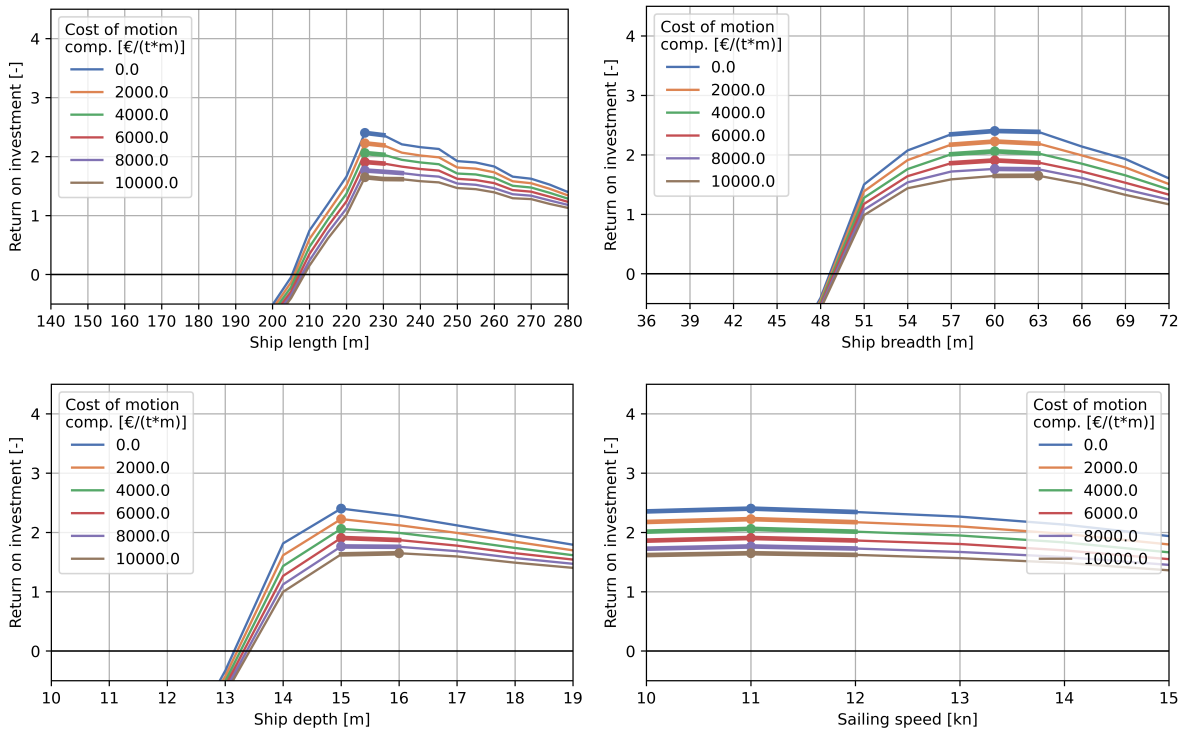

Figure K.2: Visualization of the financial results while weathervaning with a maximum H_s requirement of 1.5 meters.

The results show that the lines representing different cost levels are closer to each other, this is a result of the lower motions associated with the H_s As expected, the overall ROI for the configurations is lower because of the lower workability. Regarding the optimal ship parameters, some interesting observations can be made. The optimal length remains consistent with the original analysis with an H_s of 2.5 meters. However, at the highest cost level, the optimal ship length is at a lower value. The optimal ship breadth remains the same. At the highest cost level, the optimum shifts to wider ships. Ship depth exhibits similar behavior to the analysis with a 2.5 meters H_s limit. The optimal range at the highest cost level is the same. Interestingly, the optimal sailing speed is lower with the lower H_s limit, at 11 knots. Additionally, the optimal range is narrower. The reason for this shift to lower optimal speed is not entirely clear, but may be attributed to the reduced revenue and the lower investment costs associated with a smaller propulsion installation.

K.2. Significant wave height limit of 3.5m

Below, a graph with the MPE motion displacements for different ship displacements is presented. As expected, the MPE displacements will be higher compared to the base case with a operational H_s limit of 2.5 meters.

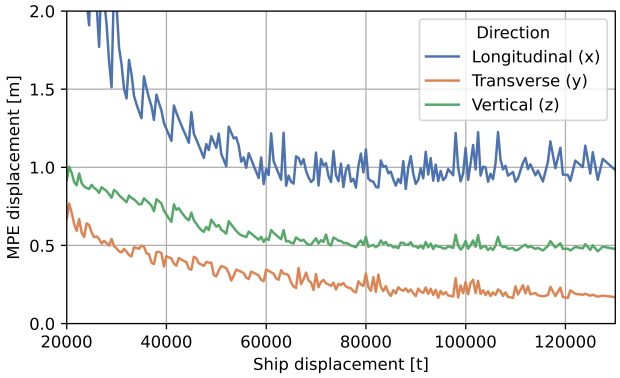

Figure K.3: Visualization of the MPE displacements while weathervaning with a maximum H_s of 3.5 meters.

With the operational H_s limit increased to 3.5 meters, the workability also increases from 78.2 to 88.6 percent. This increase would enable *Moonshot* to install more turbines per year, resulting in increased revenue. The financial results for the different ship parameters, also accounting for the cost of motion compensation, are displayed in the following graphs.

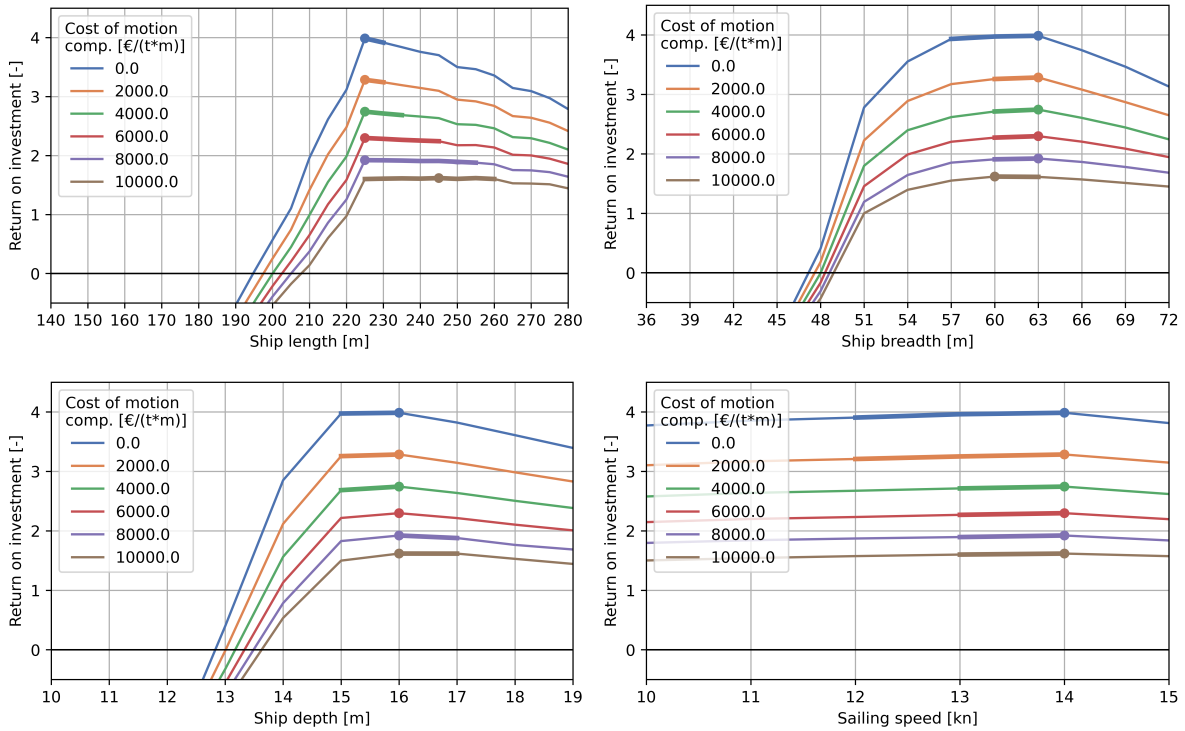

Figure K.4: Visualization of the financial results while weathervaning with a maximum H_s requirement of 3.5 meters.

As anticipated, the ROI of the configurations at a zero-cost level is higher, which is visible in the graphs above. The relative distance between the lines representing different cost-levels is significantly larger when comparing it to the results for the base-case with an H_s limit of 2.5 meters (Figure 5.19 in Chapter 5). This is a result of the increased motions, increasing

the costs significantly for increasing cost-levels. In terms of optimal length, the results reveal that the optimal length remains the same for the lower costs levels when compared to the results for 2.5 meters. However, as the motion penalty increases, the optimal length also increases, and the range becomes broader. This is because of the lower longitudinal motions for longer ships. Regarding breadth, a shift of optimal ship breadth towards larger values is visible. What stands out, is that the optimal breadth shifts to a lower value again at the highest cost level. Regarding depth, a shift to larger values than for a H_s limit of 2.5 meters can be observed. The optimal range also included 15 meters at lower costs levels. However, as the penalty increases, the range becomes smaller and eventually widens to 17 meters depth at the two highest cost levels. This change is driven by improved seakeeping behavior at increased depths.

Interestingly, the optimal ship speed increases to 14 knots, which is higher than for H_s limits of 1.5 and 2.5 meters. This increase in optimal ship speed is not what you would expect and appears to be a flaw of the model. In*Blended Design*, seakeeping behavior is only calculated at zero ship speed during turbine installation. It does not take into account motions during transit. Typically, seakeeping during transit is worse at higher sailing speeds, particularly in higher sea states. Therefore, it could be valuable to incorporate an analysis of seakeeping behavior during transit, in addition to offshore operations, to assess if seakeeping in transit conditions would be a critical factor.

Small analysis on environmental performance

A small analysis on environmental performance has been done. This aspect was omitted from the performance evaluation in Chapter 5, because it would be too extensive to evaluate the entire environmental performance for all ship configurations across various alternative fuels and different scenarios. Instead, a small portion will be included here,focusing on the evaluation of the Energy Efficiency eXisting ship Index (EEXI). This metric displays the energy efficiency of the ship and indicates the carbon emission depending on amount of transported cargo in tonnes and the sailing distance in miles. The formula for calculating the EEXI provided below. In general, ships with the lowest EEXI are considered to be the most environmentally efficient. The same displacement as derived from the maximum ROI will be used. Within this constraint displacement, different combinations of ship parameters will be explored.

$$\text{EEXI} = \frac{CO_2 \text{ emissions}}{\text{Transportation work}} =$$

Emissions main engine(s) | Emissions aux. engine(s) | Energy savings aux. engine(s) | Energy savings main engine(s)

$$\frac{\left(\prod_{j=1}^{M} f_j\right)\left(\sum_{i=1}^{nME} P_{ME(i)} \cdot C_{FME(i)} \cdot SFC_{ME(i)}\right) + (P_{AE} \cdot C_{FAE} \cdot SFC_{AE}) + \left(\left(\prod_{j=1}^{M} f_j \cdot \sum_{i=1}^{nPTI} P_{PTI(i)} - \sum_{i=1}^{neff} f_{eff(i)} \cdot P_{AEeff(i)}\right) C_{FAE} \cdot SFC_{AE}\right) - \left(\sum_{i=1}^{neff} f_{eff(i)} \cdot P_{eff(i)} \cdot C_{FME} \cdot SFC_{ME}\right)}{f_i \cdot f_c \cdot f_l \cdot capacity \cdot f_w \cdot V_{ref} \cdot f_m}$$

Transportation work

In this case, transportation work is calculated as the annual transported turbine weight multiplied by the sailing distance. The environmental performance outcomes for different ship parameters, while maintaining a fixed displacement of 70,000 tonnes, are depicted in the graphs below. Please refer to Figure 5.1 in Chapter 5 for guidance on interpreting these plots.

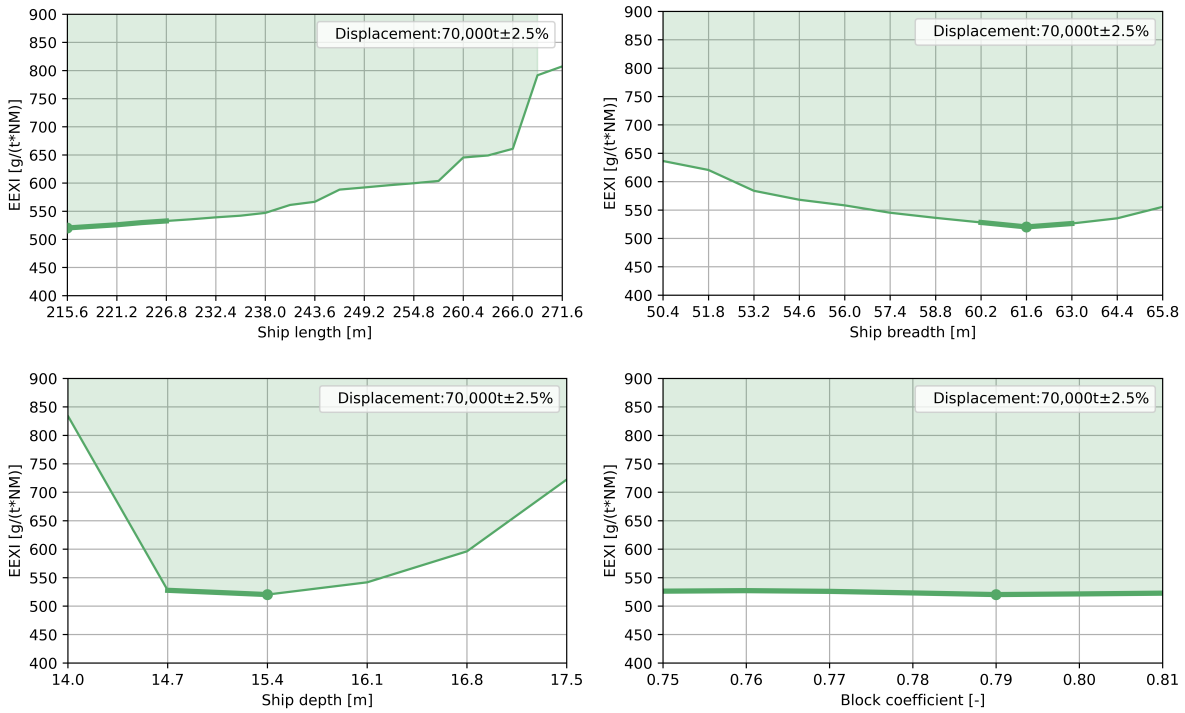

Figure L.1: Visualization of the environmental performance results for the 20 MW *Moonshot* with a fixed displacement.

The observed EEXI values are high compared to other ship types. For instance, a bulk carrier typically has an EEXI below 10 [203]. The large difference can be attributed to the relatively light mass of turbine components, while their footprint is large. In terms of emissions per transportation work, turbine components are thus one of the worst types of cargo, unlike bulk cargo such as rocks.

The results reveal that the block coefficient does not significantly influence the EEXI. However, there is a clear optimum observed for ship depth and ship breadth. The EEXI increases rapidly for values outside the optimal depth or breadth. The optimal depth for environmental performance falls within the optimal depth range for financial performance but is lower than for optimal seakeeping performance. Likewise, the optimal breadth range for environmental performance aligns with the optimal financial performance breadth range. However, it would fall outside the optimal breadth range for seakeeping behavior. The optimal ship length is as short as possible. For longer ships, the EEXI increases very rapidly beyond ship lengths of 257.6 meters. This is primarily because of the displacement constraint, as large longer ships would require a smaller breadth or draft, impacting the number of turbines a configuration can carry and thus affecting the transportation work in the EEXI formula.

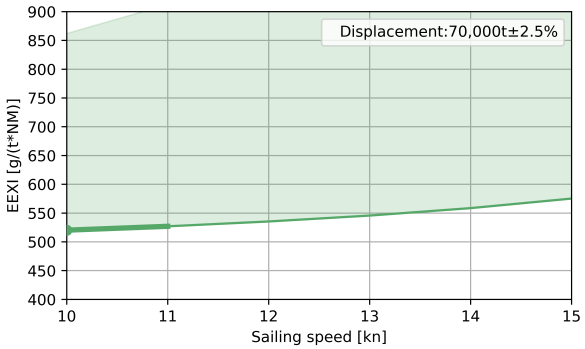

Figure L.2: Visualization of the environmental performance results for sailing speed.

The plot for sailing speed is shown in the figure above. Generally, as speed increases, so does the EEXI. Therefore, the optimal speed would ideally be as low as possible. With increasing speeds, the EEXI also increases, but the increase is not very steep.

(This page intentionally left blank)

M

Artist impressions of Moonshot

The contents of this appendix have been excluded from the repository due to confidentiality reasons.